

**ASYMMETRIC RELATIONSHIP OF NINO
INDICES WITH RAINFALL EXTREMES
OVER WESTERN GHATS AND COASTAL
REGION OF KARNATAKA**

Thesis

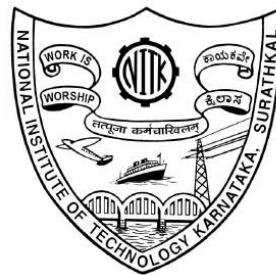
Submitted in partial fulfillment of the requirements for the
degree of

DOCTOR OF PHILOSOPHY

By

VINAY D C

(123041 AM12F07)



DEPARTMENT OF APPLIED MECHANICS AND HYDRAULICS
NATIONAL INSTITUTE OF TECHNOLOGY KARNATAKA
SURATHKAL, MANGALURU-575 025

Feb – 2020

**ASYMMETRIC RELATIONSHIP OF NINO
INDICES WITH RAINFALL EXTREMES
OVER WESTERN GHATS AND COASTAL
REGION OF KARNATAKA**

Thesis

Submitted in partial fulfillment of the requirements for the
degree of

DOCTOR OF PHILOSOPHY

By

VINAY D C

Under the guidance of
Prof. AMBA SHETTY

Professor

Dept. of Applied Mechanics & Hydraulics
NITK, Surathkal



DEPARTMENT OF APPLIED MECHANICS AND HYDRAULICS
NATIONAL INSTITUTE OF TECHNOLOGY KARNATAKA
SURATHKAL, MANGALURU-575 025

Feb – 2020

D E C L A R A T I O N

By the Ph.D. Research Scholar

I hereby *declare* that the Research Thesis entitled **ASYMMETRIC RELATIONSHIP OF NINO INDICES WITH RAINFALL EXTREMES OVER WESTERN GHATS AND COASTAL REGION OF KARNATAKA** which is being submitted to the **National Institute of Technology Karnataka, Surathkal** in partial fulfilment of the requirements for the award of the Degree of **Doctor of Philosophy** in **Applied Mechanics and Hydraulics Department** is a *bonafide report of the research work* carried out by me. The material contained in this Research Thesis has not been submitted to any University or Institution for the award of any degree.

123041 AM12F01, VINAY D C

(Register Number, Name & Signature of the Research Scholar)

Department of Applied Mechanics and Hydraulics
National Institute of Technology Karnataka, India

Place: NITK-Surathkal

Date: 14-02-2020

C E R T I F I C A T E

This is to *certify* that the Research Thesis entitled **ASYMMETRIC RELATIONSHIP OF NINO INDICES WITH RAINFALL EXTREMES OVER WESTERN GHATS AND COASTAL REGION OF KARNATAKA** submitted by **VINAY D C** (Register Number: 123041 VINAY D C) as the record of the research work carried out by her, is *accepted as the Research Thesis submission* in partial fulfilment of the requirements for the award of degree of **Doctor of Philosophy**.

Prof. Amba Shetty

Research Guide

(Name and Signature with Date and Seal)

Chairman - DRPC

(Signature with Date and Seal)

Department of Applied Mechanics and Hydraulics

National Institute of Technology Karnataka, India

ACKNOWLEDGEMENTS

गुरुः ब्रह्मा गुरुः विष्णु गुरुर्देवो महेश्वरा, गुरुः साक्षात् परब्रह्म तस्मै श्री गुरुवे नमः ।

गुरु बिन ग्यान नहीं , ग्यान बिन आत्मा नहीं।

To my guide, **Prof. Amba Shetty**, I owe it all to you. Many many Thanks!

Completion of this research work was possible with the support of several people. I would like to express my sincere gratitude to all of them. First of all, I am extremely grateful to research supervisor **Prof. Amba Shetty**, Department of Applied Mechanics and Hydraulics, National Institute of Technology Karnataka, for logical and tactical suggestions, wholehearted co-operation, constructive criticism and continuous encouragement during the development of the research work. With moral support and guidance of the supervisor, this research work could be completed and I could publish my work in recognized good journals.

I thank the former Director of the Indian Institute of Tropical Meteorology (IITM), Pune, Prof. B. N. Goswami, for granting permission to attend the classes and utilize institutional infrastructure facilities. I thank Ramesh H Kripalani, Senior Scientist, former Head of CAT program, and Dr. Roxy Mathew Koll, Scientist E, Centre for Climate Change (CCC), IITM for granting the permission to attend classes and supported to carry out my research work.

I am grateful to Research Progress Assessment Committee members, **Prof. Subhash C Yaragal** and **Prof. Amai Mahesha**, for their critical evaluation and useful suggestions during the progress of the work.

Much obliged to Mr. Bhupendra Bahaddur Singh, Mr. Pramit Deburman, Scientist at IITM (CCC), Dr. Manjunath Patel G C, Dr. Gebremedhin Kiros, Dr. Amogh Mudbhatkal and Dr. Chandre Gowda, Doctorols of NITK, and Suman K, Sujay Ragavendra reseach scholar of AMD, NITK and friend Rajesh for support to carryout my research work.

I am thankful to Prof. Swapan Bhattacharya, Former Director of NITK, Prof. Katta Venkataramana, former Dean of Academics, NITK and Prof. Subba Rao, former Head, Department of Applied Mechanics and Hydraulics, NITK for granting permission to attend classes at IITM, Pune.

I Thank to Prof. Mahesha A, and Prof. M K Nagaraj, Prof. Dwarakish G S, Prof. Subba Rao, former Head, Department of applied Mechanics and hydraulics during research program. I wish to thank Prof. Lakshman Nandagiri, Prof. Kiran G Shirlal, Dr. Ramesh H, Dr. Paresh Chandra Dekha, Dr. Varija, Dr. Prithviraju, Dr. B M Doddamani, Dr. Vadivuchezhian K, Dr. Manu, Dr. Naser, Dr. Debabrata Karmakar Faculty members, Department of Applied Mechanics and hydraulics.

I am thankful to **Mr. Muralidhar N, Dr. Suparno Ghosh, Dr. Bhojaraj B E, Dr. Geetha Kuntogi, Dr. Sreedhara B M, Mr. Harish Kumar, Mr. Arun Kumar Yadav, Mr. Raveesha**, Research Scholars of AMD, **Mr. Kalay Tesfye**, Research Scholar of Civil Engineering, NITK for kind support and motivating during the period of research program.

I sincerely acknowledge the help and support rendered by all the faculties, staffs and research scholars of Department of Applied Mechanics and Hydraulics, NITK Surathkal.

I thank the authors of all those research publications which have been referred to in preparing this thesis. I also express my gratitude to reviewers of journals for their excellent input for this work.

I express profound gratitude to family members and friends for their encouragement and moral support on the path to the journey of my research.

Besides all, I express my worshipful gratitude to the Almighty, the source of strength during the entire endeavor.

Vinay D C

Dedication

To my father Sri. B Chandrashekar and mother Smt. Shailaja D B for all their love and support and putting me through the best education as possible,

To Prof. Amba Shetty and all my former teachers through whom the Almighty led me to the world of knowledge and wisdom,

&

To my loving wife Smt. Parinika G (Ashwini) and in-laws for constant source of encouragement and inspiration during the period of my research.

ABSTRACT

Climate variability and change has increased extreme rainfall events. There is an underreporting and limited analysis, which often have significant impact with extreme rainfall events at regional scale. The magnitude of variability of the rainfall extremes varies according to locations. Among subdivisions of Western Ghats of India maximum rainfall occurs over Coastal Karnataka. Examining the extreme events of rainfall provide an idea of the probable occurrence of severity conditions in future in the context of changing climate. Extreme rainfall indices to identify the variation of rainfall patterns such as the number of rainy days, total rainfall, daily intensity index, one and five-day maximum rainfall, dry spells and threshold intensity rainfall frequency indices were considered as per the norms suggested by Expert Team on Climate Change Detection (ETCCDI) of Intergovernmental Panel on Climate Change (IPCC). These rainfall extremes indices are analyzed using IMD gridded high resolution daily rainfall data for the period 1901-2013. Statistical trend analysis techniques namely Mann–Kendall test applied for extreme rainfall indices and Theil-Sen estimator perceive nature and magnitude of slope in rainfall indices. The trends show contrasting spatial variations of extreme rainfall indices in Coastal region (low land) and Western Ghats (high land) regions of Karnataka. The changes in daily rainfall events in the lowland region primarily indicate statistically significant (varies from 95% to 99.9% confidence level) positive trends in the annual total rainfall, 1-day, and 5-day maximum rainfall, frequency of very heavy rainfall, and heavy rainfall as well as medium rainfall events. The seasonal variation of rainfall exhibits mixed trend, however significantly rising trend is witnessed in the southern coastal plains and the adjacent Western Ghats region during the pre-monsoon. But, southern coastal plains show a decreasing trend in the monsoon period (JJAS). Furthermore, the overall annual rainfall strongly correlated with all the rainfall indices in both regions, especially with indices that represent heavy rainfall events which are responsible for the total increase of rainfall.

The interannual variability of rainfall and its extreme events over study region is observed to be associated with ENSO cycle, whereas Nino indices are asymmetric over the study region. The trends in ETCCDI extreme rainfall indices analyzed as an issue of climate change and the possible teleconnection with the ENSO mode as a concern of natural climatic variability have been analyzed over the study region. Nevertheless, differences are found

between the spatial extent of correlation coefficients and their magnitudes. Using most significant time lag between the extreme rainfall indices (dependent variable) and the November-January (ONDJ) seasonal average of Niño indices (independent variable). The best model with the highest coefficient of determination was identified by Step wise regression analysis. The teleconnection between the Niño indices (Niño 1+2, Niño 3, Niño 3.4 and Niño 4) and the rainfall extremes with 0-year and 1-year ahead are at different phases, regional response of rainfall extremes to these indices are dissimilar. This analysis provides insights into regional response of rainfall extremes to global climate indices over the study region.

The large-scale phenomenon over the pacific ocean with rainfall over the study region provide a scientific basis for understanding and developing credibility in future regional climate. A significant lag correlation between the summer monsoon rainfall and Niño indices was revealed by the seasonal lead-lag correlation analysis, Niño 3(t-4) at 90% confidence level, remaining Niño 3.4(t-2), Niño 4(t-2), and Niño 4(t-3) at 95% confidence level shows a significant relationship at respective lag period from onset of summer monsoon rainfall. In order to investigate the combined lagged effects of the potential climate predictors for monsoon rainfall using multiple linear regression as a linear method compared to neural network as a nonlinear method have been employed to examine the predictability of the summer monsoon rainfall. The principal component analysis of predictors aids to represent in one-dimensional space using the eigen vector that corresponds to the covariance matrix's largest eigen value. Whereas first principal component explains about 72% of the variance of the predictors. Thus, PC1 considered as predictor in regression equation and input layer in neural network models to avoid over fitting. The attained prediction on the basis of the overall performance of the prediction models, feed forward neural network model shows a better prediction compared to other models with a good correlation coefficient and RMSE of 0.53 and 1.6 for training case, and 0.72 and 1.63 for testing case, respectively. From the time series analysis for period 1951-2013 of standardized monsoon rainfall Index selected the positive episodes values having standardized value greater than +1 (excess) and similarly with negative episodes values with standardized values less than -1 (deficit). The mean anomalous SST values for the region Niño 3.4 for the season DJF (-2) for positive episode is 0.1719°C and the negative episode is -0.5133°C. The two SST means are significantly different at confidence level of 87.15% through the Student's t-test.

In awaken of climate change, this study is a contribution in the on-going research of extreme events over mountainous terrain including disaster management study. The sequential daily rainfall extremes and other atmospheric parameters may be utilized for the now-casting of extreme rainfall events. Further the relationship between topography and other atmospheric parameters influence for rainfall extremes should be studied separately to get better insight. This research may also be useful for the modifications in rainfall extremes retrieval methods over the Western Ghats mountainous terrain.

Key Words: ENSO Indices, extreme rainfall, neural network, regression model, Stepwise regression, summer monsoon, teleconnection, Western Ghats of Karnataka.

CONTENTS

Abstract	i
Contents	v
List of figures	x
List of tables	xiv
Nomenclature	xv
CHAPTER 1 INTRODUCTION	1
1.1 Introduction	1
1.2 Rainfall distribution	1
1.2.1 Causes of Spatial Variability of Rainfall	3
1.3 Factors influencing precipitation	4
1.4 Influence of climatic factors for extreme rainfall	5
1.5 Assessment of extreme precipitation variability	7
1.6 Rainfall variability over west coast of India	8
1.7 Teleconnection of ENSO with rainfall	10
1.7.1 Assessment of Oceanic Nino index	10
1.8 Importance of the study	12
1.9 Statement of Problem	13
1.10 Objectives of the study	14
1.11 Organization of the report	14
CHAPTER 2 LITERATURE REVIEW	15
2.1 Background	15
2.2 Exploratory Analysis of Rainfall	15
2.2.1 Trend analysis of rainfall in India	16
2.2.2 Variation in frequency of extreme rainfall events and its trend	16
2.3 Association of Precipitation with Sea Surface Temperature	21
2.3.1 Impacts of climate change on water resources	22

2.3.2 Local impacts of climate change in India and the Western Ghats	22
2.4 Sea surface temperature anomalies teleconnection with monsoon rainfall	26
2.5 Literature gap and Summary	31
CHAPTER 3 MATERIALS AND METHODOLOGY	33
3.1 Introduction	33
3.2 Study Area	33
3.2.1 Climatic characteristics	38
3.3 Data sets	41
3.4 Details of tools used for the study	43
3.5 Overall Methodology	44
CHAPTER 4 TREND ANALYSIS OF EXTREME RAINFALL INDICES	47
4.1 Introduction	47
4.2 Extreme rainfall analysis in Western Ghats	47
4.3 Methods for trend analysis	48
4.4 Methodology	50
4.4.1 Schematic flow of extreme rainfall analysis	50
4.4.2 Assessment of Changes in Rainfall Extreme Events	52
4.4.3 Statistical Tests for Trend Detection	54
4.4.3.1 Serial Correlation	54
4.4.3.2 Autocorrelation Removal	54
4.4.3.3 Non-Parametric Versus Parametric Methods	55
4.4.3.4 Background and Purpose of Mann-Kendall test	56
4.4.3.5 Assumptions and Requirements	56
4.4.3.6 Calculation of Mann-Kendall trend test	57
4.4.3.7 Modified Mann-Kendall (MMK)	58
4.4.3.8 Magnitude of Trend (Sen's Slope)	58

4.5 Results and Discussion	60
4.5.1 Spatio-temporal patterns and Variability of Rainfall	60
4.5.2 Trend analysis of ETCCDI rainfall Indices	61
4.5.2.1 Significance of ETCCDI extreme rainfall indices	64
4.6 Spatial distribution of interannual precipitation indices and its trend	65
4.6.1 Spatial distribution and trends in Annual Total Rainfall (RR) and Simple Daily Rainfall Intensity (SDII) Indices	65
4.6.2 Changes in the Extreme Rainfall Depth and Intensity Indices	69
4.6.3 Inference of interannual temporal variation of extreme rainfall Indices	71
4.7 Seasonal analysis of precipitation indices and trend	72
4.7.1 Spatial distribution of extreme precipitation indices during monsoon season	72
4.7.2 Spatial patterns of temporal trends of the extreme rainfall indices during monsoon season	75
4.7.3 Spatial distribution of extreme precipitation indices during pre-monsoon Season	77
4.7.4 Spatial patterns of temporal trends of the extreme rainfall indices during pre-monsoon season	79
4.7.5 Spatial distribution and temporal trends of the extreme rainfall indices during post-monsoon season	81
4.8 Spatial Distribution of Threshold Precipitation Indices	84
4.9 Correlation of annual precipitation Indices	88
4.10 Conclusions	91
CHAPTER 5 ENSO INDICES MODULATION ON EXTREME RAINFALL EVENTS	95
5.1 Introduction	95
5.2 Spatial patterns and teleconnection of rainfall extremes	95
5.3 Methodology	96
5.3.1 Stepwise regression analysis	98
5.3.2 Bivariate Correlation	100

5.4 Results and Discussion	100
5.4.1 Analysis of teleconnection between rainfall extreme indices and ENSO Indices	100
5.4.2 Temporal patterns of Nino Indices	101
5.4.3 Possible teleconnections of rainfall extremes with ENSO indices	102
5.4.4 Characteristics of Sea surface temperature	106
5.4.5 Correlation Analysis between ENSO Indices and extreme Rainfall events	106
5.4.5.1 Influence of Niño 1+2 on extreme precipitation indices	107
5.4.5.2 Influence of Niño 3 on extreme precipitation indices	113
5.4.5.3 Influence of Niño 4 on extreme precipitation indices	118
5.4.5.4 Influence of Niño 3.4 on extreme precipitation indices	123
5.5 Conclusions	128
CHAPTER 6 ESTIMATION OF SUMMER MONSOON PRECIPITATION	131
6.1 Introduction	131
6.2 Importance of estimation of seasonal rainfall	132
6.3 Methodology	133
6.3.1 Temporal variation of monsoon season rainfall	134
6.3.2 Multiple linear regression model	135
6.3.3 Principle component Analysis	136
6.3.4 Artificial Neural network	137
6.3.5 Statistical Performance	140
6.4 Seasonal precipitation anomaly associated with sea surface temperature	140
6.5 Temporal variation of Sea Surface Temperature anomalies over Equatorial Pacific Ocean associated with ENSO phases	143
6.6 Seasonal Lead-lag correlation of summer monsoon precipitation index with Niño indices	144
6.7 Models for estimation of summer monsoon precipitation	147
6.8 Results and discussion	148

6.8.1 Assessing SST-SMP association with identifying predictors and comparison of models	149
6.8.2 Rainfall Anomaly teleconnected with ENSO Events	153
6.9 Conclusion	155
CHAPTER 7 SUMMARY AND CONCLUSIONS	157
7.1 Summary	157
7.2 Conclusions	158
7.3 Limitations of the study	161
7.4 Scope for future study	161
References	163
Appendix	177
Publications	199
Biodata	a

LIST OF FIGURES

Figure 1.1 Annual mean rainfall map of India	3
Figure 1.2 Schematic representation of the processes involved in increasing moisture content in the atmosphere and how they influence extreme precipitation	7
Figure 1.3 Pacific Ocean Areas with Sea-surface temperatures averaged for Niño Indices	11
Figure 3.1. Geographical Location of (a) Coastal region and Western Ghats of Karnataka and (b) regional distribution of grid point in the study area	36
Figure 3.2 Flowchart of the steps involved in research methodology	44
Fig. 4.1 Schematic flow chart for evaluating the trend of extreme precipitation indices of ETCCDI	50
Figure 4.2 Variation of precipitation with elevation at each grid points over (a) Low Land (Coastal region) and (b) High Land (Western Ghats)	51
Fig. 4.3 Annual Rainfall in the (a) Low Land (Coastal Region) and (b) High Land (Western Ghats) regions of the west coast of Karnataka	61
Fig. 4.4 Spatial distribution of annual rainfall indices (a) RR and (b) SDII (c) CWD and (d) CDD	66
Fig. 4.5 Spatial patterns of temporal trends of the rainfall indices (a) RR, (b) SDII, (c) CWD and (d) CDD	68
Fig. 4.6 Spatial distribution of annual rainfall indices (a) Rx1 and (b) Rx5	69
Fig. 4.7 Spatial patterns of temporal trends of the rainfall indices (a) Rx1, (b) Rx5	70
Fig. 4.8 Spatial distribution of precipitation indices over the study region - Monsoon (JJAS) average values (a) RRTOT, (b) CWD, (c) SDII and (d) R2.5_65	74
Fig. 4.9 Spatial patterns of trends for precipitation indices over the study region - Monsoon (JJAS) period (a) RRTOT, (b) CWD, (c) SDII and (d) R2.5_65	76
Fig. 4.10 (a-d) Spatial distribution of mean values of precipitation indices over the study region - Pre-Monsoon (March-May)	78
Fig. 4.11 (a-d) Spatial patterns of trends for precipitation indices period over the study region - Pre-Monsoon (March- May)	80
Fig. 4.12 (a-d) Spatial distribution of average values of precipitation indices over the study region - Post-Monsoon (October-November)	82

Fig. 4.13 (a-d) Spatial patterns of trends for precipitation indices over the study region - Post-Monsoon (October-November)	83
Fig. 4.14 (a-d) Spatial distribution of average values of the extreme precipitation event frequency indices during 1901-2013	85
Fig. 4.15 (a-d) Spatial patterns of trends for the frequency of extreme precipitation indices over the study region during 1901-2013	87
Fig. 4.16 (a-j) Correlation between total annual rainfall and annual precipitation indices	89
Figure 5.1 Schematic flow chart to identify the asymmetric relationship of ENSO indices with ETCCDI extreme rainfall Indices	97
Figure 5.2 Interannual variability of sea-surface temperature anomalies over Niño region during ONDJ (October-January) season	101
Figure 5.3 (a-f) Rainfall indices identified grid points influenced by the Niño Indices based on the stepwise regression method	103
Figure 5.4 (a-e) Absolute threshold intensity rainfall frequency indices identified grid points influenced by the Niño Indices based on the stepwise regression method	104
Figure 5.5 (a-f) Grid points with the precipitation extremes influenced by the Niño 1+2 with 1-year and 0-year ahead, respectively	109
Figure 5.6: The Pearson's correlation between Niño 1+2 and general extreme precipitation indices	110
Figure 5.7 (a-f) Absolute threshold intensity rainfall frequency indices influenced by the Niño-1+2 with 1-year and 0-year ahead, respectively.	111
Figure 5.8: The Pearson's correlation between Niño 1+2 and frequency of extreme precipitation indices	112
Figure 5.9 (a-f) Grid points with the precipitation extremes influenced by the Niño-3 with 1-year and 0-year ahead, respectively.	114
Figure 5.10: The Pearson's correlation between Niño 3 and general extreme precipitation indices	115
Figure 5.11 Absolute threshold intensity rainfall frequency indices influenced by the Niño-3 with 1-year and 0-year ahead, respectively	116
Figure 5.12: The Pearson's correlation between Niño 3 and frequency of extreme precipitation indices	117

Figure 5.13 (a-f) Grid points with the precipitation extremes influenced by the Niño-4 with 1-year and 0-year ahead, respectively.	119
Figure 5.14: The Pearson's correlation between Niño 4 and general extreme precipitation indices	120
Figure 5.15 (a-f) Absolute threshold intensity rainfall frequency indices influenced by the Niño-4 with 1-year and 0-year ahead, respectively	121
Figure 5.16: The Pearson's correlation between Niño 4 and intense rainfall frequency of extreme precipitation indices	122
Figure 5.17 (a-f) Grid points with the precipitation extremes influenced by the Niño-3.4 with 1-year and 0-year ahead, respectively	124
Figure 5.18: The Pearson's correlation between Niño 3.4 and general extreme precipitation indices	125
Figure 5.19 (a-e) Absolute threshold intensity rainfall frequency indices influenced by the Niño-3.4 with 1-year and 0-year ahead, respectively	126
Figure 5.20: The Pearson's correlation between Niño 3.4 and frequency of extreme precipitation indices	127
Figure: 6.1 Flow chart of the methodology adopted for estimation of SMP with Niño Indices over study region	134
Figure 6.2 Schematic representation of feed forward back propagation neural network	138
Figure 6.3 Schematic representation of generalized regression neural network	139
Figure 6.4 The time series for the period of 1951 -2013; (a) Monsoon season (JJAS) monthly precipitation, (b) Average monsoon season precipitation of study region and (c) the anomaly of the summer monsoon precipitation normalized by the standard deviation.	142
Figure 6.5 ENSO Oceanic Index (Sea surface temperature anomaly) of regions (a) Niño 1+2, (b) Niño 3 (c) Niño 3.4 and (d) Niño 4	143
Figure 6.6: Seasonal lead-lag correlation between summer monsoon precipitation index and Niño 1+2, Niño 3, Niño 3.4 index and Niño 4 indices lagging by 1-8 season	145
Figure 6.7: Scatter plot of correlation between summer monsoon precipitation index and predictors	146

Figure 6.8: The comparison of model output and observed data for multiple regression model, PC1 regression model, NN1 (FFNN) model and NN2 (GRNN) model	149
Figure 6.9: The difference of seasonal mean precipitation anomaly between model output and observed data for multiple regression model, PC1 regression model, NN1 (FFNN) model and NN2 (GRNN) model	150
Figure 6.10: Scatter plot of the model performance between training and test set of the models MR, PC1, NN1, and NN2	152
Figure 6.11: (a-d) Comparison of SMP anomaly with prediction models output during (a) El Niño and (b) La Nina period respectively	154

LIST OF TABLES

Table 1.1: Nino indices region with range of latitude and longitude (NOAA)	10
Table 2.1: Expert Team on climate change monitoring and detection indices of extreme precipitation events analysis	18
Table 2.2: Teleconnection of climate indices with rainfall extreme events	23
Table 2.3: Analysis of summer monsoon precipitation using predictors	27
Table 3.1: Tools used for the study	43
Table 4.1: Description of Annual and Seasonal Precipitation Indices	53
Table 4.2: Lag-1 significant serial correlations and MK/MMK Trend test results at the 5% level	63
Table 4.3: Correlation analysis of annual rainfall with extreme rainfall indices	88
Table 5.1 SWR analysis Coefficient of determination (%) for rainfall extreme indices	105
Table 6.1: Eigen values of principal component analysis	136
Table 6.2: Eigen vectors of the principal component analysis	136
Table 6.3: Seasonal lead-lag relationship between Niño indices and summer monsoon precipitation	146
Table 6.4: Performance of the models used in prediction of summer monsoon precipitation	151
APPENDIX 1: Annual Statistics of Individual Grid Points' Daily Gridded Precipitation over HL (the Western Ghat) and LL (coastal region)	177
Appendix 2: Cumulative probabilities for negative z-values are shown below table	178
Appendix 3: Cumulative probabilities for Positive z-values are shown below table	179
Appendix 4: Seasonal statistics of gridded points of precipitation data over the study region for the period of 1901-2013.	180
Appendix 5: The Pearson's correlation between Niño 1+2 and general extreme precipitation indices	181
Appendix 6: The Pearson's correlation between Niño 1+2 and frequency of extreme precipitation indices	183
Appendix 7: The Pearson's correlation between Niño 3 and general extreme precipitation indices	185

Appendix 8: The Pearson's correlation between Niño 3 and frequency of extreme precipitation indices	187
Appendix 9 : The Pearson's correlation between Niño 4 and general extreme precipitation indices	189
Appendix 10 : The Pearson's correlation between Niño 4 and intense rainfall frequency of extreme precipitation indices	191
Appendix 11 : The Pearson's correlation between Niño 3.4 and general extreme precipitation indices	193
Appendix 12: The Pearson's correlation between Niño 3.4 and frequency of extreme precipitation indices	195
Appendix 13: Correlation Analysis between ENSO Indices and summer monsoon precipitation index	197

NOMENCLATURE

Symbol	Description
CDO	Climate Data Operator
CLIVAR	Climate Variability and Predictability
ENSO	El Niño-Southern Oscillation
ETCCDI	Expert Team on Climate Change Detection and Indices
GrADS	Gridded data Analysis and Display System
RHtest	Relative Homogeneity Test
IMD	India Meteorological Department
IPCC	Intergovernmental Panel on Climate Change
MR	Multiple Linear Regression
PC	Principal Component
NN	Neural network
NN1	Feed forward back propagation neural network
NN1	Generalized regression neural network
NOAA	National Oceanic and Atmospheric Administration
PC	Principle Component
RClimDex	R based Climate data analysis tool
R	Coefficient of Determination
r	Co-efficient of Correlation
SMP	Summer monsoon rainfall/precipitation
SMPI	Summer monsoon rainfall/precipitation index
SSTA	Sea Surface Temperature Anomaly

CHAPTER 1

INTRODUCTION

1.1 INTRODUCTION

Rainfall is an essential element of the hydrologic cycle and displays temporal and spatial unpredictability across the globe. A reliable hydrologic cycle is critical for the maintenance of a normal existence of life. Varying quantities of rainfall are received by the earth at different regions. Several factors regulate the amount of rainfall received by a region. A significant aspect is the climate pattern across the globe that is influenced by differences in temperature between the poles and the equator.

1.2 RAINFALL DISTRIBUTION

Topography, nearness to large water bodies, and the general flow of air, affect rainfall distribution. The abundance of rainfall is greatest where moist air rises and lowest where it sinks.

- **Global distribution of rainfall**

Across the Earth, the annual average rainfall is about 1000 mm and the distribution is extremely uneven. The equator and monsoon areas of Southeast Asia are the regions which receive the highest rainfall. In contrast, moderate amounts of rainfall are received in the middle latitudes while the subtropical desert and Polar Regions receive the lowest amounts (Ekman, 1905; Hsu and Wallace, 1976).

- **Rainfall distribution over India**

The summer monsoon in India, typically manifests between June and September. During this time, greater than 80% of the total yearly rainfall is received by large portions of the central and western parts of the country, whereas the southern and north-western portions receive 50%-70% (Shukla et al., 1977; Nanjundiah et al., 2013). Figure 1.1 shows the mean annual rainfall pattern over India. The annual rainfall in the country averages to about 1120 mm. However, there are significant spatial variations. For example, heavy rainfall is received by areas in the Sub-Himalayan region in the North East, Meghalaya hills, and

Western Ghats. On the other hand, lower rainfall is received by Western Rajasthan and the Northern areas of Kashmir (Dhar et al., 1901; Rupa Kumar et al., 1992; Parthasarathy et al., 1995; Gadgil, 2003; Kothawale and Rajeevan, 2016). It can be seen that rainfall in India exhibits two significant features namely, rainfall increases eastwards in the north of India whereas it increases westwards in Peninsular India.

- **Rainfall Patterns over Karnataka**

Climatic variation in Karnataka can be attributed to its differing geographic and physiographic situations. For instance, in the plateau region, the climate varies from arid to semi-arid whereas in the Ghats, the variation is from humid to humid tropical. On the other hand, the climate in the plains of the west coast is the humid tropical monsoon type. Rainfall patterns in Karnataka were studied extensively by Krishnan (1984) who reported that, the south-west monsoon period is when the state receives 80% of its annual rainfall. This is followed by the post-monsoon period when it receives 12% and in summer it receives 7%. Only 1% of the rainfall is received in winter. Karnataka receives roughly 500 mm to 3500 mm of rainfall annually, with an annual average of 1248 mm. In south interior Karnataka, the eastern part is affected by the north-eastern monsoon between October and December accounting for 30% of the annual rainfall in the region. During this time, the rainfall over and near the Ghats increases while the region towards the West Coast sees a decrease in rainfall (Gadgil and Gowri 1988; Francis and Gadgil 2006).

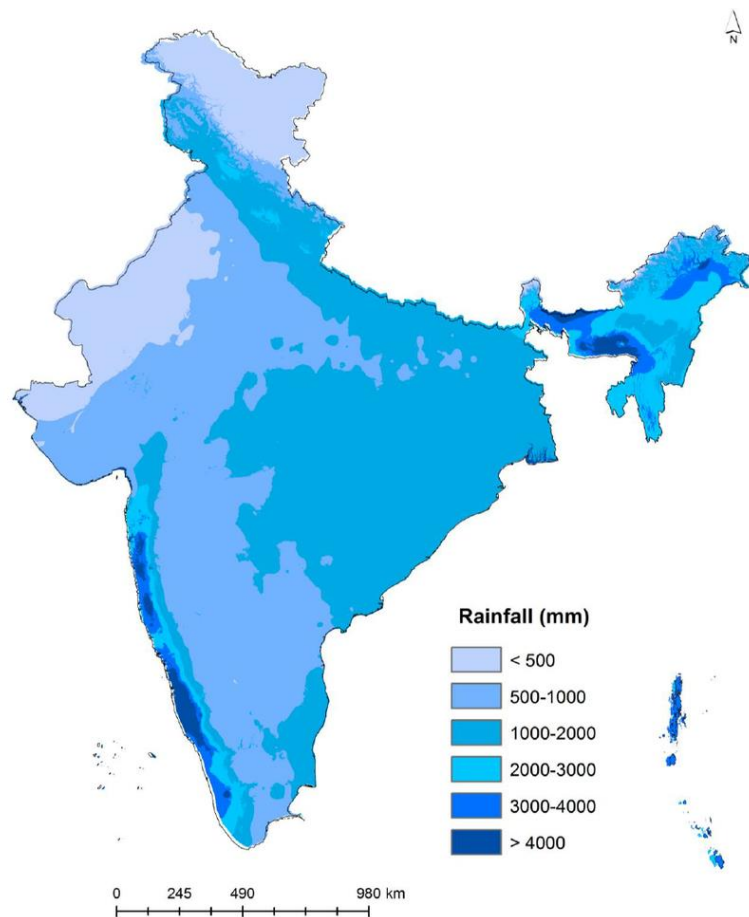


Figure 1.1 Annual mean rainfall map of India (Reddy et al. 2015).

1.2.1 Causes of Spatial Variability of Rainfall

Over time, there are variations in global and regional rainfall rates. Distinct causes lead to differing patterns of rainfall. High rainfall is received by areas near the equator since large-scale evaporation is produced by constant solar heating. Thus, convective rainfall is formed by moist air that cools with altitude. In addition, there is convergence of air masses, resulting in heavy rainfall. Convective rainfall may be experienced by mid-latitudes whereas frontal (depression) rainfall may be caused by air masses in the poles and in the sub-tropics. High levels of rainfall are received in mountain ranges because of moist air caused by relief or the orographic effect. However, this can cause a severe decrease in rainfall in the leeward region of mountains. In contrast, the Polar regions are dry as cold air holds less moisture than warm air. Moreover, the interior regions of continents are inclined to be dry due to their

lack of proximity to moisture sources. Also, clouds may lose moisture before they arrive at the middle of large continents.

1.3 FACTORS INFLUENCING RAINFALL

Several factors affect rainfall around the world. The varying effect of these factors is the reason why different parts of the Earth experience contrasting climates. The factors affecting hydrological cycle and influencing rainfall are broadly classified as;

- (a) Geography,
- (b) Climate and
- (c) Anthropogenic activity.

A brief discussion on each of the factors is given in the sections as follows:

- (a) Geography. Some important factors which affect rainfall based on the geography of the land mass are listed below.
 - Altitude or Elevation: Typically, as altitude increases, climatic conditions become colder.
 - Topography: Air movement is naturally impeded by mountain ranges.
 - Impacts of Geography: A region's location (country, state, or position) and its remoteness from mountains and significant water bodies (river/sea).
 - Earth's Surface: The amount of atmospheric heating is determined by the quantity of sunlight reflected or absorbed by the surface. In general, darker areas, such as regions with dense vegetation, are inclined to be good absorbers, whereas lighter areas, such as regions covered with snow and ice, are likely to be good reflectors.
- (b) Climate. These factors are based on the patterns of meteorological variables in a given region over a long period of time. A few important factors are discussed below:
 - Sea surface temperature: The Earth's surface contains 70% of water (sea/ocean). The spatial variations of sea surface temperature influences rainfall patterns. If sea surface temperatures vary, rainfall patterns tend to vary as well.

- Humidity: Humidity is the general term which describes the moisture content in the air. The quantity of moisture content decides the latent energy stored up in the atmosphere and indicates the potential capacity for rainfall.
 - Prevailing global wind patterns: The amount of rainfall at different regions is determined by the prevailing winds. In Southeastern Asia, for instance, monsoons are formed as a result of these winds. On the other hand, these winds cause abundant rain to be received during the winter in the West coast of South and North America.
 - Earth's rotation: The uneven heating of Earth's surface by the sun is a driving force behind the rainfall patterns.
- (c) Anthropogenic activity. These factors act as direct/indirect influences due to the interference of human activity:
- Increase in greenhouse gases due to burning of fossil fuels
 - Deforestation and land cover change.

1.4 INFLUENCE OF CLIMATIC FACTORS ON EXTREME RAINFALL

Extreme rainfall can have devastating effects on human society and the environment. There is mounting concern and emphasis on the spatio-temporal pattern of extremes of rainfall and the subsequent impact on the space-time variations of flood and droughts, taking the global warming and the subsequent modification of the hydrological cycle into consideration (Ashrit et al. 2001; IPCC 2012). With indications of global warming, there is an increased likelihood of dynamic climate systems due to the strengthening of the hydrological cycle (Fowler and Hennessy, 1995; Trenberth, 1998, 1999). In agreement with the Clausius-Clapeyron relationship, air's water-holding capacity doubles approximately with every 10°C increase in temperature (Fowler and Hennessy, 1995). Fig. 1.2 indicates a global intensification in atmospheric moisture content due to anticipated greater evaporation rates caused by warmer lower-atmosphere and oceans (Fowler and Hennessy, 1995; Trenberth 1998, 1999).

It is expected that the amount of global rainfall will increase to balance the increased evaporation. Nevertheless, the increased moisture content in the atmosphere indicates that, expected increase in total rainfall will occur predominantly as an increase in intensity of

rainfall events, rather than in frequency (Trenberth, 1999). Additionally, latent heat release in precipitating systems further enhances their intensity and the convergence of moisture into the system, causing a favorable outcome (Trenberth, 1999). This anticipated increase in total rainfall and intensity of rainfall is projected to lead to global changes. However, this global trend may not be reflected by the effects experienced at regional and at local levels. Whilst rainfall globally is anticipated to be affected by the thermo-dynamic effects on rainfall described above, the probable changes in atmospheric movement, as a secondary influence on the amount of rainfall and intensity of a warmer climate, increases the probability of localized modifications to rainfall systems (Emori and Brown, 2005). The occurrence of significant modifications to both the spatial and temporal inconsistency under a temperate climate is suggested by these alterations in rainfall characteristics. A vast body of research in recent years has scrutinized the probable alterations in temporal inconsistency of rainfall caused by these dissimilar increase in the heaviest rainfall events. In contrast, considerably less attention has been paid to modifications in the extent of local spatial consistency, which might be anticipated to be associated with a move towards greater local convective rainfall.

The Expert Team for Climate Change Detection Monitoring and Indices (ETCCDMI) specifies information concerning extreme rainfall indices (e.g., type of rainfall, intensity and extremes, frequency, etc.) (Alexander et al., 2006). Indices related to extreme rainfall can be grouped into two categories: one computes the frequency (number of instances) of the index beyond or within its specified limit (CDD, CWD, R2.5-65, R40, R65, R100, and R20), while the second assesses the depth (mm) or intensity (mm per day) of rainfall (RR, SDII, RX1day, and RX5day). The separation of frequency and magnitude is anticipated to offer additional insights into the frequently slight variances in the climatic condition across the study area. Moreover, it is evident that these indices are also significant for the evaluation of the possible effect of climate changes on sub-humid to humid tropical environments associated with agriculture, forests, sustainable development, water resources, etc.

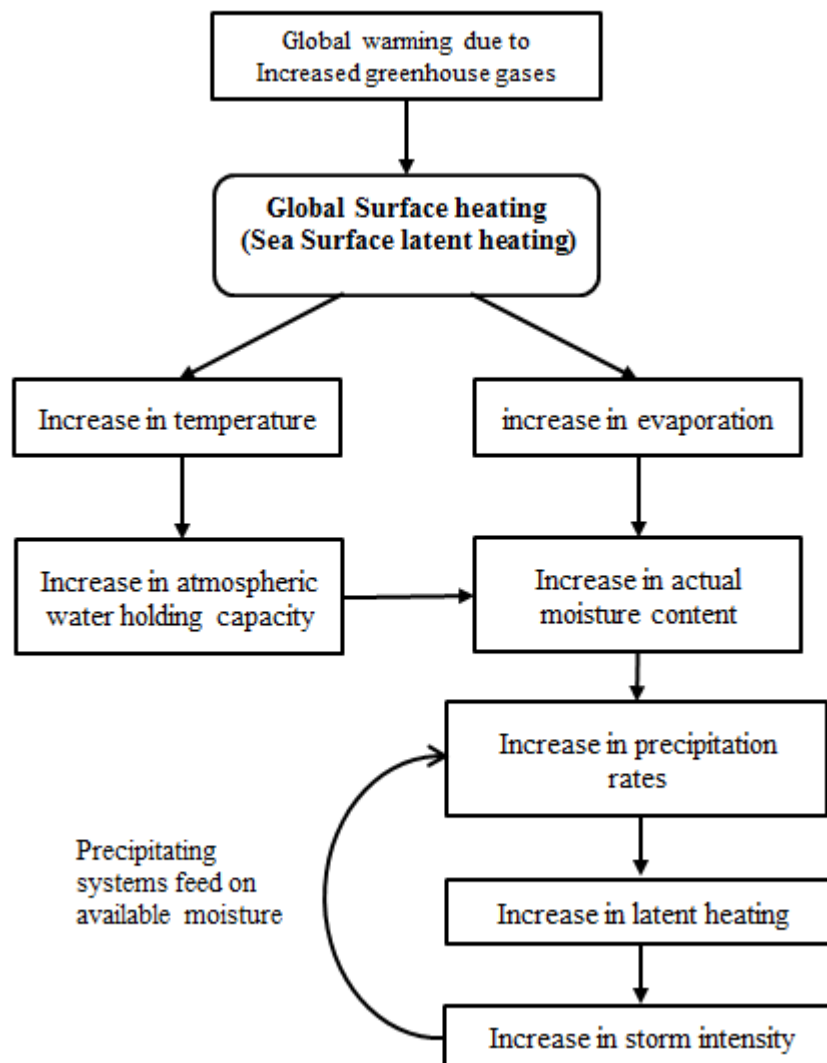


Figure 1.2 Schematic representation of the processes involved in increasing moisture content in the atmosphere and how they influence extreme rainfall (Trenberth, 1999).

1.5 ASSESMENT OF EXTREME RAINFALL VARIABILITY

The Intergovernmental Panel on Climate Change (IPCC) reported that, considerable increase in the anthropogenic emission of various GHGs (greenhouse gases) since industrialization has caused global warming (IPCC, 2007). IPCC estimates that the global mean surface temperature has increased by $0.6\text{ }^{\circ}\text{C} \pm 0.2\text{ }^{\circ}\text{C}$ since 1861 and envisages a further increase of $2\text{ }^{\circ}\text{C}$ to $4\text{ }^{\circ}\text{C}$ over the next century. Many facets of the Earth's climate system have been greatly affected by greenhouse gases, which have been at their peak for

the past few decades (Pachauri et al., 2014). Globally, changes in yearly rainfall quantity, extreme storms, and increase in total extreme rainfall events are being experienced by regions. As regions experience changes in rainfall, decisions regarding the preservation of fundamental societal standards such as, sustainable water supply, continued provision of food, and basic human comforts, need to be provided. Presently, there is limited clarity regarding the manner and extent of climate change in different regions. Policy decisions rely on different probable scenarios making it imperative that they are well understood and encompass the prospective spectrum of changes in rainfall (Jones & Patwardhan, 2014).

The analysis of annual rainfall has been the emphasis of much climate change research. Often, the impact of these changes on society are best recognized, most evident, and most visible. In contrast, there is underreporting and limited analysis about extreme rainfall events and patterns which often have significant effects on a regional scale. Numerous groups have sought to study extreme weather patterns and have used climate indices to develop frameworks. The Expert Team on Climate Change Detection and Indices (ETCCDI) is one such group which created a group of rainfall indices that could be utilized to study the extreme rainfall pattern over time. These indices aid in the specific understanding of the local climate systems which affect society.

This study attempts to analyze rainfall pattern using ETCCDI rainfall indices over the Western Ghats and Coastal regions of Karnataka. This will permit a close examination of spatial and temporal trends of extreme rainfall over the study region.

1.6 RAINFALL VARIABILITY OVER WEST COAST OF INDIA

Across India, rainfall on the spatial domain is unevenly distributed. The Western Ghats is among the areas with the maximum recorded monsoon rainfall. Due to its high elevated hilly regions, the Western Ghats obstructs the moisture-laden south-west monsoon winds crossing over the Arabian Sea. Moist air collected from the sea and oceans cools adiabatically and condenses due to dense water vapor collected from sea and oceans. Therefore, in the west coast rainfall increases along the Western side (wind ward) of Western Ghats and gradually reduces on the eastern leeward side because of the drop in moisture content. This longitudinal stretch from the Coastline to the Western Ghats could

aid in observing significant spatial and temporal variations in rainfall. As seen before, rainfall patterns depend on various factors such as, moisture availability, velocity and direction of wind, region's orography and teleconnections (Francis and Gadgil, 2006; Tawde and Singh, 2015; Revadekar et al., 2018). High altitudinal zones appear to be associated with the maximum rainfall and intense rainfall events (Patwardhan and Asnani, 2000; Tawde and Singh, 2015). Researchers also (e.g., Grossman and Durran, 1984; Ogura and Yoshizaki, 1988) have indicated that the orographic effect may extend horizontally up to 200 km in the windward direction. Therefore, the Western Ghats elevation is capable of deep convection though it is well offshore from the Arabian Sea and west coast (Vishnu et al., 2013). Among the three subdivisions of Western Ghats, the highest rainfall is received by coastal Karnataka. Moreover, the Karnataka section of the Western Ghats of Karnataka has an extensive mountain barrier (Tawde, 2013) signifying the orographic dependence.

In atmospheric science the word Teleconnection states that climate anomalies being connected to each other at large distances between land mass and oceans. Large spatio-temporal variability is displayed by the summer monsoon rainfall over Indian sub-regions. This is always regarded with the greatest concern, due to teleconnection with various phenomena pertaining to oceanic and land surfaces. The El Niño Southern Oscillation (ENSO) and monsoon teleconnections exhibit significant relationship between monsoon rainfall and different ENSO indices (Krishna Kumar et al., 1995). In recent decades, the relationship of ENSO with monsoon rainfall has been observed to be declining (Kinter et al., 2002; Revadekar et al., 2018). Considering the inconsistent outcomes reported by global warming, such a decline is possibly a short-lived feature (Ashrit et al., 2001).

1.7 TELECONNECTION OF EL NINO SOUTHERN OSCILLATION WITH RAINFALL

After the seasonal cycle, ENSO is the second most significant source of weather change which generates a substantial portion of short-term climate variation across the globe (Glantz, 2001; Rosenzweig et al., 2001; Goddard and Dilley, 2005). ENSO accounts for roughly half of the total discrepancy in local weather in some regions. ENSO, among all climate events, is unique for its strength, certainty, and widespread impact (McPhaden et al. 2006). ENSO's most direct impact on regional climate patterns are detected in the area nearest to the tropical Pacific. Nevertheless, rainfall and seasonal temperature can be transformed globally by signals of its effect (Kiladis and Diaz, 1989; Vedwan and Broad, 2003). Also known as teleconnections (Trenberth et al., 1998), these shifts originate from tropical sea surface temperatures (Fedorov and Philander, 2000).

1.7.1 Assessment of Oceanic index

The average sea surface temperature anomaly (SSTA) over various parts of the Pacific Ocean is measured by the temperature-based index (Table 1.1 and Fig. 1.3). SSTA is the variance between the real and climatological sea surface temperatures. The Tropical Atmosphere Ocean (TAO) array data provides the observed sea surface temperature (SST) and is collected in the equatorial Pacific Ocean from a network of roughly 70 deep-ocean buoys (Coles, 1999). These buoys, in different regions, record and transmit sea surface (and sub-surface) temperatures, water currents, atmospheric status, and wind data. A real average standardized anomaly of sea surface temperature from a specified climatological phase is used to derive values.

Table 1.1 Niño indices region with range of latitude and longitude (NOAA)

Index	Latitude	Longitude
Niño1+2	0° - 10° S	90° W - 80° W
Niño3	5° N - 5° S	150° W - 90° W
Niño3.4	5° N - 5° S	170° W - 120° W
Niño4	5° N - 5° S	160° E - 150° W

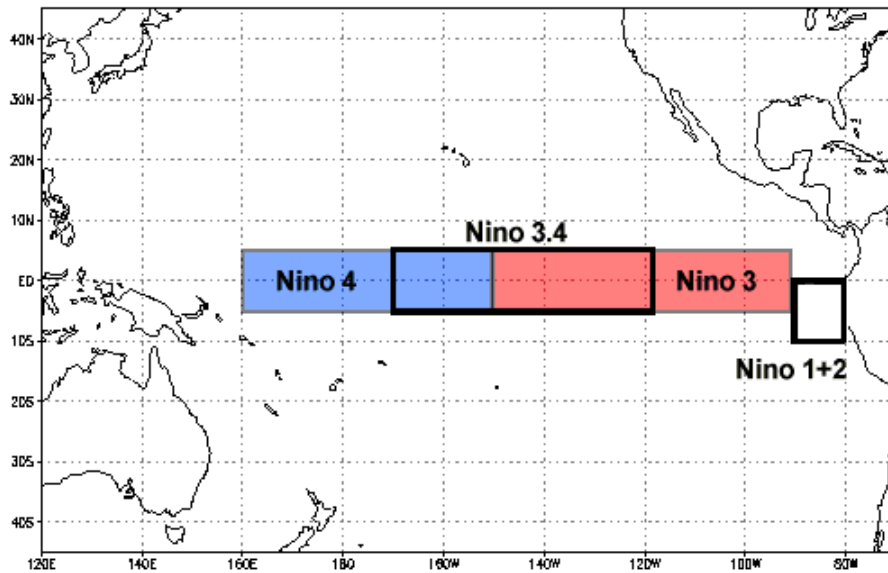


Figure 1.3 Pacific Ocean Areas with Sea-surface temperatures averaged for Niño Indices. Source (NOAA)

From Figure 1.3, it can be seen that the first region to get warm is the Niño1+2 region (near South America’s west coast) due to its quick reactions to variations, both seasonal and El Niño-related (Glantz, 2001). In contrast, the variation in temperature in the Niño3 region (cold tongue of east Pacific) is greater than others, although it has a much lower response to continental influences (Hanley et al., 2003). The shift of SSTs in the Niño4 region (warm pool of West Pacific) is linked to modifications, along the longitudinal equator, of powerful east-west temperature gradients (Glantz, 2001). Niño4 explains the extent of rainfall in regions in Southeast Asia. The most commonly used SST index is the Niño3.4 (between Niño3 and Niño4) due to its effectiveness in capturing SST inconsistency and rainfall change (NOAA). Niño3.4 defined (Bamston et al., 1997) as a more robust representative for ENSO event than Niño3, due to its greater association with the Southern Oscillation Index (SOI). Moreover, the Niño3.4 index has greater explanatory power in describing the evolution of ENSO (Trenberth and Stepaniak, 2001) and displays the highest intersection with previous occurrences (Trenberth, 1997).

1.8 IMPORTANCE OF THE STUDY

The Western Ghats and Coastal region of Karnataka are anticipated to have variation in rainfall and extreme events (Francis and Gadgil, 2006; Goswami et al., 2006; Kumar et al., 2010; Guhathakurta et al., 2011). More water vapor can be held by warmer air. In fact, the capacity of air for moisture content increases by about 7% for each degree increase in temperature. Intense rainfall events can be produced by an atmosphere with greater moisture and vice versa, which is precisely what has been detected in the Western Ghats (Kumar et al., 2014). An increased risk of drought can result from a decrease in average rainfall. On the other hand, an increased risk of flooding could be caused by an increase in average rainfall. Storm water runoff due to extreme rainfall, which often contains toxins such as, phosphorus, nitrogen, pesticides, and heavy metals, can end up in streams, lakes, and bays, harming aquatic ecosystems and reducing quality of water for human usage. The prospect of flooding is the most immediate impact of heavy rainfall. Additionally, the risk of landslides is also increased by heavy rainfall. When the groundwater table levels and saturation is raised by above-normal rainfall, slopes can become less stable, resulting in landslides. More frequent landslides are anticipated in the Western Ghats, which have an exceptionally high probability of landslides owing to their topography, due to climate change-induced increase in heavy downpours.

Increase in heavy rainfall does not necessarily result in an upsurge in seasonal or annual total rainfall. Moreover, considering climate change, calamities, such as, reduced moisture content in the ecosystem and increased incidences of fire, might be witnessed in the Western Ghats. Gopala Krishnan et al. (2011) submitted that high vulnerability to climate change was evident in the forests of the Western Ghats. Moreover, temperatures are anticipated to disproportionately increase in contrast to rainfall. The present study is motivated by such observations submitted by the scientific community to evaluate regional scale extreme rainfall events and the effect of El Niño Southern Oscillation (ENSO) over the study region.

According to IPCC-AR5 (2019), human interaction is directly affecting about 70 per cent ice-free land surface on the planet. But in India irrigation occurs prior to the start of the monsoon season and the resulting land cooling decreases the land-sea temperature contrast. This can delay the onset of the monsoon and decrease its intensity. The IPCC AR5 report

dealing with interactions between land and climate interprets that effects of irrigation on local regional and global climate very well studied. It is well established that irrigation increases total evapo-transpiration, increases the total amount of water vapour in the atmosphere, and decreases mean surface daytime temperature within the irrigated area and during the time of irrigation. Increase in vegetation, primarily due to agriculture, is weakening rainfall in early monsoon months, particularly in South and North Indian regions. At the onset of boreal spring (February to March) evapo-transpiration is already large over irrigated crops (in India) and the resulting excess moisture in the atmosphere is transported south-westward by the low-level winds. The IPCC report also said that human-induced climate change is leading to unpredictable changes, particularly in precipitation. It said that the heavy rainfall events have increased in frequency and intensity since 1950.

Climate variability have a strong effect on rainfall characteristics and extremes, but the relationship between the El Niño Southern oscillations and rainfall patterns are not well defined at regional scale. Therefore, a regional analysis considering extreme rainfall and the impact of Niño indices on variations of rainfall events would be significant. Bearing this in mind, the present research proposes to investigate the association between Niño indices and extreme rainfall events at a regional scale specifically over the coastal regions and Western Ghats of Karnataka.

1.9 STATEMENT OF PROBLEM

Better hazard management in future requires detailed analysis on the impact of changing climate on extreme precipitation. Many studies analyzed the influence of changing climate on trend of rainfall, extreme rainfall events and frequency of irregular seasons, also tried to identify the association of rainfall with topographical and Meteorological parameters. Among the subdivisions of Western Ghats, the highest rainfall is received by coastal Karnataka. This is always regarded with the greatest concern, due to teleconnection with various phenomena pertaining to oceanic and land surfaces. It is necessary to understand the teleconnections exhibit significant relationship between extreme rainfall and different ENSO indices.

1.10 OBJECTIVES OF THE STUDY

The aim of the research is to identify the variation in rainfall extreme events and their teleconnection of ENSO indices due to climate variability and change over the Western Ghats and coastal region of Karnataka.

The specific objectives of the present study are:

- 1 To investigate the variability and long term trends in synoptic extreme rainfall events using ETCCDI rainfall indices.
2. To explore the affect of Oceanic Nino indices on ETCCDI extreme rainfall indices.
3. To estimate the summer monsoon rainfall by identifying optimal Niño predictors.
4. To identify the asymmetric relationship of ENSO indices with rainfall over study region.

1.11 ORGANIZATION OF THE REPORT

The complete report comprises of seven chapters. Chapter 1 provides the overview of spatio-temporal variability of rainfall and extreme rainfall due to climate change and the basis for the research. The rest of this report is organized as follows:

Chapter 2: Offers a critical review of work associated with climate change and its effects on extreme rainfall.

Chapter 3: Describes the study region and the complete methodology adopted for the research work.

Chapter 4: Deals with seasonal rainfall variability of extreme rainfall indices with its trend and contribution of annual extreme rainfall indices to the total annual rainfall across the Coastal region and Western Ghats of Karnataka, India.

Chapter 5: Deals with understanding the role of Niño indices influence on Rainfall extreme indices considered for the study.

Chapter 6: Describes the identification of relationship with predictors and summer monsoon rainfall anomaly to estimate the seasonal rainfall using multiple regression and neural network models.

Chapter 7: Provides the summary and conclusions of the present work.

In order to attain the objective of research, existing literature pertaining to the study was scrutinized. The review of the same is presented in the following chapter.

CHAPTER 2

LITERATURE REVIEW

2.1 Background

This section deals with review of relevant literature to bring out the background of the study undertaken to accomplish the objectives of the research. The three major themes organized are namely;

- ❖ Exploratory analysis on trend analysis of rainfall and extreme rainfall indices
- ❖ Teleconnection of rainfall events association with sea surface temperature
- ❖ Analysis of monsoon rainfall with sea surface temperature as predictor variable

The survey of literature carried out under these themes is presented in the sections to follow.

2.2 Exploratory Analysis of Rainfall

The spatial and temporal distribution of rainfall is very complex and uneven (ward and Robinson, 1990). There is no established standard definition of an extreme rainfall event, hence many researchers in the past came up with objective definitions based on the statistical distributions of rainfall at a particular place. The extreme rainfall event recognized from a Intergovernmental Panel on Climate Change (IPCC) as an event that is rare within its statistical reference distribution at a particular place, usually as rare as or rarer than the 95th percentile. A broad definition identifies extreme rainfall events as a transitory localized phenomenon featuring very high intensity rainfall over a restricted region. Nevertheless, researchers have used different thresholds for the identification of extreme rainfall events. This issue brought the hydrologist and others to recognize the underlying pattern of rainfall from historical records for better prediction of rainfall. There have been many past studies, which concentrated on trend of rainfall, frequency of extreme rainfall events and its trend at regional and spatial scales. Exploratory analysis of rainfall is grouped under the following heading.

- Spatial pattern and rainfall trend in India
- Variation in frequency of extreme rainfall events and its trend

2.2.1 Trend analysis of rainfall in India

Intensification in monsoon rainfall is predicted over South Asia due to global warming as evident in climate model simulations studies (Lal et al., 2000; May, 2002; Meehl and Arblaster, 2003, May, 2004; Kumar et al., 2006; May, 2011). However, accurate assessments of future changes in the regional monsoon rainfall have remained unclear due to extensive deviations among the model projections, e.g., (Annamalai et al., 2007; Kripalani et al., 2007; Kumar et al., 2011). The simulated rainfall response to global warming by climate models is actually accompanied by a weakening of the large-scale southwest monsoon flow, e.g., among others (Kripalani et al., 2003; Krishnan et al., 2013). Several studies have tried to address the important problem of trends in rainfall in India since the last century. Several previous studies have found that there is no clear trend of either increase or decline in average annual rainfall over India (Mooley and Parthasarathy, 1984; Thapliyal and Kulshrestha, 1991; Lal et al., 2001; Kumar et al., 2010). Although no study has found long term trend in the monsoon rainfall over whole of India, but significant long term changes have been recognized (Koteswaram and Alvi, 1969; Jagannathan and Parthasarathy, 1973; Raghavendra, 1974; Dash et al., 2007; Kumar and Jain, 2010; Joshi and Pandey, 2011). Rupa Kumar et al. (1992) reports that monsoon rainfall over the west coast, central peninsular and northwest India has increased by 10% –12% of the normal rainfall during a span of 100 years.

Meteorological subdivisions over the west coast, western arid region and northeastern humid region showed significantly decreasing trends in both rainfall and rainy days. The northern hilly parts of the Himalaya were found to have a significantly increasing trend of rainfall but decreasing trend of rainy days. The north and central plains of India showed a decreasing trend of rainy days and the eastern plain was found to have a decreasing trend of rainfall during the summer monsoon period.

2.2.2 Variation in frequency of extreme rainfall events and its trend

As a consequence of the atmospheric warming, the water holding capacity of the atmosphere is also rising, which ought to result in more intense short term storms (Trenberth, 2011). Higher humidity in the atmosphere may create shift in the large rains by convective mechanisms. In many studies analyses of changes in climate extremes with coupled

atmosphere–ocean general circulation models have been performed. Rajeevan et al. (2008a) examined the variability and long term trends of extreme rainfall events over the Central India for 104 years and found 6% increase per decade is associated with the increasing trend of sea surface temperature and surface latent heat flux over the tropical Indian Ocean. Roy and Jr (2004) identified increase in the frequency of extreme rainfall events over last 10 decades in India. The increase in extreme events is strongest in regions extending from the north western Himalayas through most of the Deccan Plateau in the southern peninsular region of India and decrease in eastern part of the Gangetic Plain and parts of Uttaranchal. Guhathakurta et al. (2011) also found increase in frequency of heavy rainfall events in peninsular, east and north east India and decreasing in parts of central and north India. The extreme high and extreme low rainfall increased from the year 1930 to 2013 by 2-fold and 4-fold with high variation particularly in early 2000s in India (Jun et al. 2015).

The trend using parametric test and non-parametric test varies, as parametric t-test showed significant trend and non-parametric Mann-Kendall test resulted no significant trend of extreme rainfall events in North East Himalayan region with negative correlation between elevation and frequency of extremes exceeding percentiles (Bharti et al. 2016). Dash et al. (2009) reported a significant decline in the frequency of moderate-to-heavy rainfall events over most parts of India in the last 50 years. This was also supported by a significant rise in the frequency and duration of monsoon breaks over India during recent decades (Ramesh Kumar et al., 2009; Turner and Hannachi, 2010). The frequency of extreme rainfall events (100 mm/day) have increased in certain parts of the country (Goswami et al., 2006). Rupakumar et al. (2006) studied the effect of climate change in India by evaluating the present day simulation (1961-1990) of PRECIS climate model and reported an increase in extreme rainfall along west coast and west central India. In order to summarize the understanding of the literature on rainfall extreme events, a brief description of the most commonly used methods and the findings of extreme rainfall events for different region is summarized in Table 2.1.

Table 2.1: Expert Team on Climate Change Monitoring and Detection Indices of extreme rainfall events analysis

Sl. No	Author and Year	Region	Analyzing Method	Major Results
1	Rajeevan et al. (2008)	Central India	Absolute threshold approach (a) Heavy rainfall (≥ 100 mm/day) (b) Moderate rainfall (≥ 5 and < 100 mm/day) and (c) Very heavy rainfall (≥ 150 mm/day) events.	Positive trend in extreme active events and negative trend in moderate active events
2	Dash et al. (2009)	Six homogeneous monsoon regions in India	Low, moderate, and heavy rainy days and short, long, dry, and prolonged dry spells are analyzed	Positive trend of dry spells observed in each region Positive trend of heavy rainy days observed in North West, Central North East and North East, while negative trend is observed in other regions
3	Singh and Ranade (2010)	19 sub-regions of India	Onset, critical length, and number of wet and dry events	Reduction in longest wet spell with high intensity rainfall and enhancement in longest dry spell, which further indicates a drift toward extreme of extremes
4	Ghosh et al. (2011)	India (grid wise analysis)	Annual Maximum Series has been extracted to compute 30 year and 100 year return level using Generalized Extreme Value distribution.	Spatially non uniform trend and also increase in spatial heterogeneity is observed.

Table 2.1 Continued.....

Sl. No	Author and Year	Region	Analyzing Method	Major Results
5	Rajendran et al. (2012)	Western Ghats of India	Future climate change in mean rainfall, rainfall regimes and monsoon circulation	Analysis of observed APHRODITE rainfall shows that there is a significant decreasing trend in the monsoon rainfall over the Western Ghats mountains during the recent past. Significant reduction in orographic rainfall over the west coasts of Kerala and Karnataka along the narrow western Ghats mountains by the end of the twenty-first century.
5	Singh (2013)	India (grid wise analysis)	Standardized rainfall anomaly of +1 is active event and -1 is break event. Analysis carried out for pre-1975 and post-1977 separately	Positive trend of short break spells and moderate active spells in post-1977 is observed
6	Vittal et al. (2013)	India (grid wise analysis)	Intensity, duration, and frequency is analyzed for the Peak Over Threshold (rainfall >95th percentile) series.	Significant differences in the pattern of active rainfall extremes in India during pre-1950 and post-1950. Abrupt variations in the rainfall extreme events occurred after 1975 in most of the grids. Indication advise that this period coincides with the commencement of urbanization in India (Kishtawal et al., 2010).
7	Singh et al. (2014)	Central India	Standardized rainfall anomaly of +1 is active event and -1 is break event.	Significant increase in the frequency of dry spell and intensity of wet spell.

Table 2.1 Continued...				
Sl. No	Author and Year	Region	Analyzing Method	Major Results
8	Pai et al. (2015)	south central, north central, northeast and west coast regions of India	Variability and trends in the daily rainfall events of monsoon season over four regions.	Increased disaster potential for instant flooding over SCI and NCI due to significant increasing trends in the frequency and intensity of the HR and VHR events.
9	Varikoden et al. (2018)	Western Ghats of India	to identify changes in regional climate	the extreme events of rainfall are observed in low elevated areas with high inter-annual variability and an increase (decrease) southwest monsoon rainfall of about 1.6 mm day ⁻¹ decade ⁻¹ in certain regions of the northern (southern) Western Ghats
10	Nageswara Rao et al. (2019)	South peninsula region of India	Unveil the behavior of north east monsoon rainfall over south peninsula.	The variability of north east monsoon rainfall has increased during the period 1959–2016. The seasonal rainfall has increased over Tamil Nadu, Rayalaseema, as well as an increase in the number of high-intensity rainfall events in the recent period with respect to the earlier period (1901–1958).

2.3 Association of Rainfall with Sea Surface Temperature

Izumo et al. (2008) have stated that it is essential to understand the fundamental mechanism of sea surface temperature oscillations that control variability of rainfall intensity. The teleconnection between the tropical central eastern Pacific SST and Asian south west monsoon has been studied by researchers since Walker (1923, 1924) defined the ENSO which is very closely linked to the zonal circulation over the equator. It was further witnessed that, the Walker circulation is strongly coupled with underlying oceans, especially the sea surface temperature in the tropical central eastern Pacific (Bjerknes, 1969). Studies have been carried out to investigate the physical mechanisms responsible for the ENSO–monsoon association (Rasmusson and Carpenter, 1983; Webster and Yang, 1992; Ju and Slingo, 1995; Kirtman and Shukla, 1997). The association between ENSO events and Indian monsoon has been studied by many researchers (Krishna Kumar et al., 1999; Krishnamurthy and Goswami, 2000; Singh et al., 2011). Indian summer monsoon is weaker (stronger) than normal before (after) the peak of an El Niño in winter, and that the relationship is opposite for the monsoon and La Niña (Wu et al. 2012; Chakraborty 2018). It is also observed that, the monsoon circulation over southern Asia is generally weaker (stronger) than normal during El Niño (La Niña) summers (Webster and Yang, 1992; Lau and Yang, 1997).

Shukla (1975) evaluated physical mechanism between Arabian Sea oceanic parameters and Indian monsoon rainfall. Aforementioned research explained that, the reduction in monsoon rainfall amount is related to the weak wind speed over Western Arabian Sea and cold SST, which is attributed to reduced sea level pressure and therefore less evaporation over Arabian Sea. Shukla & Mishra (1977) studied the lead-lag relationship between Arabian Sea surface temperature affecting monsoon rainfall over central and western India. Their study found out significant positive correlation between sea surface temperature of July with August rainfall over central and western India. The study of Izumo et al. (2008) has provided the new methods for better estimate of Indian summer monsoon considering regional scale as well as ENSO cycles. Their study concludes that upwelling at Somalia coast maximizes during summer monsoon season because of south west winds. Further Izumo et al. (2008) observed that increased upwelling at Somalis coast limits the westward extent of warm pool ($SST > 28^{\circ}C$) hence decreasing rainfall at west coast of India. This is due to less evaporation and insufficient

moisture transport towards Western Ghats. The alongshore variability in wind velocities over western Arabian sea affects the upwelling at Somalia coast hence the intensity of rainfall over west coast of India. Nino 3.4 SST of previous year affects the Indian monsoon rainfall in the next season summer monsoon at west coast of India. A positive lag-correlation is observed between previous winter ENSO conditions and the subsequent Indian summer monsoon. In order to summarize the understanding of the literature on various SST indices and rainfall relationship is summarized in Table 2.2.

2.3.1 Impacts of climate change on water resources

The hydrologic system is an integral part of the global climate system and circulates water between oceans, air, and land. Climate change could lead to the disruption of the hydrological cycle leading to either intense rainfall events (causing floods and landslides) or intensified droughts leading to reduction in agricultural productivity. The increase in temperature increases the potential evapotranspiration and leads to decrease in the soil moisture and groundwater which ultimately impacts the availability of water in the form of river flow.

2.3.2 Local impacts of Climate change in India and the Western Ghats

The climate change impacts on surface water resources are expected to be severe in India. The increasing population along with the associated developmental activity has a threatening role on freshwater sources. The National Commission for Integrated Water Resources Development (NCIWRD) has made an assessment of the total freshwater resources of the country (GoI 2007). The water resources in the Indian subcontinent are expected to be stressed in the light of climate change and as much as 45% of annual runoff drains into the sea. Several schemes are proposed and under construction to minimize the loss of available runoff. But, the accomplishment of these water resource development plans in the rivers and agro-climatic zones is only possible with knowledge of spatio-temporal variation of rainfall in light of climate change.

The irrigation requirements in the non-irrigated areas are solely met by rainfall. The variation in rainfall due to climate change could strain the cultivation in these areas. Additionally, the irrigated areas may face water shortage during summer leading to scarcity of food and risk to the agricultural sector. It may be interesting to note that, the Central Statistics Office, Govt. of India (GoI 2017) reported a 4.1% growth rate of Gross Value Addition (GVA) of agricultural and allied sector in 2016-17 as first advance estimate.

Table 2.2: Teleconnection of climate indices with rainfall extreme events

Sl. No.	Author and Year	Region	Climate Indices	Major Results
1	Brown et al. (2011)	North Eastern United states	AO, ENSO (Nino 3.4), NAO, PDO, PNA (pacific north American pattern), NP (North Pacific pattern)	Rainfall indices did not display coherent associations with large-scale forcing.
2	Revadekar et al. (2011)	Individual states in India to detection of possible changes in extreme climate events on the local, regional, and national scales	scenarios under increasing greenhouse gas concentration and sulphate aerosols	Rainfall is expected to increase in calendar year, prominent changes in daily rainfall and extremes events during summer monsoon (JJAS) season. Coastal Karnataka is a remarkable region, the occurrences of heavy rainfall events are likely to reduce in the future.
3	Donat et al. (2014)	Arab Region	ENSO (Nino 3.4), NAO	The relationships of the climate extremes with NAO are stronger, strong in the western part of the Arab region (closer to the Atlantic Ocean) but the relationship with ENSO are found to be more significant towards the eastern part.
4	Casanueva (2014)	Europe	AO, NAO, Scandinavian Pattern, East Atlantic Pattern (EA), SOI, AMO (Atlantic Multidecadal Oscillation)	Dissimilar patterns of variability found for wet and dry spells in winter and summer, Opposite associations with the North Atlantic Oscillation in winter and summer, and the relationships with the Scandinavian and East Atlantic patterns as well as El Niño/Southern Oscillation events in spring and autumn gave insight into the trend differences. Significant relationships were found between the Atlantic Multidecadal Oscillation and Total volume of R95p rainfall indices.

Table 2.2 Continued...

Sl. No.	Author and Year	Region	Climate Indices	Major Results
5	Duan et al. (2015)	Japan	AMO, PDO and Southern Oscillation Index (SOI),	Climate indices shows statistically significant correlations with increasing extreme rainfall events, especially with SOI.
6	Preethi et al. (2017)	Two large regional subsystems over the Asian domain, (a) South Asian and (b) East Asian monsoons	SSTs of West pacific Ocean and West Indian Ocean, mean sea level pressure, winds at lower troposphere	The relationship of the NEI and WCI rainfall series with Nino indices reveals maximum relation with SSTs over the Nino3.4 region correlation coefficient of -0.52 with NEI and -0.43 with WCI for the period 1970–2014 at 5% significance level. Wind patterns over the Pacific intensification rainfall depicts particularly associated with the WCI.
7	Wang et al. (2017)	Tropical North Atlantic (1) the western TNA (2) the Gulf of Mexico and the western Caribbean Sea, and (3) the open ocean southeast and east of Florida.	ENSO (Nino 3.4), NAO, AMO, MDR SST (Main hurricane development region), AWP (Atlantic Warm pool)	Rainfall intense events show a minimum value in the eastern Caribbean Sea north of South America. Rainfall intense events displays both interannual and multidecadal variability, but does not show a long-term trend due to global warming. The topmost three climate index depicts high correlations with rainfall intense events are (JJASON) ENSO and Atlantic warm pool indices, and the (JFM) North Atlantic oscillation index. However, the large-scale oceanic and atmospheric variables not show an important role in rainfall intense events in the Gulf of Mexico and the open ocean southeast and east of Florida.

Table 2.2: Continued...

Sl. No.	Author and Year	Region	Climate Indices	Major Results
8	Xiao et al. (2017)	China	ENSO, PDO, IOD, NAO	The regions with rainfall extremes influenced by climate indices with 1-year and 0-year ahead identified and shows contrasting at different phases. The rainfall extremes generally tend to be decreasing in the central part at the same year of positive ENSO while increasing in the east part of China a year after the positive ENSO.
9	Li et al. (2018)	Singapore	ENSO (Nino 3.4), global mean temperature, local temperature	Significant correlations are found between rainfall extremes and all the three factors, and the signature of local effects is more evident than global warming.
10	Revadekar et al. (2018)	Western Ghats of India	ENSO Indices and IOD	Observed that Indian Ocean Dipole (IOD) plays a dominant positive role in rainfall over entire Western Ghats in summer monsoon months, whereas role of Nino regions are asymmetric with rainfall over Western Ghats. Indian summer monsoon shows negative relationship with Nino SST. Negative correlations are also seen for Western Ghats rainfall with Nino regions but only during onset and withdrawal phase. During peak monsoon months July and August subdivisions of Western Ghats show positive correlation with Nino SST.

2.4 Sea surface temperature anomalies teleconnection with monsoon rainfall

Summer monsoon rainfall over Western Ghats exhibits large spatio-temporal variability that is always viewed with greatest concern, and it is teleconnected with different oceanic and land surface phenomena (Revadekar et al. 2018; Varikoden et al. 2018a). ENSO events are well known to be associated with significant seasonal climate anomalies at many places around the globe (Walker 1923; Rajeevan and McPhaden 2004; Naidu et al. 2017). The ENSO-monsoon rainfall teleconnections involve significant simultaneous relationships between monsoon rainfall and various ENSO indices (Krishna Kumar et al., 1995). The classical relation between ENSO and summer monsoon rainfall (SMR), observation says majority of years during the ENSO warm (cold) events the SMR was below (above) normal. Almost all the statistical seasonal prediction schemes of SMR rely heavily on the change in magnitude of various ENSO indices from winter (December to February) to spring (March to May) prior to the start of monsoon season. These studies reveal that Indian summer monsoon is weaker (stronger) than normal before (after) the peak of an El Niño in winter, and that the relationship is opposite for the monsoon and La Niña. It is also observed that the monsoon circulation over southern Asia is generally weaker (stronger) than normal during El Niño (La Niña) summers (Webster and Yang, 1992; Lau and Yang, 1997). Actually, it is also associated with other oceanic regions in addition to the eastern tropical Pacific, such as the warm pool of the west Pacific Ocean, the northwest Pacific Ocean (Ju and Slingo 1995; Soman and Slingo 1997) and the Indian Ocean (Saji et al. 1999). Several studies have documented empirical links between Indian Ocean SST anomalies and monsoon variability. Negative correlations exist between the summer monsoon rainfall and 16 months earlier SST near Indonesia (Nicholls 1983). Furthermore, the links between the SMR, the Indian Ocean and the tropical eastern Pacific have shown a biennial variability (Meehl 1987, 1997). Therefore, instead of calculating various global SST indices, from the tropical Pacific Ocean and using seasonal lag (December to May) for prediction of the SMR. In order to summarize the understanding of the literature on rainfall estimation, the brief description of the recent literatures are summarized in Table 2.3.

Table 2.3: Analysis of summer monsoon rainfall by identifying predictors

Sl. No.	Author and Year	Region	Predictor	Remarks
1	Sahai et al. (2003)	India	Global SST and ENSO (Nino 3.4)	SMR-SST relationship examined from three seasons lag prior to the start of the monsoon season up to four years lag. The correlation patterns show a slow and consistent temporal evolution, predicted values explain about 80% of the observed variance of SMR in the model verification period. It is claimed that the weakening of the ENSO-SMR relationship in recent years.
2	Kumar et al. (2007)	Orissa	ENSO (Nino 3.4), Equatorial Indian Ocean Oscillation (EQUINOO), Ocean Land temperature contrast (OLTC)	The climate indices of ENSO, EQUINOO, and Ocean-Land Temperature Contrast (OLTC) have been used as predictor variables to predict the monthly as well as seasonal rainfall. Global climate variables that are highly influencing the regional monsoon rainfall. The obtained results are encouraging and show improvement in monsoon rainfall estimating. ANN is very useful to predict non-linear relationship of global climate and monsoon rainfall at regional scale.
3	Srivastava et al. (2010)	India	Southern Oscillation Index (SOI), Pacific Decadal Oscillation Index (PDOI), Global SST	SOI and PDOI alone unable to give the best model description but combination of both of these is able to produce a better forecasting model. Climatic indices and regional Sea Surface Temperature both considered as candidate predictors, showed the better performance with RMSE (root mean square error) and AAPE (average absolute percentage error) ranges from 12.85 to 29.92 mm and 1.21% to 5.01%, respectively.

Table 2.3: Continued...

Sl. No.	Author and Year	Region	Predictor	Remarks
4	Schepen et al. (2012)	Australia	Pacific Ocean indices, Indian Ocean Indices, Antarctic Oscillation	Seasonally, the strongest evidence is found from August–October to November–January and the weakest evidence is found from March–May to May–July. Climate indices derived from the Pacific region show stronger persistence in the relationship with Australian seasonal rainfall totals than SST anomalies of Indian region. Many climate indices are found to show similar supporting evidence for forecasting Australian seasonal rainfall, leading to the prospect of combining climate indices in multiple predictor models and/or model averaging.
5	Singh and Borah (2013)	India	the time series rainfall data for 140 years considered Antecedent (90 years) period data analyze the precedent (50 years)	In this study feed-forward backpropagation neural network algorithm used for SMR analysis. Based on neural network algorithm the five neural network architectures designated using three layers of neurons (one input layer, one hidden layer and one output layer). The data set is trained and tested separately for each of the neural network architecture. The predicted results obtained for the training and testing data are compared with existing model. Results clearly exhibit superiority of model over the other existing model.
6	Nanjundiah et al. (2013)	India	ENSO and EQUINOO (Equatorial Indian Ocean Oscillation)	The prediction of the phases of extreme modes of climate indices and their link with the monsoon assessed. It was found that SMR-SST relationship opposite to the observed, with the predicted SMR being negatively (instead of positively) correlated with the rainfall over the western equatorial Indian Ocean and positively (instead of negatively) correlated with the rainfall over the eastern equatorial Indian Ocean.

Table 2.3: Continued...

Sl. No.	Author and Year	Region	Predictor	Remarks
7	Ravi et al. (2013)	South India	Antarctic Circumpolar Current Index, (ACCI) Southern Indian Ocean (SIO), Bay of Bengal index (BOBI), North Equatorial Index (NEI) and Nino 3.4	Correlation analysis is done to see the effect of STIO (South and Tropical Indian Ocean) SST variability on winter monsoon rainfall index (WMRI) for South India. The significant positive correlation is found between Southern Indian Ocean (SIO) SST and WMRI in July-August-September. Maximum positive correlation of 0.61 found from the region south of 50deg. S and the negative correlations of 0.60, 0.53 and 0.57 are found with the SST of the regions SIO, Bay of Bengal and North Equatorial Ocean respectively at 99% confidence level. WMRI predicted by SST indices using regression models, individual models performed better prediction skills to capture non linearity.
8	Surendran et al. (2015)	India	ENSO (Nino 3.4) and Equatorial Indian Ocean oscillation (EQUINOO)	Interannual variation of SMR over Indian region is strongly linked with ENSO and as well as EQUINOO, the seasonal value of the ENSO being stronger than that with the EQUINOO. Results shows the variation of a composite index determined through bivariate analysis, explains 54% of SMR variance, suggesting a strong dependence of the skill of monsoon prediction on the skill of prediction of ENSO and EQUINOO.

Table 2.3: Continued...				
Sl. No.	Author and Year	Region	Predictor	Remarks
9	Dorji et al. (2018)	Bhutan	SST of AS and BB, MSLP (mean sea level pressure) of Bangladesh and northeast India, selected Northern hemisphere teleconnection indices	The monsoon rainfall mainly from the large-scale seasonal south-westerly winds from the Bay of Bengal and the Arabian Sea. The study shows high correlation with the SST and the MSLP of the Bay of Bengal and the Arabian Sea. Study shows the weakening of the relationship between ENSO and summer rainfall, ENSO/SOI was a weak predictor for summer monsoon in Bhutan. The study shows modest correlations with the Northern Hemisphere teleconnection indices.
10	Johney et al. (2018)	Kerala	Indian Ocean Dipole (IOD)	The possible teleconnection of SMR of Kerala with the Indian Ocean dipole (IOD) using the cross-correlation and ensemble empirical mode decomposition - based time-dependent intrinsic correlation analyses. The analysis has showed the dominance of negative association of IOD with SMR of Kerala in different process scales with strong positive association at localized time spells. The forecasting strategy demonstrated in the study and the evidence of IOD–SMR rainfall link are an amendment to the efforts for improving the predictability of SMR in Kerala.

2.5 Literature gap and Summary

Following inferences were drawn from the literature review

- From the review of past literature, it is evident that, the Western Ghats of India is one of the eight "hottest hotspots" of biological diversity in the world and are listed as the UNESCO World Heritage Site (UNESCO 2013). The region is facing problems related to extreme weather conditions. A great deal of research has been conducted on the changing climate of the Western Ghats of India, but few studies have been carried out on the estimation of rainfall extreme events.
- Longitudinal stretch from the coastline to the Western Ghats could aid in observing significant spatial and temporal variations in rainfall. Rainfall extremes depend on various factors such as, moisture flux, orography and teleconnections. Therefore, the Western Ghats elevation is capable of deep convection. Among the three subdivisions of Western Ghats, the highest rainfall is received by coastal Karnataka due to extensive mountain barrier signifying the orographic dependence.
- Due to changing climate, there is a change in extreme rainfall events pattern. Studies have quoted the extreme rainfall Indices derived by expert team on climate change detection and monitoring indices (ETCCDI) based on intensity, frequency and duration in daily rainfall pattern. Therefore, change in frequency of extreme rainfall events and their trend has to be given importance in West Coast of Karnataka as this region receives extreme events of rainfall all along the west coast of India.
- The recognition of prospective variations in extreme rainfall events, in terms of the occurrence, depth and interval assumes importance on the regional scales, due to the associated critical socioeconomic consequences. Therefore, it is necessary to evaluate various aspects of future projections of rainfall extremes.
- The trend analysis carried out using daily rainfall data signified that the trend is increasing in the southern India except Kerala region and decreasing in the Himalayan

region. Though there have been many studies at global and in the Indian context, very few studies accounted for the regional heterogeneity of rainfall.

- The El Nino Southern Oscillation (ENSO) is known to be a major forcing of the Earth's year-to-year climate variability. Association between ENSO and summer-monsoon rainfall over India has been rigorously studied. Whereas role of Nino regions are asymmetric over Western Ghats rainfall.
- Understanding changes in rainfall variability is essential for explanation of the extreme events response to sea surface warming (SST) and its impacts. While changes in mean rainfall have been studied intensively, rainfall extreme events variability has received less attention, despite its theoretical and practical importance.
- Analyzing the summer monsoon rainfall by teleconnection of Climate indices SST-monsoon relationship at different season. The asymmetric teleconnection of Nino indices reveals better performance of prediction using seasonal lead-lag relationship than the standard ENSO index.

Inferences drawn from the literature survey led to the formulation of the objectives of this research. Formulated objectives address few important aspects related to rainfall over Coastal region and Western Ghats of Karnataka.

Description of study area under investigation and materials used for present study are outlined in chapter 3

CHAPTER 3

MATERIALS AND METHODOLOGY

3.1 INTRODUCTION

This chapter includes the description of;

- ❖ Geographical, physical features of study region and climatic characteristics,
- ❖ Data used and,
- ❖ Overall methodology adopted for the study

3.2 STUDY AREA

The geographical location of Karnataka's coastal region and the Western Ghats is between 11° 50' to 15° 48' N latitude and 74° 5' to 76° 14' E longitude. The districts of Udupi, Dakshina Kannada, and Uttara Kannada are covered by the coastal region of Karnataka, which is spread among the Western Ghats and extends up to the Arabian Sea in the west and to the edge of the plateau of Karnataka. Several ridges and spurs of the Western Ghats span this region. The Western Ghats are parallel to the coastline and comprise of a series of mountains. Several hill peaks and ranges, waterfalls, creeks, and rivers render the Western Ghats as a difficult terrain. The Western Ghats and the plains constitute the two major physical units of the coastal region. During the summer monsoon season (JJAS), heavy rainfall is received by Karnataka's coastal region and the Western Ghats, with the average rainfall being in excess of 2500mm in some parts. Considerable damage is caused by the frequently occurring orographic effect, which is caused due to the heavy rainfall (> 150 mm/day) along the coastal plains.

A narrow stretch of marine and estuarine plains is represented by the coastal plains. The Western Ghats are formed by the precipitous rise at the eastern sides. When compared to the elevation of the northern parts (450m-600m), the elevation of the southern parts (900m-1,500m) is found to be higher. A distance of around 320km is covered from the north to the south by the 50km-80km wide coastal belt. From the point of view extreme rainfall analysis,

the study region can be conveniently divided into Coastal region as Low land (LL) and High land (HL) composes of Western Ghat. The location of the study area is shown in Figure 3.1. According to a report of the Western Ghats Ecology Expert Panel (2011), several mammals, reptiles, birds, amphibians, plants and floras are indigenous to this region and are specifically restricted to India. The rainfall received in this region during the south-west monsoon cherishes the flourishing growth of living beings. During the JJAS months, the annual averaged rainfall is found to be more than 250cm in the study region (Francis and Gadgil, 2005). According to a report by the Western Ghats Ecology Expert Panel (2011), the vegetated or forest areas with a specific altitude are mapped for defining the boundaries of the Western Ghats. In accordance with this report, the present study has considered the areas with an elevation of more than 200m as the mountain barriers of the Western Ghats (Tawde, 2013). Moist air rising from the Arabian Sea is blocked at cascaded mountains, resulting in the eastern side of the Western Ghats receiving low rainfall (Tawde and Singh, 2015). On the other hand, moist air flux rising from the Arabian Sea causes orographic effect, resulting in intense rainfall in the coastal plains and the windward side (western part) of the Western Ghats (Francis and Gadgil, 2006; Tawde and Singh, 2015).

The summer monsoon is driven by seasonal variations in land-sea temperature contrast between Asian landmass and adjacent oceans. The south-east trade winds from the southern hemisphere are drawn into Western Ghats as the south-west monsoon winds after they cross the Equator. The summer monsoon winds are divided into branches - the Arabian Sea branch and the Bay of Bengal branch. It gives very heavy rainfall (more than 200 cm), to the windward side of the Western Ghats.

Among three subdivisions of Western Ghats (Kerala, Coastal Karnataka and Konkan Goa), minimum rainfall occurs over Kerala. Maximum rainfall occurs over Coastal Karnataka which is middle subdivision and again rainfall decreases over Konkan & Goa. Thus, though all the three subdivisions of Western Ghats receive very high rainfall during the summer monsoon season, it indicates substantial spatio-temporal variation in distribution. Therefore to understand the modulation of large-scale phenomenon over the Pacific Ocean SSTs with rainfall over West coast of Karnataka, a subdivision of Western Ghats of India is considered.

Communities, economies, and ecosystems are being significantly influenced by climate change. An increased risk of flooding is caused by an increase in the mean rainfall, while

an increased risk of drought is caused by a decrease in the mean rainfall. Aquatic ecosystems are damaged and the quality of fresh water is diminished by several pollutants, such as phosphorus, nitrogen, pesticides, and heavy metals. Such pollutants are transposed by storm water runoff caused by extreme rainfall. The most immediate impact of heavy rainfall is the prospect of flooding. Moreover, there is an increased risk of landslides being caused due to heavy rainfall. A landslide is caused because of the slopes losing their stability, which is due to the rising of the water table, which is in turn caused by an above-normal rainfall. Increased heavy rainfall induced by climate change leads to the anticipated occurrence of frequent landslides in the Western Ghats of Karnataka.

Rainfall is the primary source of irrigation in non-irrigated areas. Crop cultivation in such areas could be strained due to the variation in rainfall caused by climate change. Moreover, shortage of water may be encountered in irrigated areas during the summer season, which may pose a risk to the agriculture sector and cause scarcity of food grains. Several rivers originate in the Western Ghats of Karnataka. Several problems, such as climate change and rapid changes in land use, are encountered by the people residing in this region. Water scarcity is reported during the summer in places located in the Western Ghats and the Coastal regions of Karnataka, where an annual average rainfall of more than 3000 mm is recorded.

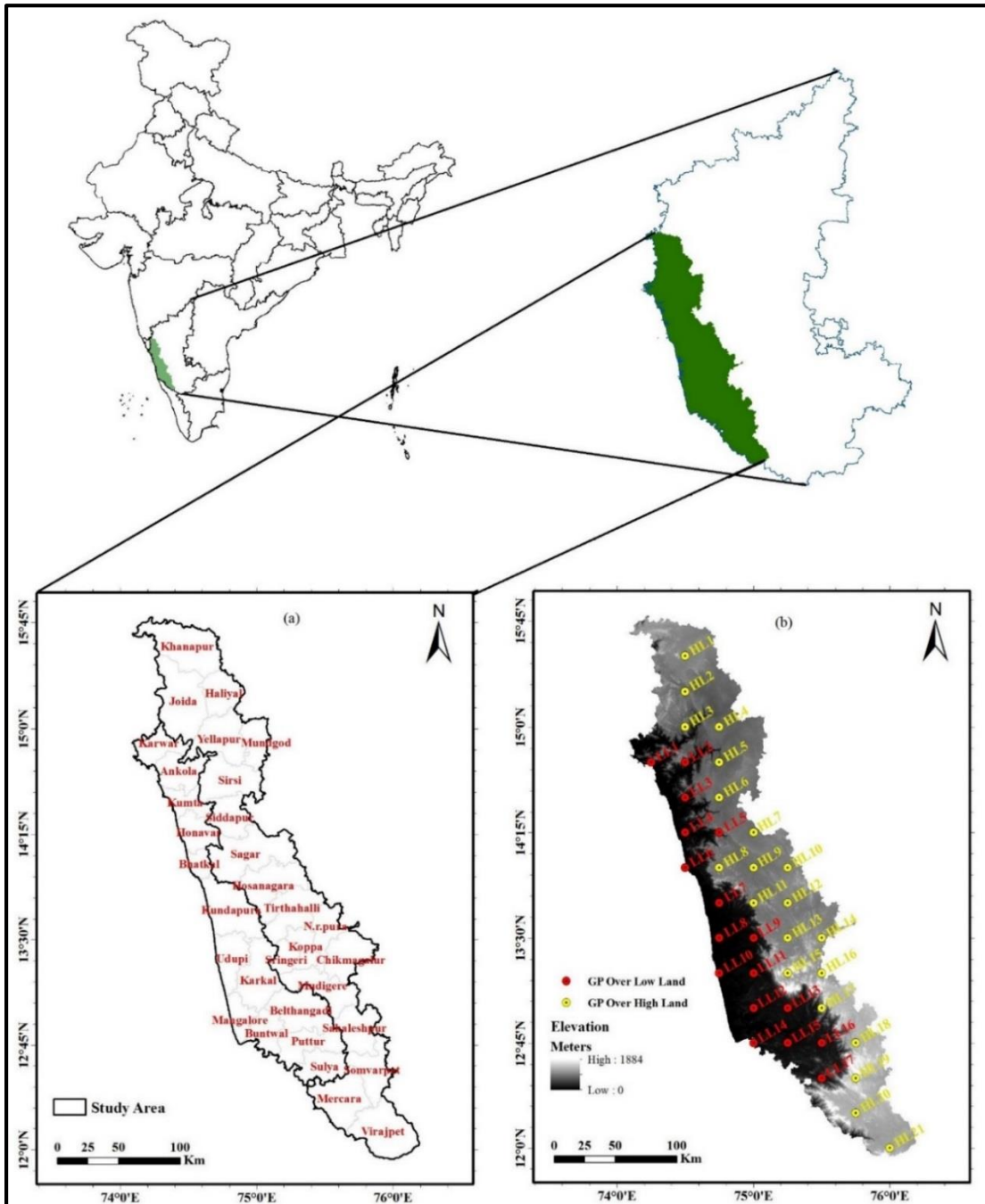


Figure 3.1. Geographical Location of (a) Coastal region and Western Ghats of Karnataka and (b) Regional distribution of grid point in the study area

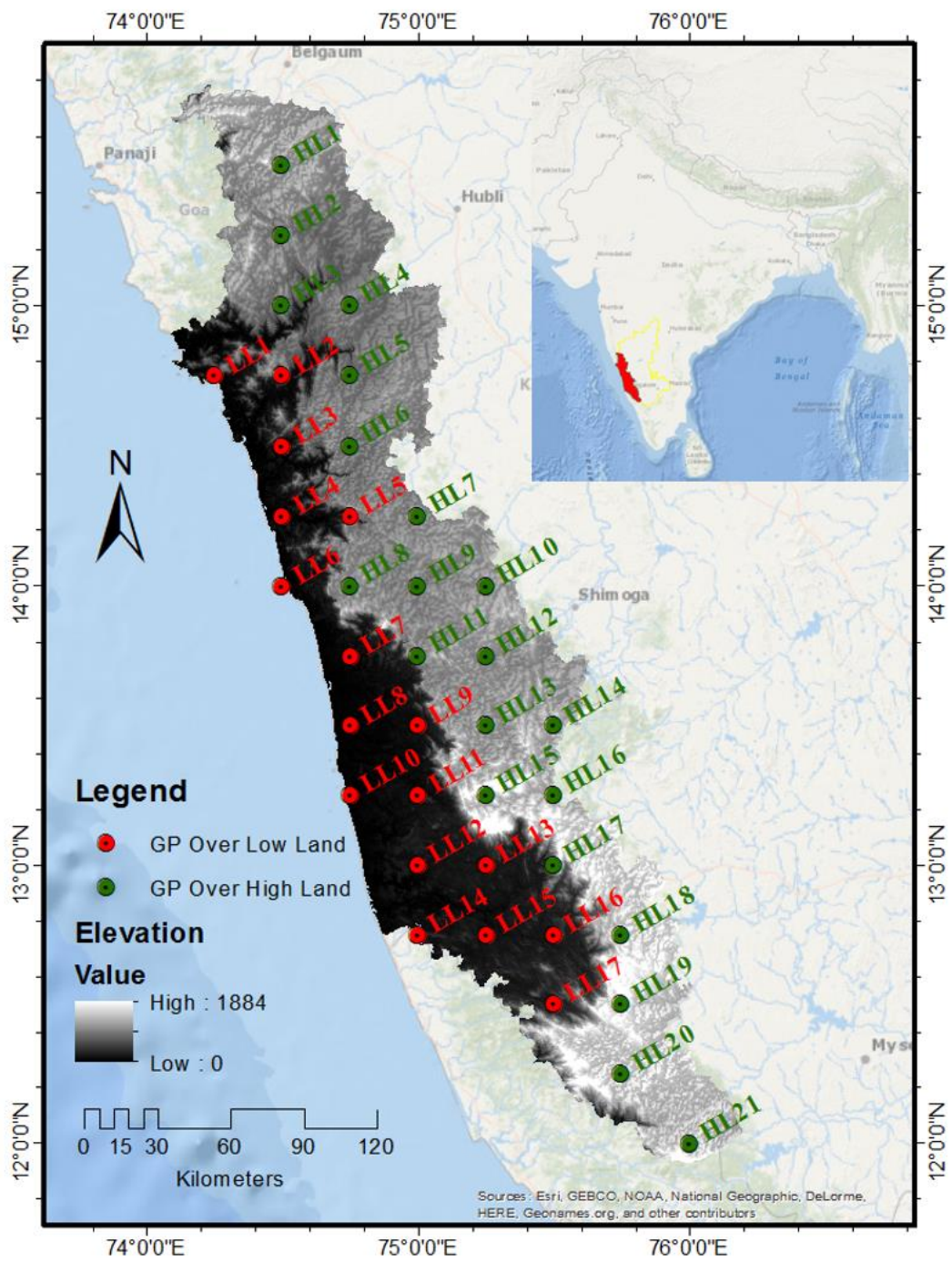


Figure 3.1b. Geographical Location of grid points of the study region

3.2.1 Climate characteristics

The distance from the sea, topography, and the land's altitude contribute towards the dynamic weather of Karnataka's coastal region and the Western Ghats. The coastal plains possess a humid tropical monsoon climate, whereas the Western Ghats possess a sub-humid to humid tropical climate. According to the Ministry of Environment and Forests, four seasons, namely, summer season, monsoon season, post-monsoon season, and winter season, are experienced by the people living in Karnataka.

- ❖ Summer: The summer season is experienced in the months of March, April, and May. The last two months prove to be the hottest, as the study area becomes uncomfortable and dry. The situation may turn worse if the pre-monsoon rainfall does not occur.

- ❖ Monsoon: The monsoon season commences in the month of June and extends up to the month of September. Although the temperature and humidity are found to be increasing in the month of June, ample rainfall is brought about by the south-west monsoon. The humidity content is demonstrated in the coastal region and the western side of the Western Ghats (100%) and also by the eastern side of the Western Ghats (60%) during the months of June and August.

- ❖ Post-Monsoon: A pleasant weather change is observed in the months of October and November that witness the post-monsoon season. The north-eastern monsoon brings about some spells of rainfall in the study region, thereby affecting other parts of Karnataka. A considerable decrease in humidity is witnessed during post-monsoon.

- ❖ Winter: The winter season is experienced in December, January and February, which are regarded as the coldest months of the year as the temperature dips to around 10°C. Consequently, the high altitude region of the Western Ghats witness a noteworthy fall in the humidity levels, resulting in a pleasant weather.

i. Rainfall

The rainfall in the study region is mainly due to cyclonic and orographic effects, the contribution of convective rainfall out of annual rainfall is negligible. The moist air being lifted due to depression over the Arabian Sea during the south-west monsoon are carried by the sea breeze towards the canopy of Western Ghats resulting in the orographic rainfall. The high lands closure to Western Ghats experience heavier rainfall and intense rainfall could be identified near narrow belt coastline. With respect to the south-west monsoon and the Arabian Sea, the study region with a tropical climate is found to be dependent on its geographic and physiographic location.

ii. Temperature

Sea breeze and land breeze primarily impact the coastal region's climate. Striking changes in temperature are demonstrated by the direction of wind over the Arabian Sea. A gradual increase in temperature is witnessed in the study region after the coldest month of January. The month of March witnesses a rapid rise in temperature. The month of May generally witnesses a peak in temperature in the coastal plains. The temperature begins to drop in the months of October and November and continues to drop further in the month of December.

iii. Wind

The winds are strong and are mainly westerly or south westerly during south west monsoon period (June and July). During the rest of the year, Winds are northeasterly. The maximum wind velocity is so far recorded is 72 km/hr on the 21st of July 1983 (IMD).

iv. Water resources

Reservoirs, waterfalls, lakes, and rivers constitute some of the available sources of surface water in Karnataka. The Western Ghats are the primary division for the river basins. About 6% of the country's surface water resources (i.e. approximately 17 lakh million cubic meters (MCM)) is accounted by the country's seventh largest (area-wise) state of Karnataka. Additionally, the state possesses a potential of about 102 cubic km of surface water. A majority of the seven river systems of Karnataka originate near the Western Ghats ridge at an elevation of 400 meters to 1,600 meters above the mean sea level. The rivers flowing towards the east (towards the Bay of Bengal) carry 60% of the state's surface water, whereas the rivers flowing towards the west (towards the Arabian Sea) carry 40% of the state's surface water. Since the rivers flowing in the western direction cannot be utilized, the average economic utilization of the river basins is estimated to be 45%. It is noteworthy that the state's ground water resources (485 TMC) are not evenly exploited in Karnataka. For instance, the irrigation and coastal areas of Malenadu possess adequate quantum of surface water; however, the ground water resources are minimally exploited.

3.3 Data sets

i. Rainfall data

The India Meteorological Department (IMD) 0.25°x0.25° high resolution (25Km grid data) gridded daily rainfall data for the period 1901 to 2013 were used. The IMD gridded data has been developed by IMD over Indian region using weighted interpolation technique on rain gauge observations. The dataset is well validated and reliable (Pai et al. 2014; 2015). The starting point of this gridded data is 6.5° N and 66.5° E with total (241x281) grid points. A total of 38 grid points were selected and extracted the individual grid point rainfall values from the IMD gridded data for the year 1901-2013. The rainfall data is available in daily series with various compatible conversion data format. In the present study netcdf format is used and extracted using the climate data analysis tools ferret and Grads. Figure 3.1b depicts geographical locations of grid points employed. The selected grid points are divided broadly into two groups based on its situated location in the study region and elevation. West coast of India, has an influence of sea/breeze circulation. Whereas horizontal extent of sea breeze is upto 75km from the sea/land interface and vertical extent of sea/land breeze circulation cell upto 1 km (Rani et al., 2010). According to the elevation values from the ASTER digital elevation model, the selected grid points are bifurcated into two zones. The high-resolution daily rainfall gridded data (for the time series of 1901-2013) was used to extract the grid points (selected for analysis within the study area) as individual points of rainfall data. In a way similar to the one followed by the state's agro metrological division, the elevation and location of the grid points were used to differentiate them within the study region. The spatial rainfall variability and the circulation of sea breeze or land breeze caused by orographic rainfall affect the west coast of India (Rani et al., 2010). Therefore, intense rainfall is prevalent in low lying areas (up to 140 m above MSL) of the Western Ghats (Tawde and Singh, 2015). Elevation values for the selected grid points are extracted from ASTER elevation data. Appendix I shows the description of selected grid over study region. The 17 grid points located towards western side of Western Ghats and elevation within 200 meters are coastal region grid points, which are also remarked as 'Low Land'. The remaining 21 grid points are spread over ridges and slope of the Western Ghats at high elevated location, which are termed as 'High Lands'. Grid points, which are located in border of Western Ghats toward inland region are near to leeward side of Western Ghats,

which receives rainfall relatively low. However, the grid points at the strip of the coastline received intense rainfall.

ii. Sea Surface Temperature

The anomaly of the sea-surface temperature (SST) is measured in °C and its monthly time series of climatic data (from 1951 to 2013) is included in the present study. The SST data is available in monthly series with various data format (www.esrl.noaa.gov) . The sea-surface temperature anomalies (SSTA) observed in the central Pacific's Niño 3.4 region defines the ENSO signal. The National Weather Service Climate Prediction Center at the National Oceanic and Atmospheric Administration (NOAA) tabulates the monthly time series of SSTA, which is derived from the NOAA Extended Reconstructed Sea Surface Temperature V3B (ERSST.V3B). SST anomalies that are averaged across a given region are used as the basis of several indices that are employed in the monitoring of the tropical Pacific. The various indices, such as the Niño 1+2, Niño 3, Niño 3.4 and Niño 4 regions, correspond with the labels assigned to ship tracks that crossed these regions. El Niño was first recognized in the coastal South American region with which the eastern-most and the smallest of the Niño SST regions (Niño 1+2 region) corresponds. It was discovered that the vital region for coupled interactions between the atmosphere and the ocean for ENSO was situated westward towards the Niño 4 region, despite the Niño 3 region once being the chief focus to monitor and predict El Niño (Trenberth, 1997). SST anomalies are captured by the Niño 4 index in the central equatorial Pacific. When compared to other Niño regions, this region has a lesser inclination to possess variance. The average equatorial SSTs from around the South American coast's dateline may be represented by the Niño 3.4 anomalies across the Pacific. As mentioned below, two different regimes (La Niña or El Niño phases) were defined using the mean value of sea-surface temperature anomaly in Niño 3.4 region for a given year.

La Niña, if mean $SSTA < -0.5^{\circ}\text{C}$;

El Niño, if mean $SSTA \geq +0.5^{\circ}\text{C}$

It is inferred from the above definition that a growing season, influenced by La Niña or El Niño, is denoted by any average values that exceed -0.5 or +0.5.

3.4 Details of tools used for the study

The following list of tools and packages were used for processing the Rainfall data and analysis are summarized in Table 3.1:

Table 3.1 Tools used for the study

Tools	Purpose
Ferret, CDO, GRADS	These are the open source tools based on Linux platform. It was used for converting raw rainfall data obtained from IMD and extraction of grid points of the study region. It is very useful in data visualization and analysis.
AnClim	Open source tool used to detect autocorrelation and homogenization in a time series.
RClimdex	A software developed by Zhang and Yang (2004) at Canadian Meteorological Services was used to obtain Rainfall Indices and analysis.
RHtetsV3	RHtest package is used to detect multiple change points that might exist in time series (Wang and Fing 2004).
ArcGIS 10.1 [®]	ArcGIS is professional GIS software developed by Environmental System Research Institute (ESRI). It is used for the generation of maps, conduct of spatial analysis and sharing of intelligent visualization for an improvised decision making. It renders a set of comprehensive data visualization and analysis tools which greatly simplify the analysis of geo-spatial data.
MATLAB [®]	A powerful mathematical data analysis tool used in neural network analysis and modeling.
Spi_sl_6	US Drought Mitigation Center definitive calculation SPI (Standardized rainfall Index) executable program (WMO adopted), WINDOWS operating system command line.
Minitab 17	A statistical analysis software helps to improve quality and verification of analysis and results.

3.5 Overall Methodology

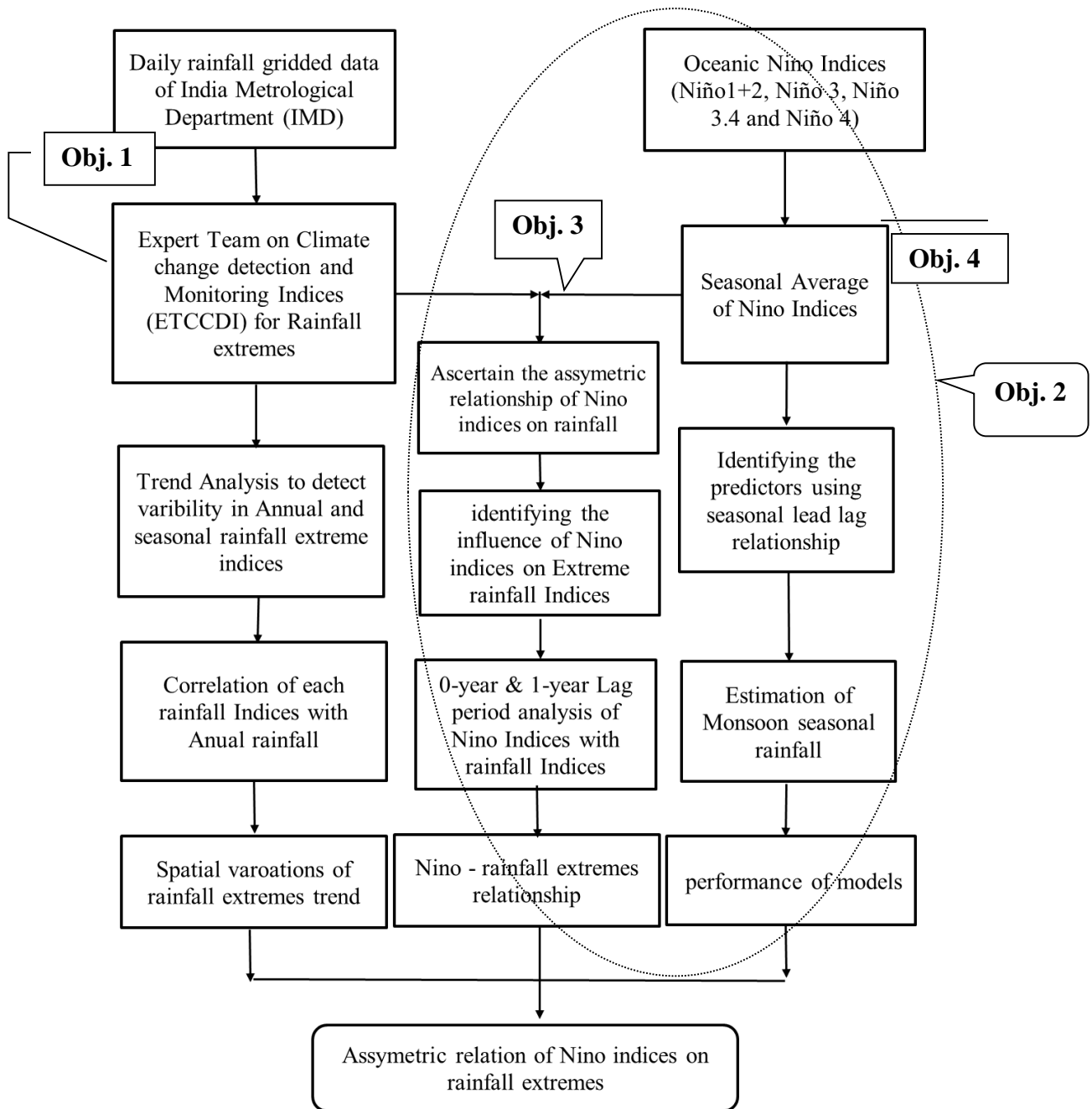


Figure 3.2 Flowchart of the steps involved in research methodology

The present study can be classified under four objectives, which are inter-related as shown in the flow chart of the overall research methodology in (Figure 3.2). By using daily time series, the ETCCDI extreme rainfall indices were computed by the high-resolution gridded rainfall IMD data for the study region. The measurement and characterization of climate variability and change is addressed by the joint Expert Team on Climate Change Detection and Indices (ETCCDI) of JCOMM/CLIVAR/CCI by providing extreme rainfall indices relevant to climate change detection which is discussed under chapter 4. Mountains with a steeply rising western face, narrow zonal width, and an orientation from the north to the south, basically constitute the Western Ghats of Karnataka. The rainfall over the study region is occurred by winds sliding over the Arabian Sea blocked by the Western Ghats and thus uplifted to generate moderate-to-heavy rainfall in an orographic manner. Whereas relationship of Nino regions with rainfall are asymmetric over the Western Coast of Karnataka, India. Hence, the effects of Nino indices with ETCCDI rainfall indices are discussed in chapter 5. The rainfall over study region is highly concentrated in monsoon season. Therefore, in chapter 6 discussed on estimation of seasonal rainfall by significantly influencing seasonal Nino Indices using lead lag relationship. Chapter 7 on summary and conclusions of all the four objectives of this research.

The next chapter explains detailed methodology, results and discussions of the objective 1 of this research.

CHAPTER 4

TREND ANALYSIS OF EXTREME RAINFALL INDICES

4.1 INTRODUCTION

Synoptic weather system variability provides insight into regional rainfall and extreme events. In recent decades, fluctuations in extreme rainfall events have attracted widespread interest by the scientific community due to their devastating impacts on both human society and natural systems. Increased concerns for extreme Rainfall events analysis is not only due to economic development, the growing need for water, and global warming, but also due to its significance in natural threats, such as droughts, soil erosion, and floods (Lopez-Moreno et al., 2009; Oguntunde et al., 2011; Wang et al., 2015; Tabari et al., 2015a). The increased concentration of greenhouse gases (GHG) has accelerated the speed of the hydrological cycle because of enhanced atmospheric warming and result in instability of the hydrological cycle system. An enhanced focus on this issue could be attributed to the varying Rainfall patterns as witnessed in several parts of the world. The changes to the rainfall due to climate change are bound to influence the review of management practices in hydrology.

4.2 EXTREME RAINFALL ANALYSIS IN WESTERN GHATS

In the Western Ghats, Rainfall often exhibits seasonality due to the periodicity of weather. The methods adopted to evaluate the trends, therefore, are required to consider the seasonality. The trend analysis of extreme Rainfall indices are explained in this chapter for the study area namely, the coastal region of Karnataka and the Western Ghats.

Of late, extreme occurrences of rainfall have become a matter of much interest as they have greater sensitivity to changes in climate than average values, within the global warming context. Extreme events are described as the “occurrence of climate variable above (or below) a threshold value near the upper (or lower) ends of the range of observed values of the variable”. Extreme events are occasional occurrences and frequently are situated beyond the scope of most monitored or computed data. Although there is a very low likelihood of these events, they are connected with abnormal effects and can result in significant losses and destruction due to their scale. These impacts may involve excessive loss of life,

economy, or both. Extreme rainfall signifies the maximum rainfall in a day within a year. Consequently, there are as many values of extreme rainfall as the total number of years.

It is widely acknowledged that rainfall events taking place in mountainous regions provide water resources for society, agriculture, industry, and the environment. But, for planners of water resources and agriculture, variability of Rainfall events is an extremely challenging issue. It is difficult to predict the risk of extreme events, but their impacts could be severe. India is of substantial interest for researchers as it is evident from several studies that a rise in GHG concentrations would markedly enhance the conveyance of moisture into the Indian west coast, causing extreme events of rainfall (Bhaskaran et al., 1995; May, 2002). Despite the significance of inflow-generating rainfall in the Western Ghats of Karnataka, a knowledge gap remains concerning the enduring, historic climatological behavior of the synoptic weather system that delivers the region's rainfall pattern. To outline the change in Rainfall extremes in the study region (i.e., Karnataka's coastal region and the Western Ghats), it is necessary to look at the historical trends of statistical properties of Rainfall extremes.

The objective of the Chapter 4 is to understand spatio and temporal behavior of the extreme rainfall events based on ETCCDI rainfall indices and its trend over study region.

4.3 METHODS FOR TREND ANALYSIS

The detection of trends can be carried out using either parametric or non-parametric tests. The linear trend in the parametric tests analyze whether there is a significant variance from zero for the slope coefficient of linear regression whereas the sign of the slope coefficient signifies a negative or positive trend. The meteorological time series are frequently encountered with non-normally distributed, censored, and missing data, making them more suitable for non-parametric methods as they are distribution free (Hirsch et al. 1991). Incorrect results leading to invalid inferences could be obtained with the use of parametric methods when the data is not normally distributed. The trend detection of meteorological variables can be performed using several non-parametric methods, such as seasonal Kendall test (Hirsch et al. 1991), Locally Weighted Scatterplot Smoothing (LOWESS) (Champely and Doledec, 1997), the wavelet based trend analysis (Craigmile et al., 2004), and the

Spearman's rank correlation test (Yue and Wang, 2002). The Mann-Kendall (MK) test is the best non-parametric approach for detecting the trend (WMO, 1988).

Mann-Kendall test with pre-whitening of time series is referred to as the Modified Mann-Kendall (MMK) test used in the present study for rectifying serially correlated data with 95% confidence interval. The slope estimator of Sen (1968) is used to estimate the magnitude of the trend in the seasonal and annual series. A robust estimate of a monotonic trend's magnitude is rendered by the non-parametric approach of Sen's slope estimator. The change in the mean of the sample over observation period is determined with an assumption of the trend to be linear. The magnitude of a trend can be gauged by analyzing the average changes over a region (Hirsch et al., 1991; Kiros et al., 2016; Mudbhatkal and Amai, 2018). The slope estimator of Sen is a widely used tool in quantifying trend in Rainfall time series (Kahya and Kalayci, 2004; Partal and Kahya, 2006; Rajeevan et al., 2008; Kiros et al., 2016; Revadekar et al., 2018).

For water management in warmer climates, an awareness of the pattern of extreme Rainfall is essential. Indeed, mobilizing and planning water resources requires analysis of trends in Rainfall time series. This analysis can facilitate adaptation planning and resilience building for droughts and flood. This study endeavors to offer greater insight regarding the development of extreme Rainfall in the Western Ghats and west coast of Karnataka at daily timescales. The chapter 4 attempts to study the historical rainfall trend of the ETCCDI extreme rainfall indices in the Western Ghats and coastal region of Karnataka.

Methodology followed in the analysis is outlined below section 4.4.

4.4 METHODOLOGY

4.4.1 Schematic flow of extreme rainfall analysis

Fig. 4.1 depicts the flow of activities undertaken by the study for the trend analysis of extreme Rainfall patterns.

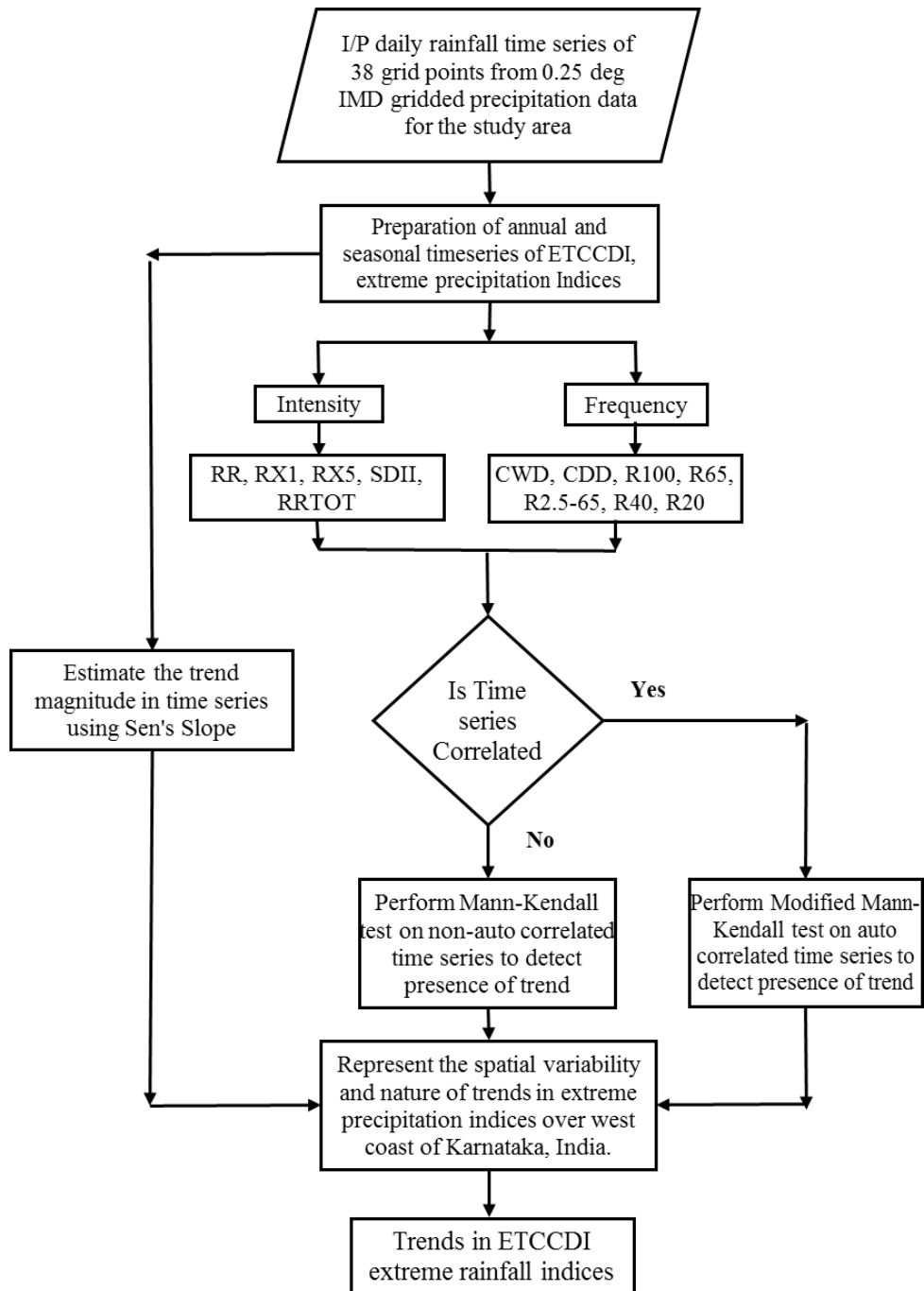


Fig. 4.1: Schematic flow chart for evaluating the trend of extreme Rainfall indices of ETCCDI

The changes in extreme rainfall events were assessed using daily Rainfall series of high-resolution gridded data of the India Meteorological Department (IMD). This dataset contains data for the period 1901-2013 (113 years) (Pai et al., 2013). The elevation information of topography is extracted using the Digital Elevation Model (DEM) of Advanced Space borne Thermal Emission and Reflection (ASTER). Within the boundary of the study area, the grid points chosen for analysis were extracted as distinct Rainfall values from the IMD dataset. Within the region, the grid points were segregated based on their elevation and location, which is also comparable with Karnataka state agro meteorological division. The circulation of breeze caused by sea or land affects the Indian west coast and the spatial Rainfall variability, because of the orographic Rainfall (Rani et al., 2010). Consequently, the low-lying areas (that is, up to 200 m above MSL) of the Western Ghats in Karnataka have a tendency for intense Rainfall (Tawde and Singh 2015).

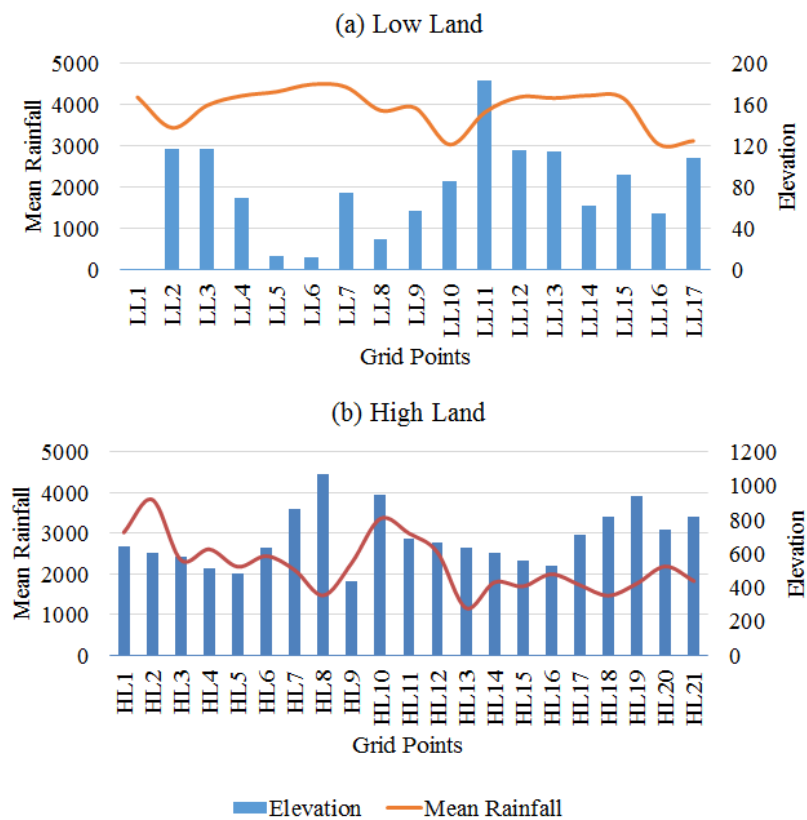


Figure 4.2: Variation of Rainfall with elevation at each grid points over (a) Low Land (Coastal region) and (b) High Land (Western Ghats)

Appendix 1 summarizes the grid points/stations utilized in this study with their elevations, coordinates, and the observed average rainfall values for the study period (i.e., 1901-2013). The ordering of the grid points was done in two categories, namely high land points (HL) and low land points (LL). The grid points were above 200 m above MSL in HL points and were below 200 m above MSL in LL points (Tawde and Singh 2015). A total of 38 grid points were scrutinized of which 21 were located in HL and 17 were located in LL. The HL points were distributed across the highly elevated areas of the Western Ghats.

Spatial variation of Rainfall at each grid point over coastal plains and highly terrain region of selected study area is depicted in Figure 4.2. A significant role is played by the hilly terrain of the Western Ghats in the suppression of Rainfall on the leeward side and intense Rainfall on the windward side. Detectable peaks and higher Rainfall over gradually increasing slopes are observed in the study region.

4.4.2 Assessment of Changes in Rainfall Extreme Events

In order to elaborate the climatology of extreme rainfall and to investigate changes in extremes (intensity and frequency), it was essential to design a set of indices that were statistically robust, covered a wide range of climates. The latent change in rainfall extremes over Karnataka's coastal region and the Western Ghats was characterized by calculating the climatic extreme indices. These indices are recommended by the Expert Team on Climate Change Detection Indices (ETCCDI) and the joint World Meteorological Organization Commission for Climatology (CCI) and World Climate Research Programme (WCRP) project on Climate Variability and Predictability (CLIVAR) (Peterson et al., 2001; Alexander et al., 2006; Zhang et al., 2011). Since extreme events have strong impact on society. These extreme rainfall indices have also been used in other studies for different regions in India and around the world (Revadekar et al. 2011; Revadekar and Preethi 2012; Hasan et al. 2018; Jiang et al. 2018; Li et al. 2018).

Table 4.1 summarizes the descriptions of the indices selected for the present study. The 12 rainfall indices were computed for each individual grid points/station at seasonal and annual (monsoon, before monsoon and after monsoon) time steps. The rainfall indices considered

in the study are based on fixed threshold (absolute) and some are based on adaptable thresholds. Data were analyzed by using the RCLimDex is an open source software developed by ETCCDI. This package was used and developed in previous studies (Croitoru et al. 2016; Demaria et al. 2013; Sharma and Singh 2017; Wang et al. 2013).

RCLimDex was used to compute extreme rainfall indices from the IMD gridded daily rainfall data. A 5% level of statistical significance was taken into consideration. The purpose of the ETCCDI process is to determine a standardized set of indices, which makes capable comparison across study region. The slopes of the annual/seasonal trends and their statistical significance to rainfall indices were calculated based on non-parametric MK/MMK test in order to detect trends within time series.

Table 4.1: Description of Annual and Seasonal Rainfall Indices

S.no.	Index	Definition	Units	Significance
1	RR	Total annual rainfall	mm	Annual magnitude of rainfall
2	CWD	Number of rainy days in a year/season (with rainfall intensity ≥ 2.5 mm/day)	days	Rainy days
3	CDD	Number of dry days in a year	Days	Dry Days
4	Rx1	One-day annual highest rainfall amount	mm	High intensity rainfall
5	Rx5	Cumulative five-day annual highest rainfall amount	mm	Intense rainfall event magnitude
6	SDII	Average intensity of daily rainfall in a year/season (with rainfall intensity ≥ 2.5 mm/day)	mm/day	Daily intensity of rainfall
7	RRTOT	Ratio of seasonal precipitation to Annual precipitation (Seasonal precipitation /Annual precipitation * 100)	%	Seasonal Ratio of Precipitation
8	R100	No. of days in a year/season with rainfall intensity ≥ 100 mm/day	days	Very heavy rainfall
9	R65	No. of days in a year/season with rainfall intensity between 100mm/day and 65 mm/day	days	Heavy rainfall
10	R2.5-65	No. of days in a year/season with rainfall intensity between 65mm/day and 2.5 mm/day	days	Moderate rainfall
11	R40	No. of days in a year/season with rainfall intensity between 65mm/day and 40 mm/day	days	Average rainfall
12	R20	No. of days in a year/season with rainfall intensity between 40mm/day and 20 mm/day	days	Low rainfall

4.4.3 Statistical Tests for Trend Detection

4.4.3.1 Serial Correlation

Serial dependence between the data is checked using Lag-1 autocorrelation (Enders, 2002; Wilks, 2006). The correlation coefficient (simple) of the first observations $N-1$, X_t , $t = 1, 2, 3, \dots, N-1$ and the next observations, X_{t+1} , $t = 2, 3, \dots, N$ is the lag-1 autocorrelation coefficient. Equation 4.1 specifies the correlation between X_t and X_{t+1}

$$r_1 = \frac{\sum_{t=1}^{N-1} (X_t - \bar{X})(X_{t+1} - \bar{X})}{\sum_{t=1}^N (X_t - \bar{X})^2} \quad (4.1)$$

where $\bar{X} = \sum_{t=1}^N X_t / N$ = Mean of the time series.

The testing of the significance of the lag-1 autocorrelation coefficient r_1 is conducted. The limits of probability on the correlogram of a two-tailed tests' independent series is specified by Equation 4.2 (Meshram et al., 2016).

$$r_1 (95\%) = \frac{-1 \pm 1.96\sqrt{N-k-1}}{N-k} \quad (4.2)$$

where k denotes the lag and N denotes the sample size.

If the value of r_1 is beyond the aforementioned confidence interval, and serially independent if otherwise, then the data are presumed to be serially correlated.

4.4.3.2 Autocorrelation Removal

The outcome of the Mann-Kendall test can be influenced by the effect of auto-correlation. The probability of the incorrect rejection of the null hypothesis at the stipulated significant level is increased by a positive autocorrelation of the time series (von Storch and Navarra, 1995). Moreover, the trend's significance can possibly be underestimated if the data contains negative serial correlations (Yue et al., 2002). The serial correlation can be eliminated using several proposed approaches. Several researchers have commonly employed "pre-whitening" on the original dataset (Douglas et al., 2000; Burn and Hag Elnur, 2001; Zhang et al., 2001; Yue et al., 2002). The method of using pre-whitening in the removal of the effect of lag-1 serial correlations was originally proposed by von Storch and

Navarra (1995); however, an erroneous evaluation of a trend's significance can be probably caused by the method's capacity of eliminating a segment of the identified trend (Yue et al., 2002; Wu et al., 2008; Shifteh Some'e et al., 2012). Therefore, in the present study, Modified Mann-Kendall test has been utilized for overcoming the autocorrelation effect on the trend estimation.

4.4.3.3 Non-Parametric Versus Parametric Methods

Hydro-climatologic data do not typically satisfy the assumptions of the parametric test (i.e., linearity, normality, and independence) (Van Belle and Hughes, 1984; Helsel and Hirsch, 1988; Huth and Pokorna, 2004). A trend's statistical significance is determined by non-parametric methods employed in several studies (Harry et al, 1999; Zhang et al., 2001; Yue and Hashimoto, 2003; Xu et al., 2003; Kahya and Kalayci, 2004; Huth and Pokorna, 2004; Partal and Kalya, 2006). It has been evidenced that non-parametric approaches are appropriate for large sample sizes and commonly skewed data (Hirsch et al., 1982). Moreover, these approaches are not only inclined to be more unaffected by misbehaving data (e.g., outliers), but additionally offer outcomes similar to their parametric counterparts. Further, these methods are found to be within the limits of confidence limits even during normal distributions (Huth and Pokorna, 2004).

The above-mentioned points indicate the suitability of non-parametric methods for trend analysis. Further, these methods are more robust than their parametric counterparts. Regarding competence, i.e., capacity to differentiate between the null and alternative hypotheses, the Mann-Kendall test for monotonic trends (Mann 1945) outperform parametric tests (Kahya and Kalayci 2004). This is a non-parametric test that has been commonly utilized for evaluating the randomness against the hydrology and climatology trends (Kahya and Kalayci 2004; Alexander et al. 2006; Partal and Kahya 2006; Kiros et al. 2016; Kumar Raju and Nandagiri 2017). The challenge in utilizing the Mann-Kendall test is that the outcome gets modified if the analyzed time series contains serial correlations. A trend that is more frequent and random than the significant level is suggested by the test because of a positive serial correlation (persistence) existing in a time series Trend analysis in Turkish Rainfall data (Partal and Kahya 2006). The elimination of the impact of serial correlation through “pre-whitening” prior to the application of the Mann-Kendall test was

proposed by Von Storch (1995). Another option is to use the Modified Mann Kendall test that removes the effect of serial correlation in the dataset (Hamed and Ramachandra Rao 1998).

4.4.3.4 Background and Purpose of Mann-Kendall test

The Mann-Kendall test is a non-parametric test for identifying trends in time series data, based on the idea that a lack of trend should correspond to a time series plot fluctuating randomly about a constant mean level, with no visually apparent upward or downward pattern. If an increasing trend really exists, the sample taken first from any randomly selected pair of measurements should on average have a lower concentration than the measurement collected at a later point. The test compares the relative magnitudes of sample data rather than the data values themselves (Gilbert, 1987). One benefit of this test is that the data need not conform to any particular distribution. Moreover, data reported as non-detects can be included by assigning them a common value that is smaller than the smallest measured value in the data set. The procedure assumes that there exists only one data value per time period. When multiple data points exist for a single time period, the median value is used.

4.4.3.5 Assumptions and Requirements:

The following assumptions underlie the MK test:

When no trend is present, the measurements (observations or data) obtained over time are independent and identically distributed. The assumption of independence means that the observations are not serially correlated over time.

The observations obtained over time are representative of the true conditions at sampling times.

The sample collection, handling and measurements be normally distributed or that the trend, if present, is linear. The MK test can be computed if there are missing values and values below the one or more limits of detection, but the performance of the test will be adversely affected by such events. The assumptions of independence requires that the time between

samples be sufficiently large so that there is no correlation between measurements collected at different times.

4.4.3.6 Calculation of Mann-Kendall trend test

As introduced in the previous section, the Mann-Kendall (MK) is a non-parametric trend test that is often utilized for the discovery of significant trends in hydrologic data series (Patra et al., 2012). Equation 4.3 explains the S statistics for a series X_1, X_2, \dots, X_n in the MK test:

$$S = \sum_{i=1}^{n-1} \sum_{j=i+1}^n \text{sgn}(X_j - X_i) \quad (4.3)$$

where $i = 1, 2, \dots, n - 1$ and $j = i + 1$ and n is the dataset's length.

$$\text{Sgn}(\theta) = \begin{cases} +1 & \text{if } (X_j - X_i) > 0 \\ 0 & \text{if } (X_j - X_i) = 0 \\ -1 & \text{if } (X_j - X_i) < 0 \end{cases} \quad (4.4)$$

An upward or a downward trend is signified by a positive or a negative value of the test statistic S . The variance of the Mann-Kendall statistics is rendered by Equation 4.5.

$$\text{var}(S) = \frac{n(n-1)(2n+5) - \sum_{p=1}^n tp(tp-1)(2tp+5)}{18} \quad (4.5)$$

where tp is the number of ties existing up to sample i .

The standardized MK test statistic (Z_{mk}) can be calculated using Equation 4.6:

$$Z_{mk} = \begin{cases} \frac{S-1}{\sqrt{\text{var}(S)}} & \text{if } S > 0 \\ 0 & \text{if } S = 0 \\ \frac{S+1}{\sqrt{\text{var}(S)}} & \text{if } S < 0 \end{cases} \quad (4.6)$$

A standard normal distribution is followed by Z_{mk} . A negative value signifies a negative trend and a positive value signifies an upward trend. The cumulative probabilities of Z -

values are presented in Appendix 2 and 3. The null hypothesis is rejected and a trend is considered significant, if $Z_{mk} > Z\alpha/2$ (where α is the level of significance).

4.4.3.7 Modified Mann-Kendall (MMK)

MMK has been utilized to identify trends in data that is serially correlated. The significant values of ρk (autocorrelation coefficient) are utilized in this method for estimating the variance correction factor n/n_s^* . The variance of S is undervalued during the positive and auto correlation of the data.

$$n/n_s^* = 1 + \frac{2}{n(n-1)(n-2)} \sum_{k=1}^{n-1} (n-k)(n-k-1)(n-k-2) \rho k \quad (4.7)$$

Equation 4.8 is used to compute the revised Variance:

$$V^*(S) = V(S)X \frac{n}{n_s^*} \quad (4.8)$$

Where $V(S)$ is the same as was estimated using the Mann-Kendall approach.

4.4.3.8 Magnitude of Trend (Sen's Slope)

Apart from identifying the existence of a trend, a slope estimator β was utilized to compute the trend's magnitude. Hirsch et al. (1982) extended this slope estimator from an original proposal by Sen (1968). β is the robust value of the trend's magnitude. That is, the median overall probable combinations of pairs for the entire dataset is indicated by the slope estimator β (Hirsch et al., 1982). An 'ascending trend' (increasing values with time) is indicated by a positive value of β , while a 'descending trend' is indicated by a negative value of β (Xu et al., 2007; Karpouzou et al., 2010). Sen's slope estimated forecasts the trend's magnitude with the slope (Q) of all pairs of data. This magnitude can be gauged by using Equation 4.9.

$$Q = \frac{x_j - x_i}{j - i} \quad (4.9)$$

where x_j and x_i are regarded as the values of data at times j and i ($j > i$), respectively.

Sen's slope estimator is calculated as the median of Q 's N values by Equation 4.10 and Equation 4.11:

$$\beta = Q \frac{(N+1)}{2} \text{ if } N \text{ is Odd,} \quad (4.10)$$

$$\beta = (Q (N/2) + Q ((N + 2)/2))/2 \text{ if } N \text{ is even} \quad (4.11)$$

A positive value of β indicates an upward (increasing) trend in the time series and a negative value of β indicates a downward (decreasing) trend in the time series.

The direction of data trend is reflected by the sign of the β value, while the steepness of the trend is indicated by its value. The confidence interval of β at a particular probability should be obtained to ascertain whether there is any statistical difference between the median slope and zero. Equation 4.12 can be used to compute the confidence interval regarding the median slope.

$$C_\alpha = Z_{1-\frac{\alpha}{2}} \sqrt{\text{Var}(S)} \quad (4.12)$$

where Variance (S) is

$$\text{Var}(S) = \frac{1}{18} [n(n-1)(2n+5) - \sum_{p=1}^q tp(tp-1)(2tp+5)] \quad (4.13)$$

The standard normal distribution table is used to derive $Z_{1-\alpha/2}$.

The confidence interval's lower bounds (M1) and upper bounds (M2), are computed using Equation 4.14 and 4.15:

$$M_1 = \frac{N - C_\alpha}{2} \quad (4.14)$$

$$M_2 = \frac{N + C_\alpha}{2} \quad (4.15)$$

Sen's slope estimator was used to gauge the trend's magnitude. The trends were detected at 0.1% (extremely significant), 1% (significant), 5%, and 10% significance levels. The annual and seasonal variations of rainfall for each station/grid point were computed with respect to the mean and the variations are plotted over time.

4.5 RESULTS AND DISCUSSION

Within the context of global warming, extreme rainfall events have recently received much attention because they are the most sensitive to climate change than mean values. Extreme events are occasional occurrences and frequently are situated beyond the scope of most monitored data. Although there is a very low likelihood of these events, they are connected with abnormal effects and can result in significant losses and destruction due to their scale. These impacts may involve excessive loss of life, economy, or both. Extreme rainfall signifies the maximum rainfall events in a day within a year. Consequently, there are as many values of extreme rainfall events as the total number of years. The results of extreme rainfall analysis is provided under the following sub-headings.

4.5.1 Spatio-temporal patterns and Variability of Rainfall

The statistical analysis of the data grid of daily Rainfall is summarized in Appendix 1. The mean annual Rainfall in the LL regions varies between 3036 mm and 4496 mm respectively for narrow mountain ranges and broader coastal strips. Fig. 4.3 shows that the average annual rainfall of LL and HL regions is 3961 mm and 2342 mm respectively for the period 1901-2013. Appendix 1 represents the variance in the skewness was between -0.089 and 1.49, while the variance in the standard deviation of Rainfall was from 581 mm to 1881 mm. The largest positive skew distribution was found to have a mean value of 0.69. The yearly Rainfall during the period 1901- 2013 was asymmetric alongside the Western Ghats' ridge line. Three grid points, namely, LL1, LL14, and LL17, were found to have been lesser than the mean (i.e., on the left) whereas the remaining were higher than the mean (i.e., on the right). The variance in the kurtosis ranged from 0.03 to 4.88 with an approximate mean value of 1.55. The variance in the coefficient of variation (CV) of Rainfall ranged between 15.74% and 36.65%, adjoining the coastline (LL12) adjacent to the bottom of the Western Ghats (LL9). The coastal region's average CV was found to be 21.75%.

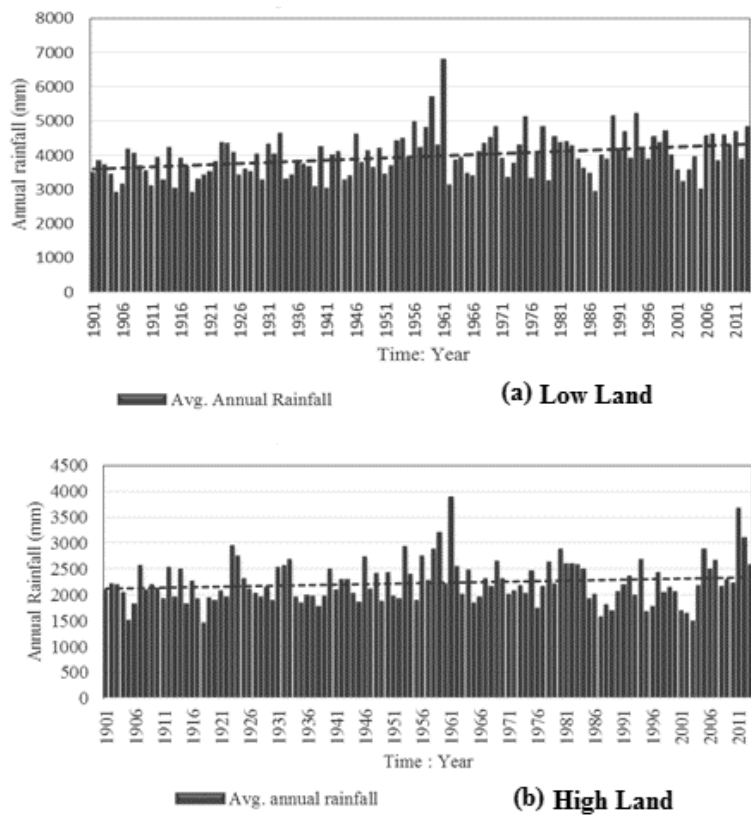


Fig. 4.3 Annual Rainfall in the (a) Low Land (Coastal Region) and (b) High Land (Western Ghats) regions of the west coast of Karnataka.

4.5.2 Trend analysis of ETCCDI rainfall Indices

The Expert Team for Climate Change Detection Monitoring and Indices (ETCCDMI) specifies information concerning extreme rainfall indices (e.g., type of rainfall, intensity and extremes, frequency, etc.) (Alexander et al., 2006). Indices related to extreme rainfall can be grouped into two categories: one computes the frequency (number of instances) of the index beyond or within its specified limit (CDD, CWD, R2.5-65, R40, R65, R100, and R20), while the second assesses the depth (mm) or intensity (mm per day) of rainfall (RR, SDII, RX1day, and RX5day). The separation of frequency and magnitude is anticipated to offer additional insights into the frequently slight variances in the climatic condition across the study area (i.e., the Western Ghats and the shoreline of Karnataka). Moreover, it is evident that these indices are also significant for the evaluation of the possible effect of climate changes on sub-humid to humid tropical environments associated with agriculture, forests, sustainable development, water resources, etc.

The trend analysis for rainfall indices was carried out for the annual and three principal seasons, namely monsoon (from June to September), north-east monsoon or post-monsoon (from October to November), and winter (from December to February). Table 4.2 summarizes the outcomes of the MK/MMK test (non-parametric) at a 5% level of significance. The majority of the Rainfall indices that were evaluated by the dataset's time series did not possess any significant lag-1 serial correlation coefficient. Table 4.2 summarizes each index's significant increasing and decreasing trends and the quantity of significant serial correlations, during the period of study from 1901 to 2013.

The outcomes of the statistical analysis for the annual rainfall trend detection at 95% confidence level revealed that the annual series (RR) was dominated by positive trends (Table 4.2). A positive trend was shown by 22 (58 %) of the 38 grid point and 16 grid points showed a negative trend. Whereas 16 grid point trends showed statistically significant increases at the 95% significance level (Table 4.2), the remaining 16 grid points showed a decreasing trend. However, only 5 grid points are statistically significant.

Table 4.2: Lag-1 significant serial correlations and MK/MMK Trend test results at the 5% level

Season	Variable	No. of significant Serial correlation	No. of Significant		No. of Non-Significant		No Trend
			increasing trend	decreasing trend	increasing trend	decreasing trend	
Annual	RR	7	16	5	6	11	--
	RX1	17	8	3	17	10	--
	RX5	9	11	5	11	11	--
	CWD	6	9	10	12	7	--
	SDII	5	14	12	8	4	--
	CDD	8	18	6	7	4	3
Monsoon	RRTOT	26	12	2	11	13	--
	CWD	14	10	4	14	10	--
	SDII	32	13	4	10	11	--
	R2.5_65	17	7	10	11	7	3
Pre- Monsoon	RRTOT	2	5	9	11	13	--
	CWD	12	2	6	5	8	17
	SDII	10	2	3	13	20	--
	R2.5_65	11	2	6	5	9	16
Post- Monsoon	RRTOT	8	--	4	10	24	--
	CWD	15	3	4	9	12	10
	SDII	10	--	3	19	16	--
	R2.5_65	17	3	4	7	13	11
Monsoon	R100	15	6	1	0	0	31
Frequency indices	R65	20	12	4	2	0	20
	R40	29	11	4	6	4	13
	R20	28	7	3	9	10	9

Similarly, the trend in total seasonal rainfall (RRTOT) reveals: (a) in monsoon season (JJAS), 23 (60%) out of 38 grid points are showed increasing trend. Whereas, 12 grid points are significant. (b) Pre-monsoon season (MAM), 16 (42%) grid points showing increasing trend and 22 grid points showing decreasing trend. Whereas, 5 and 9 grid points are showing statistically significant trends of increase and decrease. And (c) in Post-monsoon season (ON), 10 grid points showing increasing trend but not statistically significant. Whereas 28 (73%) out of 38 grid points are decreasing trend, but only 4 grid points are statistically significant.

Upon analysis of the overall trend in total rainfall of annual and seasonal regime, the results revealed increasing trend in annual rainfall due to predominant grid point are showing statistically increasing trend. In study region, about 80% of rainfall occurs in Monsoon season. Due to high contribution of monsoon rainfall to total annual rainfall, we could observe similarity in pattern of rainfall. To prove it, the monsoon season rainfall also indicating increasing trend with statistical significance. In pre-monsoon, 42% of grid points shows increasing trend and post-monsoon 73% of grid points are showing decreasing trend. From results shown above it can be concluded that there is a mixed trend of rainfall experienced in the study region (i.e., the Western Ghats and Coastal Karnataka).

4.5.2.1 Significance of ETCCDI extreme rainfall indices

The majority of indices based on extreme rainfall provide information on the “wetness”. The index CWD (Consecutive wet day) is a measure of rainy/wet day. In present study, rainy day is considered if the daily rainfall is greater than 2.5 mm according to IMD. CDD (Consecutive dry day) is the index that describes the dryness, often referred to drought indicator. The dry day is defined when daily rainfall is less than 1mm. CWD and CDD are duration indices which calculate the maximum length of wet and dry spell, respectively. Analysis of CWD and CDD could be performed using different threshold of rainfall for wet and dry days. The foremost contribution indices, RX1 and RX5, the intense 1 and 5 day intense rainfall respectively, these indices provide information of most intense-rain of the year. RX5 is a measure of short-term rainfall intensity and indicator for flood creating events. RR describes the total annual rainfall amount on wet days (CWD) of year, similarly RRTOT is a percentage ratio of seasonal rainfall with annual. SDII is a simple measure of

rainfall intensity that depicts the average amount of daily rainfall over all wet days in a year. There is no necessary relationship between RR and SDII and extremes of climate, however, these offer useful information regarding the association between changes in extreme conditions and other aspects of the distribution of daily rainfall events. The indices R100 (very heavy), R65 (heavy), R2.5-65 (moderate), R40 (average), R20 (low rainfall) are based on absolute thresholds, i.e. they directly measure the frequency of very wet days and they are highly correlated with total, annual and seasonal Rainfall.

4.6 Spatial distribution of interannual Rainfall indices and its trend

4.6.1 Spatial distribution and trends in Wet day Annual Total Rainfall (RR) and Simple Daily Rainfall Intensity (SDII) Indices

Generally any discussion on changes to extremes of rainfall begins with changes of RR index at local and regional levels. This is probably the most important parameter reflecting rainfall variations over the entire year which is one of the twelve rainfall indices analyzed in this study. Figure 4.4(a) illustrates the long-term annual Rainfall spatial distribution. The coastal region was found to have the maximum magnitude of annual Rainfall, while it decreased near the Western Ghats' eastern side. A similar outcome was derived by Tawde and Singh (2015) suggested that moist air from the Arabian Sea is raised by the mountain ranges causing a low-intensity Rainfall in the eastern side of the Western Ghats. The shoreline and areas near the coastal plains displayed intense Rainfall. In general, this is because of the orographic Rainfall Francis and Gadgil (2006). Fig. 4.4(b) depicts a low Rainfall on the Western Ghats' eastern side and a heavy Rainfall on the south-west section near the coast. The mean intensity of annual daily Rainfall (SDII), lowest value less than 6 mm/day displayed by the leeward side of the Western Ghats. Consequently, intense Rainfall was seen in the Western Ghats' windward side, i.e., the LL region. This could also be attributed to the fact that the Karnataka section of the Western Ghats is cascaded and wider resulting in intense Rainfall (Tawde and Singh, 2015; Vinay and Shetty, 2018). The range of CWD was found to be greater than 155 days in the Western Ghats and it is extended to around 65 days in the rain shadow region. Similarly the spatial variation of CDD found to be lesser than 170 days in the Western Ghats region and it extended upto about 260 days in leeward region.

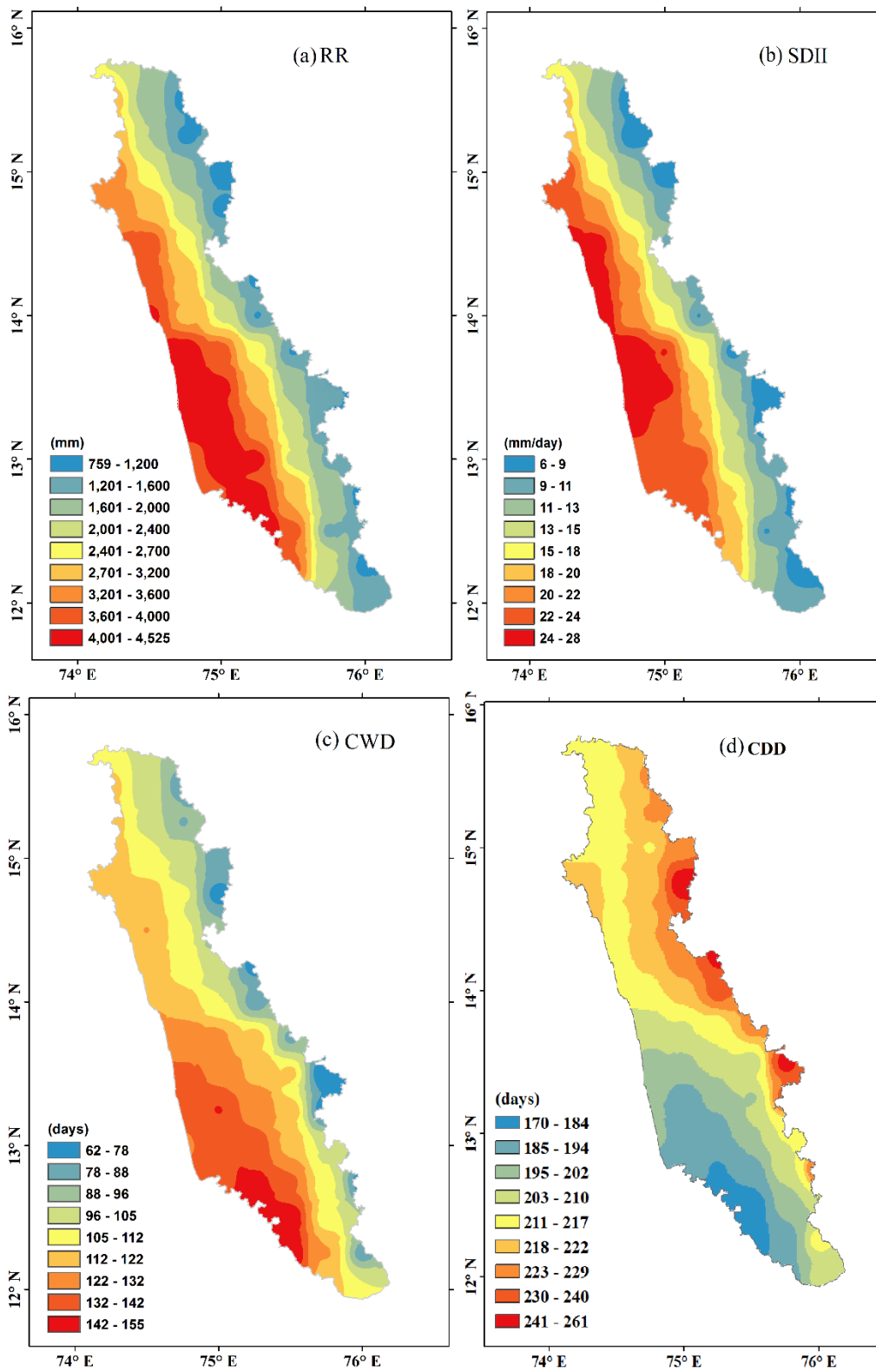


Fig. 4.4 Spatial distribution of annual rainfall indices (a) RR and (b) SDII (c) CWD and (d) CDD

With increasing gradient was demonstrated by the study regions' south-west region in the rainy days there is decreasing gradient of dry days (Fig. 4.4 ((c) & (d)).

The trend analysis outcomes for the general Rainfall indices are depicted in Fig. 4.5. The total annual Rainfall and RR illustrated a mixed trend over the 113 years of study (1901 to 2013), which ranged from -6.0 mm/year to 23 mm/year. It can be observed from Fig. 4.5 (a) that a significant increase at a confidence level of 99% was prevalent through most of the study area sections, especially the north-west region. A statistically significant rise in the trend was demonstrated by most of the grid points of the order 21 mm/year (at 99.9% confidence level) in the LL region. A mixed trend was shown by the mountainous HL region and a significant decrease in trend was shown by some of the grid points (8 mm/decade magnitude). Again, a significant rise (-2.6 days/decade to 2.4 days/decade) in trend was displayed by the study region and a mixed trend was depicted by the rainy days for most of the part (Fig. 4.5 (c)). Interestingly, a decreasing trend was observed in the number of rainy days (CWD) and an increasing trend was observed in the total annual Rainfall (RR). CWD shows mixed trend in both spatial and in significance level, but daily average and CDD are showing in agreement. Hence, a significant increase across most of the grid points could be observed in the trend of SDII with the values of SDII varying between 0.53 mm/day/decade and 1.6 mm/day/decade. These variations in trends increase the probability of the effect of topography, local urbanization, and global climate change on the Rainfall events. These outcomes are in agreement with Meher Homji's (1980) early study, which found that the intensity of Rainfall in Karnataka's Western Ghats is strengthened by the proximity of the sea.

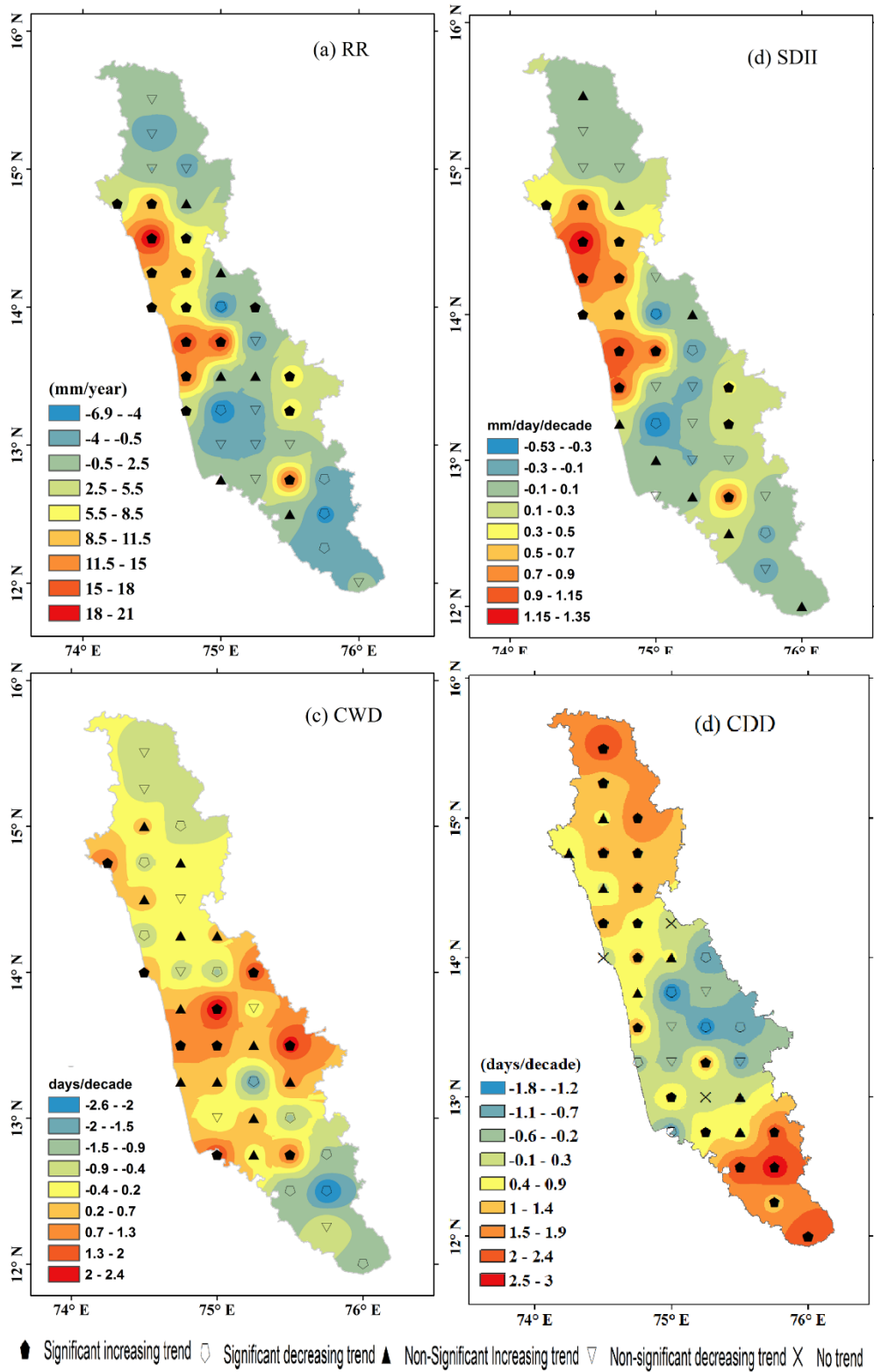


Fig. 4.5 Spatial patterns of temporal trends of the rainfall indices (a) RR, (b) SDII, (c) CWD and (d) CDD.

4.6.2 Changes in the Extreme Rainfall Depth and Intensity Indices

The index for one-day and five-day yearly highest Rainfall (Rx1 and Rx5) indicates that the LL regions' northern section and the HL regions' central section witnessed the highest values and Rx5 depicts intense rainfall along the western side of the Western Ghats (Fig. 4.6 (e)). The lowest values for Rx1 were found on Western Ghats' eastern side, that is, the eastern side of the HL region (Fig. 4.6 (b)). Rx5 is an indicator of short flood shows spatial variation is about 700mm high in along the coastal strip to about 200mm western side of the Western Ghats. Intense rainfall is related with wet and dry days, with increase in rainfall and decrease wet days (also means increase in dry days) leads to very heavy rainfall. The mean intensity of annual daily Rainfall (SDII), with intensity of Rainfall ≥ 2.5 mm/day, was almost comparable with Rx1 and Rx5 days (Fig. 4.6). Nevertheless, the northern part of LL and central part of HL displayed the highest intensity of about 28mm/day. Consequently, intense Rainfall was seen in the Western Ghats' windward side, i.e., the LL region. This could also be attributed to the fact that the Karnataka section of the Western Ghats is cascaded and wider resulting in intense Rainfall (Tawde and Singh, 2015).

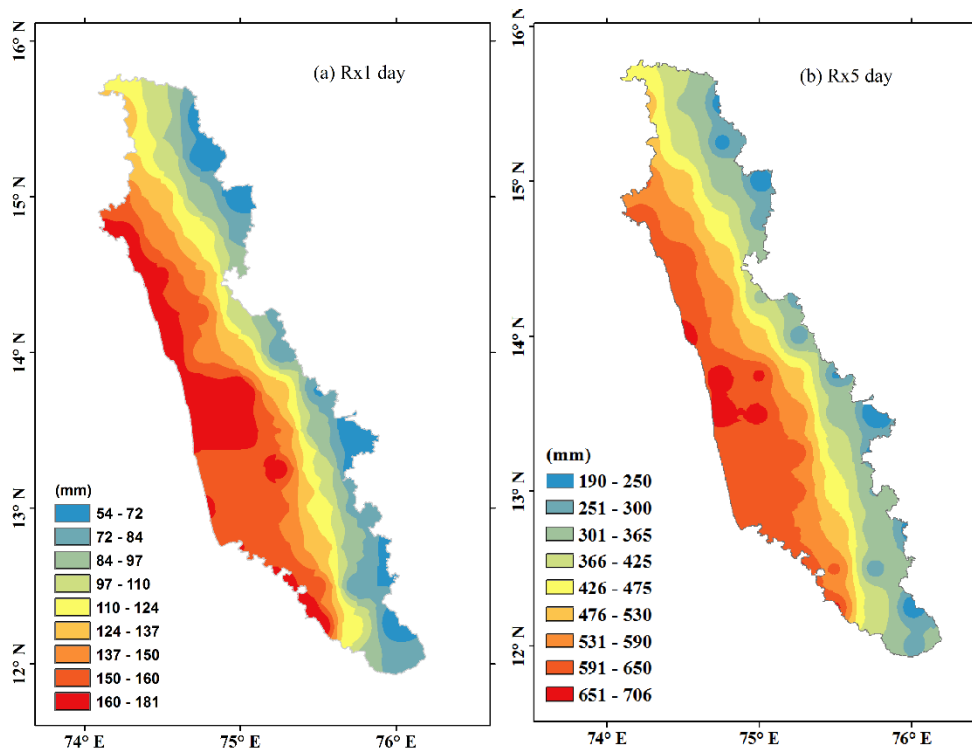


Fig. 4.6 Spatial distribution of annual rainfall indices (a) Rx1 and (b) Rx5

A decreasing trend ranging from -3 mm/decade to 9 mm/decade is shown by Rx1 in the study areas' south-east and central sections (Fig. 4.7 (a)). For the RX5 day index which corresponds to the maximum consecutive 5-day rainfall amount (a potential indicator of flood producing events). The trend magnitude varied from -14mm/decade to 32mm/decade, whereas there is significantly an increasing trend at maximum annual rainfall region of the study region. A scatter spatial distribution was possessed by the one-day and 5 day annual highest Rainfall amount (Rx1 and Rx5). Moreover, in comparison to the Rx1 index in the south of both LL and HL regions, the one in the north-west regions was found to be extremely strong. Rapid urbanization in the south-east and central HL regions of the Western Ghats could be considered to contribute to the decrease in Rx1 (Singh et al., 2014).

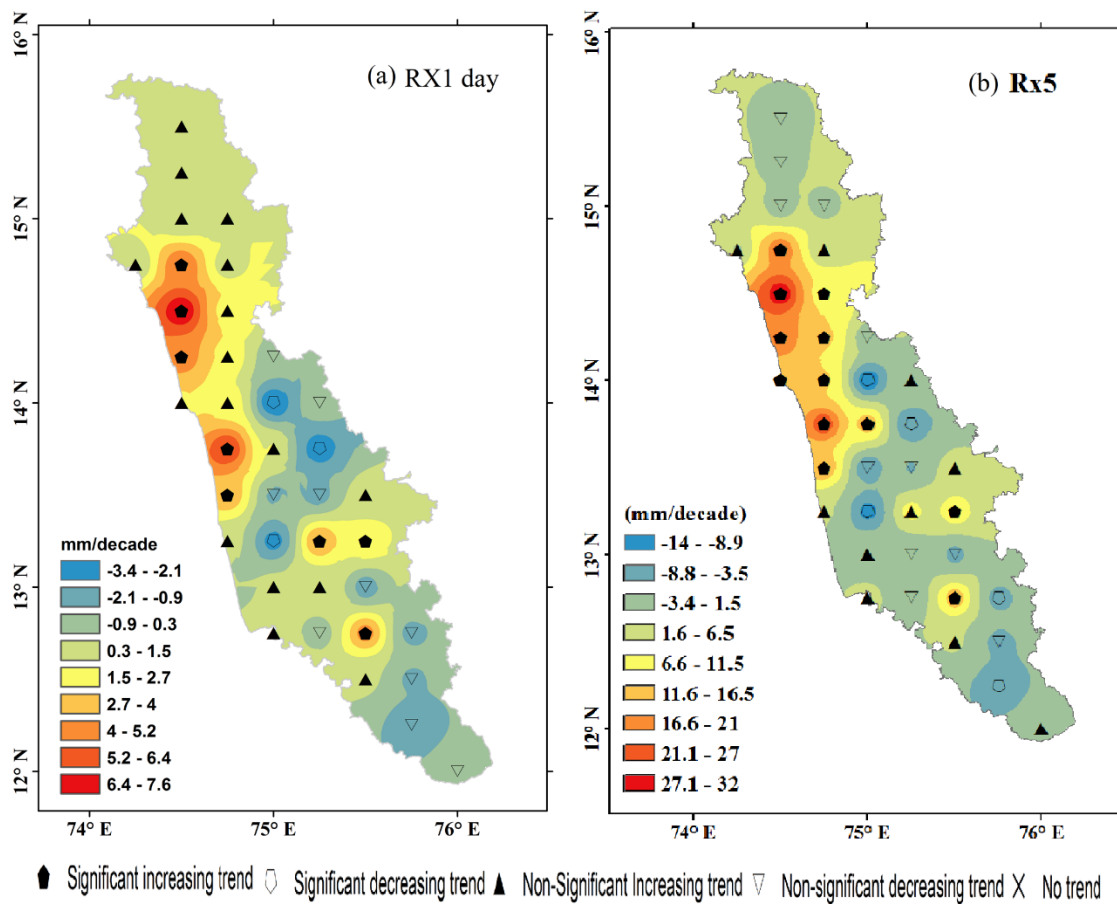


Fig. 4.7 Spatial patterns of temporal trends of the rainfall indices (a) Rx1, (b) Rx5

4.6.3 Inference of interannual temporal variation of extreme rainfall Indices

The spatial analyses of rainfall frequency suggested an increase in the frequency and contribution of the heavy rainfall in north-west portion of the LL and adjacent HL region. The study pointed out that the coexistence of shallow and deep convective clouds in the moist adiabatic stratification regime was the reason for this increase. The variations in the temporal features of the rainfall were also analyzed in the study. The study observed a decreasing trend in Rx1 in the central and south-east portion of the study area that ranges from -3 mm/decade to 9 mm/decade and also revealed an increase in the total annual rainfall (RR) and a considerable decrease in the number of rainy days.

The decrease in CWD implies a reduction in the number of wet spells, which could critically affect the water availability during the growing season of rain fed crops and result in reduced crop yields. Such spatio-temporal information would be useful for the planners and policy makers for implementation of location-specific adaptation and mitigation measures against drought vulnerability of the region. A strong correlation exists between total rainfall and other rainfall indices, especially heavy rainfall indices which are responsible for the increase in rainfall. The changes in the frequency and magnitude of extreme events would have adverse effects on human lives, infrastructure, natural resources and ecosystem.

These findings lead to the conclusion that the variations in trend is influenced by global warming, expanding urbanization and deforestation (Goswami et al. 2006; Guhathakurta et al. 2011). If the rainfall trend remains unchanged (Karuna Sagar et al. 2016), rainstorms and heavy Rainfall which may lead to serious consequences such as floods, landslides, etc. may be predicted in the future. The availability of water resources in the study region during the non-monsoon seasons may also get affected with the present trend in rainfall.

4.7 Seasonal analysis of Rainfall indices and trend

The present section to understand the seasonal variation of extreme rainfall indices of the study region. Appendix 4 presents the basic seasonal Rainfall statistical attributes of study region of Karnataka's Low Land (coastal region) and High Land (Western Ghats) regions. The CV ranges from 47.56% to 15.4% and the SD ranges from 1880mm to 398mm. The minimum Rainfall ranged from 2714mm to 609mm and the maximum Rainfall ranged from 9792mm to 3166mm, with the average Rainfall in the monsoon season ranging from 4496mm to 1168mm. The range of the mean seasonal Rainfall is from 272mm to 98.60 mm in the pre-monsoon period and from is 410mm to 152mm in the post-monsoon period. The SD ranged from 198.85 mm to 69mm in the pre-monsoon period and from 163mm to 84mm in the post-monsoon period. The CV ranged from 130mm to 44mm in the pre-monsoon period and from 63.72% to 39.53% in the post-monsoon period. These values indicate that there is more variability in regions with less rainfall than the regions with relatively greater rainfall. The data indicates that the maximum amount of Rainfall occurs with spatial variation across the study region in the monsoon season. It was found through the temporal distribution of seasonal Rainfall that the highest contribution of Rainfall was made by the monsoon season, followed by the pre-monsoon season and the post-monsoon season.

4.7.1 Spatial distribution of extreme Rainfall indices during monsoon season

A scrutiny was performed of the spatial dispersion of the average monsoon (July to September) Rainfall using values of gridded and high-resolution daily Rainfall from IMD for the study period of 110 years, which explains the study area's indices of Rainfall. The highest average magnitude of monsoon Rainfall was possessed by the coastal region whereas the lowest average monsoon Rainfall was possessed by the eastern section of the Western Ghats, i.e., the rain shadow region. Moreover, the shoreline and nearby hilly regions received intensified Rainfall, which could be explained by the orographic influence (Francis and Gadgil, 2006). Rainfall regimes display spatial variances in the area of study. It can be observed that there is a distribution of very heavy Rainfall near the coastline (Fig. 4.8a), which reduces to 20% of the maximum average daily Rainfall in the observed rain shadow region, as Tawde and Singh (2015) also described. A significant reduction in the

gradient in RR (from 4525 mm in the coastal region (low land) to 1168 mm in the Western Ghats' rain shadow region (high land)) is observed. The IMD refers to a day as rainy, if the Rainfall is either equaling or exceeding 2.5 mm. Nandargi and Mulye (2012) reported that the rainy days were approximately the same over the area of study. The norms of IMD (for a rainy day) were utilized by the present study to calculate the mean number of rainy days, since heavy Rainfall is received by the mountainous territory of the study area. It was observed that the range of consecutive wet days (CWD) was from 66 days on the Western Ghats' eastern side to 104 days on the shoreline (Vinay et al., 2017).

Further, the length of the study area's south-west portion witnessed an increased number of rainy days (Fig. 4.8b). The area composed of the northern section of the low land and the central section of the western portion of the high lands witnessed the highest intensity of the SDII's spatial distribution of more than 36 mm/day. Nevertheless, the leeward part of the Western Ghats appears to have the lowest intensity of SDII (<6mm/day). The occurrence of moderate Rainfall ($65 \text{ mm} > R \geq 2.5\text{mm}$) in the eastern portion of the Western Ghats was found to range from about 60 days to about 91 days in the study period of 110 years.

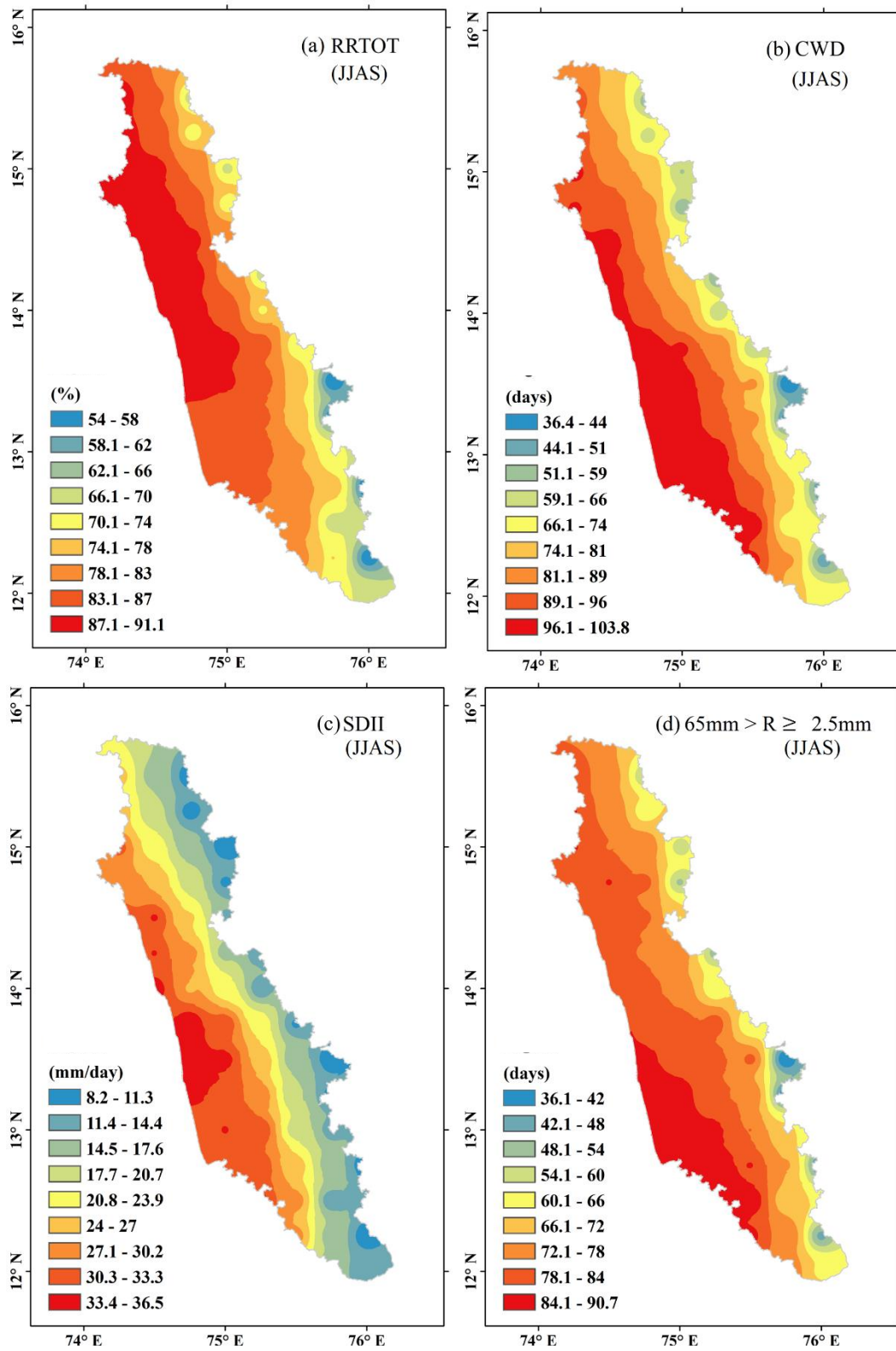


Fig. 4.8 Spatial distribution of Rainfall indices over the study region - Monsoon (JJAS) average values (a) RRTOT, (b) CWD, (c) SDII and (d) R2.5_65

4.7.2 Spatial patterns of temporal trends of the extreme rainfall indices during monsoon season

Thus, the low land region of the Western Ghats, i.e., the windward side, experiences intense Rainfall. This indicates that extreme Rainfall is caused by Karnataka's longer and broader (i.e., cascaded) mountains. In contrast, the leeward side (i.e., rain shadow region) is strengthened by the barriers formed by the mountains. Fig. 4.9 depicts the general Rainfall indices' spatial patterns from 1901 to 2013 in the study area. A trend of assertion is demonstrated by the ratio of seasonal Rainfall to total Rainfall (RRTOT). The RRTOT values range from -0.35%/decade to 0.99%/decade during the study period of 110 years (Fig. 4.9a). Moreover, a growing tendency for monsoon Rainfall is demonstrated by the neighboring mountainous regions of the southern coastal plains and a decreasing tendency for monsoon Rainfall is demonstrated by the Western Ghats, which are the neighboring regions of the southern coastal plains. On the contrary, the cascaded mountainous region (HL) rendered an assorted trend of statistically significant and insignificant values with the increasing and decreasing Sen's slope during the study period of 110 years. SDII results from increase in seasonal Rainfall and decrease in rainy days. Consequently, a significant primarily increasing trend of SDII (between -0.68 mm/day/decade and 1.79 mm/day/decade) can be seen across most of the grid points. The highest positive trends along with the almost comparable SDII patterns were displayed by the study area's north-west regions. A mixed trend of moderate Rainfall ranging from 1.62 days/decade to 1.99 days/decade was demonstrated by the study region during the study period of 110 years from 1901 to 2013. Interestingly, an increasing trend was depicted by the RRTOT, while a significant decreasing trend was depicted by the moderate Rainfall over the study region. Thus, it can be inferred that a significant increase in heavy Rainfall ($\geq 65\text{mm}$) is experienced by the northern coastal plains.

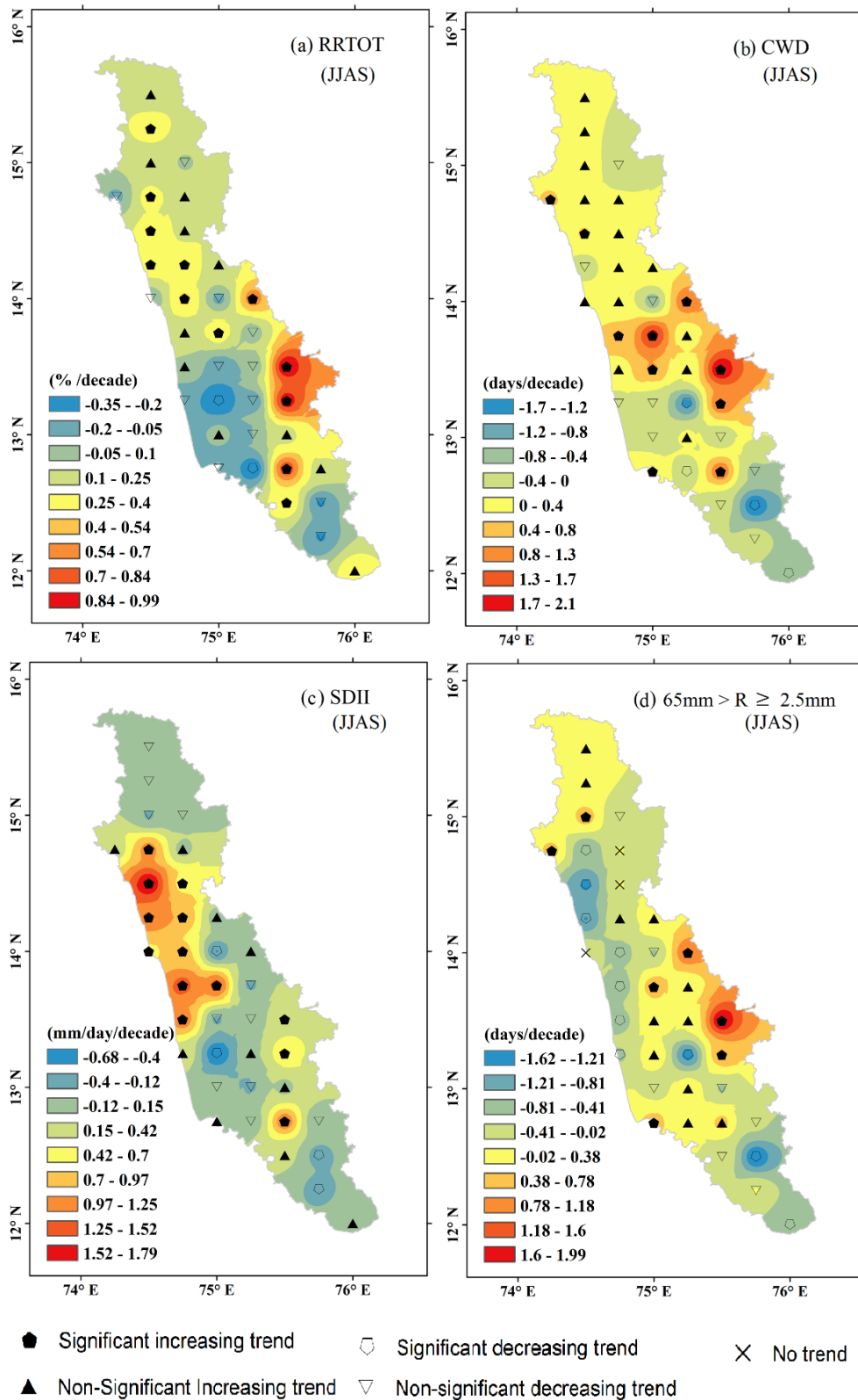


Fig. 4.9 Spatial patterns of trends for Rainfall indices over the study region - Monsoon (JJAS) period (a) RRTOT, (b) CWD, (c) SDII and (d) R2.5_65

4.7.3 Spatial distribution of extreme Rainfall indices during pre-monsoon season

The pre-monsoon season (March to May) spatial variation is depicted in Fig. 4.10. As shown in Fig. 4.10(a), the ratio of Rainfall to the total yearly Rainfall ranges between 2.9% and 21% in the pre-monsoon season. The western section of the Western Ghats was partially found to receive higher Rainfall during the pre-monsoon season than other sections. The eastern sections of the Western Ghats and the coastal plains receive a low Rainfall. The frequency and variation of the pre-monsoon Rainfall wet spell is from 6 days to 25 days. The variation in rainy days (CWD) is depicted in Fig. 4.10 (b). A decreasing gradient can be seen from the study area's south-west region to the study area's north-eastern regions. There is a variance from 7.3 mm/day to 14.3 mm/day in the simple daily Rainfall index. The rarity of heavy Rainfall events is indicated by the pre-monsoon season depiction of a similar pattern of moderate Rainfall and rainy days (CWD). The SDII in pre-monsoon season oscillates between 7.3 mm/day and 14.3 mm/day. Low magnitude Rainfall is depicted in the interior portion of the hilly terrain. Thus, the pre-monsoon season in the study area illustrates the dominance of a moderate range of Rainfall ($65 \text{ mm} > R \geq 2.5 \text{ mm}$). The spatial pattern of moderate Rainfall varies from 5.6 days to 25 days and is found to be similar to rainy days.

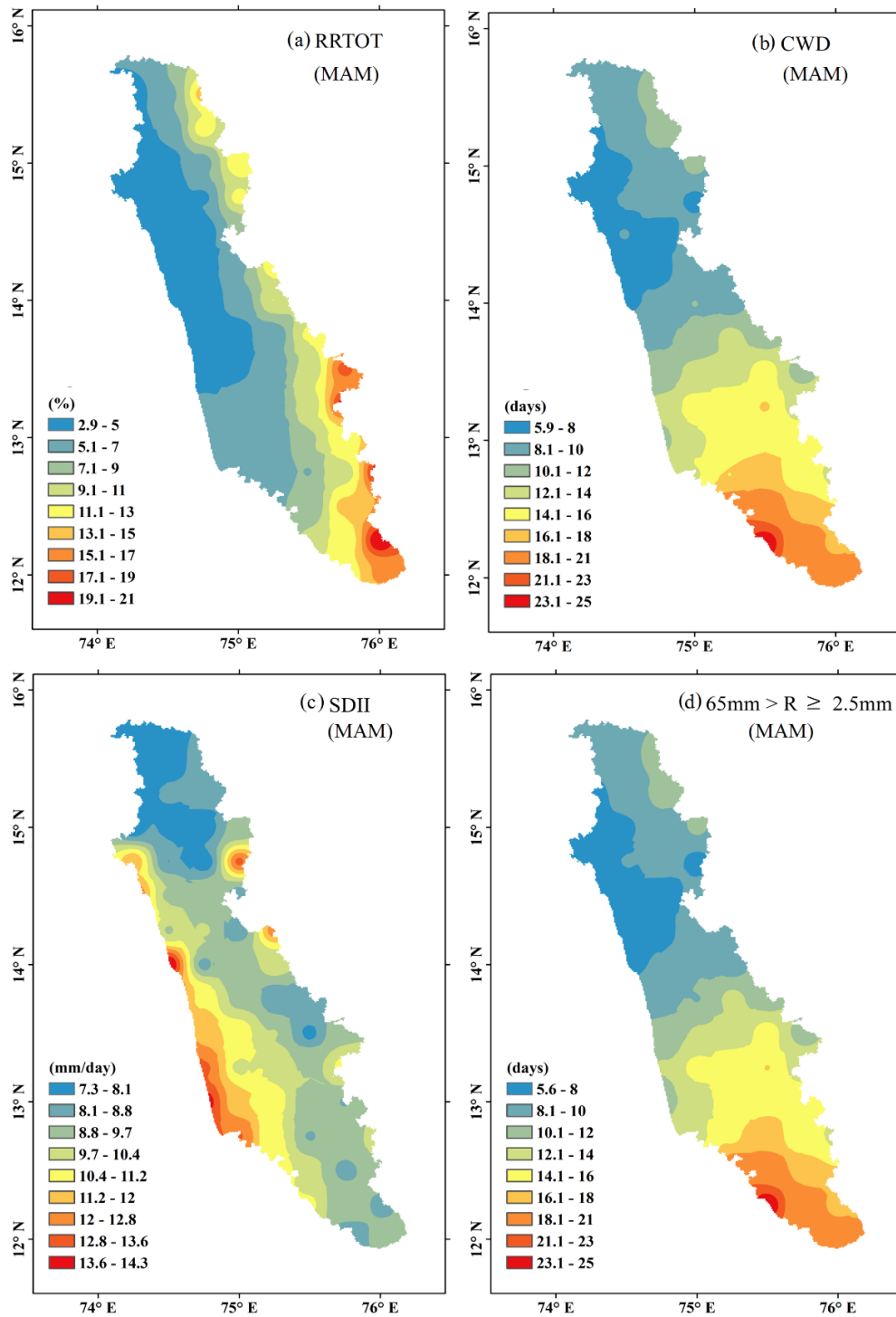


Fig. 4.10 (a-d) Spatial distribution of mean values of Rainfall indices over the study region - Pre-Monsoon (March-May).

4.7.4 Spatial patterns of temporal trends of the extreme rainfall indices during pre-monsoon season

Fig. 4.11 depicts the Rainfall trends' spatial pattern in the pre-monsoon season. An increasing trend in the range from $-0.48\%/decade$ to $0.24\%/decade$ is demonstrated by the ratio of the seasonal Rainfall to the total yearly Rainfall in the adjacent regions and the southern coastal plains of the Western Ghats. During the pre-monsoon season, significantly decreasing trends are shown by some of the grid points in the hilly terrain, denoting the presence of a high spatial variation in Rainfall. The seasonal rise in the Rainfall's intensity is indicated by the relationship of CWD, RRTOT, and SDII to surge in the seasonal Rainfall's percentage with daily intensity and rainy days. An assorted trend is shown by CWD ranging from -0.8 days/decade to 0.75 days/decade. Similarly, a mixed trend ranging from -0.55 mm/day/decade to 0.43 mm/day/decade is shown in the low magnitude daily intensity index in the Sen's slope. Similarity in the spatial variation of patterns of Rainfall, ranging from -0.8 days/decade to 0.73 days/decade, could be observed between the moderate Rainfall and CWD. The moderate Rainfall of the region and the spatial patterns of the rainy days show an increasing trend, which is in agreement with RRTOT.

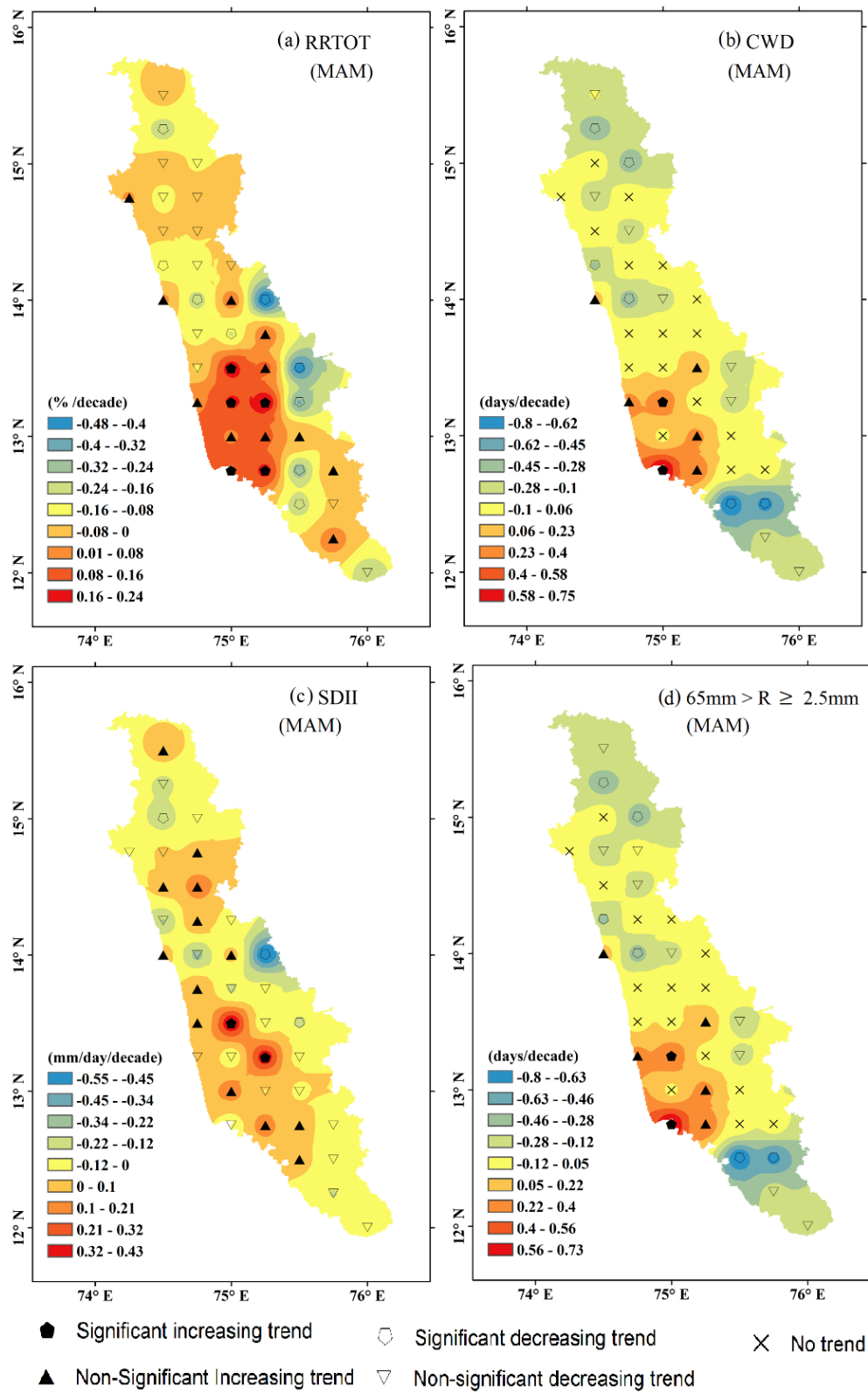


Fig. 4.11 (a-d) Spatial patterns of trends for Rainfall indices period over the study region - Pre-Monsoon (March- May).

4.7.5 Spatial distribution and temporal trends of the extreme rainfall indices during post-monsoon season

The study period's spatial patterns of Rainfall for the post-monsoon season are depicted in Fig. 4.12. A variance in the ratio of the seasonal Rainfall to the total annual Rainfall can be observed in the range from 5.5% to 25.7% (Fig. 4.12a). The frequency of rainy days varied from 9 days (in the north-east region) to 27 days (in the south-west region) in the post-monsoon season. The study area's south-west region was found to have a concentration of rainy days. The daily intensity index in the study region ranged between 9.3mm/day and 15.3mm/day in the post-monsoon season. In the south-west region, moderate Rainfall was found to resemble CWD with a range of 9 days to 27 days.

The trends of the seasonal Rainfall's (post-monsoon) spatial patterns for the study period are depicted in Fig. 4.13. A mixed trend was observed in the ratio of post-monsoon season Rainfall (RRTOT) ranging from -0.43% to 0.17%, with a principally decreasing trend. Some of the grid points showed significantly reducing trends in the post-monsoon season. A primarily declining trend ranging from -0.48 days/decade to 0.64 days/decade is seen in the post-monsoon season for CWD. In contrast, an increasing trend is shown by some grid points in the neighboring mountainous regions and the southern part of the coastal plain. The daily intensity index depict an increasing trend in the northern section of the study area, and a mixed trend in the remaining sections. Moderate Rainfall and CWD were comparable with values ranging from -0.51 days/decade to 0.62 days/decade.

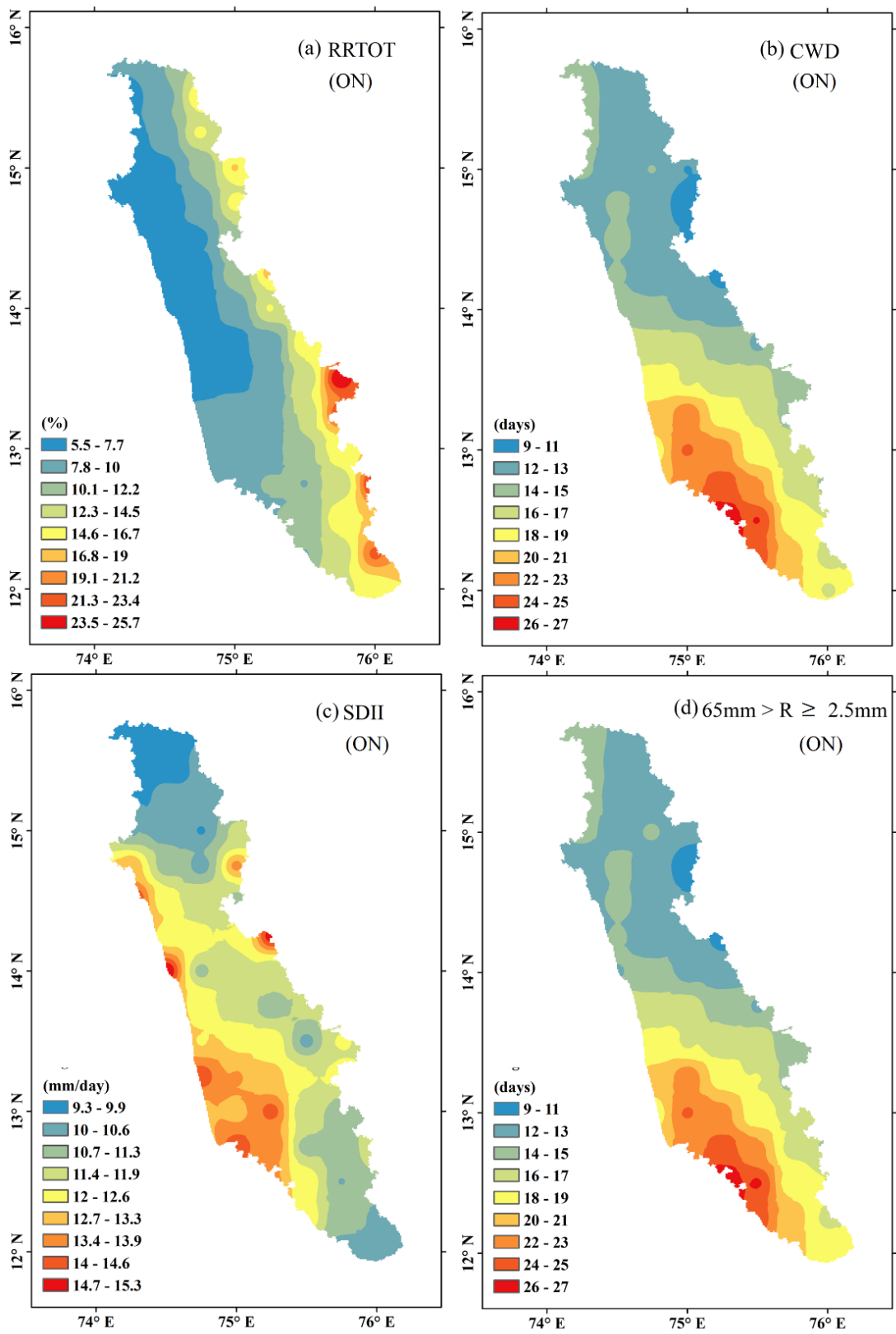


Fig. 4.12 (a-d) Spatial distribution of average values of Rainfall indices over the study region - Post-Monsoon (October-November).

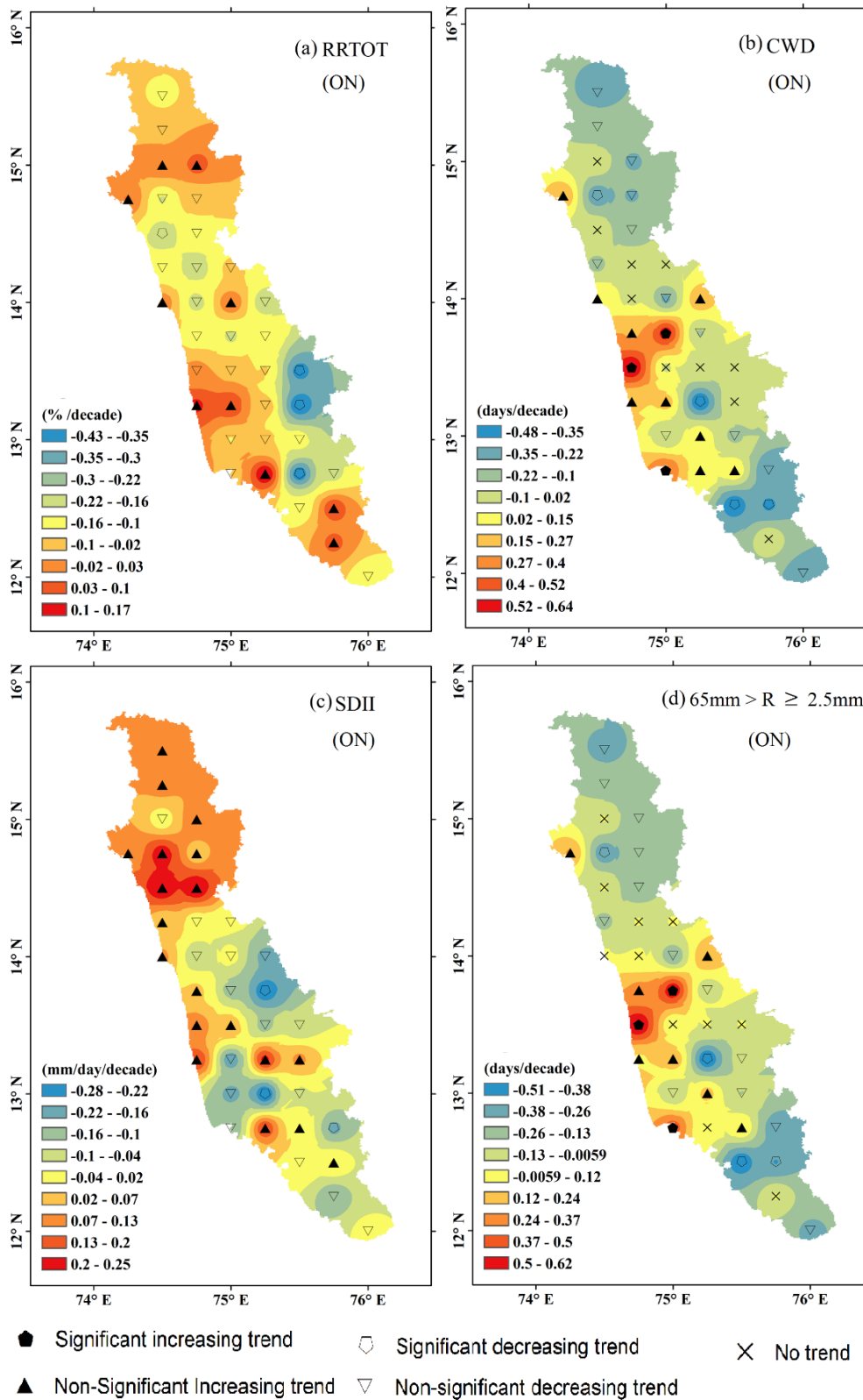


Fig. 4.13 (a-d) Spatial patterns of trends for Rainfall indices over the study region - Post-Monsoon (October-November).

4.8 Spatial Distribution of Threshold Rainfall Indices

The spatial distribution of the monsoon season averages of the indices for extreme Rainfall event frequency during 1901-2013 over the LL and HL regions is depicted in Fig. 4.14. Intense Rainfall is demonstrated by the confluence section between the shoreline and the coastal plains and the Western Ghats (western part). The coastal regions witnessed a common occurrence of intense rain events, which is in harmony with the outcomes. Moreover, comparable outcomes have been reported previously (e.g., Konwar et al., 2012; Francis and Gadgil, 2006). Interestingly, the spatial distribution of Rainfall was dominated by moderate Rainfall over the HL (elevated) regions (Konwar et al., 2012, 2014). A decreasing gradient was evident on the Western Ghats' eastern side (from west to east) due to the events of very heavy rainfall (R100) for more than 8 days and heavy rainfall (R65) for more than 12 days in the LL region (Fig. 4.14 (a and b)). The spatial distribution of average threshold Rainfall was between 1 day and 35 days, and the spatial distribution of moderate threshold Rainfall was between 62 days and 139 days (Fig. 4.14 (c and d)). The process of condensation over the HL region (i.e., mountainous terrain) was forced by the induced shallow convective orographic clouds resulting in low Rainfall (Revadekar et al., 2011; Konwar et al., 2012, 2014). The variance in the R20's spatial distribution was 7 to 36 days (Fig. 4.14 (e)). The study area's south-western region had a higher number of low Rainfall days. The spatial distribution shows consistent values for the indices for heavy Rainfall to low Rainfall intensity days. While the coastal region witnessed the extreme values, the leeward side of the study area displayed a decreasing gradient of low intensity Rainfall.

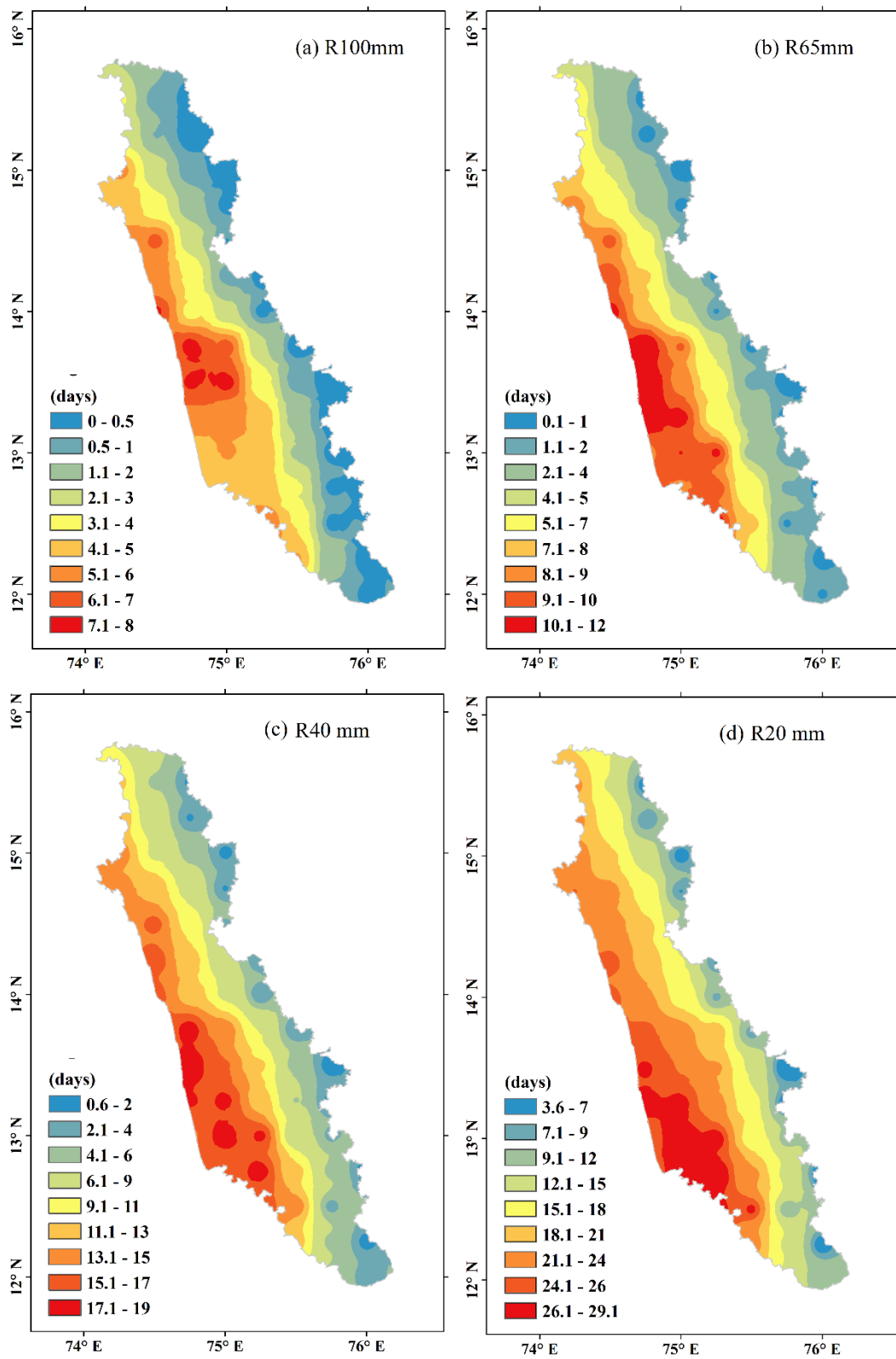


Fig. 4.14 (a-d) Spatial distribution of average values of the extreme Rainfall event frequency indices during 1901-2013.

Fig. 4.14 demonstrates the spatial patterns of trends over the study area with regards to the frequency of Rainfall indices. No trend was identified by the spatial patterns of the Rainfall frequency indices (used for present study) in some of the grid points in both LL regions and HL regions. The indices for heavy rainfall (R65) and very heavy rainfall (R100) indicate a significant rise in the trend. However, a decline in the trend (ranging between 0.74 days/decade and -0.217 days/decade and between 0.73 days/decade and 0.51 days/decade) is illustrated by some of the grid points (Fig. 4.14 (a and b)). Fluctuating between -2.61 days/decade and 1.96 days/decade, an assorted trend was demonstrated by the moderate rainfall event (R2.5-65) (Fig. 4.14 (c)). An increase in trend from both regions by 17 grid points is exhibited by the R40 index; whereas, a significant increase in trend of magnitude 0.81 days/decade was observed in LL. A significant decrease in the trend is shown in some of the grid points, whereas a significant increase in the trend is shown in the R20 rainfall event in the HL region. The overall range varied between 9.37 days/decade and 0.605 days/decade. A comparable pattern of spatial distribution was found in the Rainfall indices of mean to very heavy Rainfall frequencies, with a significant increase and decrease in trends.

Consequently, an increase in the contribution and frequency of heavy Rainfall in the neighboring HL regions and the north-west portion of the LL is suggested by the preceding spatial analysis of Rainfall frequency. This finding is in agreement with the findings of Mahesh Kumar et al. (2014) who demonstrated a significantly increasing trend in Rainfall events in the western sections of the HL and the LL regions of the Western Ghats. The present research contended that such a finding could be chiefly attributed to the co-occurrence, in the moist adiabatic stratification system, of deep and shallow convective clouds. Moreover, the observations of the present study are also supported by the study of Francis and Gadgil (2006), who posited that offshore vortices and troughs cause heavy rainfall between mid-June and mid-August.

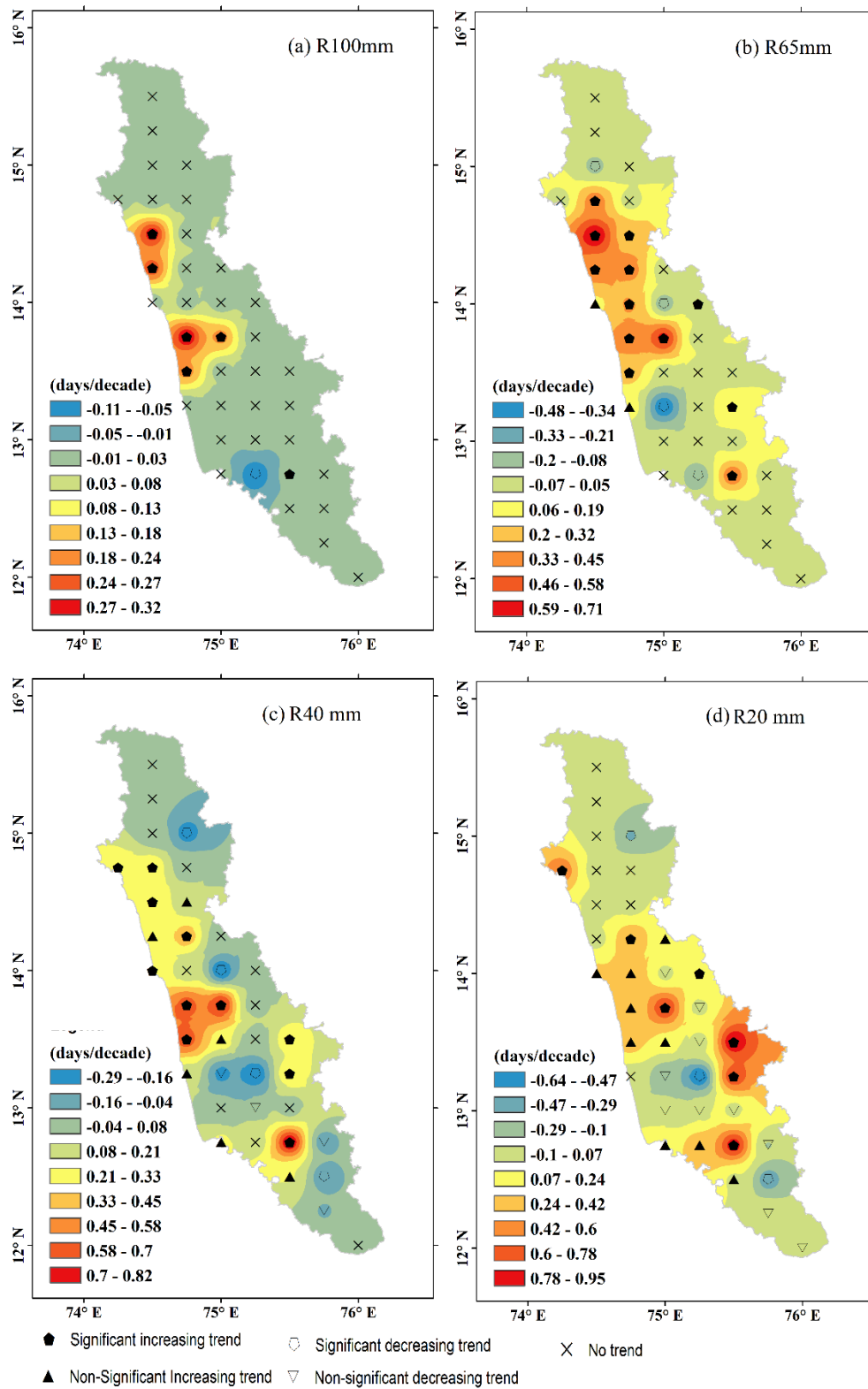


Fig. 4.15 (a-d) Spatial patterns of trends for the frequency of extreme Rainfall indices over the study region during 1901-2013.

4.9 Correlation of annual Rainfall Indices

Fig. 4.15 shows the relationship between the indices for annual Rainfall with mean annual Rainfall and assessed at 99% confidence level. The outcomes signify a high correlation among the indices of rainfall frequency (R20, R40, R65, and R100). Moreover, the total yearly rainfall over the HL and the LL regions concurred with the current study. The correlation of ETCCDI extreme rainfall Indices with total rainfall over HL and LL tabulated in the Table 4.3. The coefficients of correlation were 0.83, 0.84, 0.78, and 0.42 over the LL region; whereas, the correlation coefficients were 0.71, 0.79, 0.83, and 0.66 over the HL region (Fig. 4.13 (d-f)). At a confidence level of 0.01, the coefficients of correlation were found to be statistically significant. Over the LL region, the heavy rainfall was found to contribute to the increase in the rainfall during the study period. Nevertheless, low rainfall indices illustrate the significant relation of R20 in the HL regions and R40 in the LL regions. Additionally, at a confidence level of 99%, the coefficients of correlation for RR and Rx1 day, SDII, and CWD were found to be significant (Fig. 4.15 (a-c)), with values of 0.57, 0.59, and 0.88 (HL region) and 0.55, 0.54, and 0.86 (LL region). The correlation coefficient (for moderate rainfall (R2.5-65)) was statistically insignificant (<0.30) in the LL region and 0.33 in the HL region. Rainy days and one-day maximum rainfall caused lesser impact and lower variation on the total annual rainfall during the study period (1901-2013) over both the regions.

Table 4.3: Correlation analysis of annual rainfall with extreme rainfall indices

Indices	Co-efficient correlation (r)		Indices	Co-efficient correlation (r)	
	HL	LL		HL	LL
(a) Rx1	0.57	0.56	(f) R100	0.71	0.83
(b) Rx5	0.73	0.72	(g) R65	0.79	0.84
(c) CWD	0.51	0.54	(h) R40	0.83	0.78
(d) SDII	0.88	0.86	(i) R20	0.65	0.42
(e) CDD	-0.35	-0.29	(j) R2.5_65	0.33	0.13 [#]

statistically insignificant at 1% significance level

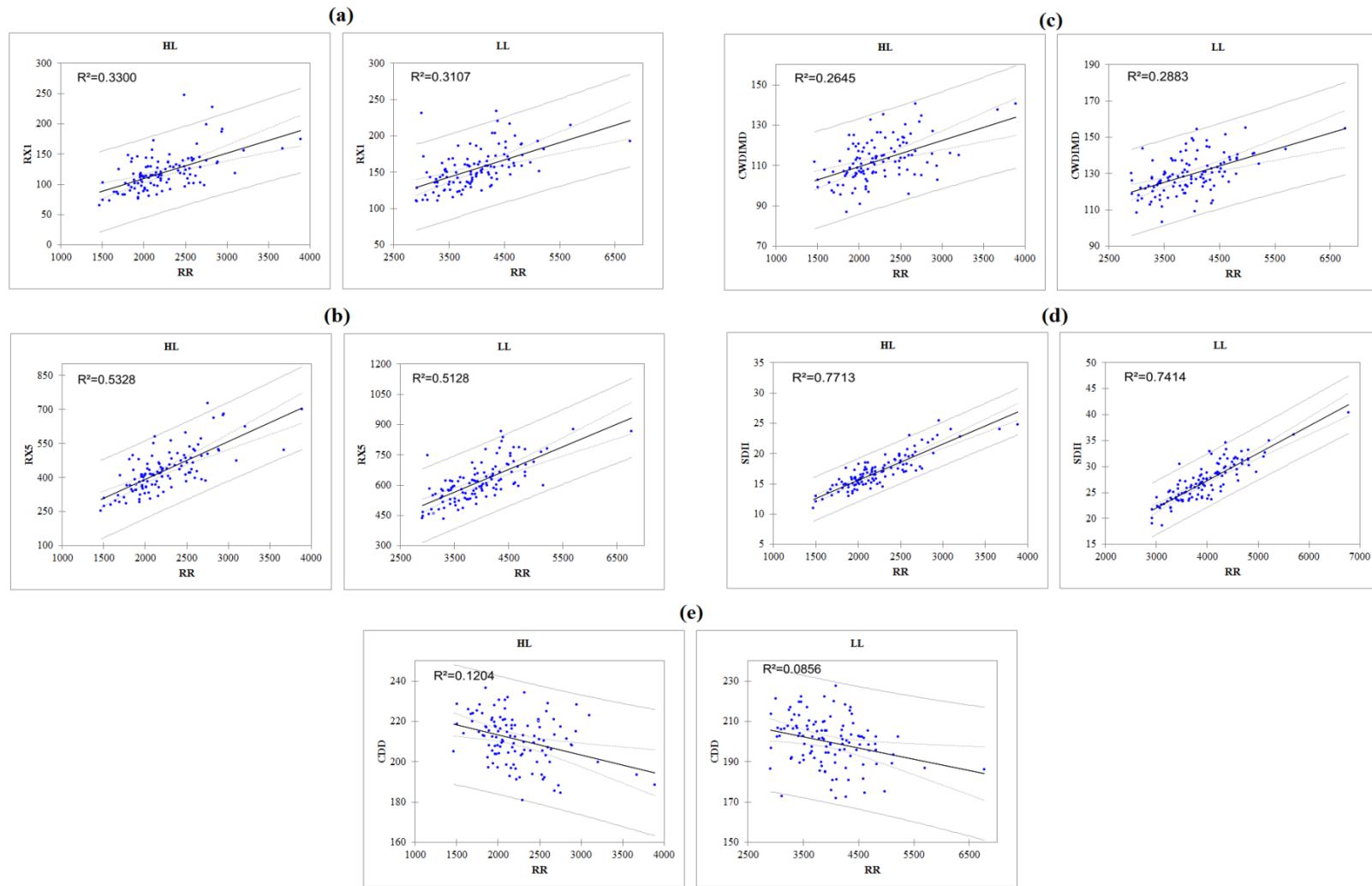


Fig. 4.16 (a-j) Correlation between total annual rainfall and annual Rainfall indices over LL and HL regions during 1901-2013.

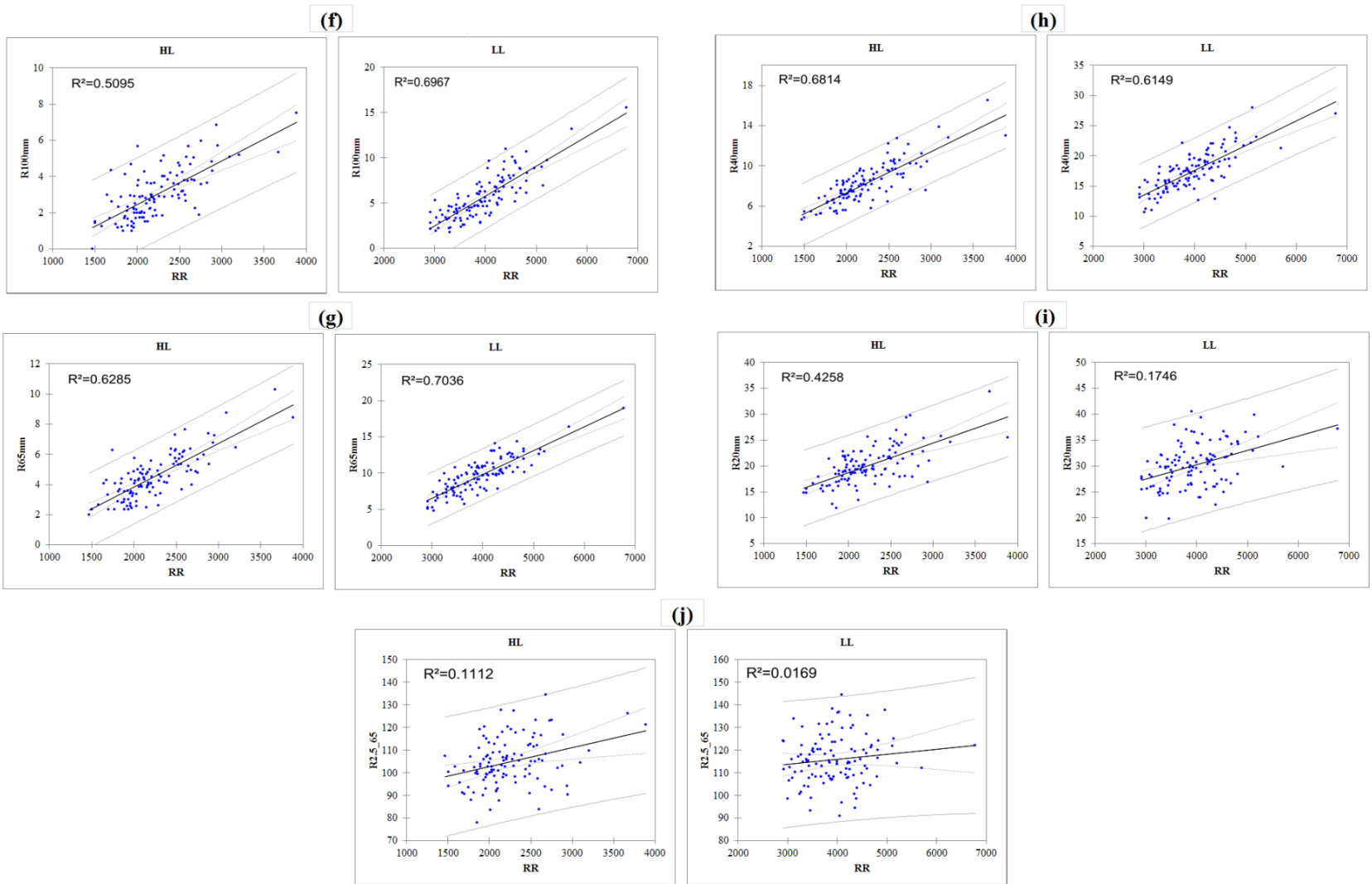


Fig. 4.15 Continued

4.10 Conclusions

The present study was taken up for the analysis of annual and seasonal Rainfall variation with the association of ETCCDI extreme Rainfall indices. The analysis was based on the frequency and the intensity. Based on the trend analysis of Rainfall indices, the following conclusions are drawn:

- The annual rainfall spatial variation shows intense towards western side of the Western Ghats due to orographic effect and gradually decreases towards eastern side of Western Ghats due to losing moisture flux in transition from west to eastern side of the study region. Lesser the advection time leads to more carry-over of moisture content to the peak of mountain (Jiang and Smith 2003). Daily average (SDII) and annual rainy days (CWD greater than equal to 2.5mm) varies in similar pattern of highest 28mm/day to least 6mm/day and 155 days to 62 days from west to eastern side of Western Ghats of Karnataka. Similar results found with Varikoden et. al., (2019) shows negative trends in rainfall in the southern region, with high values (more than 1.6 mm day⁻¹ decade⁻¹) over the area bounded by 75.5°E–76.5°E and 11°N–12°N. The coastal regions south of 13°N experience dry conditions as evidenced by the negative trends in rainfall. In the northern region, an increasing trend is observed north of 13.5°N up to 17°N. The wetting trend is more in the low altitude plains, oriented southeast to northwest between longitudes 73.75°E and 74.75°E and latitudes 14°N and 16°N, and is exceeding 1.6 mm day⁻¹ decade⁻¹.
- The intense rainfall indices Rx1 and Rx5 are observed during the months of the monsoon season (JJAS), one day intense rainfall is concentrated at center region of coastal region and towards northern portion of the coastal region because of high orographic effect due to local topography. Rx5 is an indicator of short flood shows spatial variation is about 700mm (15 % of annual rainfall) high in along the coastal strip and southern portion of western side of the Western Ghats. The time series average (113 years) of intense rainfall indices gradually decreases towards eastern side of Western Ghats. Intense rainfall is directly related with wet and dry days, with increase in rainfall and decrease wet spells leads to very heavy rainfall.

- The spatial pattern of trend in rainfall indices show significant for all the indices at 95 to 99.9% confidence level. Trend in an annual rainfall is significantly increasing along coastal strip and depicts mixed variations at mountainous terrain. The daily average, wet and dry spells rainfall indices are interlinked each other and predominantly influence the intensity of rainfall events. CWD shows mixed trend in both spatial and in significance level, but daily average and CDD are in agreement. With increase in dry spell the daily average rainfall increases by supporting the intense rainfall events. Rx1 and Rx5 intense rainfall indices depicts mixed trend pattern but the similarity shows in significantly increasing and decreasing trend and are in agreement. Vinnasri and Dhanya (2016) though characteristics of extremes are observed to be highly localized, apparent signs of wet regions turning drier and dry regions turning wetter are obtained at Indian scale.
- The monsoon season temporal trend shows significant spatial variations over the study region. The seasonal ratio of Rainfall (RRTOT) exhibits a mixed trend, but a significantly rising trend is witnessed in the southern coastal plains and the adjacent Western Ghats region during the pre-monsoon. The southern coastal plains show a decreasing trend in the monsoon period (JJAS). Possible shift in pattern of rainfall is estimated by determining the changes in the onset and return levels (Vinnarasi and Dhanya 2016).
- The rainy days and the mean daily intensity of Rainfall are correlated to seasonal Rainfall. The rainy days show the spatial variation to be similar to the seasonal ratio of Rainfall, whereas the daily intensity Rainfall depicts a substantially increasing trend in the northern coastal plains and its adjacent terrain region.
- In the pre- and post-monsoon rainy days, the daily intensity index illustrates a mixed trend over the study region. Most of the grid points show no trend for rainy days and moderate Rainfall. A few grid points depict a mixed trend with a low magnitude of Sen's slope.
- The present trend in the contribution of Rainfall over the Western Ghats and the west coast of Karnataka is observed during the monsoon season followed by the pre-monsoon and the post-monsoon seasons. Vinnarasi and Dhanya (2016) detailed investigation on various characteristics of extreme events though provides sufficient proof regarding the abrupt variations in the rainfall distribution; however, no generic statement of increase or

decrease in extremes derived since the rainfall seems to be significantly influenced by local factors than global influences.

- A statistically significant increasing trend exists in the frequency of very heavy and heavy Rainfall events and a significantly decreasing trend exists in the frequency of moderate Rainfall at the region of heavy Rainfall events. This observation is in contrary with the observation made by Jun et al. (2015) over Indian scale.
- A strong correlation exists between the total Rainfall and other Rainfall indices, especially the heavy Rainfall indices. The magnitude of intense Rainfall is responsible for the increase in the annual total Rainfall.

The asymmetric relationship of individual Nino indices with rainfall extremes discussed in Chapter 5.

CHAPTER 5

ENSO INDICES INFLUENCE ON EXTREME RAINFALL EVENTS

5.1 INTRODUCTION

The chapter 4 shows the spatio-temporal variation in ETCCDI extreme rainfall indices in the Western Ghats and the Coastal region of Karnataka. The region's climate is modulated by many large scale atmospheric controls. The variations in rainfall over the study region are significantly influenced by the El Niño Southern Oscillation (ENSO) which is one of the teleconnections (Revadekar et al. 2018). The fifth chapter aims to identify influence of ENSO on extreme rainfall indices over the study region.

5.2 SPATIAL PATTERNS AND TELECONNECTION OF RAINFALL EXTREMES

It is well known that the climatology of the Western Ghats and the Coastal region of Karnataka is characterized by pre-monsoon, summer monsoon, post-monsoon and annual total rainfall. Tawde and Singh (2015) observed a variation in the rainfall in the coastal plains and the Western Ghats' eastern part. The planning and management of the region's agricultural development is directly influenced by the water resources' spatio temporal patterns, which are significantly impacted by the rainfall's spatio temporal variations. Researchers like Goswami et al. (2006) and Pai et al. (2015) have specifically heeded extreme rainfall events and have discussed the variations in rainfall. Moreover, the possible teleconnection with the ocean-atmospheric modes must be examined as an issue of natural climatic variability and the trends of extreme rainfall indices must be examined as an issue of climate change, because the natural climatic variability and the climatic changes cause spatiotemporal variations of extreme rainfall regimes.

Large-scale circulation causes changes in rainfall extremes. The relationship between hydrological variables and ocean-atmospheric modes can be identified, because it has been established that ocean-atmospheric interactions are not random or chaotic due to the progress made in the field of synoptic climatology. The precipitation extremes can be forecast through related studies. Various land surface and oceanic phenomenon are

teleconnected to the Indian rainfall as evidenced by prior studies. The Asian monsoon dominates the Indian west coast's climate, which is significantly influenced by ENSO (Kripalani and Kulkarni, 2001; Kumar et al., 2007). Simultaneous and significant associations between various ENSO indices and monsoon rainfall are involved in the ENSO-monsoon teleconnections (Kumar et al., 1999). The Niño regions depicted asymmetric relationship over the rainfall in the subdivisions of the Western Ghats, whereas Revadekar et al. (2018) found that the sub-divisions of the Indian west coast were highly connected with the spatial variation of rainfall, indicating an asymmetric relationship. Therefore, it is vital to examine the impact of Niño indices on regional rainfall extremes in the study region of the Western Ghats and the Coastal region of Karnataka.

5.3 METHODOLOGY

Monthly Niño Indices are available from the period 1951 onwards, therefore, accordingly, IMD's gridded daily rainfall data for a 63-year period (1951 to 2013) were chosen for the study period. Extreme rainfall indices are statistically stronger because the rainfall extremes generally occur several times in a year. Therefore, the observation of extremes may not be possible during certain years and the measure of extremes is far enough in the distribution's tails. Significant responses to the eminent patterns of the climate system's internal variability are demonstrated by certain grid points. The association between the indices representing the state of Niño regions and the indices of calculated rainfall extremes is examined in this study. The strongest correlation of total rainfall is caused by the variability patterns of Niño indices, which are also the most evident for annual rainfall. The International Research Institute (IRI) considers the indices of climate variability from October to January (ONDJ), whose outcomes are presented in this study. It was found that after (before) El Niño's peak, the Indian summer monsoon is stronger (weaker) than normal in winter. Revadekar et al. (2018) identify the associations between cold SSTs and floods and between warm SSTs and droughts over the equatorial Pacific SSTA. Extreme precipitation is facilitated by influencing the association between the rainfall and ENSO. The ENSO-monsoon teleconnection has been examined from various perspectives in earlier studies. The present study attempts to understand the relationship of ETCCDI extreme rainfall indices with ENSO indices (Niño 1+2, Niño 3, Niño 3.4 and Niño 4) using the stepwise regression method. Pearson's linear correlation was used as the basis for examining

the correlation between Niño indices and the annual extreme rainfall indices. Hodrick Prescott filter was used to eliminate the trend's influence and to detrend the grid points with extreme rainfall indices (Harvey and Trimbur, 2008; Yu et al., 2018). Nevertheless, the trend for the Niño indices is not processed for maintaining the consistency of data. The impacts of Niño indices with 1-year and 0-year of monsoon year on the annual rainfall extremes are examined as the rainfall extremes of the present and forthcoming years were influenced by Niño indices.

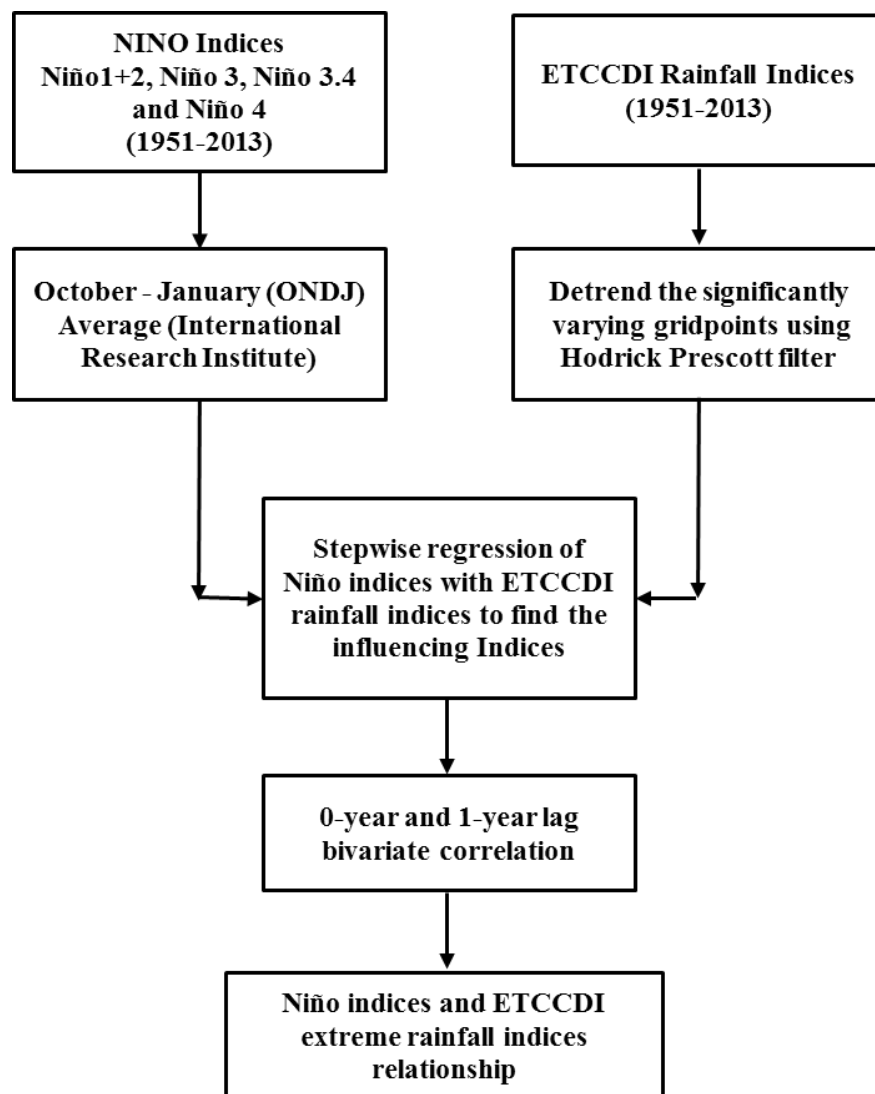


Figure 5.1 Schematic flow chart to identify the asymmetric relationship of ENSO indices with ETCCDI extreme rainfall Indices.

5.3.1 Stepwise regression analysis

Draper and Smith (1981) employ an automated process to select the predictive variables in stepwise regression (SWR), which is a type of regression model. SSTA (Niño indices) data set, which impact the rainfall extremes, is considered for the procedure of the stepwise regression. The goal of SWR is to render a simple regression model with predictive ability through the selection of predictor variables. The effect of orography influence in the study region is due to topography. Hence, a significance level of 0.01 is chosen in the present study for including most of the predictors. Let x represent the observed SSTA variable (Niño Indices) matrix (predictor data, input) and y be the vector of observed precipitation in sequence (predicted data, output). The basic steps involved in the stepwise regression are as follows:

The start of process: A level of significance termed as **Alpha-to-Enter** significance level has to be established for entering a predictor into the stepwise model and is denoted as α_E . A level of significance termed as **Alpha-to-Remove** significance level is required for removing a predictor from the stepwise model and is denoted as α_R . In other words:

- An Alpha-to-Enter level of significance, which is not greater than the usual level of 0.05, has to be specified to ensure that predictors are easily entered into the model on the basis of SST anomaly relationship and rainfall indices.
- An Alpha-to-Remove level of significance, which is not greater than the usual level of 0.01 has to be specified to ensure that predictors are not easily removed from the model. The level of significance must be set to $\alpha_R = 0.01$ or more by default.

First step: The following has to be done after specifying the levels of significance:

1. Each of the one-predictor model has to be fitted. In other words, regress y on x_1 , regress y on x_2, \dots and regress y on x_{p-1} .
2. Among the predictors having P -value lesser than $\alpha_E = 0.01$, the predictor with the smallest P -value is first put in the stepwise model.
3. The process has to be stopped if no predictor has a P -value less than $\alpha_E = 0.01$.

Step #2. Then:

1. If x_1 possessed the t -test P -value lower than $\alpha_E = 0.01$, then it is viewed as the optimal single predictor originating from the first step.

2. Now, every two-predictor model, which includes x_1 as a predictor, must be fitted. In other words, y must be regressed on x_1 and x_2 , y must be regressed on x_1 and x_3 , ..., and y must be regressed on x_1 and x_{p-1} .
3. Among the predictors with P -value less than $\alpha_E = 0.01$, the predictor possessing the smallest P -value is the second predictor placed in the stepwise model.
4. The process has to be stopped if none of the predictors have a P -value less than $\alpha_E = 0.01$. The final model will be the one with a predictor received from the first step.
5. However, if x_2 is viewed as the optimal second predictor, then it would be entered into the stepwise model.
6. Since the first predictor in the model was x_1 , it must be ascertained whether or not the significance of the x_1 predictor is affected by the entering of x_2 into the stepwise model. In other words, the P -value must be checked for testing $\beta_1 = 0$. If the P -value is greater than $\alpha_R = 0.01$, that is, if the t -test P -value for $\beta_1 = 0$ has become non-significant, then x_1 must be removed from the stepwise model.

Step #3. Then:

1. Let us assume that both x_1 and x_2 entered and remained in the two-predictor stepwise model.
2. Each of the three-predictor models, which include x_1 and x_2 as predictors, must now be fitted. In other words, y must be regressed on x_1 , x_2 , and x_3 , y must be regressed on x_1 , x_2 , and x_4 , ..., and y must be regressed on x_1 , x_2 , and x_{p-1} .
3. Among the predictors with a P -value less than $\alpha_E = 0.01$, the predictor with the smallest P -value is the third predictor placed in the stepwise model.
4. The process must be stopped if none of the predictors has a P -value less than $\alpha_E = 0.01$. The final model will be the one that contains two predictors received from the second step.
5. However, if x_3 is viewed as the optimal third predictor, then it would be entered into the stepwise model.
6. Since the first predictors in the model were x_1 and x_2 , it must be ascertained whether or not the significance of the x_1 and the x_2 predictors is affected by the entering of x_3 into the stepwise model. In other words, the P -values must be checked for testing $\beta_1 = 0$ and $\beta_2 = 0$. If the P -value is greater than $\alpha_R = 0.01$, that is, if the t -test P -value for either $\beta_1 = 0$ or $\beta_2 = 0$ has become non-significant, then the predictor must be removed from the stepwise model.

Stopping the process

Unless a t -test P -value below $\alpha_E = 0.01$ is not yielded by an additional predictor, the aforementioned steps have to be continued.

5.3.2 Bivariate Correlation

In the present study, correlation analysis is used to identify the grid points that possess the annual rainfall extremes, which are determined by the Niño indices with 0-year and 1-year of monsoon year lagged relationship. The linear correlation between two variables x and y is measured by the Pearson correlation coefficient, which is referred to as several terms, such as the bivariate correlation, the Pearson product-moment correlation coefficient (PPMCC), and Pearson's ' r '. The Pearson correlation coefficient has a value between -1 and $+1$, where -1 is the total negative linear correlation, 0 is no linear correlation, and $+1$ is total positive linear correlation. It is commonly utilized in atmospheric science's discrete statistical analysis (Pearson, 1895).

$$\text{Pearson's } r = \frac{n(\sum xy) - (\sum x)(\sum y)}{\sqrt{[n\sum x^2 - (\sum x)^2][n\sum y^2 - (\sum y)^2]}} \quad (5.1)$$

where x, y are the variables. n is length of the data.

P -value is less than 0.05 and the correlation between Niño indices and rainfall indices is significant at 5% and more.

P -value is more than 0.05 and the correlation between Niño indices and rainfall indices is significant at $>5\%$ and less.

5.4 Results and Discussion

A distinct response to each of the circulation regimes is depicted by the indices, which evidences that extreme precipitation is affected by large circulation regimes. The discussion of a detailed study of outcomes for each of the large-scale circulation regimes can be found subsequently are discussing under the section 5.5 of this chapter 5.

5.4.1 Analysis of teleconnection between rainfall extreme indices and ENSO Indices

This section presents the teleconnection between ETCCDI rainfall extremes and El Niño Southern Oscillation (ENSO) indices. The SSTA of ONDJ (October to January) shows a strong influence on the rainfall extreme indices. The multiple indices influence was detected by using a step wise regression method and each of the ENSO indices correlation was detected for 0-year lag and 1-year lag by using Pearson correlation analysis.

5.4.2 Temporal patterns of Niño Indices

Examining the temporal patterns of SSTs, anomalies over the Niño regions play a key role in investigating the linkage among them and the observed rainfall indices over the study region. Figure 5.2 presents the inter-annual variability of sea-surface temperature anomalies over Niño regions during the ONDJ season.

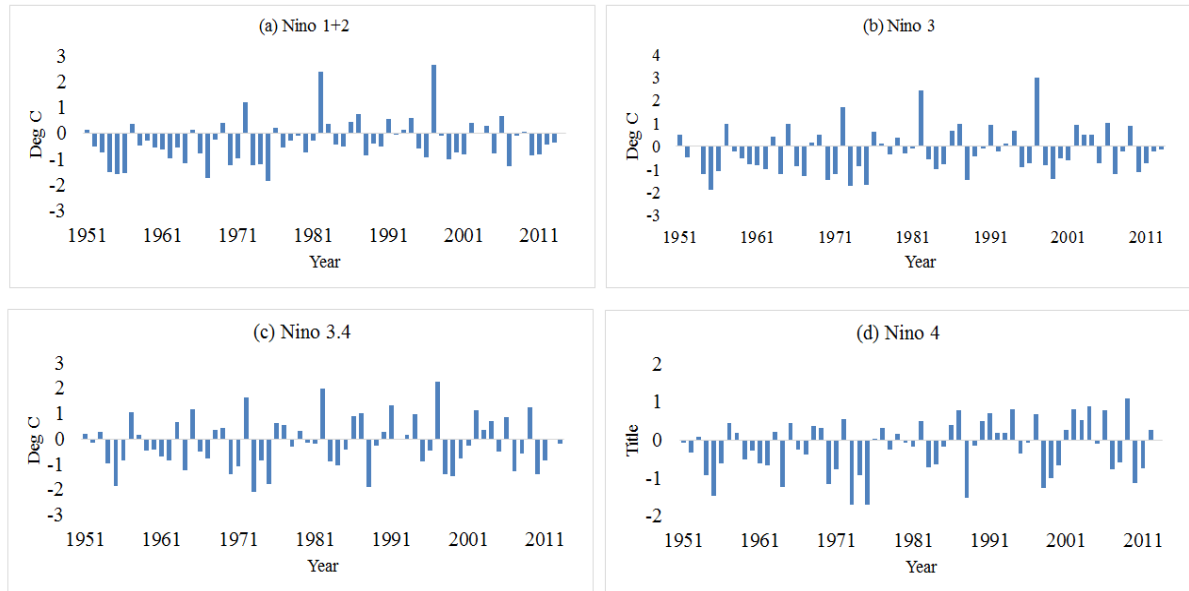


Figure 5.2 Interannual variability of sea-surface temperature anomalies over Niño region during ONDJ (October-January) season.

5.4.3 Possible teleconnections of Rainfall extremes with ENSO indices

A series of regressions on an array of potential explanatory Niño indices are executed by a multiple linear regression model termed as Step Wise Regression (SWR) analysis. The statistical significance of Niño indices determines either their addition or removal from the model at each step. The p -value of a variable's coefficient estimate is used by each step to calculate its predictive value. The testing against the model, with and without the potential parameter, is conducted by each step. When the model cannot be improved by any of the additional variables, then the method is concluded. Non-significant indices were discarded and all extracted indices were included as potential explanatory variables for the prediction of precipitation and greenness at each site. In order to identify the optimal model with the highest coefficient of determination (R^2) value, a variable lagged SWR analysis was performed. The R^2 value is regarded as the most significant time lag between the extreme rainfall indices (dependent variable) and the Niño indices (independent variable), which

leads to the generation of optimal causal association to explain the teleconnection signal propagation, regarding the Niño regions' multiple index.

The rainfall extremes of the current and the forthcoming years may be influenced by the ENSO indices. A study was conducted on the influences of Niño 1+2, Niño 3, Niño 3.4 and Niño 4 with 0-year and 1-year ahead on the annual rainfall extremes. The ENSO indices with 0-year and 1-year ahead were considered as the candidate predictor variables for each of the grid points in the study region. Later, step wise regression was used to select the robust combinations of predictor variables for predicting the rainfall extremes in each of the grid points. This was followed by the identification of extreme rainfall regions that were significantly affected by the ENSO indices (Figure 5.3 and Figure 5.4). It can be observed that the influences of certain Niño indices are invariably regulated by another Niño region, because the Niño regions influence the annual extreme rainfall indices in the most of the grid points and more than one Niño index influences a few of the grid points. In particular, the grid points with intensity index influenced less due to the orographic effect of study region's topography feature. The rainy days (CWD) and dry days (CDD) are more influenced by the modulation of climate index. Table 5.1 shows that the asymmetric relationship of SSTA is detected in the study region through the coefficient of determination between the SSTA over the Niño regions and rainfall extreme indices.

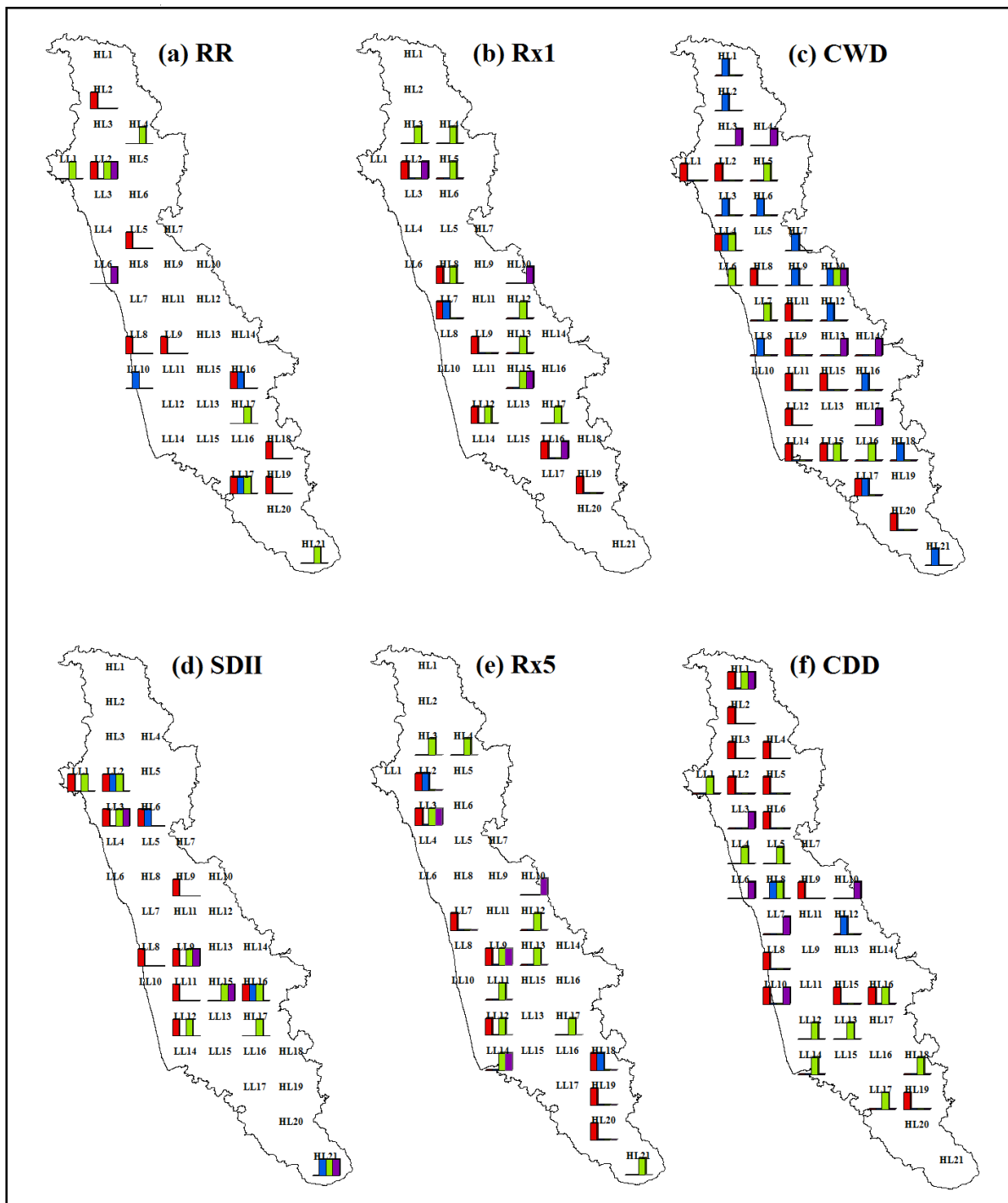


Figure 5.3 (a-f) Rainfall indices identified grid points influenced by the Niño Indices based on the stepwise regression method.

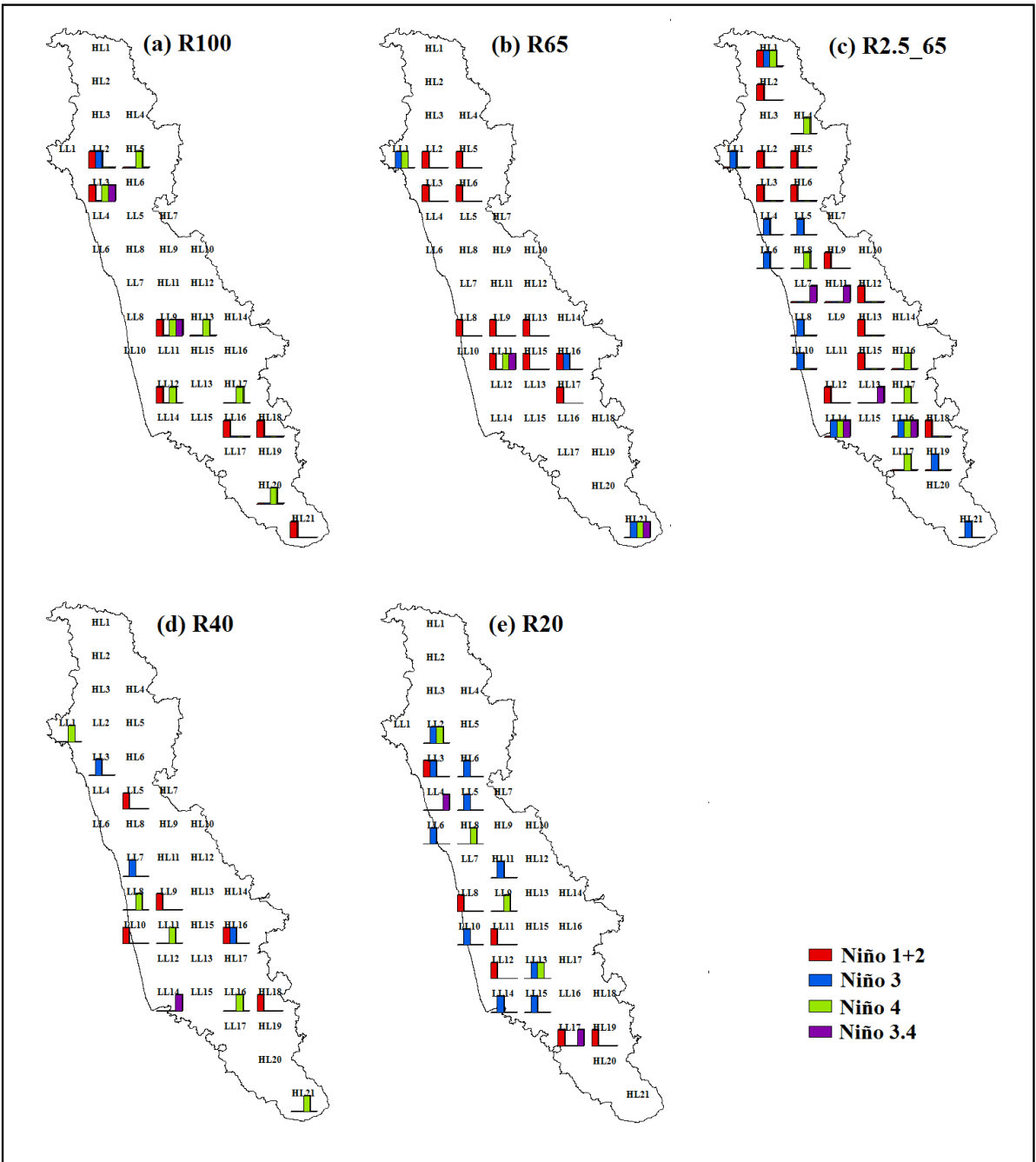


Figure 5.4 (a-e) Absolute threshold intensity rainfall frequency indices identified grid points influenced by the Niño Indices based on the stepwise regression method.

Table 5.1 SWR analysis Coefficient of determination (%) for rainfall extreme indices.

GP	RR	RX1	CWD	SDII	RX5	CDD	R100	R65	R2.5_65	R40	R20
LL1	15.7	-	6.39	13.3	-	11.5	-	14.5	17.79	6.79	-
LL2	31.14	19.8	5.03	31.2	18.0	13.1	15.8	14.9	25.32	-	25.3
LL3	-	-	3.63	32.3	25.7	3.94	30.0	8.36	25.95	7.96	12.2
LL4	-	-	12.7	-	-	10.74	-	-	22.2	-	16.3
LL5	12.0	-	-	-	-	9.28	-	-	9.65	4.66	3.4
LL6	3.96	-	6.42	-	-	4.18	-	-	11.06	-	13.4
LL7	-	11.45	7.77	-	4.79	6.1	-	-	18.41	14.5	-
LL8	9.75	-	2.91	4.64	-	6.78	-	7.55	9.88	15.9	11.1
LL9	7.84	7.56	14.0	18.3	17.8	-	18.3	7.8	-	6.01	4.31
LL10	3.83	-	-	-	-	8.35	-	-	10.13	13.2	9.31
LL11	-	-	13.9	7.74	3.91	-	-	10.4	-	11.4	8.62
LL12	-	9.32	9.8	7.46	11.6	6.55	14.6	-	16.94	-	17.2
LL13	-	-	-	-	-	3.16	-	-	11.25	-	17.2
LL14	-	-	6.71	-	14.9	3.62	-	-	15.57	3.9	14.0
LL15	-	-	9.31	-	-	-	-	-	-	-	4.36
LL16	-	6.76	9.69	-	-	-	4.59	-	27.04	10.7	-
LL17	20.1	-	7.49	-	-	4.1	-	-	13.23	-	19.0
HL1	-	-	14.24	-	-	17.87	-	-	15.89	-	-
HL2	3.19	-	13.9	-	-	5.83	-	-	10.59	-	-
HL3	-	7.44	11.4	-	4.12	5.62	-	-	-	-	-
HL4	4.16	4.81	3.79	-	3.91	6.81	-	-	7.49	-	-
HL5	-	3.06	6.61	-	-	10.86	5.63	3.98	14.68	-	-
HL6	-	-	3.74	18.2	-	6.53	-	10.3	19.44	-	3.24
HL7	-	-	22.4	-	-	-	-	-	-	-	-
HL8	-	5.85	11.1	-	-	9.01	-	-	6.97	-	6.95
HL9	-	-	4.13	4.39	-	8.13	-	-	17.66	-	-
HL10	-	3.95	22.7	-	3.44	3.6	-	-	-	-	-
HL11	-	-	13.9	-	-	-	-	-	6.63	-	4.14
HL12	-	5.34	9.01	-	3.14	4.56	-	-	9.68	-	-
HL13	-	6.08	9.31	-	6.59	-	3.7	4.27	8.22	-	-
HL14	-	-	11.9	-	-	-	-	-	-	-	-
HL15	-	16.0	6.87	20.4	-	6.3	-	3.63	8.93	-	-
HL16	20.4	-	18.6	20.2	-	8.62	-	15.3	6.99	17.3	-
HL17	5.88	4.44	8.07	3.96	5.88	-	5.12	3.44	3.98	-	-
HL18	4.8	-	17.6	-	6.21	6.66	6.14	-	4.4	7.36	-
HL19	4.5	4.79	-	-	4.53	4.23	-	-	3.4	-	4.62
HL20	-	-	15.6	-	3.93	-	4.59	-	-	-	-
HL21	3.57	-	16.6	18.0	4.72	-	5.84	16.1	3.19	6.03	-

5.4.4 Characteristics of Sea surface temperature

The study region's rainfall is recognized for the out-of-phase relationship with the Niño indices. The ocean is capable of absorbing, storing and transporting solar heat energy and therefore plays a vital role in influencing the climate. Consequently, different characteristic features in variability, trends, anomalies and annual cycles are demonstrated by the rainfall events over the Western Ghats. The atmospheric temperature and circulation is affected by the temperature of sea/ocean surface all over the globe. The proximity to the Arabian Sea and the orographic effect jointly influence the study region's climate. The correlation coefficient between the ENSO indices and the rainfall extreme events is thereby computed. Floods are associated with cold SSTs and droughts are associated with warm SSTs over the equatorial Pacific Ocean. Hence, a negative correlation is observed between the ENSO indices and the rainfall over the study region. This negative correlation is also observed for the rainfall in study region.

5.4.5 Correlation Analysis between ENSO Indices and extreme Rainfall events

In order to identify the optimal time shifts that maximize the correlation between the ENSO indices and the meteorological variables, the 0-year lag correlation and the 1-year lag correlation are applied. This is due to the frequent time delays of climatic responses to large-scale atmospheric controls. The lag correlation of individual oceanic ENSO indices with the annual average of regional averages of extreme rainfall indices is used to serve this purpose.

The tropical Pacific is monitored by using several indices that are based on SST anomalies, which are averaged across a specific region. The computation of anomalies is generally based on a period of 30 years. This index has an inclination of possessing the Niño SST indices' largest variance. External influences in the analysis (local factors, seasonal factors, altitude, etc.) are explicitly avoided because each of the time series is in its standardized version.

The concluding section contains an analysis of the similarities and differences among various outcomes. The following sections contain an analysis of the temporal and spatial climatic patterns among the outcomes from relationships with the ENSO indices.

5.4.5.1 Influence of Niño 1+2 on extreme precipitation indices.

Niño 1+2 (0-10S, 90W-80W): The Niño 1+2 region corresponds with the South American coastal region that was acknowledged by the local populations and is the smallest and the eastern-most of the Niño SST regions (Trenberth, 2011). Essentially, when linear correlation analyses are applied, then there is a synchronized time between the region's precipitation and the ENSO indices' time series. This statement holds true in all cases except for the ones in which wet spells are correlated with dry spells.

Figure 5.5 and Figure 5.7 depict the extract of the regions with the annual rainfall extremes that are affected by Niño 1+2 with 1-year and 0-year, respectively. Figure 5.6 and Figure 5.8 (Appendix 5 and 6) illustrate each grid point's correlation values for 1-year and 0-year, respectively. The modulation of Rx1 day and R100 with climate modes is similar, because of their close relation to Rx5 day and R65, respectively. The figures depict the rainfall indices and the spatial patterns. It can be observed that when the Niño 1+2 is at different lag periods, then the regional responses of annual extreme rainfall indices to the Niño 1+2 are different (Figure 5.5 and Figure 5.6). In general, a negative but less influencing and insignificant correlation is demonstrated by most of the grid points; whereas, a positive correlation is demonstrated by Rx1 day and Rx5 day. However, both positive and negative significant correlations are demonstrated by RR, SDII and CWD at different stages. Moreover, the Niño 1+2 simultaneously affect some grid points for general precipitation indices.

The frequency indices of intense rainfall events are positively correlated for R100 (very heavy rainfall) and R65 (heavy rainfall) with Niño 1+2 simultaneously at different stages. The moderate, average and low rainfall (R2.5-65, R40 and R20) indices show a significant negative correlation at different stages simultaneously (Figure 5.8). In comparison to the

5% and 1% level of significance, some of the significant correlation between Niño 1+2 and regional rainfall indices are found to be better. Normally, the intense extreme rainfall indices' frequency modulation is associated with wet spells. The grid points possessing statistically significant correlation demonstrate a consistent pattern of climate. The grid points over the study area's coastal (low land) region exhibited the greatest correlation among all statistically significant outcomes (Figure 5.6 and Figure 5.8 with respect to Appendix 6).

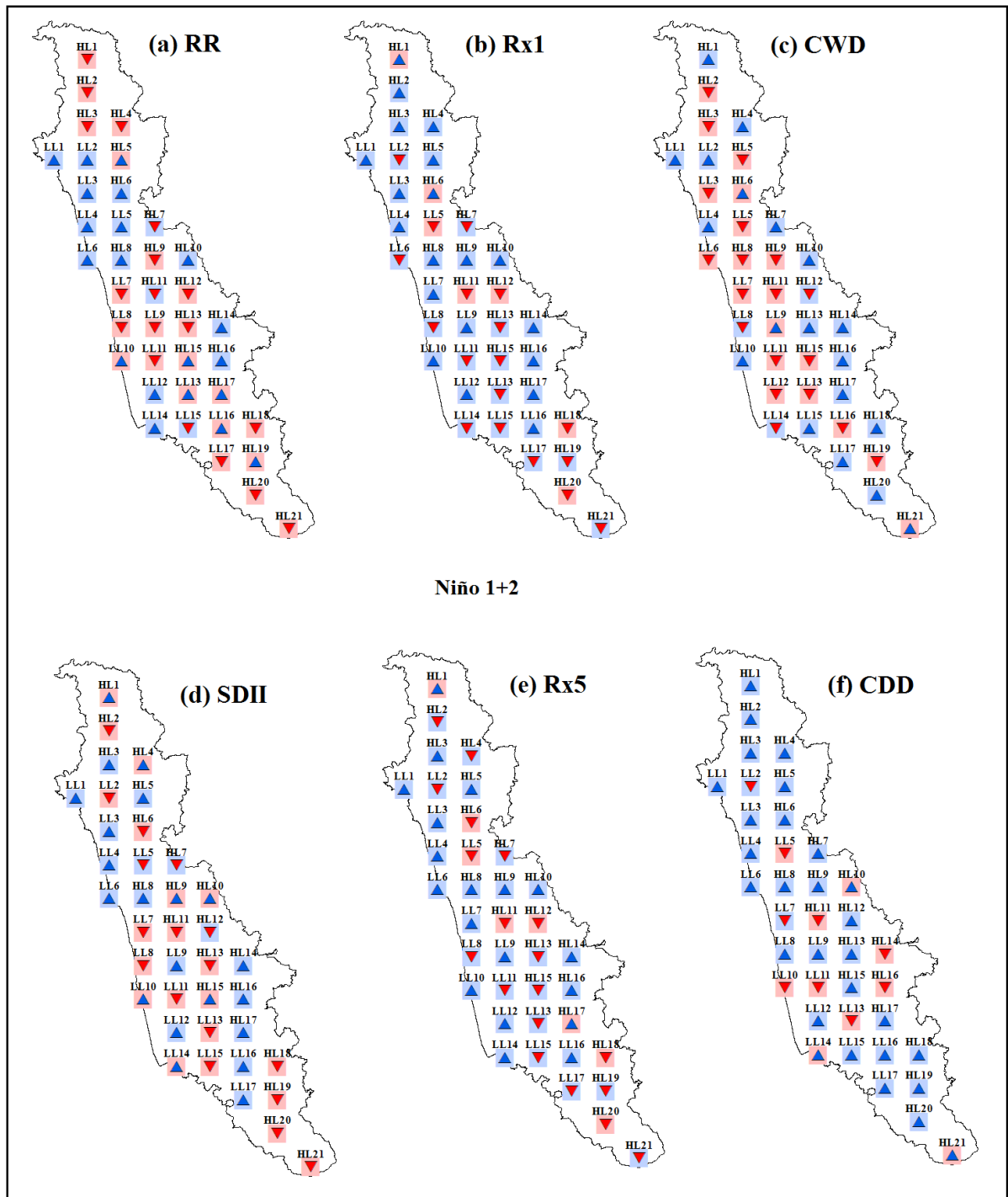


Figure 5.5 (a-f) Grid points with the precipitation extremes influenced by the Niño 1+2 with 1-year and 0-year ahead, respectively.

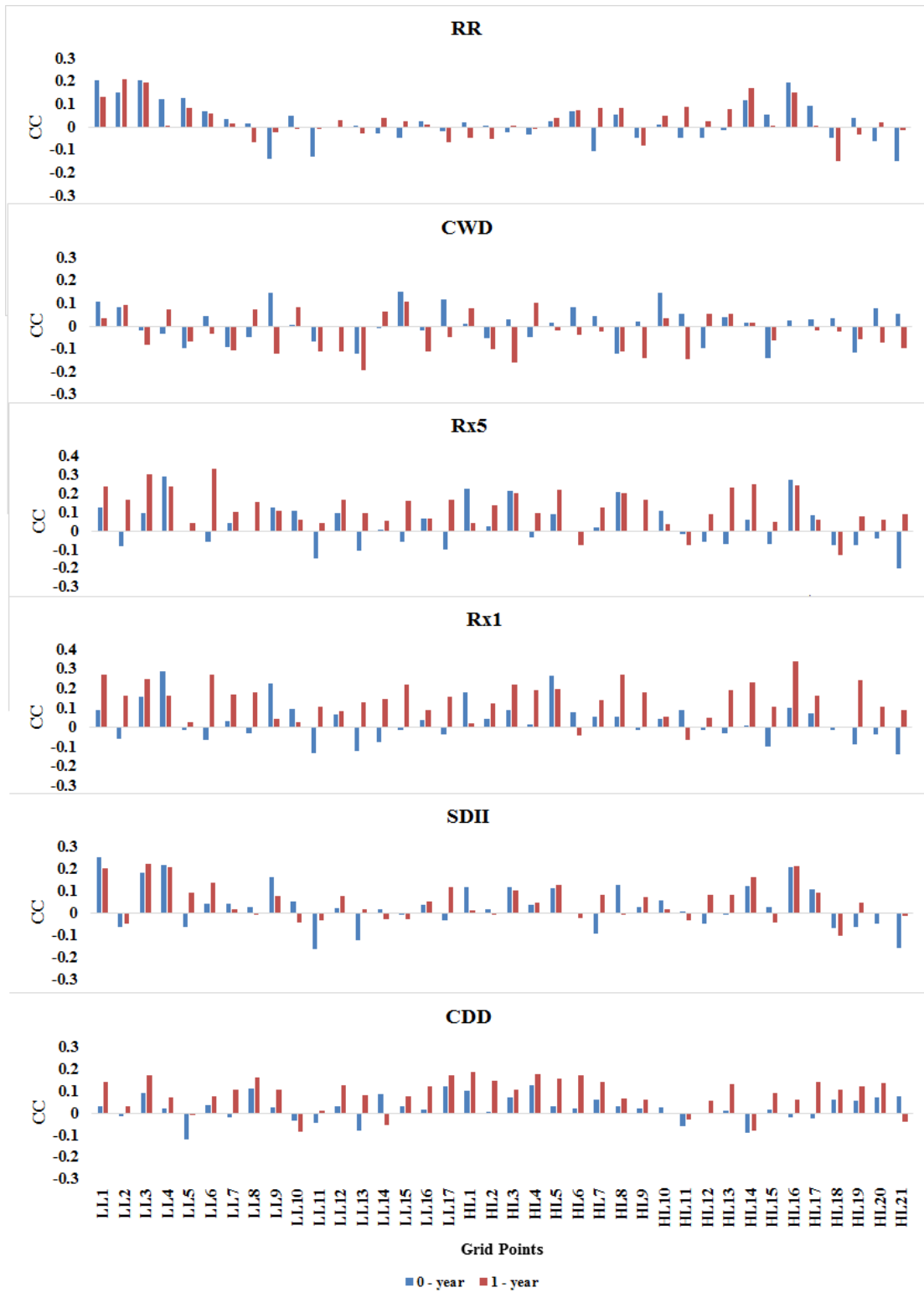


Figure 5.6: The Pearson's correlation between Niño 1+2 and general extreme precipitation indices

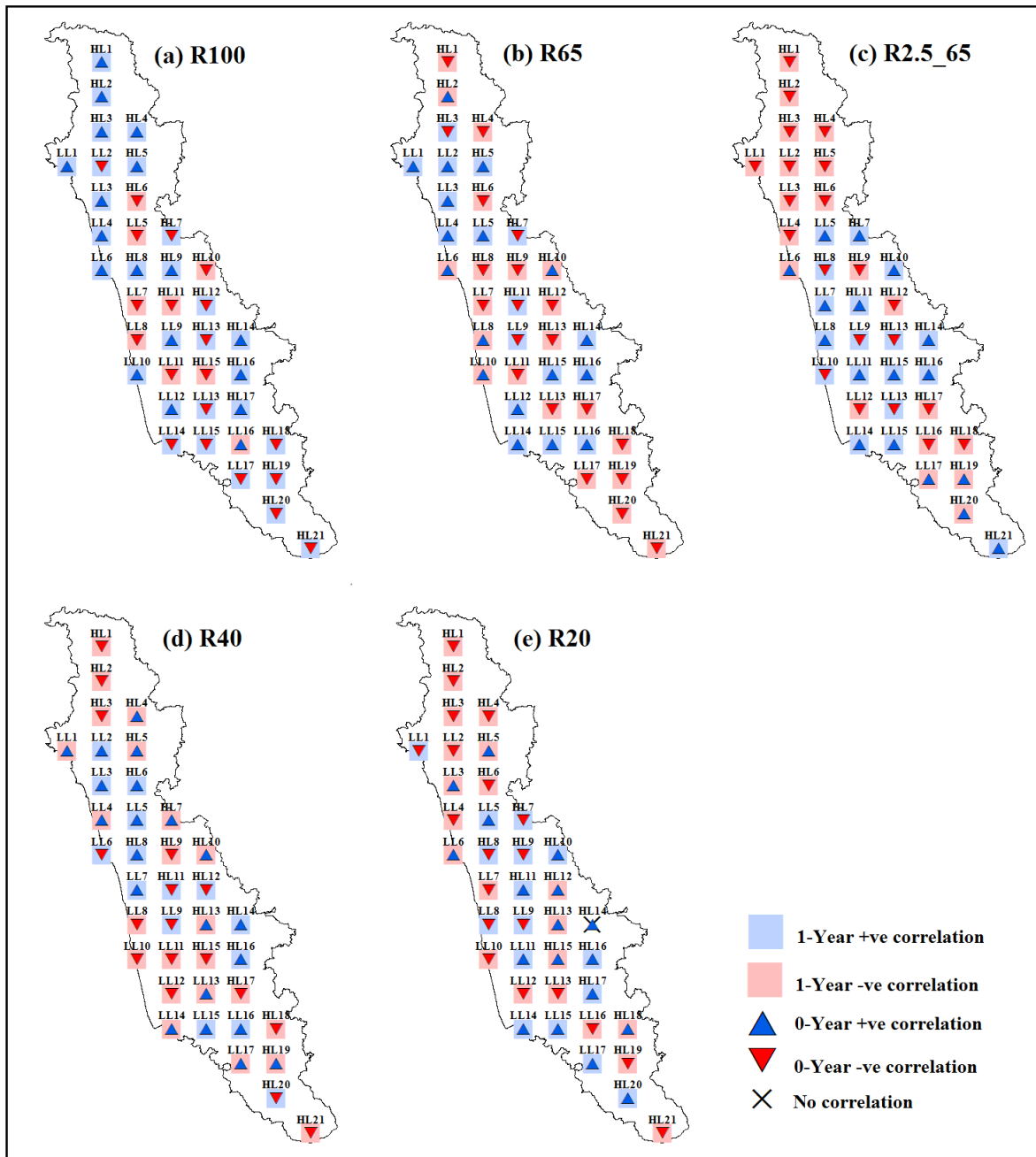


Figure 5.7 (a-f) Absolute threshold intensity rainfall frequency indices influenced by the Niño-1+2 with 1-year and 0-year ahead, respectively.

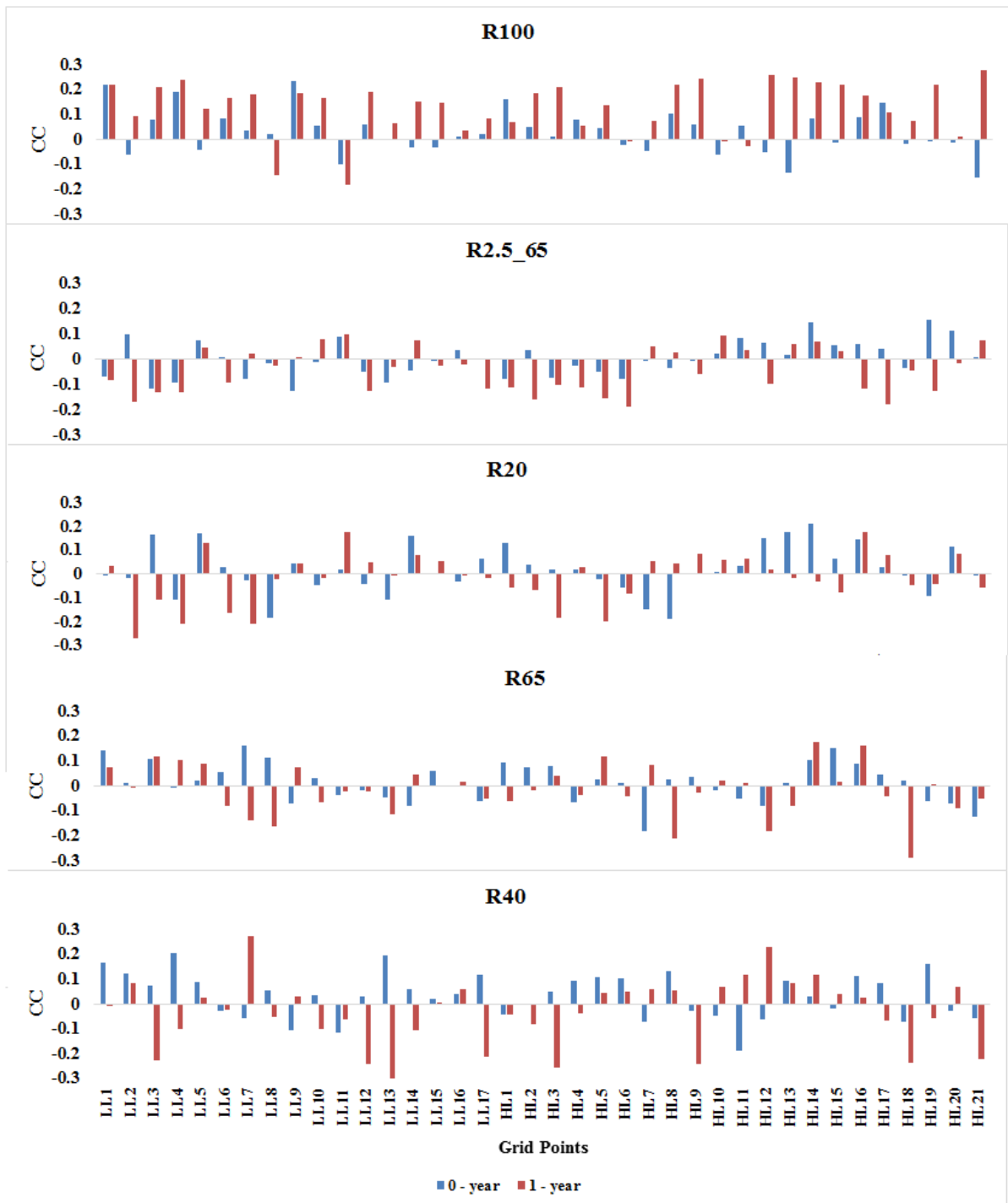


Figure 5.8: The Pearson's correlation between Niño 1+2 and frequency of extreme precipitation indices

5.4.5.2 Influence of Niño 3 on extreme precipitation indices.

Niño 3 (5N-5S, 150W-90W): Although researchers found that the vital region for coupled ocean-atmosphere interactions for ENSO was further west, Niño 3 was regarded as the prime region for the monitoring and prediction of ENSO extreme events (Trenberth, 1997). Figure 5.9 depicts the general highest magnitude rainfall indices and Figure 5.11 depicts the frequency of intense rainfall events, which illustrate the regions with extreme rainfall events determined by the Niño 3 with 0-year ahead and 1-year ahead, respectively. It shows that there is no significant correlation with RR, CWD and CCD general rainfall indices at both 0-year and 1-year ahead. This evidences that at a considered period of lag, the general rainfall indices' regional responses to the Niño 3 are not significant; whereas, a significant but not simultaneous correlation at different stages is demonstrated by the highest intensified rainfall indices Rx1 day and Rx5 day. The modulation of Niño 3 shows a strong relationship with intense magnitude and a weak relationship with the frequency of the wet and dry spell indices. The interesting characteristic could be identified from the relationship between extreme rainfall indices and Niño 3 is a significant positive correlation in general rainfall indices.

The influence of Niño 3 on the frequency of intensity of extreme rainfall indices with 0-year and 1-year ahead, respectively, is graphically represented in Figure 5.11 and its correlation values are represented by Figure 5.12 and tabulated in Appendix 7. The Niño 3 shows a strong and positive correlation with R100 (very heavy rainfall) indices over the mountainous region of the study area. The influence of Niño 3 on the frequency of intensity of rainfall indices of heavy rainfall (R65) and moderate rainfall (R2.5_65) shows an insignificant relationship. However, most of the grid points in moderate rainfall indices present a negative correlation at different stages. The relationship with average intense rainfall (R40) shows a negative, but statistically significant correlation. The low rainfall (R20) indices show a significant correlation, but most of the grid points show a negative relationship with Niño 3. It is observed from the above results that Niño 3 strongly influences very heavy rainfall by suppressing the low intensity rainfall events.

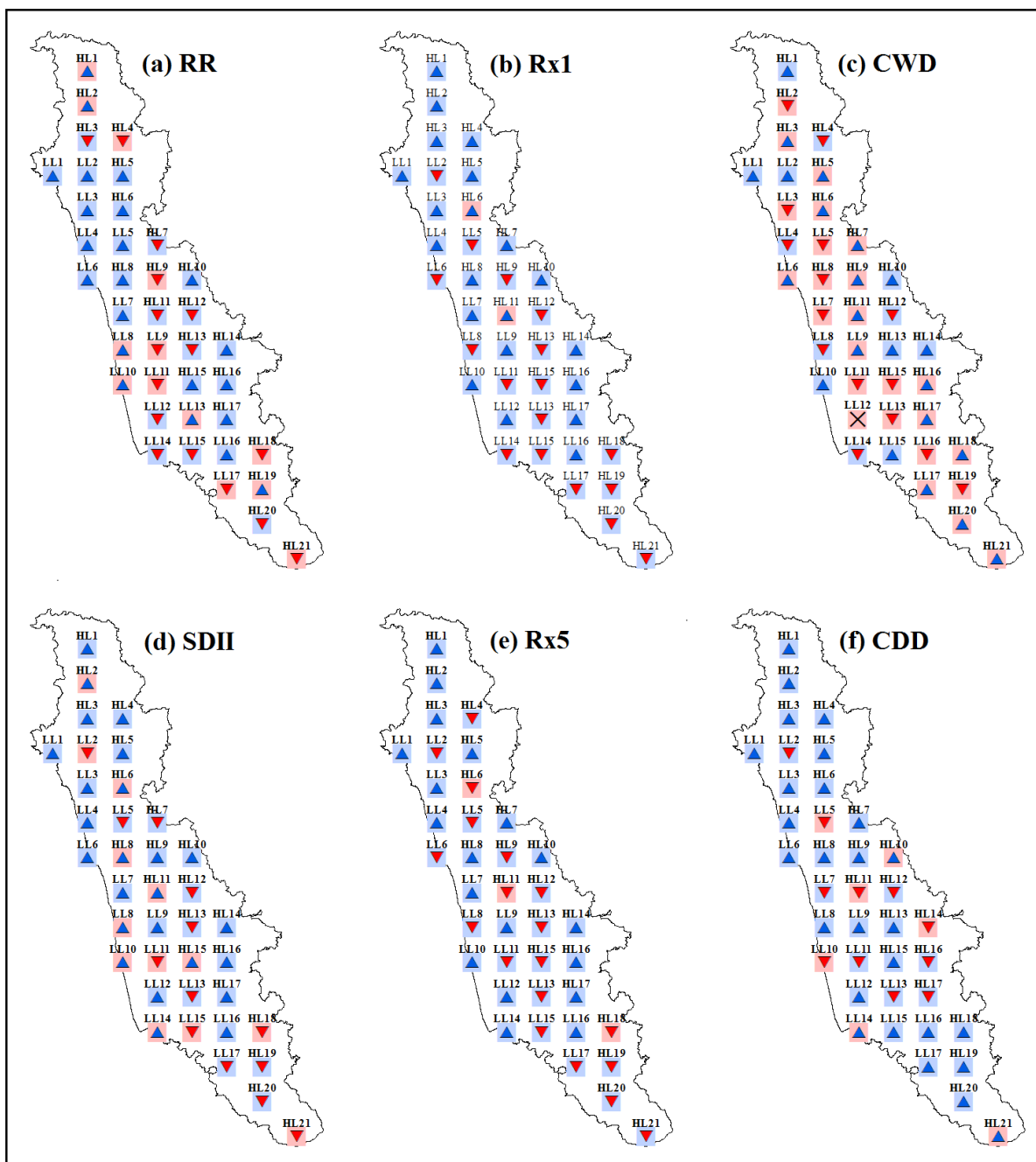


Figure 5.9 (a-f) Grid points with the precipitation extremes influenced by the Niño-3 with 1-year and 0-year ahead, respectively.

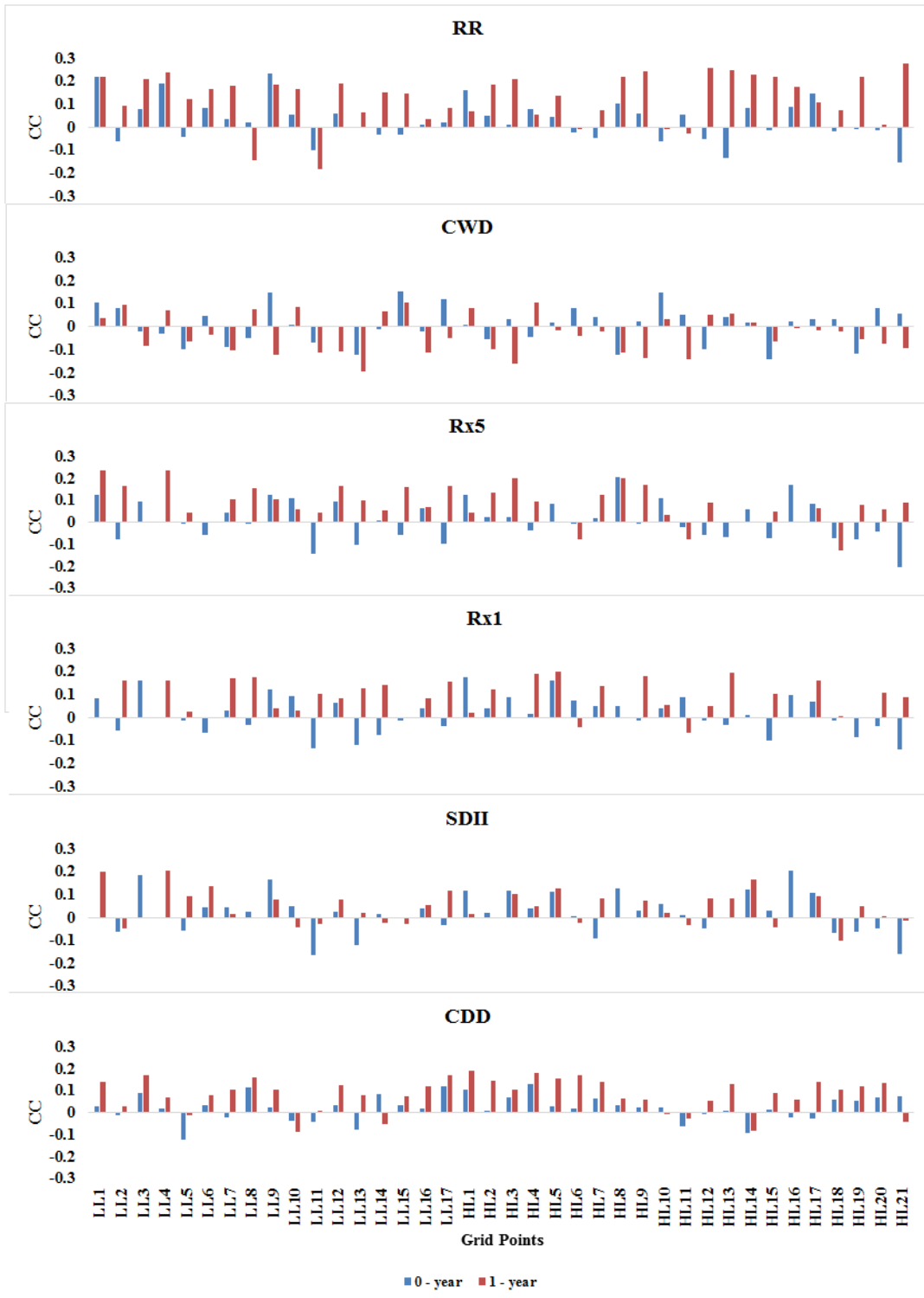


Figure 5.10: The Pearson's correlation between Niño 3 and general extreme precipitation indices

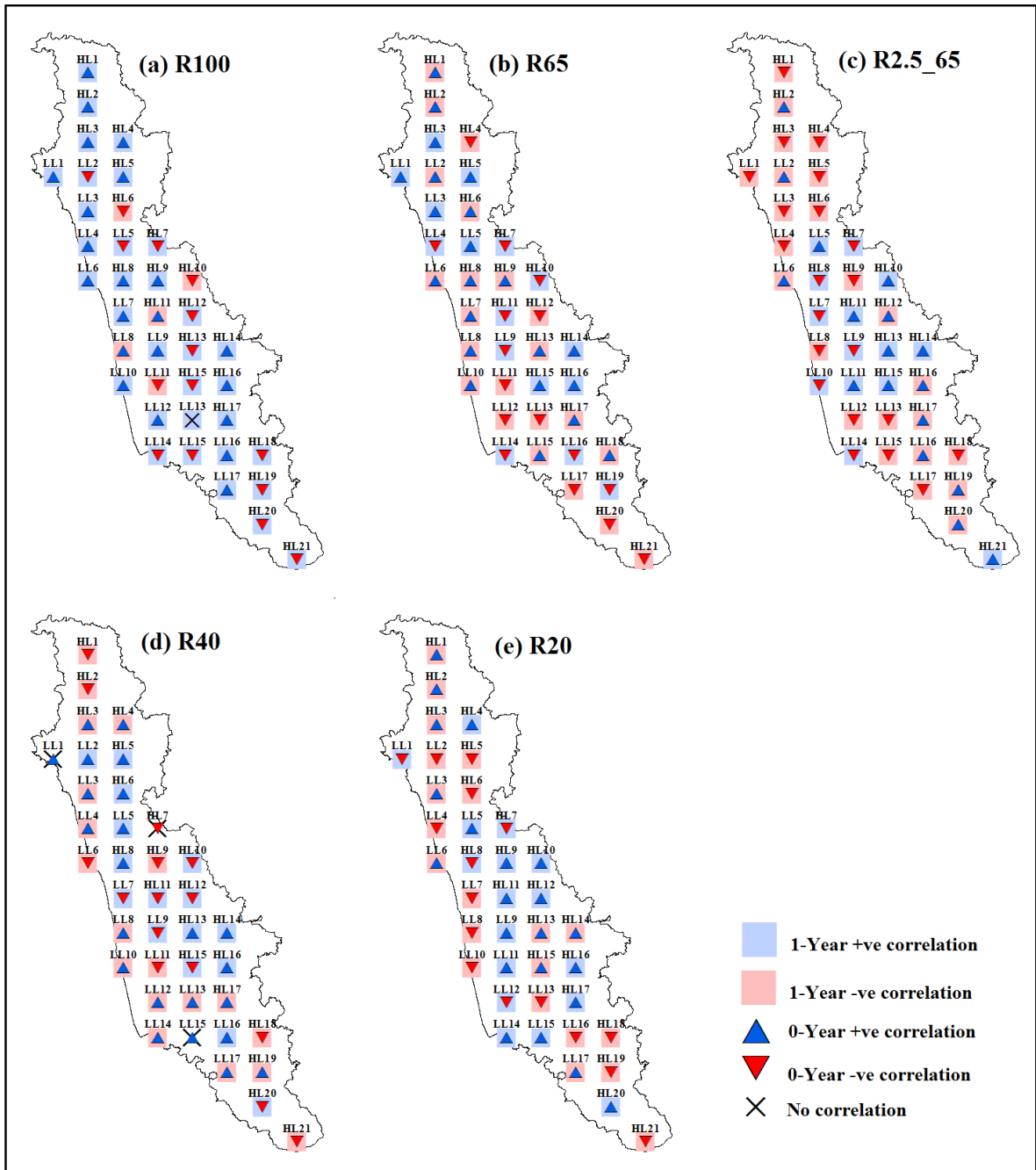


Figure 5.11 Absolute threshold intensity rainfall frequency indices influenced by the Niño-3 with 1-year and 0-year ahead, respectively.

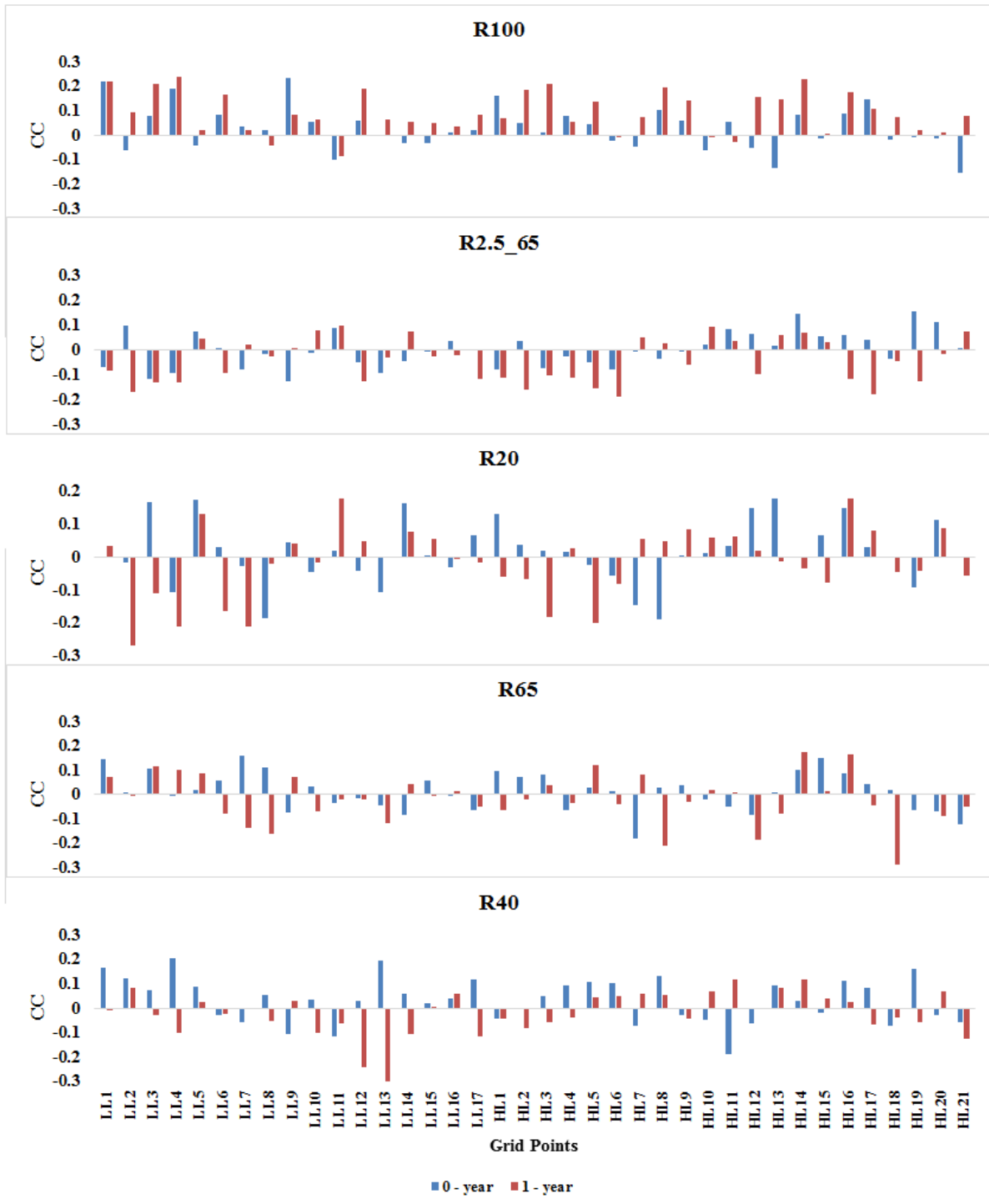


Figure 5.12: The Pearson's correlation between Niño 3 and frequency of extreme precipitation indices

5.4.5.3 Influence of Niño 4 on extreme precipitation indices

Niño 4 (5N-5S, 160E-150W): In comparison to other Niño regions, the central equatorial Pacific region is inclined to have a less variance and the SST anomalies in this region are captured by the Niño 4 index. In contrast with other Niño indices, Niño 4 shows a significant positive correlation with the annual rainfall over the study region. Due to weak and insignificant relationship with wet spells (CWD) and dry spells (CDD), a low significant relationship is illustrated with the daily average rainfall (SDII) at different stages of 0-year and 1-year (Figure 5.13 and 5.14). This indicates that regional responses to total rainfall modulation by Niño 4 is better than any other general rainfall indices at no lag. Niño 4 modulates the highest magnitude rainfall (Rx1) at lagged period with decent positive correlation, when compared to the cumulative of intense rainfall (Rx5) that shows moderately positive but statistically insignificant correlation at different stages. Overall, Niño 4 indicates a good relationship with the total rainfall and the magnitude of intense rainfall, when compared to other rainfall indices.

The modulation of Niño 4 with intense rainfall frequency of extreme rainfall indices shows a moderate relationship over the study region shown in figure 5.15 and 5.16. The frequency of very high rainfall (R100) shows a decent positive relation and a low negative correlation. The Niño 4 depicts a negative correlation with moderate rainfall (R2.5-65) at both 0-year and 1-year ahead. The remaining intense rainfall frequency indices R40 and R20 show a low mixed relationship at different stages. In the same pattern, it also indicates a low and mixed combination of correlation for heavy rainfall (R65). The comparison of these types of Niño 4 modulations with the frequency of intense rainfall indices indicates that Niño 4 is a modulator for very high rainfall. There is a consistent relation between very heavy rainfall and annual rainfall and this implies the influence of Niño 4 on very heavy extreme rainfall. The positive relation of Niño 4 strengthens the extreme precipitation events by contributing to the annual rainfall. Whereas, the increase in extreme events reduces the strength of the low frequency of rainfall and it could be observed from the relationship of other rainfall indices. In other words, it justifies that Niño indices are showing an asymmetric relation for extreme rainfall events over the study region of Karnataka's west coast. The correlation values of Niño 4 are listed in the table Appendix 9 and 10.

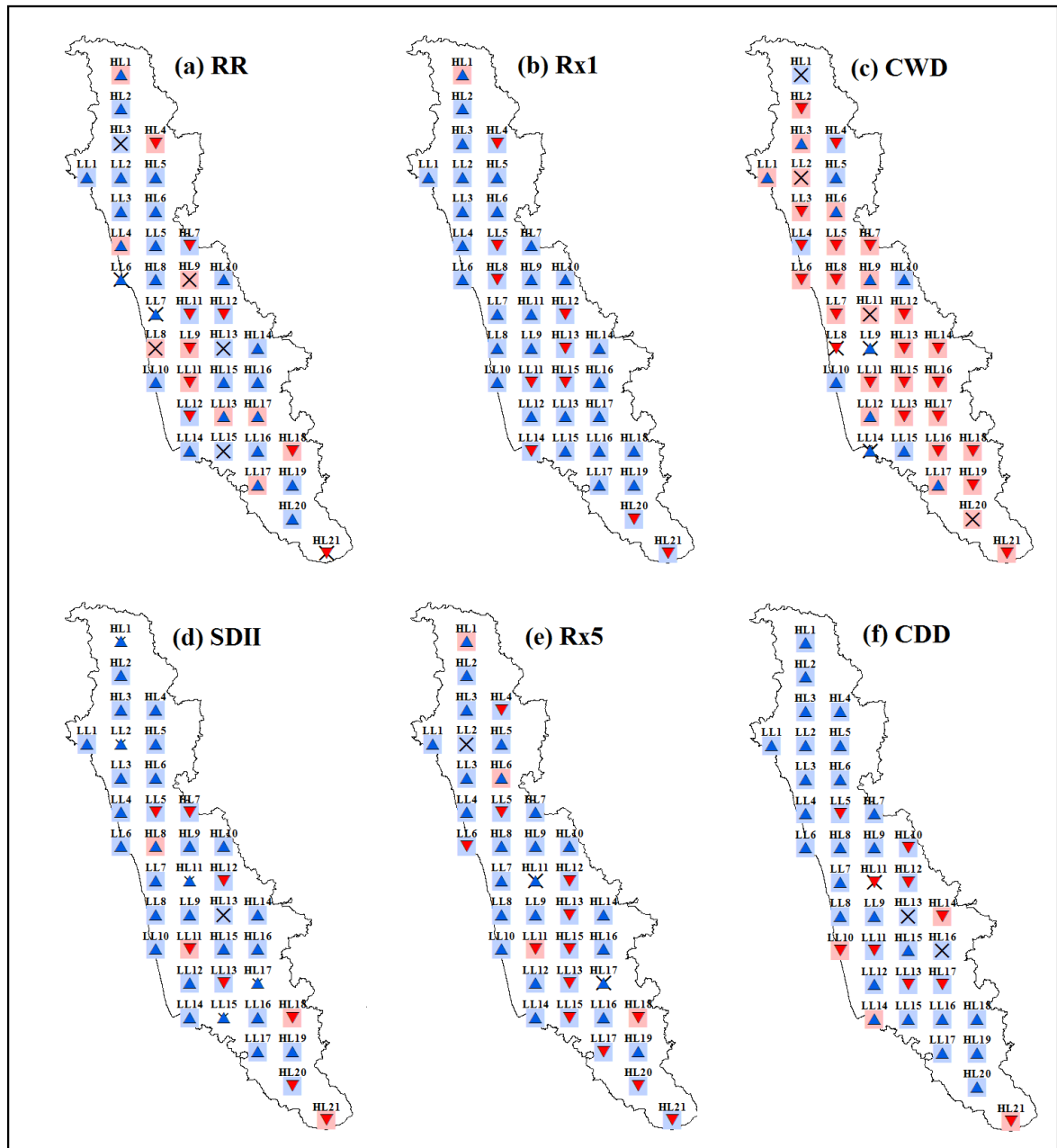


Figure 5.13 (a-f) Grid points with the precipitation extremes influenced by the Niño-4 with 1-year and 0-year ahead, respectively.

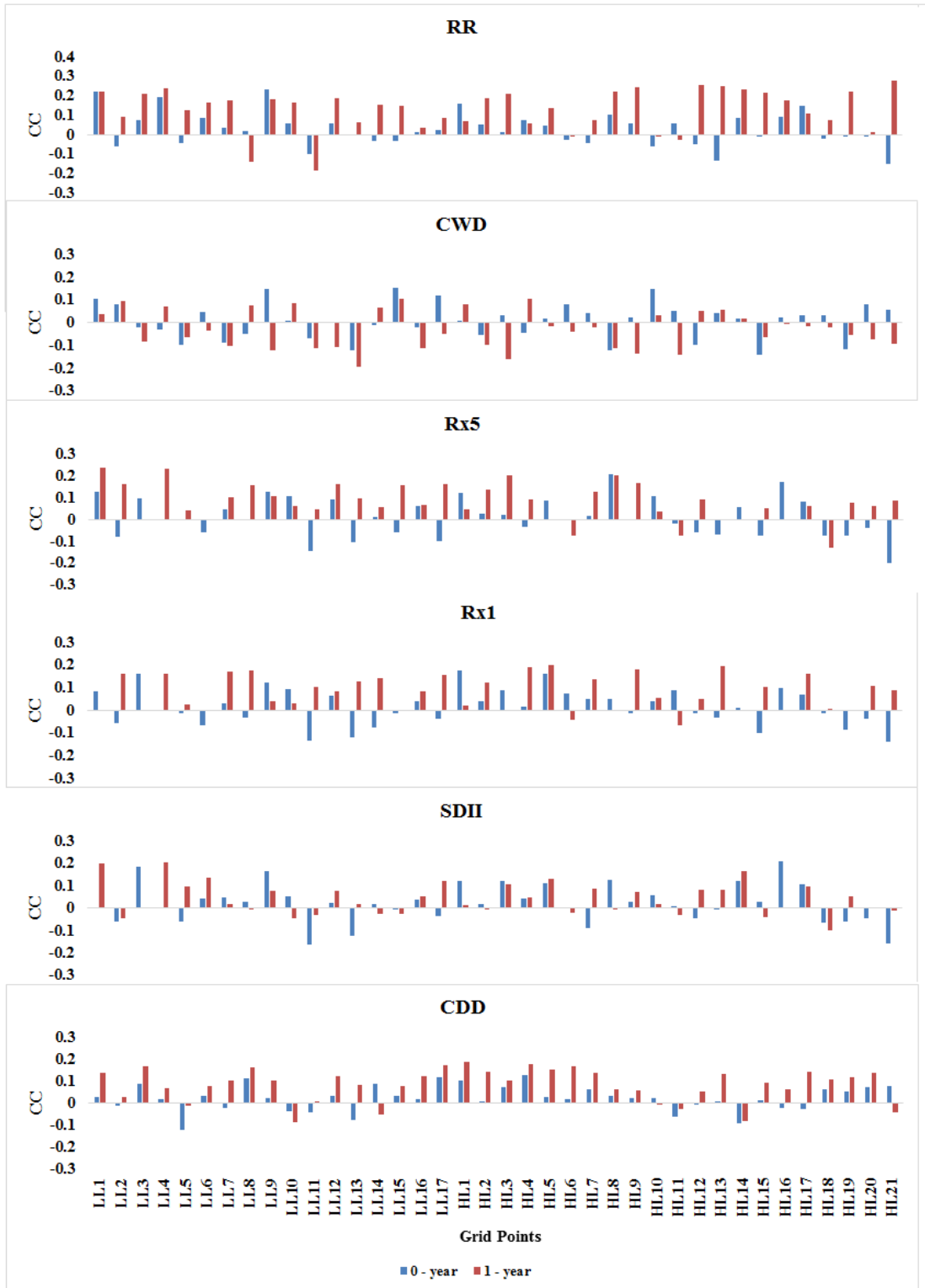


Figure 5.14: The Pearson's correlation between Niño 4 and general extreme precipitation indices

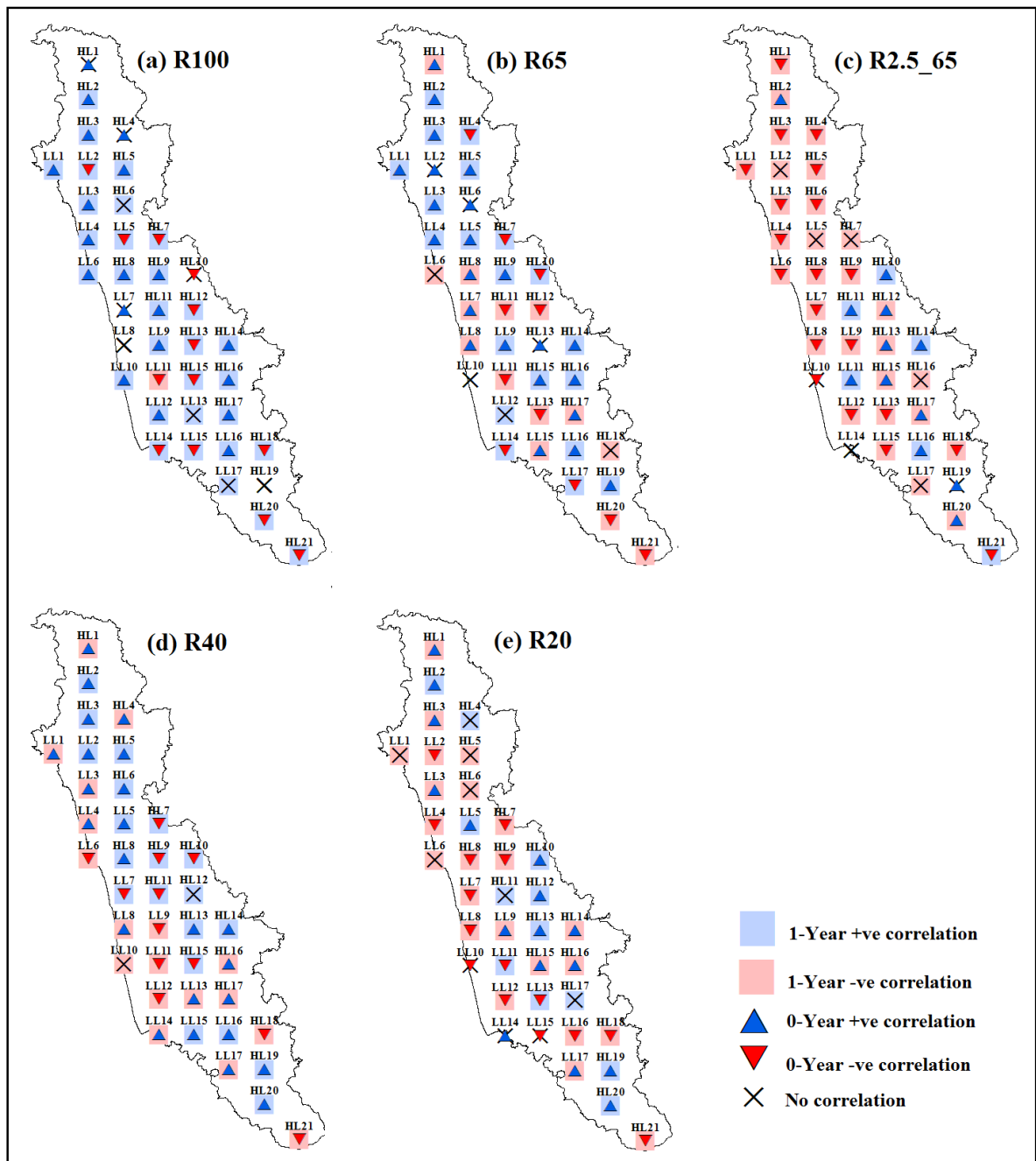


Figure 5.15 (a-f) Absolute threshold intensity rainfall frequency indices influenced by the Niño-4 with 1-year and 0-year ahead, respectively.

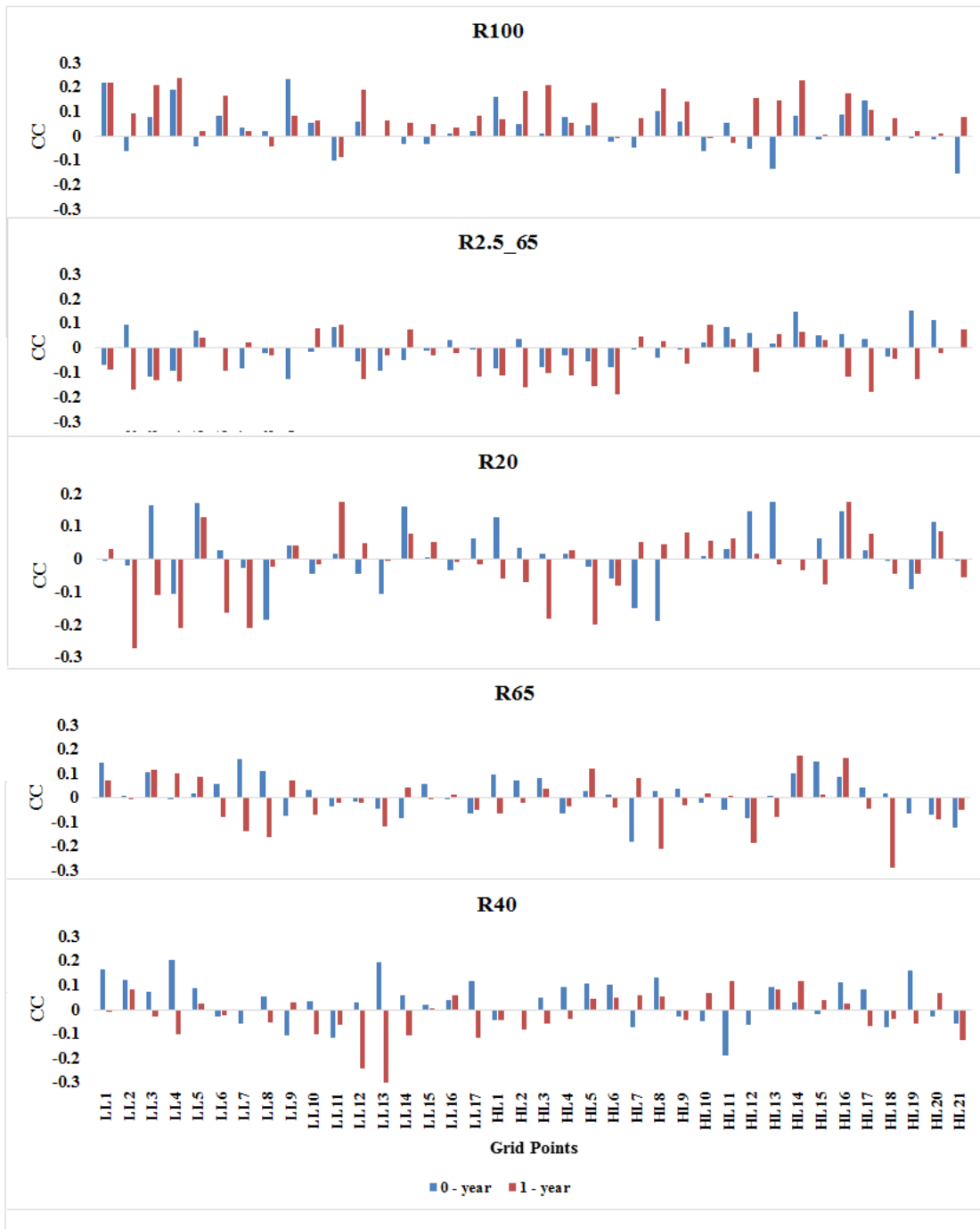


Figure 5.16: The Pearson's correlation between Niño 4 and intense rainfall frequency of extreme precipitation indices

5.4.5.4 Influence of Niño 3.4 on extreme precipitation indices

Niño 3.4 (5N-5S, 170W-120W): The average equatorial SSTs across the Pacific are perceived to be represented by the Niño 3.4 anomalies from around the dateline to the South American coast. When the Niño 3.4 SSTs exceed $\pm 0.4^{\circ}\text{C}$ for a period of six months or more, then the El Niño or La Niña events are defined and the Niño 3.4 index is generally utilized as the standard ENSO index. Figure 5.17 and Figure 5.19 depict the extract of the region with the annual rainfall extremes affected by Niño 3.4 with 1-year ahead and 0-year ahead, along with the linear correlation for every grid point of each of the extreme rainfall indices (Appendix 11). Specifically, the annual rainfall is influenced by 0-lag period of Niño 3.4; the more the lag period, the less the correlation noted. Intense rainfall indices Rx1 day and Rx5 day show a good, but not simultaneous correlation at different stages. The wet and dry spells show no significant relationship, such that the modulation of the frequency of rainfall indices with Niño 3.4 is statistically insignificant. Due to the insignificance of wet spell with Niño 3.4, SDII also represents a similar statistically insignificant relationship at different stages. The strong relationship of ENSO index with rainfall shows a significant positive correlation.

The frequency of extreme rainfall indices (Figure 5.19) influenced by Niño 3.4 has a moderate correlation with the very heavy (R100) and heavy rainfall events (R65) at no lag period. Few grid points over low land regions show a significant positive correlation, most of the grid points over high lands show a negative relationship with a low correlation, due to the effect of topography and less spatial correlation. The events of moderate rainfall (R2.5_65), average rainfall (R40), and low rainfall (R20) depict a negative correlation (Appendix 12). It is generally found that a certain Niño index always modulates another Niño index and when the climate indices are at different stages, the regional responses of extreme rainfall events to the climate indices differ and some regions get simultaneously impacted by the climate index. These outcomes are vital for either predicting or mitigating the risks caused by droughts or floods. The ENSO influences the extreme rainfall at the same point of time, specifically, in Karnataka's Western Ghats. The agricultural activities and water resources across the coastal region and the Western Ghats of Karnataka can be optimally planned and managed if the impact of climate indices on agriculture and regional response of rainfall extremes is comprehended.

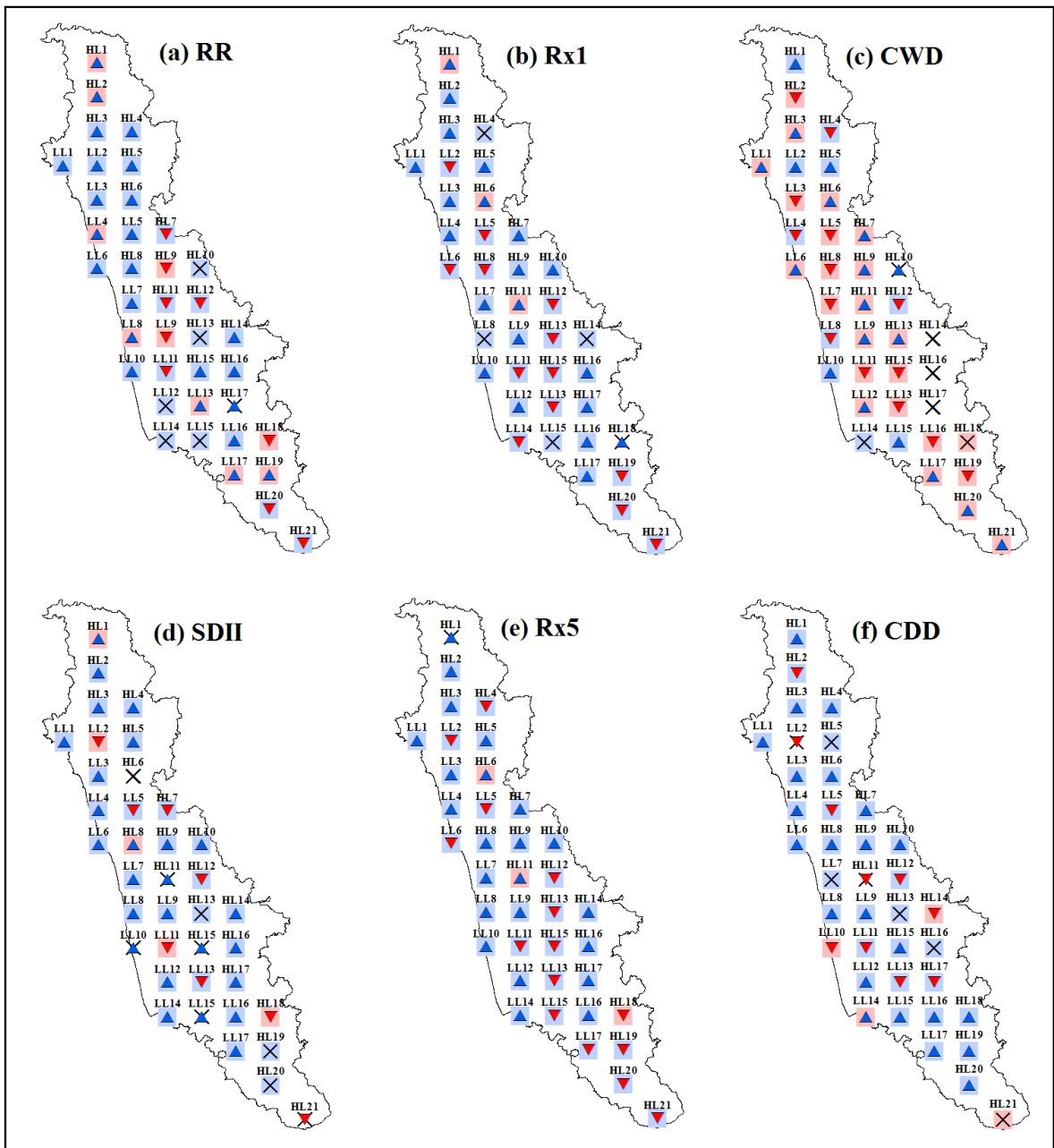


Figure 5.17 (a-f) Grid points with the precipitation extremes influenced by the Niño-3.4 with 1-year and 0-year ahead, respectively.

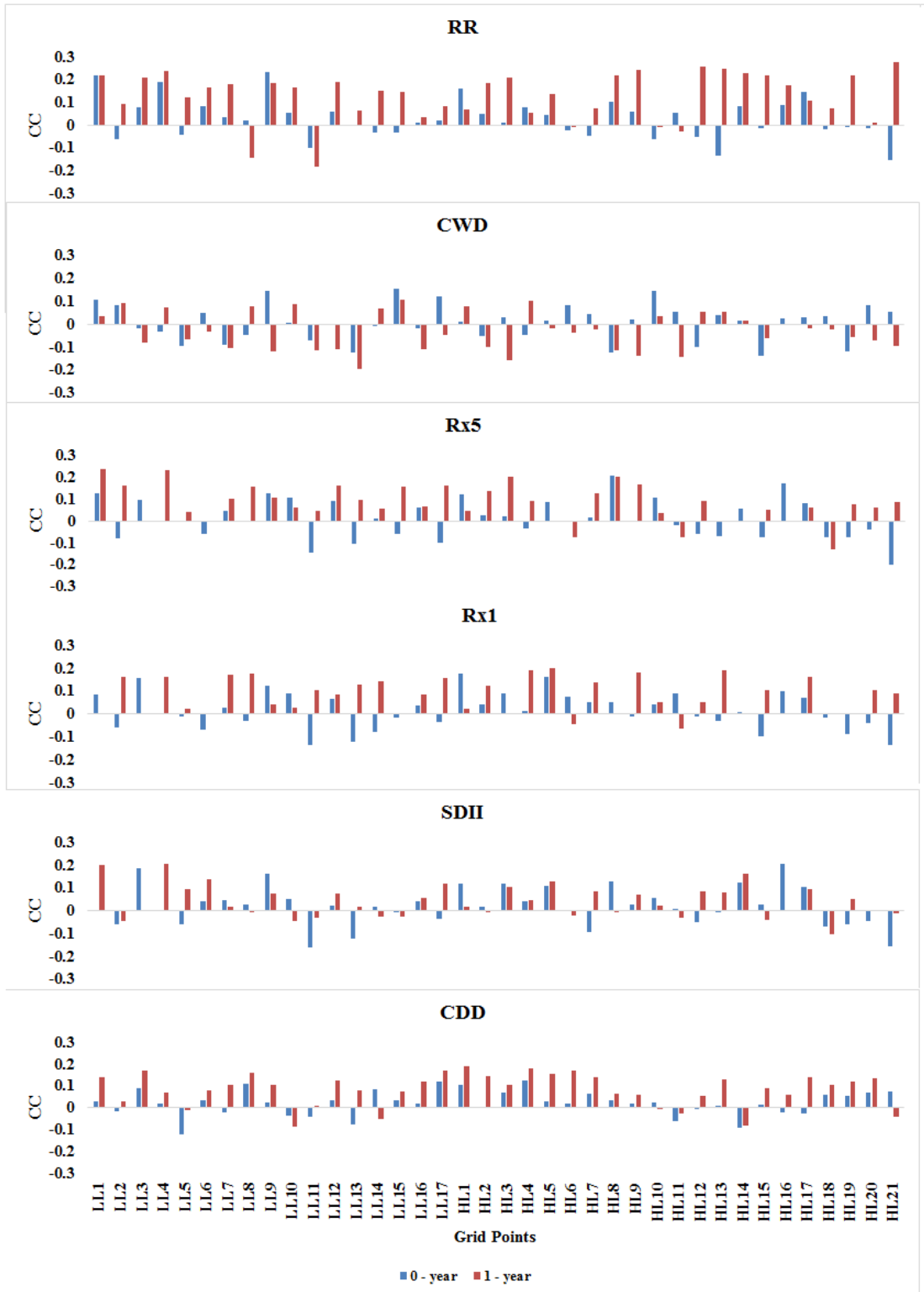


Figure 5.18: The Pearson's correlation between Niño 3.4 and general extreme precipitation indices

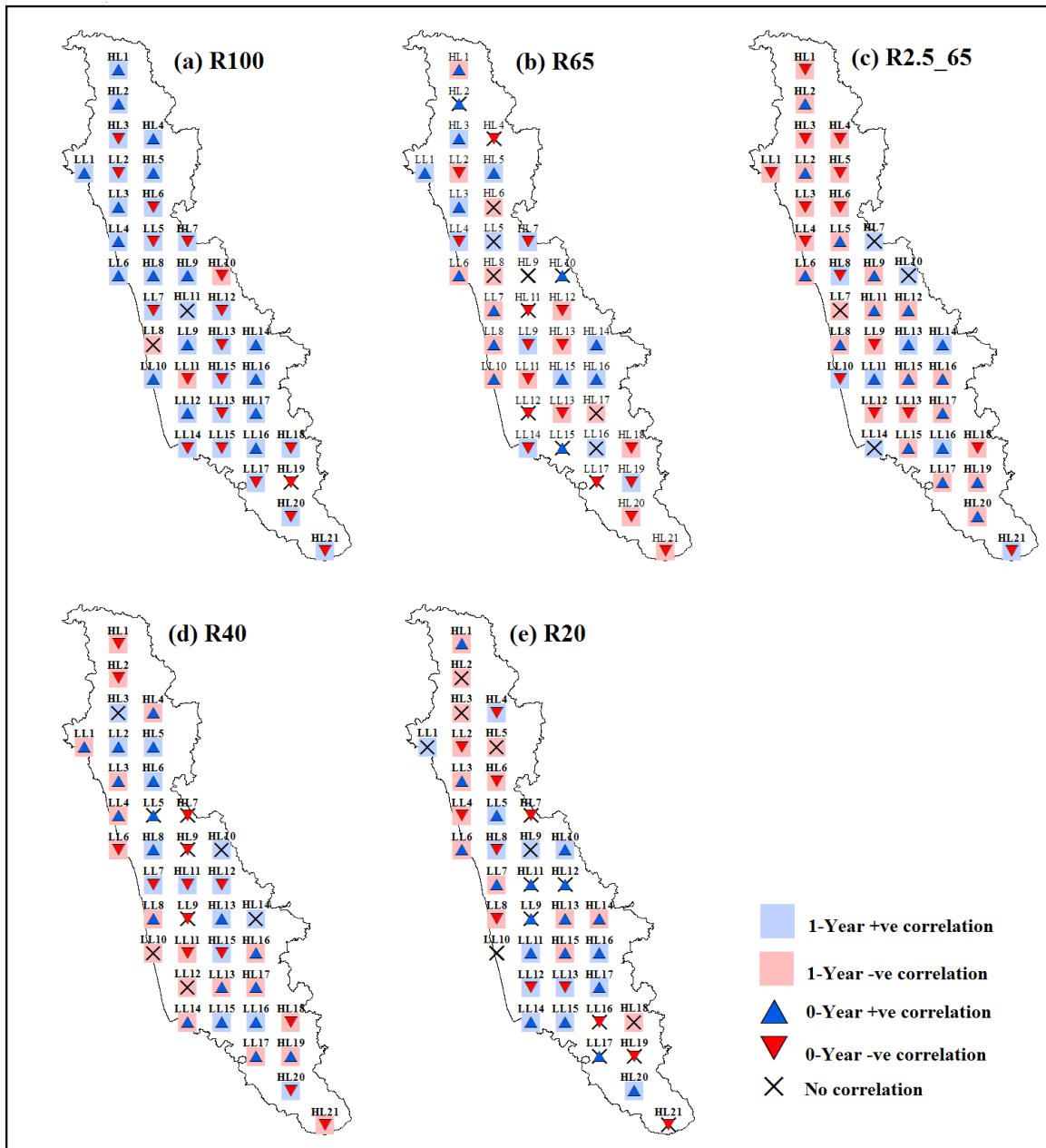


Figure 5.19 (a-e) Absolute threshold intensity rainfall frequency indices influenced by the Niño-3.4 with 1-year and 0-year ahead, respectively.

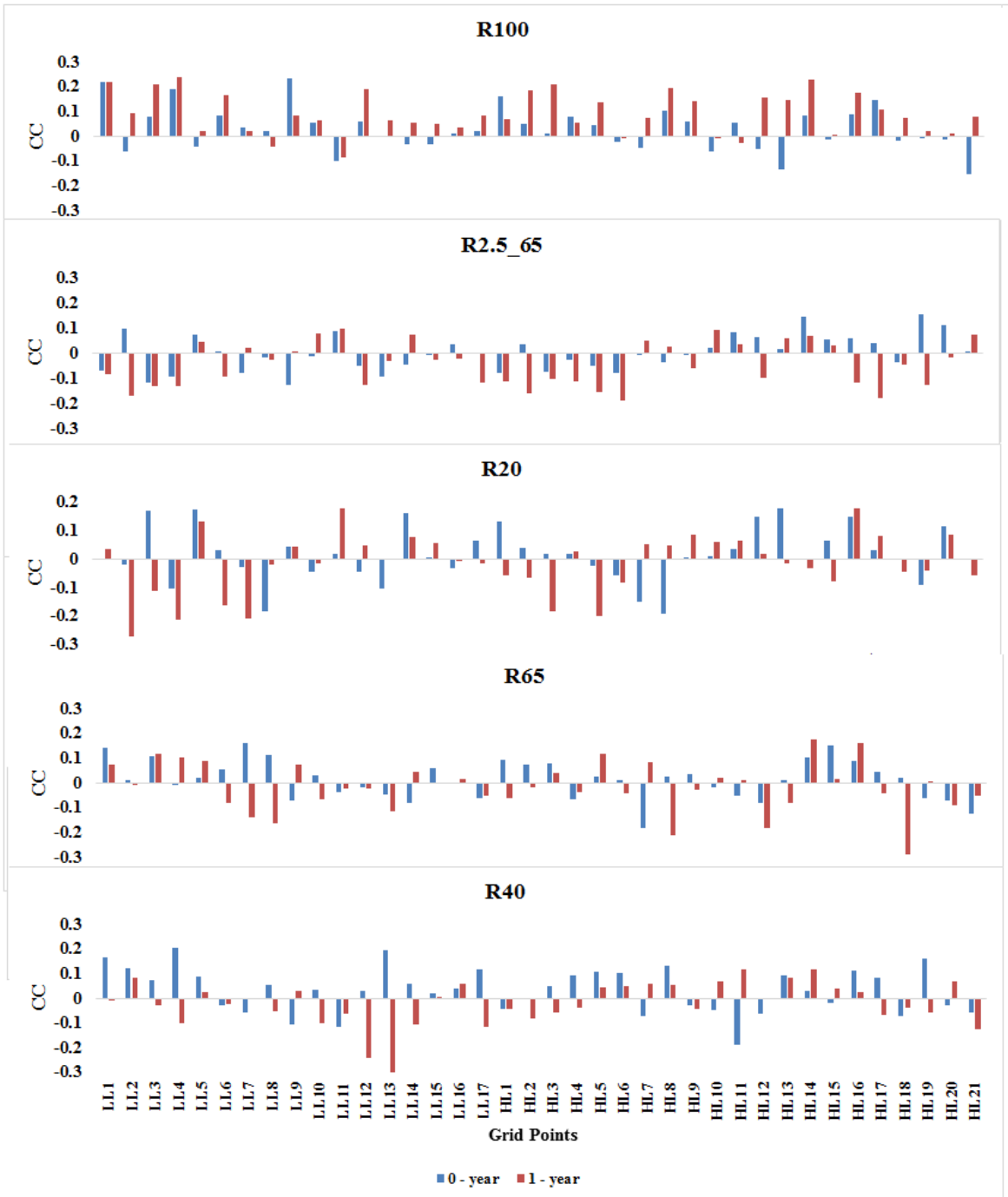


Figure 5.20: The Pearson's correlation between Niño 3.4 and frequency of extreme precipitation indices

5.5 Conclusions

The contrast in the land and sea temperatures between the Asian landmass and the adjacent oceans determines the rainfall in the west coast of Karnataka, India. The moisture laden monsoon winds from the equatorial Pacific Ocean further intensify the low pressure existing over the northern plain. The Indian subcontinent that adjoins the Bay of Bengal and the Arabian Sea receives low-level cross-equatorial south-west monsoon winds, which flow in a westerly direction over the Indian Ocean. The south-east trade winds cross the Equator from the southern hemisphere and are drawn as south-west monsoon winds in the Western Ghats of Karnataka. The summer monsoon winds render very heavy rainfall (more than 3000mm) to the study region's windward side and are divided into two, namely, the Arabian Sea branch and the Bay of Bengal branch.

Correlation coefficients between the SSTs over Niño regions and ETCCDI extreme rainfall indices of the coastal region and the Western Ghats of Karnataka are identified with the asymmetric effects of global SSTs on the extreme rainfall indices. Nevertheless, differences are found between the spatial extent of correlation coefficients and their magnitudes. The following conclusions are drawn after considering the association between ENSO indices and the monsoon.

- Regarded as the most significant time lag between the extreme rainfall indices (dependent variable) and the Niño indices (independent variable), the best model with the highest coefficient of determination was identified by SWR analysis. The teleconnection signal propagation, with respect to multiple index of Niño regions, is explained by the best causal relationship thus generated. Xavier et al., (2018) the large-scale advection of moisture brought about by strengthening of monsoon low level jet (MLLJ) is shown to be a prerequisite for heavy rainfall over the Indian subcontinent.
- The rainfall extreme regimes over the west coast of Karnataka are characterized by analyzing the ETCCDI extreme rainfall indices. If more extreme rainfall (Rx1, Rx5) is less spatially correlated and if it is represented by an annual extreme rainfall index, then the local topography is likely to influence the index. Krishnaswamy et al., (2015) ENSO

positively influences extreme rainfall events below a threshold of 100 mm day^{-1} for Indian region.

- With the intense rainfall events (Rx1 and Rx5) being spatially and sparsely coherent, the regional topography is more likely to impact the synoptic weather system. Attention must be paid to the less spatially correlated precipitation extremes as they are either dominated by a significant trend or are influenced by the regions, in spite of the mounting concern of the hydrological cycle's regional response to climate change.
- The teleconnections between the Niño indices (Niño 1+2, Niño 3, Niño 3.4 and Niño 4) and the rainfall extremes have been examined. The identification of grid points with rainfall extremes affected by ENSO indices with 0-year and 1-year ahead analyzed. It is found that if the Niño indices are at different phases, then the regional response of rainfall extremes to these indices are different. Preethi et al., (2017) the West Pacific SSTs appear to be related with the rainfall over southern parts of India.

CHAPTER 6

ESTIMATION OF SUMMER MONSOON PRECIPITATION

6.1 INTRODUCTION

The chapter 5 shows the teleconnection of Nino indices at 0-year and 1-year lag period for specific seasonal average with ETCCDI extreme rainfall indices. Similarly, considering the consecutive seasonal average of Nino indices identifying the teleconnection of monsoon rainfall at various seasons with respective lag period as predictors.

The south Asian summer monsoon is one the most noteworthy seasonal developments in the world that occurs between June and September. Water managers and irrigators can take informed decisions and formulate risk-management strategies by using the estimation of probabilistic seasonal rainfall. Such estimation can be made up to one year in advance using both dynamical and statistical prediction systems of climate (Goddard et al., 2001). The stationary relationships between the variables and the availability of long term data records are crucial for a statistical prediction system as it is based on empirical associations among the observed variables. In comparison with a statistical climate prediction system, a dynamical prediction system is more expensive for implementation and operation and it is based on such numerical simulations that model physical processes directly (Anderson et al., 1999). ENSO and other climate variables are predicted by simple statistical prediction systems, which are found to be consistently outperform sophisticated dynamical prediction systems, despite such systems being backed by significant technological advances and research studies (Barnston et al., 1999; Quan et al., 2006; Halide and Ridd, 2008). The dominance of statistical prediction system in the forecasting of seasonal rainfall will continue unless there is a significant improvement in the dynamical prediction systems (Rajeevan et al., 2007). A significant temporal and spatial variability is exhibited by the summer monsoon precipitation (SMP), despite the wind patterns' consistent reversal of seasons (Parthasarathy et al., 1995). The Western Ghats is one of the regions that receive the maximum monsoon precipitation, which is unevenly distributed on the Indian spatial domain. Elevated summits and cascaded topography basically comprise the Western Ghats. Heavy precipitation is generated due to the Western

Ghats' abstraction of the summer monsoon winds passing above the Arabian Sea. The highest monsoon seasonal precipitation is received by coastal Karnataka among the Western Ghats' subdivisions (Tawde and Singh, 2015). The association of El Niño-Southern Oscillation (ENSO) with the Indian summer monsoon has been evidenced in several studies, wherein it is proved that large spatial variability is depicted by the Indian SMP (Kripalani and Kulkarni, 1996; Mooley, 1997; Webster et al., 1998; Varikoden and Babu, 2015). The Western Ghats' precipitation is asymmetrically affected by the Niño regions (Revadekar et al., 2018), whereas substantial simultaneous relationships between various ENSO indices and monsoon seasonal precipitation are involved in the ENSO-monsoon teleconnections (Krishna Kumar et al., 1995). The effects of the SMP over the Niño indices, the Western Ghats and the coastal region of Karnataka are being investigated in the present research study.

6.2 IMPORTANCE OF ESTIMATION OF SEASONAL RAINFALL

Among three subdivisions of west coast of India (Kerala, Coastal Karnataka and Konkan Goa), minimum rainfall occurs over Kerala. Maximum rainfall occurs over Coastal Karnataka which is middle subdivision and again rainfall decreases over Konkan & Goa. Thus, though all the three subdivisions of WG receive very high rainfall during the summer monsoon season, it indicates substantial spatio-temporal variation in distribution. Therefore to understand the influence of large-scale phenomenon over the Pacific Ocean SSTs with precipitation over Western Ghats and coastal region of Karnataka, is considered in the study (Tawde and Singh 2015; Revadekar et al. 2018).

Several fields, such as water resource management, food security, fisheries, energy and agriculture, need the prediction of seasonal precipitation, which proves useful for the ground users. More than one hundred years ago, the SMP was estimation in the long range for the first time. The seasonal forecast of the Indian summer monsoon's precipitation has been empirically investigated in several studies (Krishna Kumar et al., 1997; Rajeevan et al., 2004). Several dynamic and statistical forecasting techniques have been tried and tested since then. The forecast of the monsoon remains indefinable, despite a few statistical models functioning better than the dynamic ones (Gadgil et al., 2005). Several studies have investigated the relationship between the ENSO events and the Indian

summer monsoon (Krishna Kumar et al., 1999; Singh et al., 2011; Preethi et al., 2017; Roy 2017). It was found from these research studies that before (after) an El Niño's peak, the Indian summer monsoon is weaker (stronger) than normal in winter. Additionally, this relationship was found to be the opposite for La Niña and monsoon. Further, it was ascertained that during the La Niña (El Niño) summers, the circulation of monsoon was usually stronger (weaker) than normal (Liu and Chan, 2018).

It has been evidenced that El Niño events (with the warmest SST anomalies) were found to be more effective in the central Pacific than in the eastern equatorial Pacific (Krishna Kumar et al., 2006; Varikonden and Babu, 2015). The use of neural network (NN) methods has become popular in climate and atmospheric studies (Gardner & Dorling, 1998) after the derivatives were successfully determined by the Artificial Intelligence (Bishop, 1995). Researchers are now increasingly comparing the conventional and modern methods of forecasts. Lagged associations between the combinations of Niño indices and the SMP at the regional scale are used with the Neural Networks and statistical regression models to predict the summer monsoon precipitation (SMP) in the present study.

6.3 Methodology

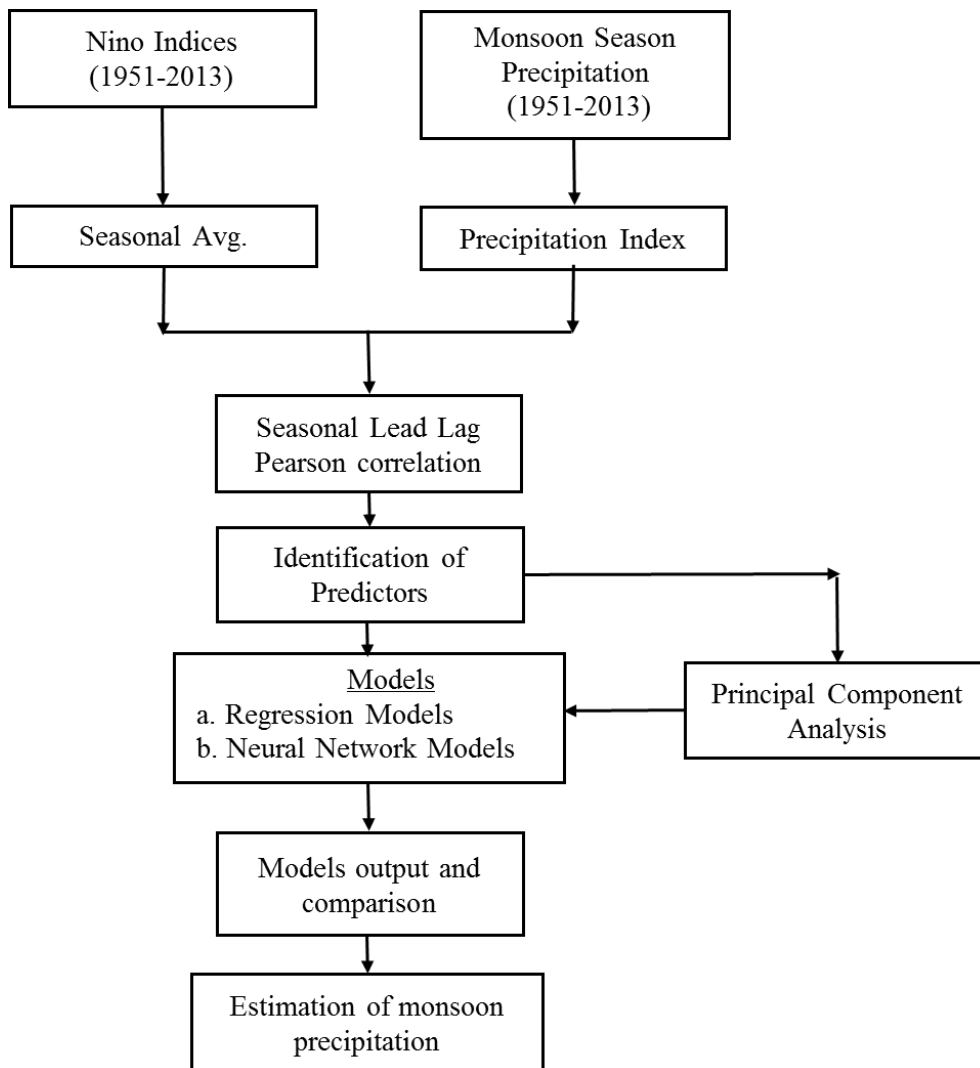


Figure: 6.1 Flow chart of the methodology adopted for estimation of SMP with Niño Indices over study region.

6.3.1 Temporal variation of monsoon season rainfall

In recent years hydro-meteorological disasters such as floods and drought are considered the major sources of losses of unknown percentage Gross Domestic Product (GDP) due to lack of documented information concerning the recurrence of these Rainfall extremes. In this section, Precipitation Index (SPI) was used to assess the recurrence of rainfall pattern. Precipitation index over study region has been estimated to find out in-out phase relationship with ENSO indices over study region as follows:

$$\text{Precipitation Index} = \frac{(\text{climatology of obsrved monthly precipitation} - \text{mean precipitation})}{\text{Std. deviation of time series}}$$

SMP Anomaly = climatology of monthly *average of precipitation* – mean of the *precipitation* time series.

Summer monsoon Precipitation (SMP) anomaly calculated for each months of monsoon season (June-July-August-September) using Thiessen polygon area weighted of grid points partially covered and averaged over study region.

6.3.2 Multiple linear regression model

The extent of association among the variables is determined by utilizing the multiple linear regression analysis. The least square regression analysis can be extended to cases where there are more than one independent variables. Let y the dependent variable (Rainfall) and X_1, X_2, \dots, X_p be the independent variables (Nino Indices). The multiple linear regression equation is represented as:

$$Y = d_0 + d_1X_1 + d_2X_2 + \dots + d_pX_p \quad (6.2)$$

where d_0, d_1, \dots, d_p are the regression constants (coefficients) to be determined. Denoting the observations on the variable as $(Y, X_1, X_2 \dots X_p)$.

The averaging and the anomaly series over the summer season were calculated to construct the summer monsoon precipitation anomaly and were equated with selected potential predictors. The models were developed through the selection of predictor values having a threshold confidence level. Eventually, the predictors in a model are usually subjected to tests and the selected ones are included for making predictions. The final regression equation generally comprises of such predictors only. Another regression model using the first principle component as predictor constructed regression equation. The developed models constructed to predict monsoon precipitation over study region, west coast of Karnataka, India.

6.3.3 Principle Component Analysis

The number of independent variables in principal component analysis was defined considering a set of components accounting for highest total variance (Jolliffe 2002). The mathematical transformation of a number of latently correlated variables into a fewer number of uncorrelated variables is termed as Principal Component Analysis (PCA). Principal components possess the original variables' linear combination and are also known by the generation of a new set of variables by PCA.

Table 6.1 Eigen values of principal component analysis

	PC1	PC2	PC3	PC4
Eigenvalue	2.9024	0.6307	0.3553	0.1116
Variability (%)	72.5592	15.7685	8.8815	2.7907
Cumulative %	72.5592	88.3277	97.2093	100.0000

Table 6.2 Eigen vectors of the principal component analysis

	PC1	PC2	PC3	PC4
Niño4 _(t-2)	0.4172	0.4881	0.0185	-0.2240
Niño4 _(t-3)	0.5464	-0.0726	-0.4635	0.4694
Niño3 _(t-4)	0.4997	-0.2196	0.8268	0.1358
Niño3.4 _(t-2)	0.5269	-0.4137	-0.3181	-0.6708

Table 6.1 illustrates that the variances and eigen values of each component's four-dimensional parameters are gauged by PCA. A majority of the total variance (72.5%) is accounted by the first PC component. The eigen vectors of the four predictor's principal component analysis are shown in Table 6.2. Thus, the data in a one-dimensional space can be represented using the eigen vector that corresponds to the covariance matrix's largest eigen value (PC1 explains about 72% of the variance of the predictors) (Chate et al., 2018). This one dimensional PC is used as predictor in regression equation and input layer as neural network models to avoid over fitting of the model for estimation of seasonal precipitation.

6.3.4 Artificial Neural network

An artificial neural network (ANN), or simply neural network (NN), is a mathematical or computational representation of a model inspired by neural networks of the biological nervous system. The neural networks are able to capture complex patterns that exist in the data, and to solve problems that are difficult for conventional computers or human beings (Chowdary 2007). Generally, the network models have been found to outperform the traditional empirical, statistical or numerical models (Singh & Borah, 2013). Since 1980s, several models of neural networks with different learning algorithms and topologies have been formulated (Rumelhart et al., 1985). Several fields (including atmospheric science) utilize neural networks.

Among the different kinds of existing Artificial Neural Networks, the present study has focused on generalized regression neural network and feed-forward neural network.

i. Training of an Artificial Neural Network

The rules of learning are used to implement the process of learning, which is termed training. The rules of learning are classified into supervised learning and unsupervised learning.

- Supervised learning: The given inputs are used by the network in determining the predictive performance. Both the inputs and the outputs are known in supervised learning.
- Unsupervised learning: The neurons have to manage the outputs, as they are not known in unsupervised learning.

In present study, supervised learning method is used with potential selected predictors with training period from 1951 to 2000 and test period of 2001 to 2013 by trail method.

ii. Feed Forward Back Propagation Neural Network

Figure 6.2 depicts a typical feed forward back propagation neural network. Complicated problems are solved by such network types, as they utilize one or multiple layers hidden

between the output layers and the input layers. The number of neurons is fixed in the input layer and in the output layer after the determination of the number of inputs and outputs. However, the optimal count of neurons hiding in the hidden layer has to be selected. Several trial and errors are required to determine the optimum quantity of hidden layers. A good initial value can be selected and the quantity of the input parameters must be used to initiate the finding, followed by the increment in the quantity of hidden layers. The disability of classifying non-linear functions is solved through the utilization of feed forward networks.

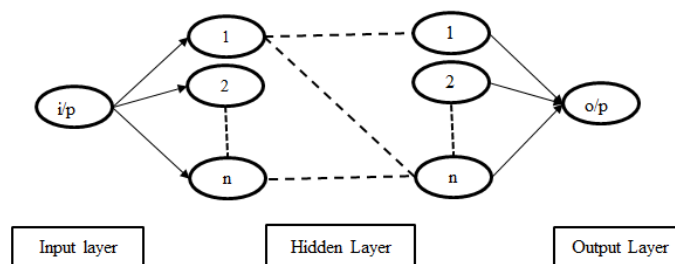


Figure 6.2 Schematic representation of feed forward back propagation neural network

The training of a supervised neural network is based on back propagation. A set of outputs is attained after the data is transmitted in the form of inputs (layer by layer) through the network. The weights of the network are set during this forward pass. A comparison is made between the desired outputs and the obtained outputs. In order to decrease the magnitude of the error, the difference between the calculated outputs (error) and the desired outputs is utilized for adjusting the network's weights as a backward pass. Unless an acceptable magnitude of errors is attained, this process is continuously repeated. Epoch is a term given to the processing of the whole set of data, both as a forward pass as well as a backward pass, by the network. Unless an acceptable magnitude of error is attained, each of the epochs decreases the error, and the network is thus trained in an approach termed as error back-propagation training.

In the current study, PC1 used at input layer, Sigmoid functions at hidden layer and 1 output at output layer selected.

iii. Generalized Regression Neural Network

Specht (1991) proposed generalized regression neural network (GRNN). Like typical feed forward back propagation neural network, GRNN will not require iterative training procedure for approximation of solutions. The GRNN comprises the radial basis function neural network method. Its topology looks similar to typical feed forward neural network, which is used in back propagation training but its operation is different from typical NN. The theory of estimating function is utilized as the basis for the GRNN. The GRNN shows consistent approximation, if a large number of training set is used then the error move towards zero with smaller constraints on the function. The GRNN is based on Nadaraya Watson Kernel regression and it is used to estimate the solutions similar to regression techniques. The GRNN is used in prediction of probability density function of dependent and independent variables. The schematic representation of GRNN is shown in Figure 6.3.

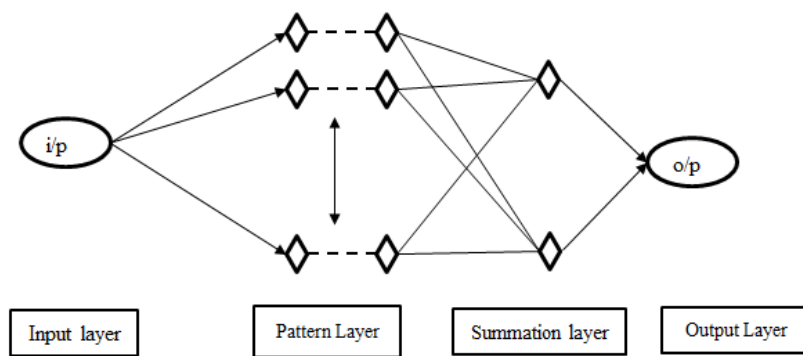


Figure 6.3 Schematic representation of generalized regression neural network

Four layers constitute the GRNN, Wherein the input layer is the first, which depends on the number of inputs considered. The first layer is connected to the second layer, which is called as pattern layer. Each neuron in pattern layer passes through training pattern, which

is processed as output. The pattern layer is then summed up in third layer, called as summation layer. The output layer is the fourth layer with the output neuron. The exponential activation is used at pattern layer and linear activation is used at output layer in the study. GRNN has been used in many hydrological applications and modelling.

In the current study, PC1 used at input layer, Radial Basis function at hidden layer and 1 output at output layer selected.

6.3.5 Statistical Performance

Root Mean Square Analysis

$$RMSE = \sqrt{\frac{\sum_{i=1}^n (F_i - A_i)^2}{n}} \quad (6.3)$$

F_i and A_i are the predicted and observed values of SMP time series data set for year i respectively, and n is the time period.

6.4 Seasonal Precipitation anomaly associated with sea surface temperature

The observed precipitation data used for the period 1951–2013, w.r.to availability of corresponding monthly SSTA time series. The averaging and anomaly series over the summer season (JJAS) is calculated to derive the summer monsoon precipitation index. Figure 6.4 shows standardized precipitation index used for analyzing seasonal relationship of monsoon precipitation and sea surface temperature. Figure 6.4(a) depicts monsoon months precipitation, whereas peak precipitation observed during the month of July and least at withdrawal phase of September month. Figure 6.4(b) shows average monsoon precipitation for the time series with mean of 2706.74 mm and standard deviation 495.6 mm. Monsoon precipitation anomaly normalized by the standard deviation, also termed as standardized monsoon precipitation index (SMPI) calculated for each months of monsoon season (June-July-August-September) and averaged over study region. Years with magnitude of normalized anomaly greater than 1 are excess rainfall seasons, for positive anomalies and negative anomalies less than -1 for deficient rainfall seasons.

The SST of the ENSO indices is utilized as different Niño indices (Niño-1+2, Niño-3, Niño-3.4 and Niño-4), as shown in Figure 6.5 (Trenberth and Stepaniak, 2001; Trenberth, 1997). The actual indices are computed as the specified region's area-averaged sea surface temperature anomalies ($^{\circ}\text{C}$) (Table 1.1 and Figure 1.1 in the first chapter). Corresponding to the times when SST anomalies exceeded 0.4°C in the Niño-3.4 region or when SST anomalies exceeded 0.5°C in the Niño-3 region, the quantification of El Niño is in terms of simple indices. This is apparently sufficient to generate detectable effects in the Pacific rim nations (e.g., USA, South Korea, Russia, Philippines, India, Japan, Colombia, China, Canada, Australia, etc.) (Trenberth, 1997).

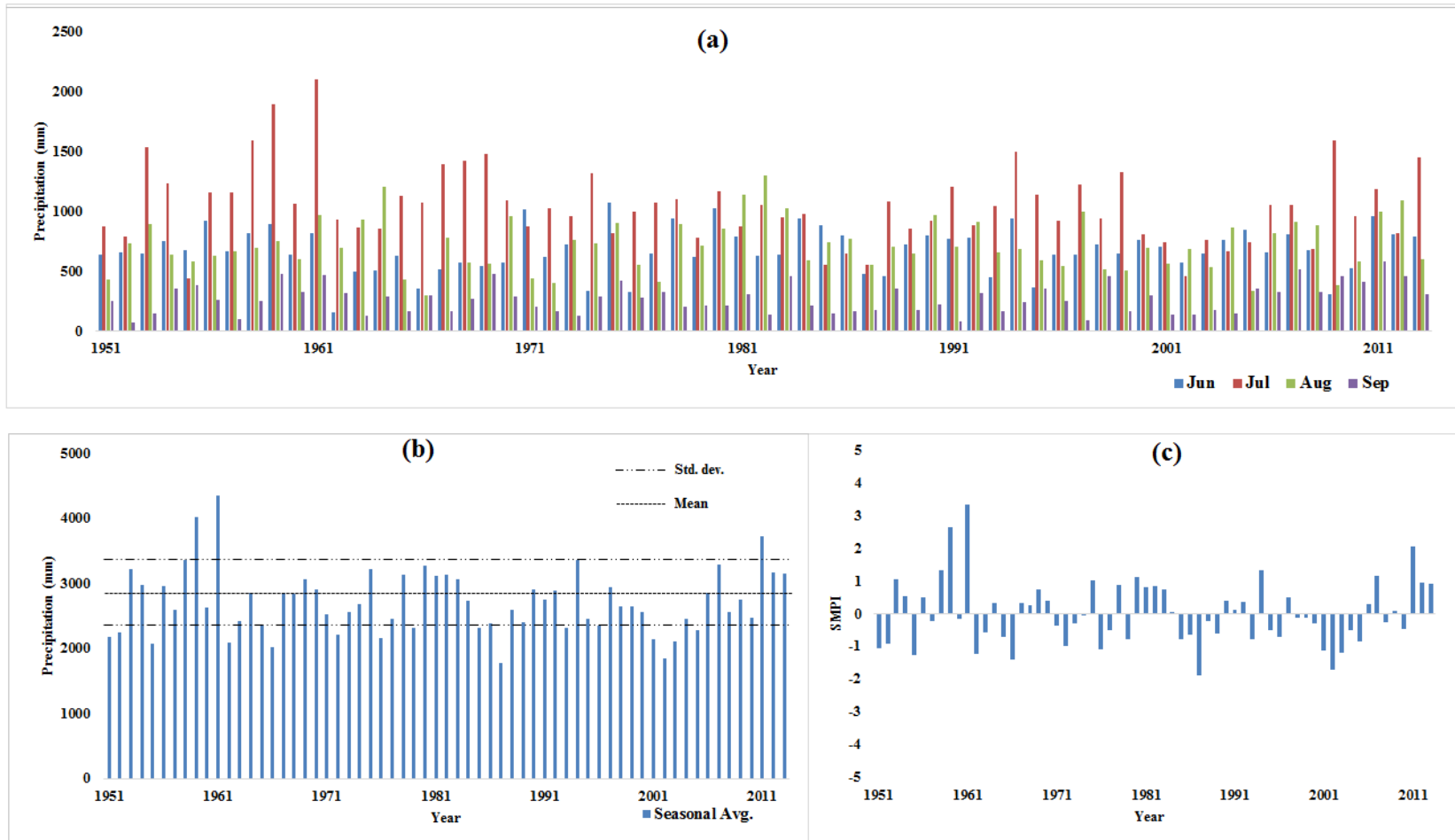


Figure 6.4 The time series for the period of 1951 -2013; (a) Monsoon season (JJAS) monthly precipitation, (b) Average monsoon season precipitation of study region and (c) the anomaly of the summer monsoon precipitation normalized by the standard deviation.

6.5 Temporal variation of Sea Surface Temperature anomalies over Equatorial Pacific Ocean associated with ENSO phases

The temporal variation of SSTA over the Niño 3.4 region play a key role in exploring the recurrence of weak, moderate and strong ENSO events and the linkage between them and the observed rainfall anomalies over study region west coast of Karnataka. Figure 6.5 presents the inter-annual variability of sea-surface temperature anomalies. The three month seasonal average of Niño region during the MAM, JJA, SON and DJF seasons are considered in the study. There are recurrences of the years with the warm and the cold ENSO phases. These warm and cold ENSO events are classified as weak, moderate and strong El Niño and La Niña. Weak El Niño and La Niña events are defined as the years during which the SSTA range between the standardized values of positive/negative 0.5-0.75. Moderate El Niño and La Niña events are defined as the years during which the sea-surface anomaly range between positive/negative 0.75- 1.0 standardized values.

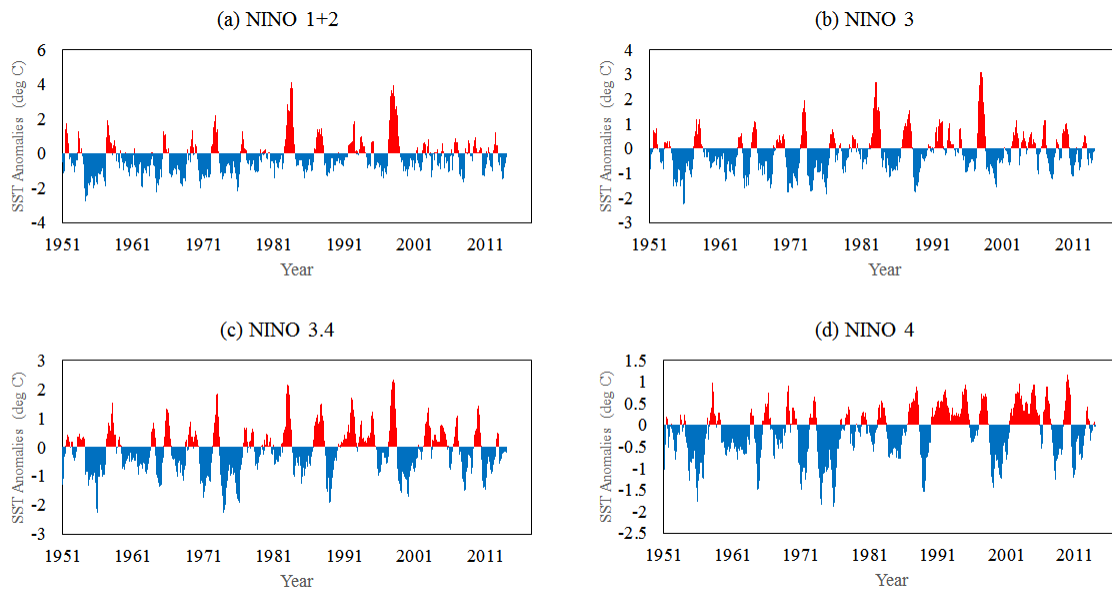


Figure 6.5 ENSO Oceanic Index (Sea surface temperature anomaly) of regions

(a) Niño 1+2, (b) Niño 3 (c) Niño 3.4 and (d) Niño 4

6.6 Seasonal Lead-lag correlation of summer monsoon precipitation index with Niño indices

The correlation of the summer monsoon precipitation index (SMPI) with the Niño indices over the study area is depicted by Figure 6.6. The recording of the concerned SST before the onset of monsoon is demonstrated by the parenthesized negative number on the x-axis. The recording of the SST anomaly after the onset of monsoon is illustrated by the positive numbers. Therefore, such cases are considered for the correlation analysis. Pearson's correlation analysis was used and it was found that the SMP anomaly was correlated with the following predictors for a period of 50 years (1951-2000). Table 6.3 and Figure 6.6 shows the Pearson's correlation of summer monsoon precipitation index with Niño indices. Niño 3 index is correlated with a lag of four seasons and correlation coefficient of 0.25 at 10% significance level. Niño 3.4 index is correlated with a lag of two seasons and correlation coefficient of 0.285 at 5% significance level. Niño 4 index is correlated with a lag of two and three seasons with a correlation coefficient of 0.315 and 0.294 at 5% significance level. From this analysis, it is observed that Niño 4 index has a good relationship with the monsoon over the study region.

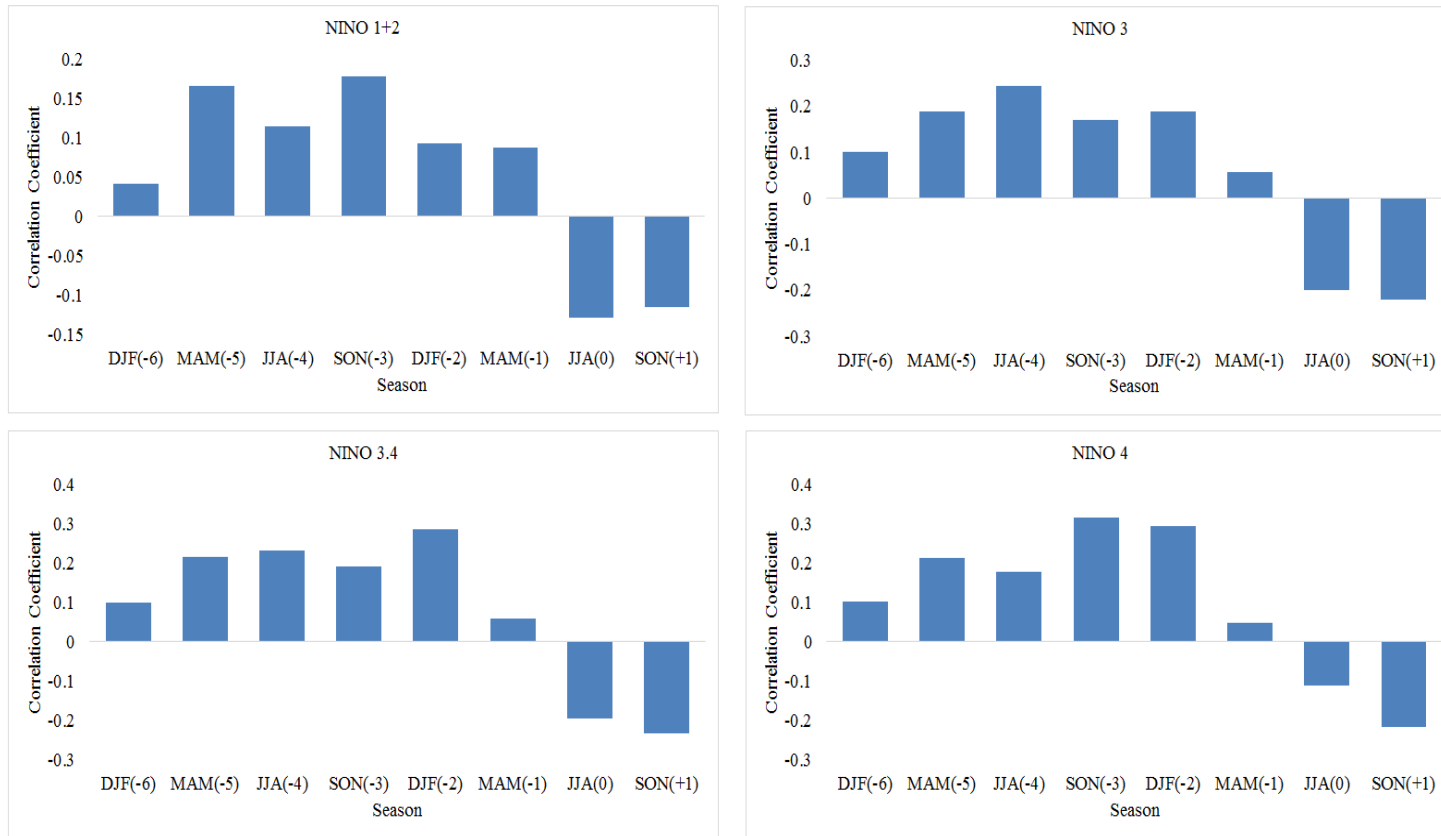


Figure 6.6 Seasonal lead-lag correlation between summer monsoon precipitation index and Niño 1+2, Niño 3, Niño 3.4 index and Niño 4 indices lagging by 1-8 season.

Table 6.3 Seasonal lead-lag relationship between Niño indices and summer monsoon precipitation.

Niño indices	Lag period in season	Correlation coefficient
Niño 3	4 season	0.245**
Niño 3.4	2 season	0.285*
Niño 4	2 season	0.315*
Niño 4	3 season	0.294*

significance level, * 5% significance level

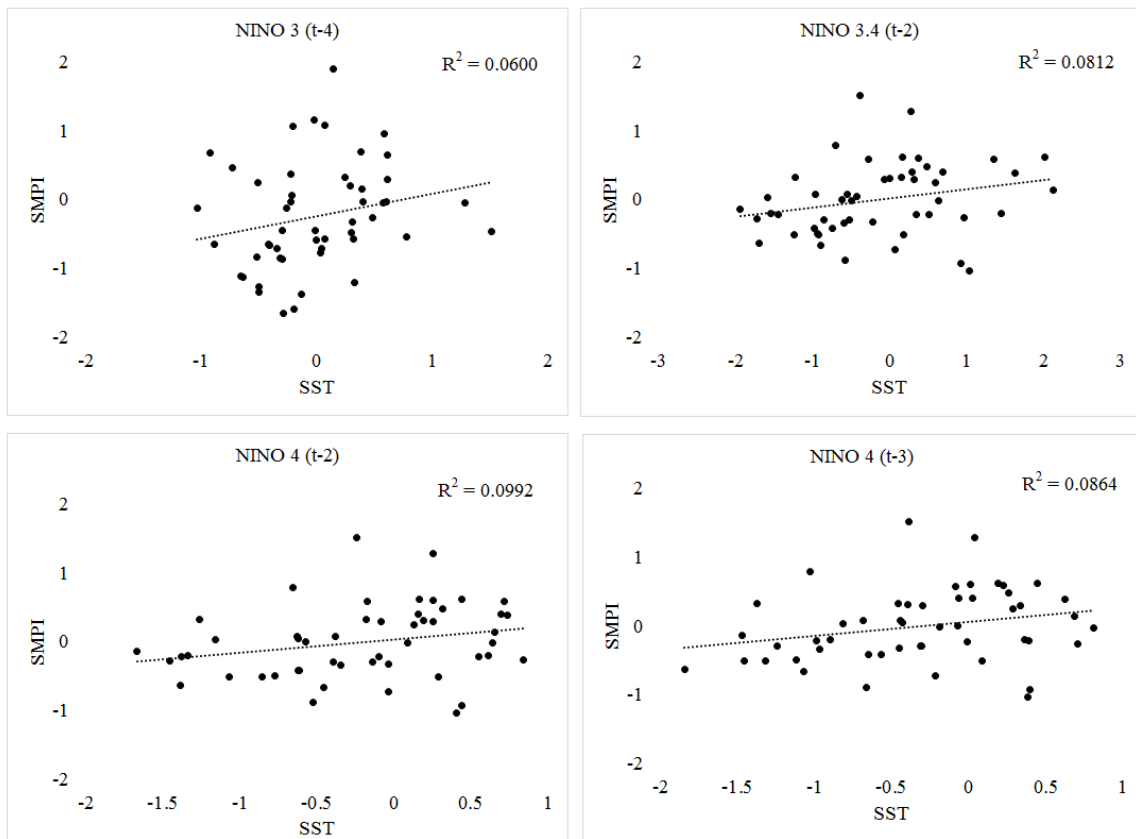


Figure 6.7 Scatter plot of correlation between summer monsoon precipitation index and predictors

The results of seasonal lead-lag correlation are presented in Appendix 13. In the present analysis, Niño 3_(t-4), Niño 3.4_(t-2), Niño 4_(t-2), and Niño 4_(t-3) shows a significant relationship with the summer monsoon precipitation over the study region of Karnataka (Table 6.3). Therefore, these indices have been selected as the predictors. Niño 1+2 index demonstrate a significance level lesser than 80% for any of the lag values. Therefore Niño 1+2 is not considered as a predictor of the analysis. The obtained results are in agreement with studies based on standard ENSO index (Tawde, 2013) with summer monsoon precipitation over Western Ghats.

6.7 Models for estimation of summer monsoon precipitation

The results obtained lead lag correlation of seasonal rainfall anomalies and Niño indices at lagged are significantly correlated at various confidence level. It should be noted that due to the low correlations obtained between the variables under correlation considered in the study, the constructed regression models were based only on the significance greater than 10% of variability for Niño indices. Below equations illustrates the models constructed between seasonal rainfall and Niño indices. The results indicated the regression models constructed were far from being optimal and model not able to capture some peaks observed in the observed rainfall anomalies.

Multiple linear regression models (Wilks 2006) have been formulated for the prediction of the summer monsoon precipitation (SMP) with Niño indices as the threats of over-fitting are avoided and the quantity of free parameters is considerably reduced in the network by the utilization of the first PC as a predictor for neural network. These models are summarized by the following regression equations.

a) Multiple Linear Regression Model

- i. MR = Significant lagged Niño indices included as predictors

$$SMP_t = -20.4 + 0.494 * Niño\ 4_{(t-2)} + 0.034 * Niño\ 4_{(t-3)} + 0.017 * Niño\ 3_{(t-4)} - 0.228 * Niño\ 3.4_{(t-2)} \quad (6.4)$$

- ii. PC = Predictor was used from principal component analysis

$$SMP_t = -15.28 + 0.561 * PC1 \quad (6.5)$$

b) Artificial neural network model

i. NN1 = Feed forward back propagation neural network model (6.6)

ii. NN2 = Generalized regression neural network model (6.7)

Overall, four methods have been developed such as regression method using lagged Niño indices and first principle component, NN1 model using feed forward back propagation neural network, and NN2 model using generalized regression neural network. The models on unseen patterns (test set) were evaluated by using 13 patterns and the coefficients were determined by using 50 patterns in the training set. The correlation coefficient (r) and the root mean square error (RMSE) were used with the observed precipitation for evaluating the models' skills. An analysis of the observed and the predicted precipitation's standard deviation (SD) was also conducted. The standard deviation and the mean of the observed SMP anomaly were 1.9 and 10.6 mm, respectively, for the train series, and 2.12 and 10.45 mm, respectively, for the test series.

6.8 Results and discussion

The global-scale tropical Sea Level Pressure associated with the Southern Oscillation occur in conjunction with the episodes of large-scale sea surface temperature (SST) anomalies (El-Nino/La Nina) over the tropical Pacific region. The intensities of El-Nino events are generally assessed on the basis of the average SSTs over the Nino regions in the Pacific Ocean (Table 1). Subsequently the detection of strong links between the El-Nino Southern Oscillation (ENSO) and the Indian monsoon rainfall (Sikka et al. 1980; Rasmusson et al. 1983; Rao 1999), the empirical models for monsoon prediction have developed rapidly. Many studies have used the relation of ENSO-Rainfall over the Indian sub-continent (Kumar et al. 2007; Gill et al. 2015; Azad and Rajeevan 2016). Parthasarathy et al. (1988) found that Niño 4 region having significant relation with the Indian rainfall, whereas others observed that Niño 3 region (Ashok et al. 2004), and Niño 3.4 region (Gadgil et al. 2003 and 2004) present better relationship with Indian rainfall. Few studies were analyzed for ENSO-rainfall over Karnataka region (Tawde 2013; Revadekar et al. 2018; Amat and Ashok 2018).

6.8.1 Assessing SST-SMP association with identifying predictors and comparison of models

As seen in Figure 6.8, the observed SMP is compared with the model output SMP in the training and the test case for the NN1 model, the NN2 model, the PC1 regression model, and the multiple regression model. Figure 6.9 depicts the difference of SMP between model output and observed data. It may be noted that from Earth System Research Laboratory (NOAA), there were fourteen El Niño (warm phase) and years in the period of the times series (1951-2013).

The NN1 model optimally predicted the El Niño precipitation (Figure 6.11 (a-d)). The NN2 model optimally predicted the La Niña precipitation and the precipitation was predicted with corresponding skill by the multiple regression model. The scatter plot of various anomalies, such as NN1 predicted precipitation, NN2 predicted precipitation, PC predicted precipitation, multiple linear regression predicted precipitation, and observed precipitation, for the training and test cases is depicted in Figure 6.10. It can be seen in Figure 6.10 that the observed precipitation anomalies are in tandem with the precipitation anomalies in the test case.

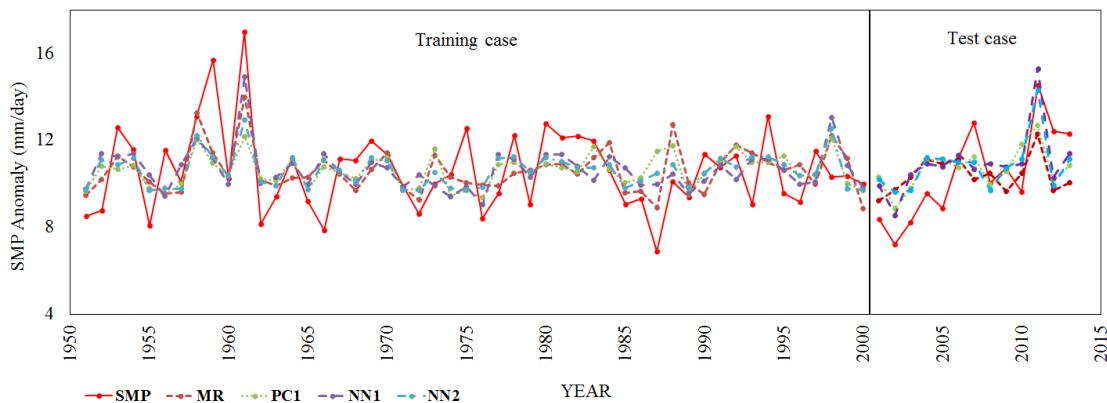


Figure 6.8 The comparison of model output and observed data for multiple regression model, PC1 regression model, NN1 (FFNN) model and NN2 (GRNN) model.

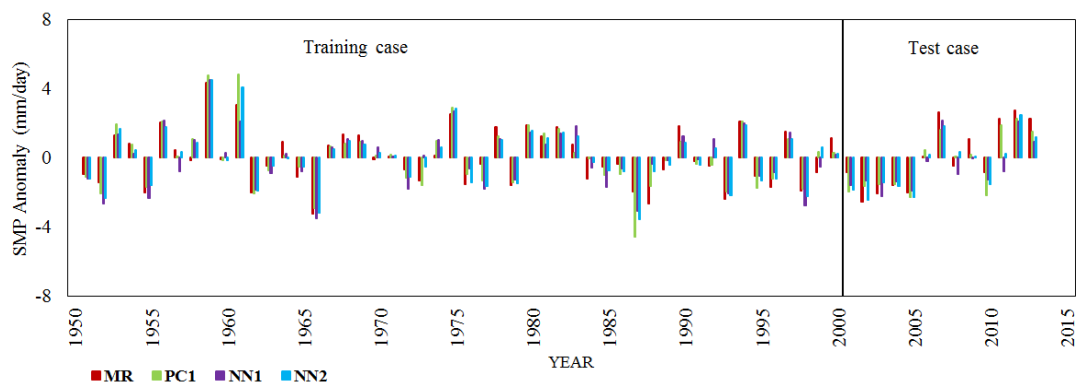


Figure 6.9 The difference of seasonal mean precipitation anomaly between model output and observed data for multiple regression model, PC1 regression model, NN1 (FFNN) model and NN2 (GRNN) model.

The models' prediction skills for the training case and the test case are summarized in Table 6.4. The RMS errors of the model and the NN1 model's better performance (on the basis of the correlation with the observed precipitation) for the training and test cases are depicted in Table 6.4. The NN1 model output's correlation coefficient was found to be 0.53 for the training case and 0.72 for the test case. The NN1 model's RMS error was 1.60 for the training case and 1.63 for the test case. In comparison with the NN2 model, the model output's correlation coefficient was 0.55 for the training case and 0.66 for the test case. The NN2 model's RMSE was 1.61 for the training case and 1.58 for the test case. The prediction was found to be better than the mean prediction, because the standard deviation of the observed data was significantly larger than the RMS error of NN models for the test case. Moreover, the regression models had more RMS errors in the training case and in the test case, when compared with the NN models. When compared to the observed standard deviation, the NN1 model's test case standard deviation was 1.5 (Table 6.4). The test case standard deviation of the multiple linear regression model and the NN2 model was 1.22. Therefore, the variance explained by the NN2 model was found to be slightly lower than that of the NN1 model.

Therefore, when El Niño and La Niña years are pertained, the accuracy of predicting the seasonal precipitation is compared between the multiple linear regression model and the

NN models. Nevertheless, the overall prediction skill of the multiple regression model is less accurate than that of the NN1 model. It is important to observe that the SST values' spatial variability in the aforementioned Niño regions is equally important as the actual values of sea surface temperature in individual regions. This is due to the fact that the second PC of the Niño indices is predicted by the first one, which is correlated with the SMP anomaly. The multivariate regression model's performance establishes the linear regression model, which is not able to discover the complex relationship between the summer monsoon precipitation anomaly and the sea surface temperature's spatial variability in the aforementioned Niño regions. The outcomes discussed above depict that the variability's non-linear feature is successfully captured by the NN1 model with the individual predictors.

Table 6.4 Performance of the models used in prediction of summer monsoon precipitation.

Predictor Models	Training				Test			
	r	RMSE	SD	RSD	r	RMSE	SD	RSD
MR	0.54	1.59	1.03	1.85	0.43	1.84	0.82	2.59
PC1	0.39	1.74	0.75	2.54	0.64	1.63	0.96	2.22
NN1	0.53	1.60	0.97	1.97	0.72	1.63	1.50	1.42
NN2	0.55	1.61	0.76	2.52	0.66	1.58	1.22	1.73

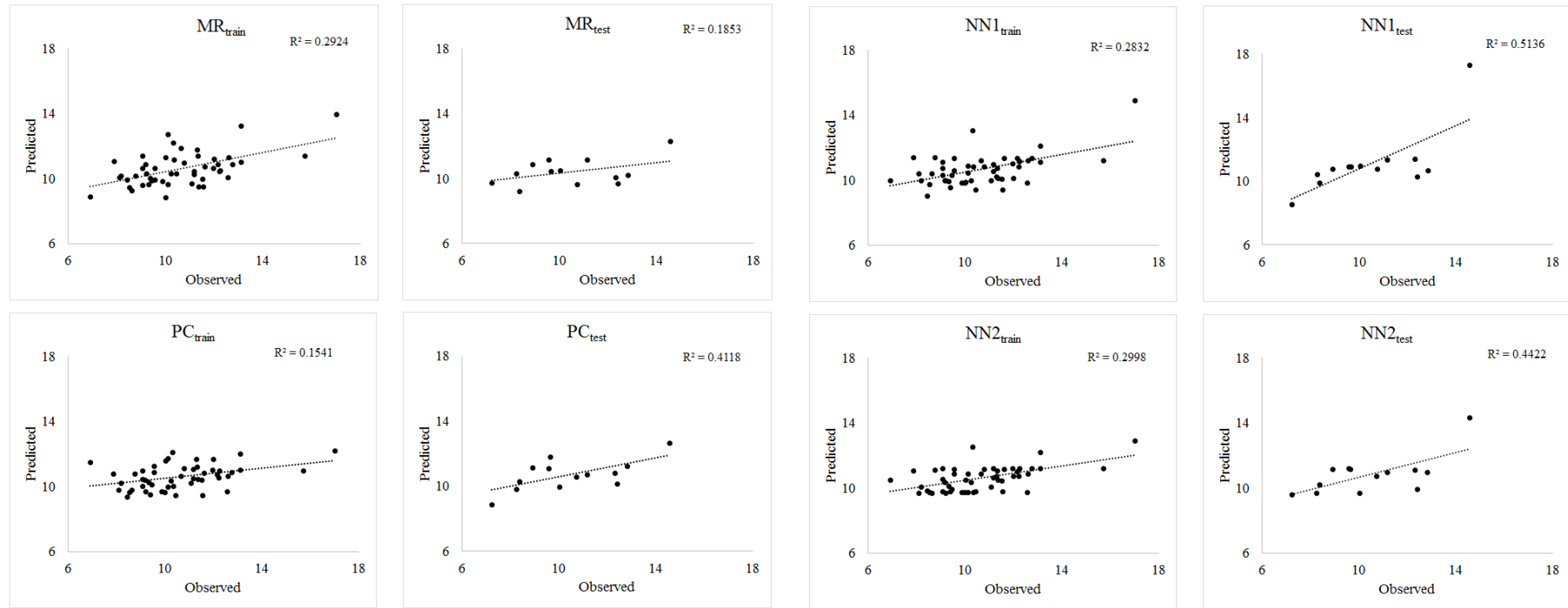


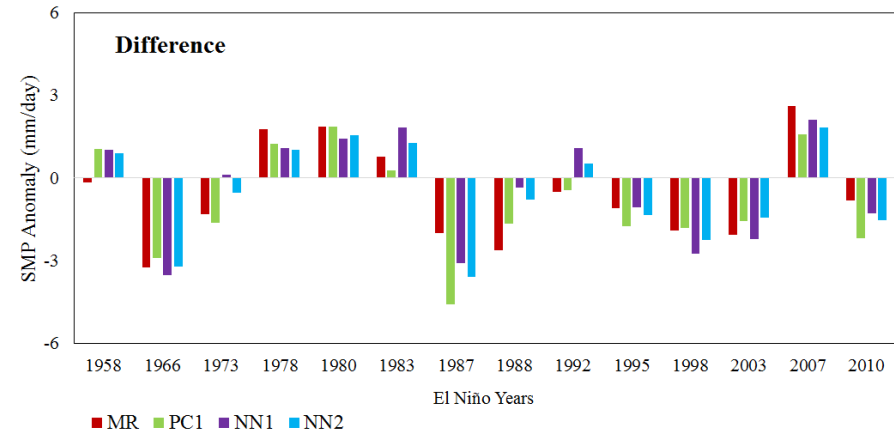
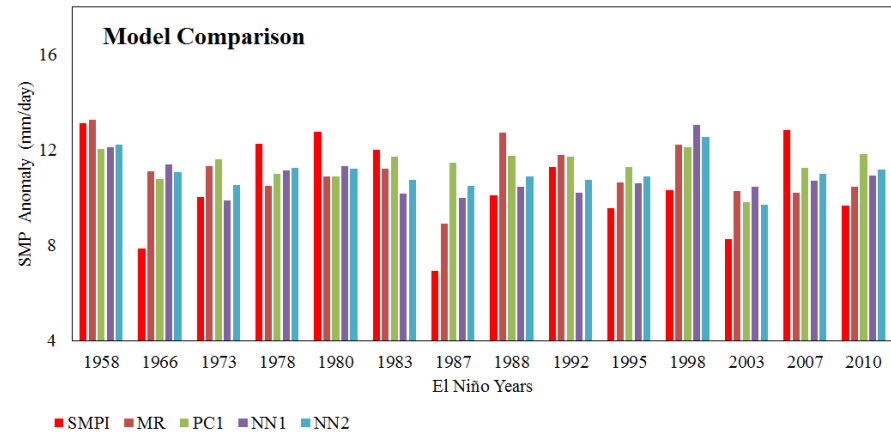
Figure 6.10 Scatter plot of the model performance between training and test set of the models MR, PC1, NN1, and NN2.

6.8.2 Rainfall Anomaly teleconnected with ENSO Events

The evaluation of rainfall anomalies over west coast of Karnataka region during ENSO years is very important for risk assessment and damage associated with climate extremes. This helps in anticipating the type of risk associated with ENSO as part of early warning processes. The analysis is based on evaluation of rainfall performance corresponding to the timing of the ENSO and composite analysis of rainfall anomalies patterns corresponding to El Niño and La Niña events, to define performance of models (wet and dry conditions) during these episodes (Figure 6.11). The results shows the strong evidences that dry, wet and normal conditions are recurrent in study region during weak, moderate, and strong ENSO (El Niño and La Niña) events. Moreover, the results show that some of the driest and the wettest years over the study region coincide with the strength of the ENSO events.

From the time series 1951-2013 of standardized monsoon precipitation Index (Figure 3c) selected the positive episodes values having standardized value greater than +1 (excess) and similarly with negative episodes values with standardized values less than -1 (deficit). The mean anomalous SST values for the region Nino 3.4 for the season DJF (-2) for positive episode is 0.1719°C and the negative episode is -0.5133°C. These two SST means are found significantly different at confidence level of 87.15% through the Student's t-test.

(a) El Niño



(b) La Niña

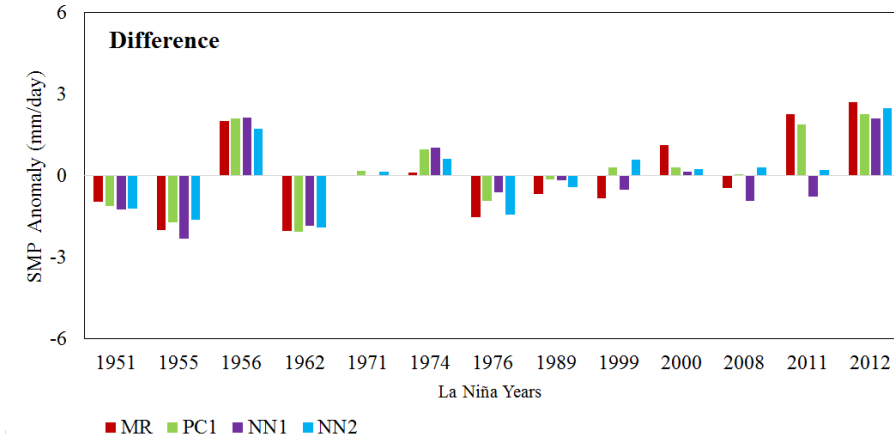
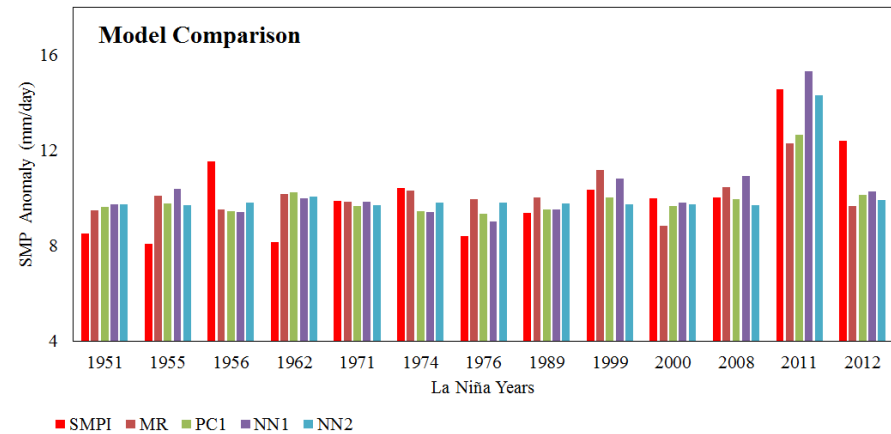


Figure 6.11 Comparison of SMP anomaly with prediction models output during (a) El Niño and (b) La Niña period respectively.

6.9 Conclusions

ENSO indices of different Niño regions show asymmetric relationship with summer monsoon precipitation over the study region. The models need to be subjected to constant changes and scrutiny for a better prediction, because of the prediction models' underlying problems like varying predictability, variation in the predictor-predictand relationship, etc. Changing the training period's length, analyzing the predictors' combination, changing the size of the model, etc. are some of the ways to implement the changes. The demonstration of a better performance by the models during a common test period results in the changes being acceptable. The prediction of seasonal summer monsoon precipitation over the study region is the outcome of the ceaseless efforts put in for adopting better skills.

A significant lag correlation between the summer monsoon precipitation and four Niño indices was revealed by the seasonal lead-lag correlation analysis, which helped to select significantly influencing four predictors based on this analysis. In order to investigate the combined lagged effects of the potential climate predictors for west coast and Western Ghats of Karnataka summer monsoon precipitation using multiple linear regression as a linear method compared to neural network as a nonlinear method have been employed to examine the predictability of the summer monsoon precipitation by utilizing the selected Niño indices as the predictors.

Generalized regression neural network (NN2) model is able to predict better in comparison with NN1 neural network model during El Nino phase. The attained prediction by feed forward back propagation neural network model (NN1) utilized in the prediction of SMP are significantly better than other selected models. However, the comparison of the standard deviation and the Root Mean Square error of the observed precipitation reveals that the mean prediction was better. This study basically concluded that non-linear relationship between the summer monsoon precipitation and the Niño indices over the study region and neural network modelling technique is able to provide a better prediction of precipitation.

Based on the modelling of monsoon season rainfall using ENSO indices, the following conclusions were drawn:

- The analysis of the Niño indices with the summer monsoon rainfall reveals that there is a significant lag correlation between them, which helped to select four significantly influencing predictors on the basis of correlation analysis.
- India, as a whole, receives deficit precipitation during El Niño and excess precipitation during La Niña episodes. The models using Niño indices depict a low prediction performance during El Niño period and a comparatively better prediction during La Niña period. Ihara (2007) results supports the ENSO events have strong relationship with rainfall over study region.
- Monsoon rainfall during the ENSO phases and the prediction by models MR and NN2 was good in El Niño (warm phase) years. The NN1 model showed a better prediction in La Niña (cold phase) years.
- The attained prediction on the basis of the overall performance of the NN1 (FFNN) neural network model shows a better prediction when compared to other models with a good correlation coefficient and RSD of 0.53 and 1.97 for training case, and 0.72 and 1.06 for testing case, respectively. The RMSE of NN1 was slightly higher (1.63) than that of NN2 (1.58) in the testing case, and the coefficient correlation of NN1 (0.53) was slightly lesser than that of NN2 (0.55) in the training case.
- The mean anomalous SST values for the region Niño 3.4 for the season DJF (-2) for positive episode is 0.1719°C and the negative episode is -0.5133°C . These two SST means are found significantly different at confidence level of 87.15% through the Student's t-test.
- The present study basically concludes that non-linear relationship between the Niño indices and the summer monsoon precipitation over the study region using neural network modeling technique is able to provide a better prediction of the rainfall.

SUMMARY AND CONCLUSIONS

7.1 SUMMARY

The focus of the present study was to assess the impacts of climate change on extreme rainfall events over the coastal region and Western Ghats of Karnataka. The primary research aims to develop a synoptic-scale rainfall climatology for the Western Ghats and Coastal region of Karnataka, assess the variability of synoptic types of extreme rainfall events using Expert team on climate change detection and monitoring Indices (ETCCDI), and to understand the asymmetric relationship of large-scale climate driver Nino indices influence on variability of extreme events. Climate of study region is dominated by the summer monsoon (JJAS), which delivers most of rainfall, which accounts for 80% of the annual rainfall. Extreme rainfall events increase along the slopes of the coastal plains and rapidly decrease on the eastern leeward side. Summer monsoon exhibits large variability in different space and time scales. The variability in rainfall is always viewed of concern and it is teleconnected with ENSO indices. However, studies on regional scale variability and their teleconnection are meagre. In view of this, trend and variability in extreme rainfall events in annual and seasonal is examined.

This chapter presents the conclusions drawn from the present investigation. The conclusions are presented sequentially in line with the framed objectives for convenience. Further, the limitations of the present study and scope for further research are also highlighted.

7.2 CONCLUSIONS

Conclusions drawn from the research with respect to the four objectives are discussed in this section.

Objective 1: Trend and variability and long term trends in synoptic extreme rainfall events using ETCCDI rainfall indices.

- The spatial pattern of rainfall indices shows a significant trend for all the indices at 95 to 99.9% confidence levels. Trend in total annual rainfall is significantly increasing along coastal strip and depicts mixed variations at mountainous terrain. The daily average, wet and dry spells rainfall indices are interlinked with each other and predominantly influence the intensity of rainfall events. CWD shows magnitude of Sen's slope -2.6 days/decade to 2.4 days/decade with mixed trend in both spatial and at the significance level (>5%), but daily average and CDD are showing in agreement. With increase in dry spell the daily average rainfall increases by supporting the intense rainfall events.
- Rx1 has decreasing trend ranging from -3mm/decade to 9 mm/decade and Rx5 corresponds to maximum consecutive 5-day rainfall a potential indicator of flood producing event depicts mixed trend with Sen's slope of -14mm/decade to 32mm/decade.
- The monsoon season temporal trend shows significant spatial variations over the study region. The seasonal ratio of rainfall (RRTOT) exhibits a mixed trend with magnitude of -0.35%/decade to 0.99%/decade, but a significantly rising trend is witnessed in the southern coastal plains and the adjacent Western Ghats region during the pre-monsoon. The southern coastal plains show a decreasing trend in the monsoon period (JJAS).
- In the pre- and post-monsoon rainy days, the daily intensity index illustrates a mixed trend over the study region. Most of the grid points show no trend for rainy days and moderate rainfall. A few grid points depict a mixed insignificant trend with a low magnitude of Sen's slope.
- A statistically significant increasing trend exists in the frequency of very heavy and heavy rainfall events with sen's slope of 0.32 days/decade and 0.71 days/decade

respectively, and a significantly decreasing trend exists in the frequency of moderate rainfall (-0.29 days/decade to 0.82 days/decade) at the region of heavy rainfall events.

- A strong correlation exists between the total rainfall and other extreme rainfall indices, especially the heavy rainfall indices with correlation coefficient of 0.8. The intense rainfall is responsible for increase in annual total rainfall.

Objective 2: Influence of oceanic Niño indices on ETCCDI extreme rainfall indices.

- The Step wise regression analysis in order identify the optimal model with highest coefficient of determination for variable lagged Nino Indices at 95% Confidence level. The Consecutive wet days (CWD), Rx5, and Rx1 depicts R^2 of 0.22, 0.25 and 0.19 at 5% significance level.

- Nino 1+2 is having positive correlation with Rx1 and Rx5 at 95% confidence level. Whereas RR, SDII and CWD are showing significant correlations but different stages.

- Nino 3 influence on frequency of intense rainy days, and R100 at both 0-year and 1-year lag period at 95% confidence level. Henceforth, the correlation with lower magnitude rainy days depicts negative relationship. Nino 3 strongly influence the very heavy rainy days by suppressing low intensity rainfall events.

- Nino 4 has positive significant correlation with total annual rainfall at 0-year lag period. Similarly the Nino 3.4 shows moderate mixed relationship for total rainfall. Both Nino 4 and Nino 3.4 has positive correlation but not significant at 95% confidence level.

- The teleconnections between the Niño indices (Niño 1+2, Niño 3, Niño 3.4 and Niño 4) and the rainfall extremes have been examined. The identification of grid points with rainfall extremes affected by ENSO indices with 0-year and 1-year ahead at different scales. It is found that if the Niño indices are at different phases, then the regional response of rainfall extremes to these indices is also dissimilar. Preethi et al., (2017) the West Pacific SSTs appear to be related with the rainfall over southern parts of India.

Objective 3: Estimation of summer monsoon rainfall

- Monsoon rainfall during the ENSO phases and the prediction by models MR and NN2 was good in El Nino (warm phase) years. The NN1 model showed a better prediction in La Niña (cold phase) years. Ihara (2007) results supports the ENSO events have strong relationship with rainfall over study region.
- The attained prediction on the basis of the overall performance of the NN1 (FFNN) neural network model shows a better prediction when compared to other models with a good correlation coefficient and RSD of 0.53 and 1.97 for training case, and 0.72 and 1.06 for testing case, respectively. The RMSE of NN1 was slightly higher (1.63) than that of NN2 (1.58) in the testing case, and the coefficient of correlation of NN1 (0.53) was slightly lesser than that of NN2 (0.55) in the training case.
- The mean anomalous SST values for the region Nino 3.4 for the season DJF (-2) for positive episode is 0.1719°C and the negative episode is -0.5133°C. These two SST means are found significantly different at confidence level of 87.15% through the Student's t-test.
- The present study concludes that non-linear relationship between the Niño indices and the summer monsoon rainfall over the study region. The neural network models are able to capture nonlinearity of ENSO-monsoon relationship and provide better prediction of the monsoon rainfall.

Objective 4: Asymmetric affect of Nino indices with rainfall extremes

- The ENSO-rainfall teleconnections involve simultaneous relationships between different ENSO indices and rainfall at different stages.
- Deficient rainfall is associated with warm SSTs and excess rainfall (extreme events) with cold SSTs over equatorial Pacific. Therefore negative correlations are seen over equatorial Pacific SSTs. Such negative relationship perceived for coastal region and Western Ghats of Karnataka.

- Asymmetric impacts of global SSTs are observed on the rainfall through correlation coefficients between the SSTs at different seasonal average over Nino regions with rainfall over the study region. SSTs over Nino regions are seen for their negative impact on rainfall over the coastal region and Western Ghats of Karnataka, however the magnitudes of correlation coefficients and their spatial extent shows differences.

The results presented in this study are statistically significant nevertheless more studies coupled with general circulation models should be carried out to establish the robustness of the results.

7.3 LIMITATIONS OF THE STUDY

The present study attempted to analyze the association of asymmetric impact of ENSO indices on ETCCDI extreme rainfall indices. However it is known that rainfall is also dependent on large scale climate drivers and its teleconnection with wind speed, wind direction temperature and climatic parameters of the region. Studying rainfall variation by considering all these parameters may give better insight into the rainfall variability in zones of Western Ghats of India. The relation between elevation and frequency of extreme rainfall events should be studied. This study has been limited to examining the ETCCDI extreme rainfall indices exclusively, however, other topographical factors like slope, aspect and geometry of the region may also be the reason for such dissimilar results which need to be studied elaborately.

7.4 SCOPE FOR FUTURE STUDY

The recommendations from current study are:

- a. The study is limited to ENSO indices, the combination of various land and sea climatic indices could able to establish variations of rainfall patterns at local scale.
- b. In recent days the rainfall events are highly varied at local regions, such that it is necessary to identify the local parameters affecting rainfall events.
- c. Recent report states that land covering patterns and irrigation system has significant impact on rainfall. Modelling of irrigation system and rainfall events with respect to climates indices could be established.

In the study area, selected regions having high decreasing or increasing trends or increase in frequency of extreme rainfall events or its trends, the rationale behind this change can be analyzed by incorporating historical change in land cover/land use, variation in temperature, long term trend of aerosol compositions, impact of humidity. The space-time variation in rainfall with wind speed, wind direction and temperature, humidity, aerosol contents can be analyzed considering long period data.

According to recent report IPCC (AR5, 2019) due to Irrigation (Peninsular India) prior to the start of the monsoon season and the resulting land cooling decreases the land-sea temperature contrast. This can delay the onset of the monsoon and decrease its intensity. Irrigating farms in India may be having an unfavourable outcome within its national boundaries but it's probably having some beneficial impact in faraway places. Therefore, based on the current study in future could establish the relationship of rainfall and irrigation management system over Peninsular India. Kerala is the gateway of monsoon for India and in other words it is highly dependent on agro based socio-economic system. Most of the rivers are originated from Western Ghats and irrigation facilitated.

Humans have altered the earth's surface - primarily by urbanization and agricultural activities (IPCC, 2013). Use of land for agriculture, which is often accompanied by irrigation, modifies the land surface through changes in the water and energy balance between land surface and atmosphere. This further influences climatic parameters like temperature, rainfall and cloud formation. The effect is more pronounced on local as compared to global climate. India is one of the regions of the world with a large irrigated area. The practice of irrigation has changed in recent years resulting in depletion of groundwater. In future, as the groundwater sources get depleted, the effect on agriculture and climate are bound to be locally significant.

Irrigating farms in India may be having an unfavourable outcome within its national boundaries but it's probably having some beneficial impact in faraway places. According to a global modelling study, irrigation in India is increasing rainfall in the Horn of Africa.

REFERENCES

- Alexander, L.V., Zhang, X., Peterson, T.C., Caesar, J., Gleason, B., Klein Tank, A.M.G., Haylock, M., Collins, D., Trewin, B., Rahimzadeh, F., Tagipour, A., Rupa Kumar, K., Revadekar, J., Griffiths, G., Vincent, L., Stephenson, D.B., Burn, J., Aguilar, E., Brunet, M., Taylor, M., New, M., Zhai, P., Rusticucci, M. and Vazquez-Aguirre, J.L. (2006). "Global observed changes in daily climate extremes of temperature and precipitation." *J. Geophys. Res. Atmos.*, 111(5), 1–22.
- Amat, H.B. and Ashok, K. (2018). "Relevance of Indian Summer Monsoon and its Tropical Indo-Pacific Climate Drivers for the Kharif Crop Production." *Pure Appl. Geophys.*, 175(6), 2307–2322.
- Anderson, J., Van Den Dool, H., Barnston, A., Chen, W., Stern, W. and Ploshay, J. (1999). "Present-day capabilities of numerical and statistical models for atmospheric extratropical seasonal simulation and prediction." *Bulletin of the American Meteorological Society*, 80(7), 1349-1362.
- Annamalai, H., Hamilton, K. and Sperber, K.R. (2007). "The South Asian summer monsoon and its relationship with ENSO in the IPCC AR4 simulations." *J. Clim.*, 20:1071-1092.
- Ashok, K., Guan, Z., Saji, N.H. and Yamagata, T. (2004). Individual and combined influences of ENSO and the Indian Ocean dipole on the Indian summer monsoon." *J. Clim.*, 17, 3141-3155.
- Ashrit, R.G., Kumar, K.R. and Kumar, K.K. (2001). "ENSO-monsoon relationships in a greenhouse warming scenario." *Geophys. Res. Lett.*, 28(9), 1727.
- Azad, S. and Rajeevan, M. (2016). "Possible shift in the ENSO-Indian monsoon rainfall relationship under future global warming." *Sci. Rep.*, 6(1), 20145.
- Barnston, A.G., Chelliah, M. and Goldenberg, S.B. (1997). "Documentation of a highly ENSO-related SST region in the equatorial Pacific: Research note." *Atmosphere-ocean*, 35(3), 367-383.
- Barnston, A.G., Glantz, M.H. and He, Y. (1999). "Predictive skill of statistical and dynamical climate models in SST forecasts during the 1997–98 El Niño episode and the 1998 La Niña onset." *Bulletin of the American Meteorological Society*, 80(2), 217-244.
- Bharti, V. and Singh, C. (2015). "Characteristics of the spatiotemporal pattern of Extreme Rainfall event over the state of Uttarakhand, India." *In ICUC9-9th International Conference on Urban Climate jointly with 12th Symposium on the Urban Environment Characteristics.*
- Bjerknes, J. (1969). "Atmospheric teleconnections from the equatorial Pacific." *Monthly weather review*, 97(3), 163-172.
- Brown, P.J., Bradley, R.S. and Keimig, F.T. (2011). "Changes in Extreme Climate Indices for the Northeastern United States, 1870–2005." *J. Clim.*, 23:6555–6572. doi: 10.1175/2010JCLI3363.1

- Casanueva, A. (2014). "Variability of extreme precipitation over Europe and its relationships with teleconnection patterns." 709–725. doi: 10.5194/hess-18-709-2014
- Chakraborty, A. (2018). "Preceding winter La Niña reduces Indian summer monsoon rainfall." *Environ Res Lett.*, 13:054030. doi: 10.1088/1748-9326/aabdd5
- Chate, G.R., Patel, G.C.M., Kulkarni, R.M., Vernekar, P., Deshpande, A.S. and Parappagoudar, M.B. (2018). "Study of the Effect of Nano-silica Particles on Resin-Bonded Moulding Sand Properties and Quality of Casting." *Silicon*. 10(5), 1921-1936.
- Chowdary, B.V. (2007). "Back-propagation artificial neural network approach for machining centre selection." *J. Manuf. Technol. Manag.*, 18(3), 315–332.
- Coles, P. (1999). "All eyes on El Nino." *The Unesco Courier* 52(5): 30.
- Croitoru, A.E., Piticar, A. and Burada, D.C. (2016). "Changes in precipitation extremes in Romania." *Quat. Int.*, 415, 325–335.
- Dash, S., Jenamani, R., Kalsi, S. and Panda, S. (2007). "Some evidence of climate change in twentieth century." *India Climatic change*, 85:299-321.
- Dash, S.K., Kulkarni, M., Mohanty, U.C. and Prasad, K. (2009). "Changes in the characteristics of rain events in India." *J. Geophys. Res.*, 114.
- Demaria, E.M.C., Maurer, E.P., Sheffield, J., Bustos, E., Poblete, D., Vicuña, S. and Meza, F. (2013). "Using a Gridded Global Dataset to Characterize Regional Hydroclimate in Central Chile." *J. Hydrometeorol.*, 14(1), 251–265.
- Dhar, O.N., Kulkarni, A.K. and Ghose, G.C. (1978). "Rainfall distribution over Indian subdivisions during the wettest and the driest monsoons of the period 1901–1960." *Hydrological Sciences Journal*, 23(2), 213-221.
- Donat, M.G., Peterson, T.C., Brunet, M. (2014). "Changes in extreme temperature and precipitation in the Arab region: Long-term trends and variability related to ENSO and NAO." *Int J Climatol.*, 34:581–592. doi: 10.1002/joc.3707
- Dorji, S., Herath, S., Mishra, B.K. and Chophel, U. (2018). "Predicting summer monsoon of Bhutan based on SST and teleconnection indices." *Meteorol Atmos Phys.*, 1–11. doi: 10.1007/s00703-018-0589-2
- Duan, W., He, B. and Takara, K. (2015). "Changes of precipitation amounts and extremes over Japan between 1901 and 2012 and their connection to climate indices." *Clim Dyn.*, 45:2273–2292. doi: 10.1007/s00382-015-2778-8
- Emori, S. and Brown, S. J. (2005). "Dynamic and thermodynamic changes in mean and extreme precipitation under changed climate." *Geophys. Res. Lett.*, 32(17).
- Enders, W. (2002). "Applied econometric time Series 4th ED." *Retail Trade*, 2–43.
- Fedorov, A.V. and Philander, S.G. (2000). "Is El Niño changing?." *Science*, 288(5473), 1997-2002.

- Fowler, A.M. and Hennessy, K.J. (1995). "Potential impacts of global warming on the frequency and magnitude of heavy precipitation." *Natural Hazards*, 11(3): 283-303.
- Francis, P.A. and Gadgil, S. (2006). "Intense rainfall events over the west coast of India." *Meteorol Atmos Phys.*, 94, 27-42.
- Gadgil, S. (2003). "The Indian monsoon and its variability." *Annual Review of Earth and Planetary Sciences*, 31(1), 429-467.
- Gadgil, S. and Gowri, R. (1988). "Coherent rainfall zones: Case study for Karnataka." *Earth Planet. Sci.*, 97(9), 63-79.
- Gadgil, S., Rajeevan, M. and Nanjundiah, R. (2005). "Monsoon prediction - Why yet another failure?" *Curr. Sci.*, 88:1389-1400
- Ghosh, S., Das, D., Kao, S. C., & Ganguly, A. R. (2011). Lack of uniform trends but increasing spatial variability in observed Indian rainfall extremes. *Nature Climate Change*, 2(2), 86.
- Gill, E.C., Rajagopalan, B. and Molnar, P. (2015). "Subseasonal variations in spatial signatures of ENSO on the Indian summermonsoon from 1901 to 2009." *J. Geophys. Res.*, 120(16), 8165-8185.
- Glantz, M.H. and Glantz, M.H. (2001). "Currents of change: impacts of El Niño and La Niña on climate and society." Cambridge University Press.
- Goddard, L. and Dilley, M. (2005). "El Nino: catastrophe or opportunity." *J. Clim.*, 18(5), 651-665.
- Goddard, L., Mason, S., Zebiak, S., Ropelewski, C., Basher, R. and Cane, M. (2001). "Current approaches to seasonal to interannual climate predictions." *Int. J. Climatol.*, 21, 1111-1152.
- Goswami, B.N., Venugopal, V., Sengupta, D., Madhusoodanan, M.S. and Xavier, P.K. (2006). "Increasing Trend of Extreme Rain Events Over India in a Warming Environment." *Science*, 314(5804), 1442-1445.
- Grossman, R.L. and Durran, D.R. (1984). "Interaction of low-level flow with the western Ghat Mountains and offshore convection in the summer monsoon." *Monthly Weather Review*, 112(4), 652-672.
- Guhathakurta, P., Sreejith, O. and Menon, P. (2011). "Impact of climate change on extreme rainfall events and flood risk in India." *Journal of Earth System Science*, 120(3), 359-373.
- Halide, H. and Ridd, P. (2008). "Complicated ENSO models do not significantly outperform very simple ENSO models." *International Journal of Climatology*, 28(2), 219-233.
- Hamed, K.H. and Ramachandra Rao, A. (1998). "A modified Mann-Kendall trend test for autocorrelated data." *J. Hydrol.*, 204(1-4), 182-196.

- Harvey, A. and Trimbur, T. (2008). "Trend estimation and the Hodrick-Prescott filter." *Journal of the Japan Statistical Society*, 38(1), 41-49.
- Hasan, M.A., Mouw, C., Jutla, A. and Akanda, A.S. (2018). "Quantification of Rotavirus Diarrheal Risk Due to Hydroclimatic Extremes Over South Asia: Prospects of Satellite-Based Observations in Detecting Outbreaks." *Geo Health*, 2(2), 70–86.
- Helsel, D.R. and Hirsch, R.M. (1988). "Applicability of the t-Test for Detecting Trends in Water Quality Variables," *Journal of the American Water Resources Association*, 24(1), 201-204.
- Hirsch, R.M., Alexander, R.B. and Smith, R.A. (1991). "Selection of methods for the detection and estimation of trends in water quality." *Water Resour. Res.*, 27(5), 803–813.
- Hirsch, R.M., Slack, J.R. and Smith, R.A. (1982). "Techniques of trend analysis for monthly water quality data." *Water resources research*, 18(1), 107-121.
- Huth, R. and Pokorna, L. (2004). "Parametric versus non-parametric estimates of climatic trends." *Theoretical and Applied Climatology*, 77(1-2), 107-112.
- Ihara, C., Kushnir, Y., Cane, M. A., & De la Pena, V. H. (2007). "Indian summer monsoon rainfall and its link with ENSO and Indian Ocean climate indices". *International Journal of Climatology: A Journal of the Royal Meteorological Society*, 27(2), 179-187.
- IPCC. (2007). "The physical science basis." *Contribution of Working Group I to the fourth assessment report of the Intergovernmental Panel on Climate Change*, 996.
- IPCC. (2012). "Managing the risks of extreme events and disasters to advance climate change adaptation: special report of the intergovernmental panel on climate change." *Cambridge University Press*.
- Izumo, T., Montegut, C.B., Luo, J.J., Behera, S.K., Masson, S. and Yamagata, T. (2008). "The role of the Western AS Upwelling in Indian Monsoon Rainfall Variability." *J. Clim.*, 21(21), 5603-5623.
- Jagannathan, P. and Parthasarathy, B. (1973). "Trends and periodicities of rainfall over India." *Monthly Weather Review*, 101:371-375.
- Jiang, R., Wang, X., Xie, J. and Gan, T.Y. (2018). "Discussion of 'Uses of Precipitation-Based Climate Indices in Drought Characterization' by Chandramouli V. Chandramouli, Nicholas Kaoukis, Mohammad Karim, and Leslie Dorworth." *J. Hydrol. Eng.*, 23(9), 07018008.
- Johny, K., Pai, M.L. and Adarsh, S. (2019). "Empirical forecasting and Indian Ocean dipole teleconnections of south–west monsoon rainfall in Kerala." *Meteorology and Atmospheric Physics*, 131(4), 1055-1065.
- Jolliffe, I.T. (2002). "Principal component analysis." *Technometrics*, 45(3), 276.
- Joshi, M.K. and Pandey, A. (2011). "Trend and spectral analysis of rainfall over India during 1901–2000." *Journal of Geophysical Research: Atmospheres*, 116.

- Ju, J. and Slingo, J. (1995). "The Asian summer monsoon and ENSO." *Quarterly Journal of the Royal Meteorological Society*, 121(525), 1133-1168.
- Juan Li, Bin Wang and Young-Min Yang, (2016). "Retrospective seasonal prediction of summer monsoon rainfall over West Central and Peninsular India in the past 142 years." *Climate Dynamics*, 48, 7-8, (2581-2596), doi: 10.1007/s00382-016-3225-1.
- Jun, T., Munasinghe, L., & Rind, D. H. (2015). "A new metric for Indian monsoon rainfall extremes." *Journal of Climate*, 28(7), 2842-2855.
- Kahya, E. and Kalayci, S. (2004). "Trend analysis of streamflow in Turkey." *J. Hydrol.*, 289(1-4), 128-144.
- Karpouzou, D.K., Kavalieratou, S. and Babajimopoulos, C. (2010). "Non- parametric trend analysis of precipitation data in Pieria Region (Greece)." *Eur Water*, 30:31-40
- Karuna Sagar, S., Rajeevan, M. and Vijaya Bhaskara Rao, S. (2016). "On increasing monsoon rainstorms over India." *Nat. Hazards*, 85(3), 1-15.
- Kiladis, G.N. and Diaz, H. F. (1989). "Global climatic anomalies associated with extremes in the Southern Oscillation." *J. Clim.*, 2(9), 1069-1090.
- Kinter, I.L., Miyakoda, K. and Yang, S. (2002). "Recent change in the connection from the Asian monsoon to ENSO." *J. Clim.*, 15(10), 1203-1215.
- Kiros, G., Shetty, A. and Nandagiri, L. (2016). "Analysis of variability and trends in rainfall over northern Ethiopia Analysis of variability and trends in rainfall." *Arab. J. Geosci.*, 9(6), 451.
- Kirtman, B.P. and Shukla, J. (1997). "Influence of the Indian summer monsoon on ENSO." *Quarterly Journal of the Royal Meteorological Society*, 126(562), 213-239.
- Konwar, M., Parekh, A. and Goswami, B.N. (2012). "Dynamics of east-west asymmetry of ISMR trends in recent decades." *Geophys. Res. Lett.*, 39, 10708.
- Koteswaram, P. and Alvi, S. (1969). "Trends and periodicities in rainfall at west coast stations in India." *Curr Sci.*, 38:229-231.
- Kothawale, D.R. and Rajeevan, M. (2016). "Monthly, seasonal and annual rainfall time series for all-India, homogeneous regions and meteorological subdivisions: 1871-2016." Indian Institute of Tropical Meteorology, Pune.
- Kripalani, R., Kulkarni, A., Sabade, S. and Khandekar, M. (2003). "Indian monsoon variability in a global warming scenario." *Natural Hazards*, 29:189-206.
- Kripalani, R., Oh, J., Kulkarni, A., Sabade, S. and Chaudhari, H. (2007). "South Asian summer monsoon precipitation variability: coupled climate model simulations and projections under IPCC AR4." *Theoretical and Applied Climatology*, 90:133-159.
- Kripalani, R.H., Kulkarni, A. (1996). "Assessing the impacts of El Nino and non-El Nino related droughts over India." *Drought Netw. News*, 8, 11-13.

- Krishna Kumar, K., Rajagopalan, B. and Cane, M.A. (1999). "On the weakening relationship between the monsoon and ENSO." *Science*, 284, 2156–2159.
- Krishna Kumar, K., Rupa Kumar, K. and Pant, G.B. (1997). "Pre-monsoon maximum and minimum temperature over India in relation to the summer monsoon rainfall." *Int. J. Climatol.*, 17: 1115–1127.
- Krishna Kumar, K., Soman, M.K. and Rupa Kumar, K. (1995). "Seasonal forecasting of Indian summer monsoon rainfall: a review." *Weather*, 50(12): 449–467.
- Krishna Kumar, K., Soman, M.K. and Rupa Kumar, K. (1995). "Seasonal forecasting of Indian summer monsoon rainfall: a review." *Weather*, 50, 449–467.
- Krishnamurthy, V. and Goswami, B.N. (2000). "Indian monsoon–ENSO relationship on interdecadal timescale." *J. Clim.*, 13(3), 579–595.
- Krishnan, A. (1984). "Analysis of Trends in the Rainfall and Droughts Occurring in the Southwest Monsoon and Northeast Monsoon Systems in the Southern Peninsular India." *Mausam*, 35(3).
- Krishnan, R. (2013). "Will the South Asian monsoon overturning circulation stabilize any further?." *Climate dynamics*, 40:187–211
- Krishnaswamy, J., Vaidyanathan, S., Rajagopalan, B., Bonell, M., Sankaran, M., Bhalla, R. S., & Badiger, S. (2015). "Non-stationary and non-linear influence of ENSO and Indian Ocean Dipole on the variability of Indian monsoon rainfall and extreme rain events." *Climate Dynamics*, 45(1-2), 175–184.
- Kumar Raju, B.C. and Nandagiri, L. (2017). "Analysis of historical trends in hydrometeorological variables in the upper Cauvery Basin, Karnataka, India." *Curr. Sci.*, 112(3), 577–587.
- Kumar, D.N., Reddy, M.J. and Maity, R. (2007). "Regional Rainfall Forecasting using Large Scale Climate Teleconnections and Artificial Intelligence Techniques." *J. Intell Syst.*, 16:307–322. doi: 10.1515/JISYS.2007.16.4.307
- Kumar, K.K., Patwardhan, S.K., Kulkarni, A., Kamala, K., Rao, K.K. and Jones, R. (2011). "Simulated projections for summer monsoon climate over India by a high-resolution regional climate model (PRECIS)." *Curr Sci.*, 101(3), 312–326.
- Kumar, K.K., Rajagopalan, B. and Cane, M.A. (1999). "On the weakening relationship between the Indian monsoon and ENSO." *Science*, 284(5423), 2156–2159.
- Kumar, K.R., Sahai, A.K., Kumar, K.K., Patwardhan, S.K., Mishra, P.K., Revadekar, J.V. and Pant, G.B. (2006). "High-resolution climate change scenarios for India for the 21st century." *Curr sci.*, 90(3), 334–345.
- Kumar, V., Jain, S. K., and Singh, Y. (2010). "Analysis of long-term rainfall trends in India." *Hydrol. Sci. J.*, 55(4), 484–496.

- Lal, M., Meehl, G.A. and Arblaster, J.M. (2000). "Simulation of Indian summer monsoon rainfall and its intraseasonal variability in the NCAR climate system model." *Regional Environmental Change*, 1:163-179.
- Lal, M., Nozawa, T., Emori, S., Harasawa, H., Takahashi, K., Kimoto, M. and Numaguti, A. (2001). "Future climate change: Implications for Indian summer monsoon and its variability." *Current science*, 1196-1207.
- Lau, K.M. and Yang, S. (1997). "Climatology and interannual variability of the Southeast Asian summer monsoon." *Advances in Atmospheric Sciences*, 14(2), 141-162
- Li, M.F., Luo, W., Li, H., Liu, E. and Li, Y. (2018). "Daily extreme precipitation indices and their impacts on rice yield—A case study over the tropical island in China." *Theor. Appl. Climatol.*, 132(1–2), 503–513.
- Li, X., Wang, X. and Babovic, V. (2018). "Analysis of variability and trends of precipitation extremes in Singapore during 1980–2013." *Int. J. Climatol.*, 38:125–141. doi: 10.1002/joc.5165
- López-Moreno, Juan, I., Hess, T.M. and White, S.M. (2009). "Estimation of reference evapotranspiration in a mountainous mediterranean site using the Penman-Monteith equation with limited meteorological data." *Pirineos*, 164, 7-31.
- Mann, H.B. (1945). "Nonparametric Tests Against Trend." *Journal of Econometric Society*, 245-259.
- May, W. (2002). "Simulated changes of the Indian summer monsoon under enhanced greenhouse gas conditions in a global time-slice experiment." *Geophys. Res. Lett.*, 29.
- McPhaden, M.J., Zebiak, S.E. and Glantz, M. H. (2006). "ENSO as an integrating concept in earth science." *Science*, 314(5806), 1740-1745.
- Meehl, G.A. (1987). "The annual cycle and interannual variability in the tropical Pacific and Indian Ocean regions." *Monthly Weather Review*, 115(1), 27-50.
- Meehl, G.A. (1997). "The south Asian monsoon and the tropo- spheric biennial oscillation." *J. Clim.*, 10: 1921–1943
- Meher-Homji, V.M. (1980). "Repercussions of deforestation on precipitation in Western Karnataka, India." *Archiv Fuer Meteorologie, Geophysik und Bioklimatologie, Serie B*, 28(4), 385-400.
- Meshram, S.G., Singh, V.P., Meshram, C. (2016). "Long-term trend and variability of precipitation in Chhattisgarh State, India." *Theoretical and Applied Climatology*, 1-16.
- Mooley, D. and Parthasarathy, B. (1984). "Fluctuations in all-India summer monsoon rainfall during 1871–1978." *Climatic Change*, 6:287-301.
- Mooley, D.A. (1997). "Variation of summer monsoon rainfall over India in El-Ninos." *Mausam*, 48, 413-420.

- Mudbhatkal, A. and Amai, M. (2018). "Regional climate trends and topographic influence over the Western Ghat catchments of India." *Int. J. Climatol.*, 38(5), 2265–2279.
- Nageswararao, M.M., Sannan, M.C., Mohanty, U.C. (2019). "Characteristics of various rainfall events over South Peninsular India during northeast monsoon using high-resolution gridded dataset (1901–2016)." *Theor Appl. Climatol.*, 1–21. doi: 10.1007/s00704-018-02755-y
- Naidu, C.V., Dharma Raju, A., Vinay Kumar, P. and Satyanarayana, G.C. (2017). "Perceptible changes in Indian summer monsoon rainfall in relation to Indian Monsoon Index." *Glob Planet Change*, 157:83–92. doi: 10.1016/j.gloplacha.2017.08.016
- Nandargi, S. and Mulye, S.S. (2012). "Relationships between rainy days, mean daily intensity, and seasonal rainfall over the koyna catchment during 1961–2005." *The Scientific World Journal*, 2012.
- Nanjundiah, R.S., Francis, P.A., Ved, M. and Gadgil, S. (2013). "Predicting the extremes of Indian summer monsoon rainfall with coupled ocean-atmosphere models." *Curr Sci.*, 104:1380–1393.
- Nicholls, N. (1983). "Impact of the Southern Oscillation on Australian crops." *J. Climatol.*, 5(5), 553-560.
- Oguntunde, P.G., Abiodun, B.J. and Lischeid, G. (2011). "Rainfall trends in Nigeria, 1901–2000." *Journal of Hydrology*, 411(3-4), 207-218.
- Oruga, Y. and Yoshizaki, M. (1988). "Numerical study of orographic-convective precipitation over eastern AS and the Ghat mountains during the summer monsoon." *J. Atmos.Sci.*, 45, 2097-2121.
- Pachauri, R.K., Allen, M.R., Barros, V.R., Broome, J., Cramer, W., Christ, R. and Dubash, N.K. (2014). "Climate change 2014: synthesis report." Contribution of Working Groups I, II and III to the fifth assessment report of the Intergovernmental Panel on Climate Change, 151.
- Pai, D.S., Sridhar, L., Badwaik, M.R., Rajeevan, M. (2015). "Analysis of the daily rainfall events over India using a new long period (1901–2010) high resolution ($0.25^\circ \times 0.25^\circ$) gridded rainfall data set." *Clim Dyn.*, 45(3-4), 755–776. doi: 10.1007/s00382-014-2307-1
- Pai, D.S., Sridhar, L., Rajeevan, M., Sreejith, O.P., Satbhai, N.S. and Mukhopadyay, B. (2014). "Development of a new high spatial resolution ($0.25^\circ \times 0.25^\circ$) Long Period (1901-2010) daily gridded rainfall data set over India and its comparison with existing data sets over the region." *Mausam*, 65(1), 1–18.
- Partal, T. and Kahya, E. (2006). "Trend analysis in Turkish precipitation data." *Hydrol. Process*, 20(9), 2011–2026.
- Parthasarathy, B. (1995). "Monthly and seasonal rainfall series for all India, homogeneous regions and meteorological subdivisions: 1871-1994." *Indian Institute of Tropical meteorology Research Report*.

- Parthasarathy, B., Diaz, H.F. and Eischeid, J.K. (1988). "Prediction of all-India summer monsoon rainfall with regional and large-scale parameters." *J. Geophys. Res. Atmos.*, 93(D5), 5341-5350.
- Patra, J.P., Mishra, A., Singh, R. and Raghuwanshi, N.S. (2012). "Detecting rainfall trends in twentieth century (1871–2006) over Orissa State, India." *Climatic Change*, 111(3-4), 801-817.
- Patwardhan, S.K. and Asnani, G.C. (2000). "Meso-scale distribution of summer monsoon rainfall near the Western Ghats (INDIA)." *Int. J. Climatol.*, 20(5), 575–581.
- Preethi, B., Mujumdar, M., Kripalani, R.H., Prabhu, A., and Krishnan, R. (2017). "Recent trends and teleconnections among South and East Asian summer monsoons in a warming environment." *Clim. Dyn.*, 48(7–8), 2489–2505.
- Quan, X., Hoerling, M., Whitaker, J., Bates, G. and Xu, T. (2006). "Diagnosing sources of U.S. seasonal forecast skill." *J. Clim.*, 19, 3279–3293.
- Raghavendra, V. (1974). "Trends and periodicities of rainfall in sub-divisions of Maharashtra state." *Indian Journal of Meteorology and Geophysics*, 25.
- Rajeevan, M. and McPhaden, M.J. (2004). "Tropical Pacific upper ocean heat content variations and Indian summer monsoon rainfall." *Geophys. Res. Lett.*, 31(18).
- Rajeevan, M., Bhate, J., and Jaswal, A. K. (2008). "Analysis of variability and trends of extreme rainfall events over India using 104 years of gridded daily rainfall data." *Geophys. Res. Lett.*, 35(18), 1–6.
- Rajeevan, M., Pai, D.S., Dikshit, S.K. and Kelkar, R.R. (2004). "IMD's new operational models for long-range forecast of southwest monsoon rainfall over India and their verification for 2003." *Curr. Sci.*, 86(3): 422–431.
- Rajeevan, M., Pai, D.S., Kumar, R.A. and Lal, B. (2007). "New statistical models for long-range forecasting of southwest monsoon rainfall over India." *Climate Dynamics*, 28(7-8), 813-828.
- Rajendran, K., Kitoh, A., Srinivasan, J., Mizuta, R. and Krishnan, R. (2012). "Monsoon circulation interaction with Western Ghats orography under changing climate." *Theor Appl. Climatol.*, 110:555–571. doi: 10.1007/s00704-012-0690-2
- Ramesh Kumar, M., Krishnan, R., Sankar, S., Unnikrishnan, A.S. and Pai, D.S. (2009). "Increasing trend of "break-monsoon" conditions over India—role of ocean–atmosphere processes in the Indian Ocean." *IEEE Geoscience and Remote Sensing Letters*, 6(2), 332-336.
- Rani, S.I., Ramachandran, R., Subrahmanyam, D. B., Alappattu, D. P. and Kunhikrishnan, P.K. (2010). "Characterization of sea/land breeze circulation along the west coast of Indian sub-continent during pre-monsoon season." *Atmospheric Research*, 95(4), 367-378.
- Rao, G.N. (1999). "Variations of the SO Relationship with Summer and Winter Monsoon Rainfall over India: 1872–1993." *J. Clim.*, 12(12), 3486–3495.

- Rasmusson, E.M., Carpenter, T.H., Rasmusson, E.M. and Carpenter, T.H. (1983). "The Relationship Between Eastern Equatorial Pacific Sea Surface Temperatures and Rainfall over India and Sri Lanka." *Mon. Weather Rev.*, 111(3), 517–528.
- Ravi, P.S., Rai, S. and Pandey, A.C. (2013). "Southern and Tropical Indian Ocean SST : A Possible Predictor of Winter Monsoon Rainfall over South India." *Atmos Clim Sci.*, 2013:440–449. doi: 10.4236/acs.2013.34045
- Reddy, C.S., Jha, C.S., Diwakar, P.G. and Dadhwal, V.K. (2015). "Nationwide classification of forest types of India using remote sensing and GIS." *Environ. Monit. Assess.*, 187(12), 777.
- Revadekar, J.V., Patwardhan, S.K. and Rupa Kumar, K. (2011). "Characteristic Features of Precipitation Extremes over India in the Warming Scenarios." *Adv Meteorol.*, 2011:1–11. doi: 10.1155/2011/138425
- Revadekar, J.V., Patwardhan, S.K. and Rupa Kumar, K. (2011). "Characteristic Features of Precipitation Extremes over India in the Warming Scenarios." *Adv. Meteorol.*, 2011, 1–11.
- Revadekar, J.V., Varikoden, H., Murumkar, P.K. and Ahmed, S.A. (2018). "Latitudinal variation in summer monsoon rainfall over Western Ghat of India and its association with global sea surface temperatures." *Sci Total Environ.*, 613–614:88–97. doi: 10.1016/j.scitotenv.2017.08.285
- Rosenzweig, C., Iglesias, A., Yang, X.B., Epstein, P.R. and Chivian, E. (2001). "Climate change and extreme weather events; implications for food production, plant diseases, and pests." *Global change & human health*, 2(2), 90-104.
- Roy, I., Tedeschi, R.G. and Collins, M. (2017). "ENSO teleconnections to the Indian summer monsoon in observations and models." *Int. J. Climatol.*, 37(4), 1794-1813.
- Rumelhart, D.E., Hinton, G.E. and Williams, R.J. (1985). "Learning internal representations by error propagation (No. ICS-8506)." *California Univ San Diego La Jolla Inst for Cognitive Science*.
- Rupa Kumar, K., Pant, G.B., Parthasarathy, B. and Sontakke, N. (1992). "Spatial and sub-seasonal patterns of the long-term trends of Indian summer monsoon rainfall." *Int. J. Climatol.*, 12: 257-268.
- Sahai, A.K., Grimm, A.M., Satyan, V. and Pant, G.B. (2003). "Long-lead prediction of Indian summer monsoon rainfall from global SST evolution." *Clim Dyn.*, 20:855–863. doi: 10.1007/s00382-003-0306-8
- Saji, N.H., Goswami, B.N., Vinayachandran, P.N. and Yamagata, T. (1999). "A dipole mode in the tropical Indian Ocean." *Nature*, 401:360–363. doi: 10.1038/43854
- Schepen, A., Wang, Q.J. and Robertson, D. (2012). "Evidence for using lagged climate indices to forecast Australian seasonal rainfall." *J. Clim.*, 25:1230–1246. doi: 10.1175/JCLI-D-11-00156.1

- Sen, P.K. (1968). "Estimates of the regression coefficient based on Kendall's tau." *Journal of the American Statistical Association*, 63(324), 1379-1389.
- Sharma, S. and Singh, P. (2017). "Long Term Spatiotemporal Variability in Rainfall Trends over the State of Jharkhand, India." *Climate*, 5(1), 18.
- Shukla, J. (1975). "Effect of Arabian sea-surface temperature anomaly on Indian summer monsoon: A numerical experiment with GFDL model." *J. Atmos. Sci.*, 32, 503-511.
- Shukla, J. and Mishra, B.M. (1977). "Relationships between Sea Surface Temperature and Wind Speed over the Central AS, and Monsoon Rainfall over India." *Monthly weather review*, 105, 998-1002.
- Sikka, D.R., Gadgil, S., Sikka, D.R. and Gadgil, S. (1980). "On the Maximum Cloud Zone and the ITCZ over Indian, Longitudes during the Southwest Monsoon." *Mon. Weather Rev.*, 108(11), 1840–1853.
- Singh, N. and Ranade, A.A. (2009). "Climatic and hydroclimatic features of wet and dry spells and their extremes across India." Indian Institute of Tropical Meteorology.
- Singh, P. and Borah, B. (2013). "Indian summer monsoon rainfall prediction using artificial neural network." *Stoch. Environ. Res. Risk Assess.*, 27(7), 1585–1599.
- Singh, R.B., Singh, A. and Kumar, A. (2014). "Climate Change Variability in Coastal Karnataka, India." *In Climate Change and Biodiversity*, Springer, Tokyo., 15-26.
- Smith, R. B., Jiang, Q., Fearon, M. G., Tabary, P., Dorninger, M., Doyle, J. D., & Benoit, R. (2003). "Orographic precipitation and air mass transformation: An Alpine example". *Applied meteorology and physical oceanography*, 129(588), 433-454.
- Soman, M.K. and Slingo, J. (1997). "Sensitivity of the asian summer monsoon to aspects of sea-surface-temperature anomalies in the tropical pacific ocean." *Quarterly Journal of the Royal Meteorological Society*, 123(538), 309-336.
- Soman, M.K., Krishnakumar, K. and Singh, N. (1988). "Decreasing trend in the rainfall of Kerala." *Curr Sci.*, 57: 5 – 12.
- Srivastava, G., Panda, S.N., Mondal, P. and Liu, J. (2010). "Forecasting of rainfall using ocean-atmospheric indices with a fuzzy neural technique." *J. Hydrol.*, 395:190–198. doi: 10.1016/j.jhydrol.2010.10.025
- Surendran, S., Gadgil, S., Francis, P.A. and Rajeevan, M. (2015). "Prediction of Indian rainfall during the summer monsoon season on the basis of links with equatorial Pacific and Indian Ocean climate indices." *Environ Res Lett.*, 10(9), 094004. doi: 10.1088/1748-9326/10/9/094004
- Tabari, H., Taye, M.T. and Willems, P. (2015). "Statistical assessment of precipitation trends in the upper Blue Nile River basin." *Stochastic environmental research and risk assessment*, 29(7), 1751-1761.

- Tawde, S. A. and Singh, C. (2015). "Investigation of orographic features influencing spatial distribution of rainfall over the Western Ghats of India using satellite data." *Int. J. Climatol.*, 2280–2293.
- Tawde, S.A. (2013). "Investigation of orographically induced rainfall over Western Ghats and its association with other monsoon parameters." MTech thesis, Andhra University, Visakhapatnam.
- Thapliyal, V. and Kulshrestha, S. (1991). "Climate changes and trends over India." *Mausam*, 42:333-338.
- Trenberth, K.E. (1997). "The definition of El Nino." *Bull. Amer. Meteor. Soc.*, 78, 2771–2777.
- Trenberth, K.E. (1998). "Atmospheric moisture residence times and cycling: implications for rainfall rates and climate change." *Climatic Change*, 39: 667-694.
- Trenberth, K.E. (1999). "Conceptual Framework for Changes of Extremes of the Hydrological Cycle with Climate Change." *Climatic Change*, 42(1): 327-339.
- Trenberth, K.E. (2011). "Changes in precipitation with climate change." *Climate Research*, 47(1-2), 123-138.
- Trenberth, K.E. and Stepaniak, D.P. (2001). "Indices of El Niño evolution." *J. clim.*, 14(8), 1697-1701.
- Van Belle, G. and Hughes, J.P. (1984). "Nonparametric tests for trend in water quality." *Water resources research*, 20(1), 127-136.
- Varikoden, H. and Babu, C.A. (2015). "Indian summer monsoon rainfall and its relation with SST in the equatorial Atlantic and Pacific Oceans." *Int. J. Climatol.*, 35:1192–1200. <http://dx.doi.org/10.1002/joc.4056>.
- Varikoden, H., Mujumdar, M. Revadekar, J.V., Sooraj, K.P., Ramarao, M.V.S., Sanjay, J. and Krishnan, R. (2018a). "Assessment of regional downscaling simulations for long term mean, excess and deficit Indian Summer Monsoons." *Glob Planet Change.*, 162:28–38. doi: 10.1016/j.gloplacha.2017.12.002
- Varikoden, H., Revadekar, J.V., Kuttippurath, J., Babu, C.A. (2018b). "Contrasting trends in southwest monsoon rainfall over the Western Ghats region of India." *Clim Dyn.*, 1–10. doi: 10.1007/s00382-018-4397-7
- Varikoden, H., Revadekar, J. V., Kuttippurath, J., & Babu, C. A. (2019). "Contrasting trends in southwest monsoon rainfall over the Western Ghats region of India". *Climate Dynamics*, 52(7-8), 4557-4566.
- Vishnu, R., Kumar, V.A., Varikoden, H., Krishnan, K.S., Sreekanth, T.S., Symon, V.S. and Kumar, G.M. (2013). "Convective thundercloud development over the Western Ghats mountain slope in Kerala." *Curr Sci.*, 1506-1514.

- Vittal, H., Karmakar, S. and Ghosh, S. (2013). "Diametric changes in trends and patterns of extreme rainfall over India from pre-1950 to post-1950." *Geophys. Res. Lett.*, 40(12), 3253-3258.
- Walker, G. (1923). "Correlation in seasonal variation of weather. VIII: A preliminary study of world weather." *Memoirs of India Meteorological Department*, 24, 75-131.
- Walker, G.T. (1925). "Correlation in seasonal variations of weather—A further study of world weather." *Monthly Weather Review*, 53(6), 252-254.
- Wang, C., Wang, X., Weisberg, R.H. and Black, M.L. (2017). "Variability of tropical cyclone rapid intensification in the North Atlantic and its relationship with climate variations Atlantic and its relationship with climate variations." *Clim Dyn.*, 49(11-12), 3627-3645.
- Wang, H., Chen, Y. and Chen, Z. (2013). "Spatial distribution and temporal trends of mean precipitation and extremes in the arid region, northwest of China, during 1960–2010." *Hydrological Processes*, 27(12), 1807-1818.
- Wang, S., Zhang, M., Sun, M., Wang, B. and Li, X. (2013). "Changes in precipitation extremes in alpine areas of the Chinese Tianshan Mountains, central Asia, 1961–2011." *Quat. Int.*, 311, 97–107.
- Webster, P.J. and Yang, S. (1992). "Monsoon and ENSO: Selectively interactive systems." *Quarterly Journal of the Royal Meteorological Society*, 118(507), 877-926.
- Webster, P.J., Magana, V.O., Palmer, T.N., Shukla, J., Thomas, R. A., Yanai, M. and Yasunari, T. (1998). "Monsoons: processes, predictability and the prospects of prediction." *J. Geophys. Res.*, 103, 14451–14510.
- Wilks, D.S. (Department of E. and A. S. C. U. (2006). *Statistical Methods in the Atmospheric Sciences. Meteorol. Appl.*
- WMO, (1988). *Guide to Wave Analysis and Forecasting. No. 702, Secretariat of the World Meteorological Organization, Geneva.*
- Wu, J.D., Li, N., Juan Yang, H., Hua Li, C. (2008). "Risk evaluation of heavy snow disasters using BP artificial neural network: the case of Xilingol in Inner Mongolia." *Stoch Environ Res Risk Assess.*, 22:719–725.
- Wu, R., Chen, J. and Chen, W. (2012). "Different Types of ENSO Influences on the Indian Summer Monsoon Variability." *J. Clim.*, 25:903–920. doi: 10.1175/JCLI-D-11-00039.1
- Xavier, A., Kottayil, A., Mohanakumar, K., & Xavier, P. K. (2018). "The role of monsoon low-level jet in modulating heavy rainfall events." *International Journal of Climatology*, 38, e569-e576.
- Xiao, M., Zhang, Q. and Singh, V.P. (2017). "Spatiotemporal variations of extreme precipitation regimes during 1961–2010 and possible teleconnections with climate indices across China." *Int. J. Climatol.*, 37:468–479. doi: 10.1002/joc.4719

Xu, Z.X., Li, J.Y. and Liu, C.M. (2007). “Long-term trend analysis for major climate variables in the Yellow River basin.” *Hydrological Processes*, 21(14), 1935-1948.

Yu, H., Zhang, Q., Sun, P. and Song, C. (2018). “Impact of Droughts on Winter Wheat Yield in Different Growth Stages during 2001–2016 in Eastern China.” *International Journal of Disaster Risk Science*, 9(3), 376-391.

Yue, S. and Wang, C. (2002). “The influence of serial correlation on the Mann–Whitney test for detecting a shift in median.” *Advances in Water Resources*, 25(3), 325-333.

Yue, S., Pilon, P. and Cavadias, G. (2002). “Power of the Mann–Kendall and Spearman’s rho tests for detecting monotonic trends in hydrological series.” *Journal of hydrology*, 259(1-4), 254-271.

Yue, S., Pilon, P., Phinney, B. and Cavadias, G., (2002). “The influence of autocorrelation on the ability to detect trend in hydrological series.” *Hydrological processes*, 16(9), 1807-1829.

Zhang, X. and Hogg, W.D. (2001). “Spatial and temporal characteristics of heavy precipitation events over Canada.” *J. Clim.*, 14: 1923-1936.

Tools website and references:

Current officially released version is Ferret 6.96

<https://www.ferret.noaa.gov>

Hankin, S., Harrison, D. E., Osborne, J., Davison, J., & O'BRIEN, K. (1996). “A strategy and a tool, Ferret, for closely integrated visualization and analysis”. *The Journal of Visualization and Computer Animation*, 7(3), 149-157.

Current officially released version is cdo 1.7.2

<https://code.zmaw.de/projects/cdo>

Current officially released GrADS version 2.2.1

<http://cola.gmu.edu/grads/downloads.php>

Current officially released RClimDex version 1.0 and RH Test

<http://etccdi.pacificclimate.org/soft>

Current Standardized Precipitation Index (SPI) tool documentation

<https://drought.unl.edu/droughtmonitoring/Tools.aspx>

APPENDIX 1: Annual Statistics of Individual Grid Points’ Daily Gridded Precipitation over HL (the Western Ghats) and LL (coastal regions)

Grid Points	Lat deg N	Lon deg E	Elevation meters	Mean Precipitation mm	Min Precipitation mm	Max Precipitation mm	SD mm	CV %	Kurtosis	Skew
LL1	14	74.5	000	4186	2714	7013	725	17.31	1.46	0.69
LL2	14.75	74.25	117	3442	2028	5560	581	16.87	0.74	0.53
LL3	12.75	75	117	3987	2233	6999	628	15.74	4.21	1.01
LL4	13	75	069	4220	2305	6543	650	15.40	1.23	0.44
LL5	13.25	74.75	013	4319	2438	6534	738	17.08	0.30	0.16
LL6	13.5	74.75	012	4496	2506	7988	1034	22.99	0.73	0.90
LL7	13.75	74.75	075	4433	2181	9651	1306	29.46	3.26	1.49
LL8	14	74.75	029	3864	1247	5185	781	20.21	1.09	0.65
LL9	14.25	74.5	057	3925	1964	6621	1391	35.43	1.05	1.31
LL10	14.5	74.5	086	3036	2141	8817	753	24.81	1.16	1.10
LL11	14.75	74.5	183	3819	1800	5703	717	18.76	0.57	0.04
LL12	12.5	75.5	116	4191	1853	5970	689	16.45	2.99	0.54
LL13	12.75	75.25	114	4165	2012	7218	696	16.72	4.88	0.92
LL14	13	75.25	062	4227	1939	7501	928	21.95	0.03	0.09
LL15	13.25	75	092	4155	1820	6592	1881	45.27	0.59	1.30
LL16	13.5	75	055	3049	1793	9793	754	24.74	1.42	1.00
LL17	13.75	75	108	3124	1495	8145	717	18.76	0.77	1.09
HL1	14	75	642	3028	1139	5869	818	27.00	0.10	0.53
HL2	14.25	74.75	605	3830	1765	5668	1203	31.42	1.65	1.12
HL3	14.5	74.75	582	2347	1483	4341	804	34.24	3.50	1.50
HL4	14.75	74.75	514	2611	1083	4159	574	21.98	-0.01	0.63
HL5	15	74.5	480	2179	1394	4928	483	22.17	3.03	1.14
HL6	12.25	75.75	639	2443	903	4849	589	24.09	2.22	1.02
HL7	12.75	75.5	863	2095	1618	6357	588	28.08	4.52	1.41
HL8	12.5	75.5	1066	1477	610	3196	454	30.78	1.36	0.82
HL9	13	75.5	434	2282	1161	5635	615	26.94	6.92	1.73
HL10	13.25	75.25	949	3366	1873	5771	727	21.61	0.50	0.62
HL11	13.5	75.25	692	3005	1206	5825	668	22.23	2.46	0.87
HL12	13.75	75.25	663	2536	1220	5615	629	24.82	4.57	1.28
HL13	14	75.25	637	1168	553	4314	556	47.56	19.05	4.02
HL14	14.25	75	602	1797	1021	4698	570	31.72	10.72	2.74
HL15	15	74.75	559	1699	757	3753	497	29.23	4.44	1.30
HL16	15.25	74.5	529	1998	1088	3945	511	25.58	1.79	1.07
HL17	15.5	74.5	711	1729	846	3437	500	28.93	1.26	0.89
HL18	12	76	815	1471	638	3933	442	30.01	7.74	1.71
HL19	12.75	75.75	940	1770	821	3167	398	22.51	1.77	0.63
HL20	13.25	75.5	745	2190	1312	5119	805	36.75	2.59	1.68
HL21	13.5	75.5	818	1829	839	3665	576	31.46	1.10	1.08

Appendix 2: Cumulative probabilities for negative z-values are shown below table

z	0.00	0.01	0.02	0.03	0.04	0.05	0.06	0.07	0.08	0.09
-3.4	0.0003	0.0003	0.0003	0.0003	0.0003	0.0003	0.0003	0.0003	0.0003	0.0002
-3.3	0.0005	0.0005	0.0005	0.0004	0.0004	0.0004	0.0004	0.0004	0.0004	0.0003
-3.2	0.0007	0.0007	0.0006	0.0006	0.0006	0.0006	0.0006	0.0005	0.0005	0.0005
-3.1	0.0010	0.0009	0.0009	0.0009	0.0008	0.0008	0.0008	0.0008	0.0007	0.0007
-3.0	0.0013	0.0013	0.0013	0.0012	0.0012	0.0011	0.0011	0.0011	0.0010	0.0010
-2.9	0.0019	0.0018	0.0018	0.0017	0.0016	0.0016	0.0015	0.0015	0.0014	0.0014
-2.8	0.0026	0.0025	0.0024	0.0023	0.0023	0.0022	0.0021	0.0021	0.0020	0.0019
-2.7	0.0035	0.0034	0.0033	0.0032	0.0031	0.0030	0.0029	0.0028	0.0027	0.0026
-2.6	0.0047	0.0045	0.0044	0.0043	0.0041	0.0040	0.0039	0.0038	0.0037	0.0036
-2.5	0.0062	0.0060	0.0059	0.0057	0.0055	0.0054	0.0052	0.0051	0.0049	0.0048
-2.4	0.0082	0.0080	0.0078	0.0075	0.0073	0.0071	0.0069	0.0068	0.0066	0.0064
-2.3	0.0107	0.0104	0.0102	0.0099	0.0096	0.0094	0.0091	0.0089	0.0087	0.0084
-2.2	0.0139	0.0136	0.0132	0.0129	0.0125	0.0122	0.0119	0.0116	0.0113	0.0110
-2.1	0.0179	0.0174	0.0170	0.0166	0.0162	0.0158	0.0154	0.0150	0.0146	0.0143
-2.0	0.0228	0.0222	0.0217	0.0212	0.0207	0.0202	0.0197	0.0192	0.0188	0.0183
-1.9	0.0287	0.0281	0.0274	0.0268	0.0262	0.0256	0.0250	0.0244	0.0239	0.0233
-1.8	0.0359	0.0351	0.0344	0.0336	0.0329	0.0322	0.0314	0.0307	0.0301	0.0294
-1.7	0.0446	0.0436	0.0427	0.0418	0.0409	0.0401	0.0392	0.0384	0.0375	0.0367
-1.6	0.0548	0.0537	0.0526	0.0516	0.0509	0.0495	0.0485	0.0475	0.0465	0.0455
-1.5	0.0668	0.0655	0.0643	0.0630	0.0618	0.0606	0.0594	0.0582	0.0471	0.0559
-1.4	0.0808	0.0793	0.0778	0.0764	0.0749	0.0735	0.0721	0.0708	0.0694	0.0681
-1.3	0.0968	0.0951	0.0934	0.0918	0.0901	0.0885	0.0869	0.0853	0.0838	0.0823
-1.2	0.1151	0.1131	0.1112	0.1093	0.1075	0.1056	0.1038	0.1020	0.1003	0.0985
-1.1	0.1357	0.1335	0.1314	0.1292	0.1271	0.1251	0.1230	0.1210	0.1190	0.1170
-1.0	0.1587	0.1562	0.1539	0.1515	0.1492	0.1469	0.1446	0.1423	0.1401	0.1379
-0.9	0.1841	0.1814	0.1788	0.1762	0.1736	0.1711	0.1685	0.1660	0.1635	0.1611
-0.8	0.2119	0.2090	0.2061	0.2033	0.2005	0.1977	0.1949	0.1922	0.1894	0.1867
-0.7	0.2420	0.2389	0.2358	0.2327	0.2296	0.2266	0.2236	0.2206	0.2177	0.2148
-0.6	0.2743	0.2709	0.2676	0.2643	0.2611	0.2578	0.2546	0.2514	0.2483	0.2451
-0.5	0.3085	0.3050	0.3015	0.2981	0.2946	0.2912	0.2877	0.2843	0.2810	0.2776
-0.4	0.3446	0.3409	0.3372	0.3336	0.3300	0.3264	0.3228	0.3192	0.3156	0.3121
-0.3	0.3821	0.3783	0.3745	0.3707	0.3669	0.3632	0.3594	0.3557	0.3520	0.3483
-0.2	0.4207	0.4168	0.4129	0.4090	0.4052	0.4013	0.3974	0.3936	0.3897	0.3859
-0.1	0.4602	0.4562	0.4522	0.4483	0.4443	0.4404	0.4364	0.4325	0.4286	0.4247
0.0	0.5000	0.4960	0.4920	0.4880	0.4840	0.4801	0.4761	0.4721	0.4681	0.4641

Appendix 3: Cumulative probabilities for Positive z-values are shown below table

z	0.00	0.01	0.02	0.03	0.04	0.05	0.06	0.07	0.08	0.09
0.0	0.5000	0.5040	0.5080	0.5120	0.5160	0.5199	0.5239	0.5279	0.5319	0.5359
0.1	0.5398	0.5438	0.5478	0.5517	0.5557	0.5596	0.5636	0.5675	0.5714	0.5753
0.2	0.5793	0.5832	0.5871	0.5910	0.5948	0.5987	0.6026	0.6064	0.6103	0.6141
0.3	0.6179	0.6217	0.6255	0.6293	0.6331	0.6368	0.6406	0.6443	0.6480	0.6517
0.4	0.6554	0.6591	0.6628	0.6664	0.6700	0.6736	0.6772	0.6808	0.6844	0.6879
0.5	0.6915	0.6950	0.6985	0.7019	0.7054	0.9088	0.7123	0.7157	0.7190	0.7224
0.6	0.7257	0.7291	0.7324	0.7357	0.7389	0.7422	0.7454	0.7486	0.7517	0.7549
0.7	0.7580	0.7611	0.7642	0.7673	0.7704	0.7734	0.7764	0.7794	0.7823	0.7852
0.8	0.7881	0.7910	0.7939	0.7967	0.7995	0.8023	0.8051	0.8078	0.8106	0.8133
0.9	0.8159	0.8186	0.8212	0.8238	0.8264	0.8289	0.8315	0.8340	0.8365	0.8389
1.0	0.8413	0.8438	0.8461	0.8485	0.8508	0.8531	0.8554	0.8577	0.8599	0.8621
1.1	0.8643	0.8665	0.8686	0.8708	0.8729	0.8749	0.8770	0.8790	0.8810	0.8830
1.2	0.8849	0.8869	0.8888	0.8907	0.8925	0.8944	0.8962	0.8980	0.8997	0.9015
1.3	0.9032	0.9049	0.9066	0.9082	0.9099	0.9115	0.9131	0.9147	0.9162	0.9177
1.4	0.9192	0.9207	0.9222	0.9263	0.9251	0.9265	0.9279	0.9292	0.9306	0.9319
1.5	0.9332	0.9345	0.9357	0.9370	0.9382	0.9394	0.9406	0.9418	0.9429	0.9441
1.6	0.9452	0.9463	0.9474	0.9484	0.9495	0.9505	0.9515	0.9525	0.9535	0.9545
1.7	0.9554	0.9564	0.9573	0.9582	0.9591	0.9599	0.9608	0.9616	0.9625	0.9633
1.8	0.9641	0.9649	0.9656	0.9664	0.9671	0.9678	0.9686	0.9693	0.9699	0.9706
1.9	0.9713	0.9719	0.9726	0.9732	0.9738	0.9744	0.9750	0.9756	0.9761	0.9767
2.0	0.9772	0.9778	0.9783	0.9788	0.9793	0.9798	0.9803	0.9808	0.9812	0.9817
2.1	0.9821	0.9826	0.9830	0.9834	0.9838	0.9842	0.9846	0.9850	0.9854	0.9857
2.2	0.9861	0.9864	0.9868	0.9871	0.9875	0.9878	0.9881	0.9884	0.9887	0.9890
2.3	0.9893	0.9896	0.9898	0.9901	0.9904	0.9906	0.9909	0.9911	0.9913	0.9916
2.4	0.9918	0.9920	0.9922	0.9925	0.9927	0.9929	0.9931	0.9932	0.9934	0.9936
2.5	0.9938	0.9940	0.9941	0.9943	0.9945	0.9946	0.9948	0.9949	0.9951	0.9952
2.6	0.9953	0.9955	0.9956	0.9957	0.9959	0.9960	0.9961	0.9962	0.9963	0.9964
2.7	0.9965	0.9966	0.9967	0.9968	0.9969	0.9970	0.9971	0.9972	0.9973	0.9974
2.8	0.9974	0.9975	0.9976	0.9977	0.9977	0.9978	0.9979	0.9979	0.9980	0.9981
2.9	0.9981	0.9982	0.9982	0.9983	0.9984	0.9984	0.9985	0.9985	0.9986	0.9986
3.0	0.9987	0.9987	0.9987	0.9988	0.9988	0.9989	0.9989	0.9989	0.9990	0.9990
3.1	0.9990	0.9991	0.9991	0.9991	0.9992	0.9992	0.9992	0.9992	0.9993	0.9993
3.2	0.9993	0.9993	0.9994	0.9994	0.9994	0.9994	0.9994	0.9995	0.9995	0.9995
3.3	0.9995	0.9995	0.9995	0.9996	0.9996	0.9996	0.9996	0.9996	0.9996	0.9997
3.4	0.9997	0.9997	0.9997	0.9997	0.9997	0.9997	0.9997	0.9997	0.9997	0.9998

Appendix 5: The Pearson's correlation between Niño 1+2 and general extreme precipitation indices

SL No	Grid Point	RR		RX1		CWD		SDII		RX5		CDD	
		0 - year	1 - year	0 - year	1 - year	0 - year	1 - year	0 - year	1 - year	0 - year	1 - year	0 - year	1 - year
1	LL1	0.176	0.142	0.141	0.321**	0.075	0.068	0.227*	0.173	0.168	0.279**	0.071	0.12
2	LL2	0.244*	0.253**	-0.035	0.158	0.114	0.111	-0.058	-0.024	-0.034	0.179	-0.001	0.047
3	LL3	0.315**	0.313**	0.236*	0.284*	-0.081	-0.078	0.293**	0.272**	0.207	0.344**	0.19	0.201
4	LL4	0.162	0.045	0.316**	0.212*	0.008	0.061	0.32**	0.31**	0.374**	0.315**	0.032	0.062
5	LL5	0.176	0.127	-0.019	-0.027	-0.136	-0.106	-0.065	0.022	-0.012	-0.016	-0.133	-0.065
6	LL6	0.1	0.143	-0.036	0.302**	-0.028	-0.054	0.076	0.181	0.011	0.42**	0.041	0.017
7	LL7	-0.02	-0.059	0.038	0.168	-0.182	-0.218*	-0.006	-0.087	0.042	0.075	-0.012	0.031
8	LL8	-0.033	-0.132	-0.065	0.104	-0.025	0.051	-0.017	-0.108	-0.025	0.111	0.192	0.144
9	LL9	-0.184	-0.054	0.103	0.071	0.1	-0.169	0.202	0.103	0.141	0.141	0.014	0.056
10	LL10	0.044	-0.014	0.081	0.028	0.06	0.133	0.037	-0.071	0.111	0.07	-0.057	-0.172
11	LL11	-0.218*	-0.072	-0.194	0.036	-0.102	-0.109	-0.209	-0.081	-0.194	0.005	-0.056	-0.053
12	LL12	0.1	0.034	0.121	0.127	-0.079	-0.195	0.049	0.07	0.142	0.157	0.047	0.103
13	LL13	0.08	-0.024	-0.173	0.042	-0.21*	-0.253*	-0.21*	-0.07	-0.165	0.031	-0.064	-0.001
14	LL14	0.04	0.068	-0.061	0.073	-0.048	0.043	0.009	-0.05	0.07	0.06	0.045	-0.122
15	LL15	-0.03	0.038	-0.004	0.123	0.182	0.107	-0.026	-0.059	-0.038	0.069	0.045	0.055
16	LL16	0.03	-0.028	0.05	0.031	-0.033	-0.061	0.036	0.032	0.068	0.044	0.081	0.166
17	LL17	-0.28*	-0.045	-0.069	0.088	0.182	0.122	0.002	0.111	-0.115	0.114	0.156	0.151
18	HL1	-0.115	-0.128	0.095	-0.025	0.024	0.102	0.026	-0.021	0.02	-0.008	0.273**	0.305**
19	HL2	-0.04	-0.103	0.06	0.065	-0.066	-0.091	-0.03	-0.044	-0.02	0.073	0.044	0.204
20	HL3	-0.072	-0.116	0.092	0.164	-0.026	-0.178	0.12	0.04	0.027	0.161	0.127	0.155

Table 5.2: Continued...

21	HL4	-0.092	-0.114	0.018	0.093	0.029	0.214*	0.002	-0.05	-0.052	0.001	0.261**	0.3*
22	HL5	0.019	-0.009	0.237*	0.194	-0.044	-0.097	0.193	0.162	0.161	0.239*	0.114	0.191
23	HL6	0.126	0.1	0.016	-0.127	0.067	-0.071	-0.049	-0.108	-0.055	-0.149	0.071	0.218*
24	HL7	-0.083	0.047	-0.026	0.031	0.051	0.031	-0.084	0.041	-0.023	0.053	0.008	0.079
25	HL8	0.019	0.018	0.177	0.335**	-0.292*	-0.24*	0.153	0.024	0.303**	0.249*	0.02	0.007
26	HL9	-0.117	-0.18	0.015	0.196	-0.015	-0.181	0.02	-0.006	0.034	0.168	0.068	0.024
27	HL10	0.042	0.034	0.018	0.015	0.196	0.156	0.073	-0.004	0.108	0.006	0.015	-0.022
28	HL11	-0.038	0.042	-0.082	-0.13	-0.01	-0.122	-0.049	-0.085	-0.112	-0.118	-0.077	-0.141
29	HL12	-0.092	-0.065	-0.041	-0.029	-0.059	0.115	-0.06	0.006	-0.105	-0.004	0.075	0.121
30	HL13	-0.065	-0.026	-0.101	0.048	0.019	0.052	-0.056	-0.031	-0.119	0.103	0.047	0.124
31	HL14	0.162	0.18	0.021	0.091	0.079	0.095	0.159	0.179	0.083	0.176	-0.107	-0.08
32	HL15	0.066	-0.036	-0.099	0.026	-0.195	-0.04	0.053	-0.101	-0.051	0.01	0.047	0.01
33	HL16	0.349**	0.301**	0.205	0.294**	0.06	0.018	0.363**	0.315**	0.287**	0.3**	-0.053	-0.074
34	HL17	0.045	-0.045	0.02	0.046	0.093	0.037	0.077	0.046	0.035	-0.013	0.022	0.135
35	HL18	-0.1	-0.164	-0.056	-0.05	0.091	0.036	-0.093	-0.137	-0.144	-0.173	0.107	0.063
36	HL19	0.006	-0.03	-0.082	0.19	-0.157	-0.089	-0.108	-0.004	-0.102	0.044	0.094	0.101
37	HL20	-0.101	-0.035	-0.055	-0.027	0.104	0.007	-0.103	-0.129	-0.066	-0.068	0.154	0.178
38	HL21	-0.145	-0.042	-0.134	0.026	0.048	-0.056	-0.179	-0.051	-0.194	0.047	0.076	-0.053

*Significant at 10%; ** significant at 5%

Appendix 6: The Pearson's correlation between Niño 1+2 and frequency of extreme precipitation indices

SL No	Grid Point	R100		R65		R2.5_65		R40		R20	
		0 - year	1 - year	0 - year	1 - year	0 - year	1 - year	0 - year	1 - year	0 - year	1 - year
1	LL1	0.178	0.239*	0.154	0.03	-0.029	-0.016	0.069	-0.004	-0.049	0.055
2	LL2	-0.035	0.096	0.003	0.074	-0.006	-0.169	0.278**	0.162	-0.195	-0.25**
3	LL3	0.216*	0.249*	0.084	0.064	-0.207	-0.154	0.099	0.011	0.078	-0.028
4	LL4	0.33**	0.352**	0.072	0.173	-0.119	-0.148	0.129	-0.157	-0.181	-0.168
5	LL5	-0.066	-0.028	0.09	0.032	0.133	0.102	0.152	0.028	0.183	0.164
6	LL6	0.097	0.27*	0.042	-0.029	0.063	-0.031	-0.024	0.035	0.01	-0.139
7	LL7	-0.041	-0.062	-0.008	-0.212*	0.104	0.139	0.002	0.238*	-0.011	-0.176
8	LL8	-0.035	-0.098	0.025	-0.248*	0.055	0.06	-0.005	-0.121	-0.175	0.044
9	LL9	0.27**	0.22*	-0.012	0.093	-0.128	0.049	-0.127	0.018	-0.03	0.07
10	LL10	0.066	0.084	0.042	-0.095	-0.009	0.105	-0.033	-0.122	-0.025	-0.061
11	LL11	-0.233*	-0.134	-0.1	-0.014	0.195	0.12	-0.212*	-0.128	0.167	0.165
12	LL12	0.072	0.28*	0.015	0.019	-0.08	-0.13	-0.029	-0.247*	-0.109	-0.002
13	LL13	-0.098	0.04	-0.242*	-0.164	-0.045	0.031	0.108	-0.28**	-0.218*	-0.025
14	LL14	-0.105	0.06	0.04	0.026	0.041	0.183	0.055	-0.031	0.113	0.052
15	LL15	-0.075	0.04	0.048	0.038	0.097	0.022	0.1	0.037	0.04	0.084
16	LL16	0.016	-0.015	0.04	0.038	-0.05	-0.105	0.045	0.022	-0.064	-0.043
17	LL17	-0.077	0.045	-0.074	-0.012	0.07	-0.069	0.106	-0.188	0.023	0.011
18	HL1	0.056	0.043	-0.039	-0.059	-0.307*	-0.244*	-0.212*	-0.129	-0.03	-0.129
19	HL2	0.04	0.138	0.018	-0.047	-0.02	-0.2	-0.113	-0.144	-0.056	-0.116
20	HL3	0.01	0.168	-0.007	0.02	-0.14	-0.132	-0.01	-0.138	-0.043	-0.175

Continued...

21	HL4	0.028	0.016	-0.125	-0.107	-0.177	-0.218*	0.06	-0.112	-0.111	-0.119
22	HL5	0.104	0.161	0.129	0.08	-0.141	-0.146	0.13	-0.031	0.012	-0.084
23	HL6	-0.077	-0.092	-0.056	-0.131	-0.19	-0.214*	0.039	0.043	-0.101	-0.102
24	HL7	-0.061	0.035	-0.164	0.02	0.025	0.045	0.016	-0.024	-0.117	0.039
25	HL8	0.231*	0.278**	-0.03	-0.201	-0.001	0.016	0.088	0.007	-0.23*	0.069
26	HL9	0.058	0.133	-0.061	-0.144	-0.024	-0.042	-0.105	-0.145	-0.031	0.057
27	HL10	-0.068	-0.005	0.031	-0.007	0.066	0.152	0.05	-0.002	0.054	0.06
28	HL11	-0.064	-0.076	-0.011	0.011	0.199	0.162	-0.154	0.113	0.178	0.128
29	HL12	-0.124	0.065	-0.118	-0.209	-0.034	-0.169	-0.073	0.124	0.154	-0.022
30	HL13	-0.185	0.068	-0.014	-0.121	-0.007	0.061	0.074	-0.011	0.185	-0.07
31	HL14	0.035	0.147	0.09	0.152	0.18	0.082	0.065	0.193	0.236*	0.00
32	HL15	-0.024	-0.049	0.167	0.047	0.049	0.068	-0.037	-0.004	0.166	-0.079
33	HL16	0.222*	0.274**	0.247*	0.291**	0.109	0.025	0.297**	0.123	0.343**	0.301**
34	HL17	0.085	0.037	-0.068	-0.107	-0.029	-0.176	-0.023	-0.054	0.084	0.054
35	HL18	-0.068	0.05	-0.116	-0.28*	-0.062	-0.04	-0.077	-0.074	0.014	-0.033
36	HL19	-0.049	0.047	-0.151	-0.051	0.129	-0.173	0.062	-0.021	-0.201	-0.122
37	HL20	-0.095	0.077	-0.097	-0.166	0.116	-0.01	-0.085	0.032	0.008	0.066
38	HL21	-0.152	0.07	-0.172	-0.04	0.031	0.061	-0.118	-0.116	-0.043	-0.077

*Significant at 10%; ** significant at 5%

Appendix 7: The Pearson's correlation between Niño 3 and general extreme precipitation indices

SI No	Grid Point	RR		RX1		CWD		SDII		RX5		CDD	
		0 - year	1-year	0-year	1-year	0 - year	1 - year	0 - year	1 - year	0 - year	1 - year	0 - year	1 - year
1	LL1	0.204	0.13	0.086	0.27**	0.106	0.04	0.25**	0.20	0.125	0.24	0.03	0.14
2	LL2	0.151	0.21	-0.057	0.16	0.082	0.09	-0.061	-0.05	-0.08	0.16	-0.014	0.03
3	LL3	0.205	0.19	0.159	0.25**	-0.019	-0.08	0.184	0.22**	0.094	0.3**	0.089	0.17
4	LL4	0.123	0.00	0.29**	0.16	-0.033	0.07	0.216*	0.21	0.291**	0.23	0.02	0.07
5	LL5	0.127	0.08	-0.011	0.02	-0.097	-0.07	-0.06	0.09	-0.004	0.04	-0.122	-0.01
6	LL6	0.071	0.06	-0.066	0.27**	0.046	-0.03	0.043	0.14	-0.058	0.33**	0.034	0.08
7	LL7	0.033	0.01	0.029	0.17	-0.091	-0.11	0.045	0.02	0.043	0.10	-0.02	0.10
8	LL8	0.017	-0.07	-0.032	0.18	-0.049	0.07	0.027	-0.01	-0.004	0.16	0.112	0.16
9	LL9	-0.14	-0.02	0.22*	0.04	0.145	-0.12	0.163	0.08	0.125	0.11	0.025	0.10
10	LL10	0.05	-0.01	0.092	0.03	0.007	0.08	0.051	-0.04	0.108	0.06	-0.037	-0.09
11	LL11	-0.127	-0.01	-0.134	0.11	-0.069	-0.11	-0.163	-0.03	-0.146	0.04	-0.043	0.01
12	LL12	-0.005	0.03	0.065	0.08	0	-0.11	0.023	0.08	0.092	0.16	0.032	0.12
13	LL13	0.002	-0.03	0.22*	0.13	-0.122	-0.19	-0.123	0.02	-0.105	0.10	-0.078	0.08
14	LL14	-0.029	0.04	-0.078	0.14	-0.01	0.07	0.016	-0.03	0.008	0.05	0.085	-0.05
15	LL15	-0.045	0.02	-0.014	0.21*	0.151	0.11	-0.001	-0.03	-0.06	0.16	0.032	0.08
16	LL16	0.028	0.01	0.038	0.09	-0.019	-0.11	0.039	0.05	0.063	0.07	0.017	0.12
17	LL17	-0.018	-0.06	-0.035	0.16	0.119	-0.05	-0.034	0.12	-0.099	0.16	0.119	0.17
18	HL1	0.022	-0.05	0.27*	0.02	0.008	0.08	0.118	0.01	0.22*	0.04	0.103	0.19
19	HL2	0.002	-0.05	0.041	0.12	-0.053	-0.10	0.018	0.00	0.023	0.13	0.006	0.14
20	HL3	-0.025	0.00	0.09	0.21*	0.03	-0.16	0.119	0.10	0.21*	0.20*	0.07	0.10

Table 5.4: Continued....

21	HL4	-0.031	-0.01	0.015	0.19	-0.046	0.10	0.04	0.05	-0.037	0.09	0.127	0.18
22	HL5	0.024	0.04	0.26**	0.20	0.016	-0.02	0.11	0.13	0.086	0.22*	0.03	0.15
23	HL6	0.068	0.07	0.075	-0.04	0.081	-0.04	0.003	-0.02	-0.05	-0.08	0.019	0.17
24	HL7	-0.104	0.08	0.052	0.14	0.042	-0.02	-0.092	0.08	0.016	0.13	0.063	0.14
25	HL8	0.054	0.08	0.052	0.27**	-0.122	-0.11	0.127	0.00	0.20*	0.20*	0.032	0.06
26	HL9	-0.048	-0.08	-0.011	0.18	0.02	-0.14	0.029	0.07	-0.002	0.17	0.021	0.06
27	HL10	0.013	0.05	0.042	0.05	0.146	0.03	0.057	0.02	0.108	0.03	0.023	0.00
28	HL11	-0.045	0.09	0.09	-0.07	0.053	-0.14	0.009	-0.03	-0.02	-0.08	-0.061	-0.03
29	HL12	-0.048	0.03	-0.012	0.05	-0.099	0.05	-0.048	0.08	-0.059	0.09	-0.005	0.05
30	HL13	-0.012	0.08	-0.032	0.19	0.04	0.05	-0.002	0.08	-0.068	0.23*	0.008	0.13
31	HL14	0.117	0.17	0.01	0.23*	0.016	0.02	0.122	0.16	0.058	0.25*	-0.091	-0.08
32	HL15	0.056	0.00	-0.098	0.10	-0.14	-0.06	0.029	-0.04	-0.073	0.05	0.013	0.09
33	HL16	0.197	0.15	0.099	0.34**	0.024	0.00	0.206	0.21**	0.27*	0.24*	-0.02	0.06
34	HL17	0.095	0.00	0.07	0.16	0.03	-0.02	0.106	0.09	0.083	0.06	-0.026	0.14
35	HL18	-0.049	-0.15	-0.014	0.00	0.034	-0.02	-0.068	-0.10	-0.074	-0.13	0.061	0.11
36	HL19	0.042	-0.03	-0.086	0.24*	-0.118	-0.06	-0.062	0.05	-0.076	0.08	0.053	0.12
37	HL20	-0.063	0.02	-0.039	0.11	0.08	-0.07	-0.047	0.00	-0.041	0.06	0.071	0.14
38	HL21	-0.147	-0.01	-0.137	0.09	0.054	-0.09	-0.158	-0.01	-0.202	0.09	0.075	-0.04

*Significant at 10%; ** significant at 5%

Appendix 8: The Pearson's correlation between Niño 3 and frequency of extreme precipitation indices

SI No	Grid Point	R100		R65		R2.5_65		R40		R20	
		0 - year	1 - year	0 - year	1 - year	0 - year	1 - year	0 - year	1 - year	0 - year	1 - year
1	LL1	0.219*	0.22*	0.143	0.07	-0.071	-0.09	0.165	-0.01	-0.003	0.03
2	LL2	-0.062	0.09	0.01	-0.01	0.095	-0.17	0.12	0.08	-0.019	-0.27**
3	LL3	0.077	0.21	0.108	0.12	-0.117	-0.13	0.075	-0.23*	0.166	-0.11
4	LL4	0.19	0.24*	-0.006	0.10	-0.095	-0.13	0.203	-0.10	-0.106	-0.21
5	LL5	-0.042	0.12	0.02	0.09	0.072	0.04	0.089	0.02	0.171	0.13
6	LL6	0.084	0.16	0.057	-0.08	0.005	-0.09	-0.029	-0.02	0.029	-0.16
7	LL7	0.034	0.17	0.159	-0.14	-0.082	0.02	-0.059	0.27**	-0.027	-0.21*
8	LL8	0.019	-0.14	0.113	-0.16	-0.019	-0.03	0.056	-0.05	-0.185	-0.02
9	LL9	0.234*	0.18	-0.073	0.07	-0.127	0.00	-0.106	0.03	0.042	0.04
10	LL10	0.056	0.16	0.031	-0.07	-0.014	0.08	0.032	-0.10	-0.046	-0.02
11	LL11	-0.102	-0.18	-0.037	-0.02	0.086	0.10	-0.115	-0.06	0.017	0.17
12	LL12	0.058	0.19	-0.017	-0.02	-0.054	-0.13	0.029	-0.24*	-0.044	0.05
13	LL13	0	0.06	-0.046	-0.12	-0.095	-0.03	0.193	-0.33**	-0.106	0.00
14	LL14	-0.031	0.15	-0.082	0.04	-0.048	0.07	0.057	-0.10	0.16	0.08
15	LL15	-0.032	0.15	0.059	0.00	-0.01	-0.03	0.02	0.00	0.005	0.05
16	LL16	0.011	0.03	-0.001	0.02	0.033	-0.02	0.041	0.06	-0.032	-0.01
17	LL17	0.022	0.09	-0.062	-0.05	-0.004	-0.12	0.115	-0.21*	0.065	-0.02
18	HL1	0.16	0.07	0.095	-0.06	-0.082	-0.11	-0.042	-0.04	0.13	-0.06
19	HL2	0.052	0.18	0.072	-0.02	0.036	-0.16	-0.002	-0.08	0.036	-0.07
20	HL3	0.013	0.21*	0.08	0.04	-0.077	-0.10	0.047	-0.26*	0.018	-0.18

Continued....

21	HL4	0.077	0.06	-0.065	-0.03	-0.03	-0.11	0.093	-0.04	0.016	0.03
22	HL5	0.046	0.14	0.026	0.12	-0.053	-0.15	0.106	0.04	-0.023	-0.20
23	HL6	-0.025	-0.01	0.012	-0.04	-0.08	-0.19	0.1	0.05	-0.058	-0.08
24	HL7	-0.046	0.08	-0.181	0.08	-0.007	0.05	-0.071	0.06	-0.148	0.05
25	HL8	0.101	0.22*	0.027	-0.21	-0.038	0.03	0.13	0.05	-0.19	0.05
26	HL9	0.059	0.24*	0.037	-0.03	-0.007	-0.06	-0.028	-0.24*	0.002	0.08
27	HL10	-0.06	-0.01	-0.019	0.02	0.022	0.09	-0.049	0.07	0.01	0.06
28	HL11	0.055	-0.03	-0.05	0.01	0.083	0.04	-0.189	0.12	0.032	0.06
29	HL12	-0.051	0.26*	-0.083	-0.18	0.062	-0.10	-0.061	-0.23*	0.148	0.02
30	HL13	-0.133	0.25*	0.011	-0.08	0.017	0.06	0.091	0.09	0.176	-0.01
31	HL14	0.086	0.23*	0.102	0.18	0.146	0.07	0.028	0.12	0.212*	-0.03
32	HL15	-0.011	0.21*	0.15	0.01	0.052	0.03	-0.021	0.04	0.065	-0.08
33	HL16	0.089	0.18	0.089	0.16	0.058	-0.12	0.112	0.03	0.146	-0.17
34	HL17	0.145	0.11	0.045	-0.04	0.038	-0.18	0.083	-0.07	0.029	-0.08
35	HL18	-0.019	0.07	0.02	-0.29**	-0.036	-0.05	-0.071	-0.24*	-0.001	0.05
36	HL19	-0.008	0.22**	-0.062	0.00	0.152	-0.13	0.162	-0.06	-0.091	-0.04
37	HL20	-0.013	0.01	-0.071	-0.09	0.112	-0.02	-0.031	0.07	0.113	0.09
38	HL21	-0.154	0.28**	-0.124	-0.05	0.002	0.07	-0.057	-0.22*	-0.005	-0.06

*Significant at 10%; ** significant at 5%

Appendix 9: The Pearson's correlation between Niño 4 and general extreme precipitation indices

SI No	Grid Point	RR		RX1		CWD		SDII		RX5		CDD	
		0 - year	1-year	0 - year	1-year	0 -year	1-year	0 - year	1 - year	0 - year	1 -year	0-year	1-year
1	LL1	0.201	0.03	0.153	0.24*	0.081	-0.06	0.258**	0.14	0.166	0.17	0.065	0.20
2	LL2	0.193	0.26**	0.066	0.25**	0.008	-0.08	0.021	0.1	0	0.21*	0.018	0.03
3	LL3	0.26**	0.20	0.168	0.22*	-0.075	-0.14	0.22*	0.3**	0.12	0.3**	0.096	0.22*
4	LL4	0.22**	0.29**	0.35*	0.18	-0.064	0.11	0.278**	0.22*	0.331**	0.24*	0.012	0.07
5	LL5	0.169	0.11	-0.06	0.29*	-0.046	-0.06	-0.017	0.12	-0.03	0.09	-0.09	0.07
6	LL6	0.181	0.00	0.011	0.28**	-0.014	-0.15	0.082	0.12	-0.038	0.24*	0.057	0.16
7	LL7	0.178	-0.01	0.114	0.18	-0.099	-0.09	0.113	0.04	0.096	0.09	0.014	0.17
8	LL8	-0.05	-0.08	0.184	0.29**	-0.058	0.00	0.013	0.02	0.038	0.23*	0.131	0.21*
9	LL9	0.29*	-0.15	0.157	0.05	0.102	0.00	0.234*	0.15	0.154	0.14	0.109	0.18
10	LL10	0.148	0.06	0.194	0.25*	0.098	0.15	0.055	0.06	0.176	0.14	-0.049	-0.05
11	LL11	-0.069	-0.03	-0.07	0.03	-0.02	-0.09	-0.118	-0.13	-0.112	-0.08	-0.066	0.07
12	LL12	-0.016	0.05	0.08	0.07	0.032	-0.08	0.028	0.14	0.077	0.18	0.052	0.12
13	LL13	0.143	-0.05	0.013	0.28**	-0.108	-0.28	-0.067	0.03	-0.009	0.10	-0.084	0.18
14	LL14	0.11	0.07	-0.065	0.14	0.043	0.00	0.053	0.03	0.017	0.07	0.114	-0.03
15	LL15	-0.04	0.05	0.052	0.26**	0.195	0.12	0.072	-0.01	-0.042	0.18	0.056	0.17
16	LL16	0.18	0.02	0.124	0.15	-0.031	-0.14	0.065	0.03	0.114	0.08	0.052	0.10
17	LL17	0.25*	-0.04	0.07	0.16	0.038	-0.23*	0.029	0.17	-0.054	0.12	0.158	0.21*
18	HL1	0.13	-0.04	0.191	-0.05	0	0.02	0.195	-0.01	0.184	-0.02	0.074	0.17
19	HL2	0.14	0.03	0.151	0.11	-0.113	-0.20	0.188	0.06	0.164	0.10	0.015	0.07
20	HL3	0.16	0.03	0.175	0.21*	0.047	-0.18	0.216*	0.21	0.112	0.20	0.051	0.09

Continued...

21	HL4	-0.01	-0.01	-0.031	0.11	-0.032	0.04	0.04	0.02	-0.04	0.05	0.113	0.15
22	HL5	0.22*	0.13	0.125	0.16	0.043	0.03	0.146	0.22*	0.072	0.20	0.033	0.15
23	HL6	0.116	0.15	0.09	0.01	0.079	-0.05	0.061	0.05	0.041	-0.03	0.02	0.21
24	HL7	-0.117	0.08	0.118	0.19	-0.017	-0.13	-0.092	0.09	0.03	0.15	0.093	0.18
25	HL8	0.185	0.03	-0.016	0.06	-0.037	-0.07	0.162	-0.07	0.143	0.07	0.1	0.12
26	HL9	0.28**	-0.03	0.016	0.04	0.061	-0.05	0.08	0.05	0.018	0.07	0.034	0.12
27	HL10	0.26*	0.11	0.054	0.25*	0.102	0.05	0.035	0.08	0.103	0.13	-0.06	0.03
28	HL11	-0.022	0.08	0.138	0.24*	0.002	-0.17	0.095	0.01	0.081	0.00	-0.069	0.00
29	HL12	-0.019	0.06	-0.07	0.09	-0.113	-0.07	-0.047	0.10	-0.058	0.13	-0.061	0.03
30	HL13	-0.001	0.12	-0.016	0.25**	-0.011	-0.14	-0.004	0.15	-0.075	0.22*	-0.001	0.19
31	HL14	0.27*	0.15	0.035	0.38**	-0.026	-0.05	0.186	0.14	0.115	0.3**	-0.188	-0.13
32	HL15	0.046	0.01	-0.058	0.21*	-0.133	-0.17	0.015	0.02	-0.061	0.11	0.054	0.22*
33	HL16	0.23*	0.02	0.082	0.39*	-0.064	-0.09	0.165	0.12	0.109	0.21*	0.002	0.18
34	HL17	0.21*	-0.08	0.085	0.13	-0.03	-0.06	0.1	-0.01	0.061	0.01	-0.053	0.13
35	HL18	-0.085	-0.21	0.073	0.06	-0.061	-0.16	-0.079	-0.13	-0.036	-0.12	0.138	0.21
36	HL19	0.21*	0.01	0.012	0.23*	-0.126	-0.15	0.077	0.15	0.039	0.11	0.034	0.07
37	HL20	0.24**	0.13	-0.058	0.07	0.004	-0.20	-0.016	0.04	-0.043	0.06	0.08	0.16
38	HL21	-0.158	0.00	-0.104	0.06	-0.021	-0.20	-0.185	-0.06	-0.202	0.04	-0.06	-0.08

*Significant at 10%; ** significant at 5%

Appendix 10 : The Pearson's correlation between Niño 4 and intense rainfall frequency of extreme precipitation indices

Sl No	Grid Point	R100		R65		R2.5_65		R40		R20	
		0 - year	1 - year	0 - year	1 - year	0 - year	1 - year	0 - year	1 - year	0 - year	1 - year
1	LL1	0.226**	0.13	0.084	0.09	-0.087	-0.19	0.167	-0.06	0.002	-0.04
2	LL2	-0.03	0.14	0.053	0.00	-0.007	-0.21	0.138	0.10	-0.017	-0.33
3	LL3	0.105	0.25**	0.207	0.27**	-0.185	-0.25	0.094	-0.03	0.117	-0.23
4	LL4	0.274**	0.22*	0.11	0.16	-0.188	-0.20	0.178	-0.07	-0.119	-0.25
5	LL5	-0.039	0.04	0.04	0.18	0.007	-0.12	0.106	0.05	0.155	0.07
6	LL6	0.17	0.17	0.08	-0.07	-0.047	-0.22	-0.013	-0.09	-0.007	-0.22
7	LL7	0.141	0.00	0.18	-0.04	-0.14	-0.12	-0.044	0.17	-0.081	-0.21
8	LL8	0.11	0.00	0.041	-0.16	-0.04	-0.16	0.029	-0.08	-0.192	-0.13
9	LL9	0.229**	0.18	0.029	0.07	-0.179	-0.14	-0.131	-0.08	0.052	-0.05
10	LL10	0.184	0.14	-0.003	-0.01	-0.021	-0.01	-0.003	-0.06	-0.069	-0.01
11	LL11	-0.094	-0.16	-0.025	-0.18	0.058	0.07	-0.152	-0.16	-0.023	0.16
12	LL12	0.186	0.24*	-0.005	0.02	-0.12	-0.23	-0.013	-0.21	-0.121	-0.03
13	LL13	0.19	0.09	-0.045	-0.12	-0.108	-0.14	0.157	-0.31	-0.098	0.01
14	LL14	-0.015	0.05	-0.074	0.18	-0.009	-0.02	0.049	-0.05	0.148	0.00
15	LL15	-0.031	0.06	0.085	-0.02	-0.048	-0.07	0.035	0.11	-0.033	0.00
16	LL16	0.181	0.23*	0.045	0.03	0.038	0.03	0.01	0.03	-0.041	-0.05
17	LL17	0.12	0.03	-0.055	0.02	-0.017	-0.16	0.079	-0.05	0.082	-0.04
18	HL1	0.164	0.00	0.158	-0.04	-0.075	-0.07	0.013	-0.07	0.137	-0.03
19	HL2	0.102	0.13	0.131	0.03	0.033	-0.07	0.059	0.02	0.1	0.02
20	HL3	0.20	0.20	0.109	0.12	-0.072	-0.11	0.098	0.11	0.05	-0.09

Continued....

21	HL4	0.168	-0.02	-0.074	0.03	-0.099	-0.10	0.027	-0.07	0.003	0.04
22	HL5	0.166	0.15	0.058	0.23*	-0.042	-0.16	0.166	0.20	0.016	-0.18
23	HL6	0.19	0.05	0.032	0.01	-0.12	-0.29	0.178	0.16	0.04	-0.06
24	HL7	-0.019	0.22*	-0.192	0.09	-0.009	-0.04	-0.119	0.03	-0.083	-0.01
25	HL8	0.123	0.05	0.078	-0.18	-0.133	-0.02	0.133	0.03	-0.193	-0.07
26	HL9	0.162	0.08	0.086	0.03	-0.061	-0.19	-0.013	0.04	-0.018	-0.01
27	HL10	-0.023	-0.01	-0.01	0.09	0.114	0.16	-0.05	0.13	0.04	0.09
28	HL11	0.184	0.23*	-0.021	-0.03	0.076	0.04	-0.149	0.09	0.003	0.02
29	HL12	-0.07	0.17	-0.06	-0.12	0.062	-0.09	0.004	0.24*	0.133	0.02
30	HL13	-0.167	0.12	0.024	-0.01	0.073	-0.03	0.139	0.19	0.143	0.02
31	HL14	0.178	0.22*	0.071	0.15	0.19	0.09	0.073	0.06	0.254**	-0.02
32	HL15	-0.042	0.03	0.163	0.05	0.06	-0.08	-0.023	0.02	0.04	-0.07
33	HL16	0.18	0.10	0.075	0.08	0.012	-0.29**	0.106	-0.03	0.145	-0.03
34	HL17	0.162	0.16	0.05	-0.11	0.027	-0.19	0.113	-0.17	-0.011	0.03
35	HL18	-0.037	0.19	0.006	-0.28**	-0.074	-0.11	-0.127	-0.17	-0.031	-0.06
36	HL19	0.11	-0.01	0.02	0.12	0.102	-0.01	0.22*	0.03	0.019	0.12
37	HL20	-0.03	0.15	-0.143	-0.16	0.122	-0.03	0.017	0.14	0.123	0.04
38	HL21	-0.188	0.15	-0.15	-0.11	-0.044	0.12	-0.143	-0.15	-0.05	-0.03

*Significant at 10%; ** significant at 5%

Appendix 11 : The Pearson's correlation between Niño 3.4 and general extreme precipitation indices

SI No	Grid Point	RR		RX1		CWD		SDII		RX5		CDD	
		0 -year	1-year	0 - year	1-year	0 -year	1 -year	0 - year	1 - year	0 -year	1 -year	0 -year	1 -year
1	LL1	0.321*	0.19	0.185	0.24*	0.078	-0.02	0.22**	0.17	0.143	0.18	0.02	0.14
2	LL2	0.135	0.19	-0.054	0.18	0.058	0.03	-0.036	-0.04	-0.066	0.17	-0.027	-0.01
3	LL3	0.176	0.14	0.118	0.22*	-0.034	-0.10	0.152	0.20	0.059	0.28**	0.045	0.14
4	LL4	0.11	-0.06	0.256**	0.14	-0.016	0.12	0.191	0.16	0.247*	0.19	0.018	0.05
5	LL5	0.22*	0.16	-0.034	0.04	-0.058	-0.05	-0.043	0.11	-0.017	0.06	-0.085	0.04
6	LL6	0.161	0.10	-0.082	0.25*	0.019	-0.09	0.049	0.10	-0.10	0.27**	0.042	0.09
7	LL7	0.178	0.02	0.158	0.15	-0.033	-0.05	0.103	0.04	0.174	0.09	-0.009	0.13
8	LL8	0.23*	-0.06	0.18	0.19	-0.056	0.04	0.045	0.02	0.127	0.15	0.107	0.17
9	LL9	-0.099	-0.04	0.138	0.02	0.138	-0.07	0.165	0.06	0.126	0.10	0.028	0.10
10	LL10	0.251*	0.02	0.101	0.05	0.013	0.07	0.052	-0.01	0.11	0.07	-0.035	-0.05
11	LL11	-0.066	0.01	-0.089	0.11	-0.042	-0.08	-0.117	-0.03	-0.109	0.03	-0.049	0.04
12	LL12	0.27*	0.04	0.044	0.04	0.029	-0.09	0.03	0.09	0.17	0.14	0.023	0.10
13	LL13	0.146	-0.02	-0.065	0.15	-0.079	-0.20	-0.065	0.05	-0.049	0.11	-0.097	0.11
14	LL14	-0.004	0.06	-0.08	0.15	-0.008	0.03	0.06	0.01	0.17	0.07	0.114	-0.04
15	LL15	-0.004	0.05	0.14	0.22*	0.155	0.10	0.064	0.00	-0.037	0.19	0.037	0.09
16	LL16	0.127	0.03	0.23*	0.10	-0.018	-0.11	0.042	0.06	0.165	0.08	0.026	0.10
17	LL17	0.32*	-0.05	0.14	0.16	0.084	-0.14	0.012	0.15	-0.054	0.17	0.113	0.16
18	HL1	0.184	-0.04	0.184	-0.03	0.012	0.06	0.146	-0.02	0.155	0.00	0.032	0.12
19	HL2	0.162	-0.02	0.17	0.11	-0.05	-0.09	0.086	0.01	0.175	0.12	-0.014	0.10
20	HL3	0.24*	0.04	0.12	0.22*	0.067	-0.15	0.159	0.12	0.162	0.21	0.027	0.05

Continued...

21	HL4	0.26*	0.02	0.10	0.18	-0.078	0.06	0.078	0.06	-0.01	0.10	0.065	0.12
22	HL5	0.27**	0.07	0.136	0.17	0.032	0.02	0.091	0.11	0.163	0.19	0.005	0.12
23	HL6	0.26**	0.07	0.17	-0.01	0.092	-0.03	0.015	-0.01	0.123	-0.05	0.012	0.17
24	HL7	-0.126	0.05	0.18	0.14	0.014	-0.06	-0.111	0.05	0.10	0.12	0.076	0.15
25	HL8	0.27**	0.06	-0.025	0.17	-0.053	-0.07	0.121	-0.07	0.143	0.12	0.048	0.07
26	HL9	-0.023	-0.06	0.15	0.12	0.05	-0.11	0.069	0.07	0.22*	0.13	0.029	0.10
27	HL10	-0.006	0.04	0.25*	0.07	0.095	0.00	0.036	0.02	0.296**	0.05	0.017	0.04
28	HL11	-0.039	0.09	0.181	-0.01	0.078	-0.12	0.074	0.00	0.25*	-0.02	-0.034	0.01
29	HL12	-0.03	0.03	-0.025	0.06	-0.089	0.02	-0.048	0.07	-0.045	0.10	-0.035	0.05
30	HL13	-0.006	0.09	-0.02	0.23*	0.014	-0.03	0.007	0.11	-0.059	0.24*	0.008	0.15
31	HL14	0.142	0.15	0.18	0.29**	-0.008	0.00	0.156	0.13	0.193	0.27**	-0.112	-0.08
32	HL15	0.26*	0.01	-0.073	0.15	-0.124	-0.07	0.045	0.00	-0.054	0.09	0.023	0.14
33	HL16	0.148	0.07	0.17	0.36**	0.005	0.00	0.166	0.15	0.29**	0.22*	-0.004	0.13
34	HL17	0.144	-0.01	0.14	0.18	0	-0.01	0.139	0.07	0.22*	0.08	-0.046	0.13
35	HL18	-0.029	-0.16	0.23*	0.01	-0.009	-0.06	-0.036	-0.10	-0.024	-0.12	0.079	0.14
36	HL19	0.28**	-0.01	-0.061	0.21*	-0.083	-0.05	-0.01	0.07	-0.03	0.08	0.046	0.10
37	HL20	-0.022	0.05	-0.026	0.13	0.048	-0.12	0.005	0.05	-0.013	0.10	0.043	0.11
38	HL21	-0.103	0.03	-0.108	0.09	0.024	-0.13	-0.111	0.00	-0.17	0.10	0.006	-0.08

*Significant at 10%; ** significant at 5%

Appendix 12: The Pearson's correlation between Niño 3.4 and frequency of extreme precipitation indices

SI No	Grid Point	R100		R65		R2.5_65		R40		R20	
		0 - year	1 - year	0 - year	1 - year	0 - year	1 - year	0 - year	1 - year	0 - year	1 - year
1	LL1	0.28**	0.16	0.136	0.13	-0.035	-0.13	0.141	-0.05	0.18	0.14
2	LL2	-0.08	0.10	-0.042	-0.02	0.183	-0.14	0.168	0.06	-0.052	-0.28*
3	LL3	0.18	0.20	0.182	0.13	-0.148	-0.12	0.071	-0.05	0.129	-0.17
4	LL4	0.23*	0.18	-0.124	0.08	-0.086	-0.11	0.186	-0.08	-0.104	-0.21
5	LL5	0.148	0.03	-0.004	0.09	0.10	-0.02	0.124	0.00	0.163	0.14
6	LL6	0.176	0.13	0.143	-0.09	0.144	-0.13	-0.038	-0.05	0.052	-0.16
7	LL7	0.15	0.02	0.192	-0.09	0.14	-0.03	-0.047	-0.25*	0.21	-0.21*
8	LL8	-0.04	-0.03	0.186	-0.13	0.13	-0.08	0.057	-0.05	-0.171	-0.05
9	LL9	0.22*	0.10	0.181	0.04	-0.133	-0.02	-0.119	0.01	0.17	-0.01
10	LL10	0.24*	0.08	0.142	-0.04	-0.018	0.05	0.015	-0.07	-0.016	0.02
11	LL11	0.162	-0.07	0.164	-0.07	0.152	0.05	-0.113	-0.08	0.17	0.16
12	LL12	0.143	0.19	-0.03	-0.02	-0.049	-0.12	0.008	-0.19	-0.059	0.05
13	LL13	0.163	0.18	-0.13	-0.09	-0.054	-0.05	0.177	-0.33**	-0.136	0.04
14	LL14	0.198	0.16	-0.073	0.10	-0.005	0.02	0.057	-0.09	0.179	0.08
15	LL15	0.186	0.18	0.22	-0.01	0.149	-0.03	0.046	0.03	0.133	0.05
16	LL16	0.011	0.17	0.11	0.03	-0.15	0.02	0.057	0.06	-0.036	0.00
17	LL17	-0.051	0.19	0.111	-0.01	-0.13	-0.13	0.131	-0.08	0.164	-0.02
18	HL1	0.122	0.17	0.145	-0.06	-0.145	-0.06	-0.096	-0.04	0.176	-0.04
19	HL2	0.013	0.17	0.146	0.00	0.012	-0.13	-0.085	-0.02	0.03	-0.05
20	HL3	-0.017	0.22**	0.132	0.05	-0.104	-0.09	0.012	0.02	-0.01	-0.18

Continued...

21	HL4	0.035	0.03	0.11	0.01	-0.083	-0.06	0.073	-0.02	-0.038	0.07
22	HL5	0.057	0.12	0.146	0.14	-0.085	-0.13	0.098	0.10	-0.007	-0.23*
23	HL6	-0.04	0.12	0.19	-0.03	-0.121	-0.20	0.063	0.06	-0.066	-0.08
24	HL7	-0.041	0.16	0.163	0.08	-0.005	0.02	-0.029	-0.01	-0.147	0.01
25	HL8	0.126	0.10	-0.003	0.23**	-0.015	0.07	0.139	0.04	-0.175	0.02
26	HL9	0.034	0.11	-0.015	0.00	0.046	-0.13	-0.059	-0.01	0.007	0.03
27	HL10	-0.073	-0.03	0.021	0.01	0.08	0.07	-0.005	0.08	0.024	0.05
28	HL11	-0.009	0.12	0.16	0.00	0.15	-0.01	-0.19	0.10	0.13	0.01
29	HL12	-0.062	0.16	-0.105	-0.17	0.038	-0.09	-0.079	-0.24**	0.17	0.00
30	HL13	-0.136	0.14	-0.02	-0.04	0.023	0.02	0.102	0.12	-0.27*	-0.02
31	HL14	0.133	0.24**	0.069	0.17	0.15	0.06	0.004	0.08	-0.25*	-0.07
32	HL15	-0.031	0.13	0.127	0.02	0.087	-0.03	-0.02	0.03	0.129	-0.09
33	HL16	0.201	0.14	0.127	0.10	0.087	-0.20	0.156	-0.03	-0.28*	0.07
34	HL17	0.18	0.12	-0.002	-0.05	0.014	-0.17	0.031	-0.10	0.054	0.07
35	HL18	-0.056	0.10	0.14	-0.29**	-0.011	-0.06	-0.077	-0.05	0.017	-0.06
36	HL19	-0.041	0.00	-0.102	0.02	0.168	-0.08	0.107	-0.04	-0.139	0.01
37	HL20	-0.061	0.06	-0.064	-0.10	0.112	-0.02	-0.074	0.09	0.063	0.08
38	HL21	-0.174	0.09	-0.163	-0.04	-0.012	0.13	-0.094	-0.11	-0.049	-0.01

*Significant at 10%; ** significant at 5%

Appendix 13: Correlation Analysis between ENSO Indices and summer monsoon precipitation index

Season	Nino 1+2		Nino 3		Nino 3.4		Nino 4	
	P-Value	Correlation Coefficient	P-Value	Correlation Coefficient	P-Value	Correlation Coefficient	P-Value	Correlation Coefficient
DJF(-6)	0.775	0.041	0.482	0.102	0.497	0.098	0.478	0.103
MAM(-5)	0.251	0.165	0.191	0.188	0.133	0.216	0.139	0.212
JJA(-4)	0.431	0.114	0.095	0.231**	0.104	0.232	0.215	0.178
SON(-3)	0.215	0.178	0.238	0.17	0.181	0.192	0.02	0.251*
DJF(-2)	0.522	0.093	0.19	0.188	0.045	0.246*	0.038	0.243*
MAM(-1)	0.549	0.087	0.696	0.057	0.678	0.06	0.738	0.048
JJA(0)	0.376	-0.128	0.164	-0.2	0.176	-0.195	0.447	-0.111
SON(+1)	0.428	-0.115	0.165	-0.22	0.106	-0.231	0.131	-0.216

** 10 % significance level, * 5% significance level

PUBLICATIONS

Journal Articles

Vinay D C, Amba Shetty (2019) “Estimation of monsoon seasonal precipitation teleconnection with El Niño Southern Oscillation (ENSO) indices over the Western Ghats of Karnataka”. *Asia-pacific journal of Atmospheric science*, **55(3)**. doi: [10.1007/s13143-019-00133-w](https://doi.org/10.1007/s13143-019-00133-w) (Online)

Vinay D C, Amba Shetty (2018). “Trends in extreme rainfall over ecologically sensitive Western Ghats and coastal regions of Karnataka: An observational assessment”. *Arabian Journal of Geosciences*, **11(12)**. doi: [10.1007/s12517-018-3700-6](https://doi.org/10.1007/s12517-018-3700-6) (online)

Vinay D C, Amba Shetty, Bhupendra Bahadur Singh, & Shonam Sharma, (2017). “Spatio-temporal precipitation variability over Western Ghats and Coastal region of Karnataka, envisaged using high resolution observed gridded data”. *Modeling Earth Systems and Environment*, **3(4)**, 1611-1625. doi: [10.1007/s40808-017-0395-8](https://doi.org/10.1007/s40808-017-0395-8) (Online)

Vinay D C, Amba Shetty (2019). “Modulation of El Niño Southern Oscillation indices on ETCCDI extreme rainfall indices over West coast of Karnataka”. *Atmospheric Research*, (Under review)

Conferences

Vinay D C, Amba Shetty, and Gebremedhin Kiros (2016). Trend analysis of Rainfall Using Gridded Data over the Coastal region of Karnataka, India. *International Conference on Civil, Environment and Waste Management (CEWM-16), at Mauritius*. (Best Paper Award).

Vinay D C, Amba Shetty, Ercan Yeşilirmak (2016). Spatio-temporal distribution of precipitation concentration using high resolution gridded data over the Western Ghats and west coast of Karnataka, India. *21st International Conference on Hydraulics, Water Resources and Coastal Engineering (Hydro2016), at CWPRS Pune, India, 8th – 10th December*.

BIODATA

Name : VINAY D C

Date of Birth : 05/12/1987

Address : Haralaiah Mariyappa Family
Doranaluru (P)
Tarikere (Tq), Chickmagalur (D)
Karnataka - 577228

Telephone : +91-9900990477

Email: : vinaydc@gmail.com

Qualification : B.E. (Civil Engineering)
Siddaganga Institute of Technology, Tumkur
Karnataka (2005-2009).
M.Tech (Remote Sensing and GIS)
National Institute of Technology Karnataka
Surathkal (2009-2011)

Publications : International Journal: 03
International Conference: 01
National Conference: 01